MONASH University
Engineering

Mechanical properties of ultra-high strength (Grade 1200) steel under cooling phase of a fire

Fatemeh Azhari
B.Sc., M.Sc.

A thesis submitted for the degree of Doctor of Philosophy at Monash University in 2018

Department of Civil Engineering

Copyright Notice

©The author 2018. Except as provided in the Copyright Act 1968, this thesis may not be reproduced in any form without the written permission of the author.

To my husband, Hamidreza, and my family

with love, respect and gratitude.

Abstract

During a fire hazard, when only partial damage or no damage occurs in the structure, it might be possible to reuse the structural members. However, after a structure is cooled down from a fire temperature, residual stresses/strains might be developed. In order to conduct a rational thermal analysis in which the effect of residual stresses/strains are taken into account, investigating the mechanical properties of the construction materials under cooling phase of fire is essential. Ultra-high strength steels (UHSS) with nominal yield strengths of up to 1200 MPa have shown great potential for application as construction materials in civil engineering field. While many researchers have focused on the mechanical response of mild carbon steel at fire temperatures, a few have investigated the in-fire and post-fire mechanical behaviour of the UHSS material and thus, its extent of application in civil engineering constructions has remained restricted.

In this study, the mechanical response of ultra-high strength steel at fire temperatures of up to 800°C and after cooling to room temperature is studied. In order to investigate the in-fire and post fire mechanical behaviour of UHSS, standard dog-bone coupons are taken from UHSS tubes. The residual post-fire stress-strain curves, strength and ductility of the UHSS material are discussed and compared to those of Grade 800 high strength steel (HSS) and Grade 350 mild steel (MS) materials. To simulate a realistic fire condition, the mechanical behaviour of UHSS standard coupons under a multi-phase loading scenario including fire and creep is also evaluated and compared with those of HSS and MS materials.

Based on the experimental tests results and by modifying the compound Ramberg Osgood material model, an empirical stress-strain model is first developed in terms of the maximum fire temperature for the UHSS cooled from fire temperatures to room temperature. Afterwards, in order to consider the effect of creep strain, by employing the Bernstain-Bézier functions, a material constitutive model which takes into account the post-fire behaviour of UHSS material subject to fire and sustaining axial loads is developed. This model is capable of extrapolating the stress-strain curves out of the range of the available experimental tests data. The constitutive model has the potential to be implemented into commercial finite element packages such as ANSYS and ABAQUS to carry out a rational thermal analysis and perform fire safety design.

Moreover, the mechanical response of UHSS under extreme cooling conditions is evaluated. To achieve this, the mechanical properties of UHSS cooled from fire temperatures with an extreme cooling rate or cooled from ambient state to sub-zero temperatures are characterised. The results are then compared to HSS and MS and the effect of steel grade is investigated.

The effect of manufacturing process on the post-fire mechanical response of thin-walled UHSS tubes is also investigated. Post-fire tensile mechanical properties of direct quenched UHSS material (UHSS-DQ) considered in the other parts of this study are compared to those of quenched and tempered UHSS material (UHSS-QT) with similar original room temperature stress-strain response. Then, a finite element model is developed to compare the post-fire compression behaviour of UHSS-DQ tubular stub-columns with those made of UHSS-QT material. For verification of the model, quasi-static compression tests are conducted on UHSS-QT tubular stub columns cooled from different fire temperatures to room temperature. It is shown that the manufacturing process substantially affects the mechanical properties of UHSS stub-column under cooling phase of a fire.

To interpret the experimental results, using optical and scanning electron microscopy (SEM) methods, microstructure examination on the UHSS specimens cooled from simulated fire temperatures is conducted at each stage. In addition, the plots of the thermodynamic stability of the phases present in the tested materials (UHSS, HSS and MS) are calculated. Based on these plots, the phase changes occurring during different fire temperatures are discussed and a recommendation is made for separating studies of the effect of simulated fire temperatures on the residual strength of steel into two classes of low and high temperatures. It is shown that sensitivity of the post-fire mechanical response of UHSS to the cooling rate and the time at the maximum fire temperature is different for these two temperature regimes.

The outcomes of this study are not only beneficial for the fire-resistant design of UHSS structures, but are also useful when it comes to assessing their post-fire capacity after cooling to the ambient state. Using the results of this study, guidelines can be added to the standards to take into account the in-fire and post-fire stress-strain response of UHSS materials.

Declaration

This thesis contains no material which has been accepted for the award of any other degree or diploma at any other university or equivalent institution and that, to the best of my knowledge and belief, this thesis contains no material previously published or written by another person, except where due reference is made in the text of the thesis.

Fatemeh Azhari

May 2018

Thesis including published works declaration

In accordance with Monash University Doctorate Regulation 17.2 Doctor of Philosophy and Research Master Regulations the following declarations are made:

I hereby declare that this thesis contains no material which has been accepted for the award of any other degree or diploma at any university or equivalent institution and that, to the best of my knowledge and belief, this thesis contains no material previously published or written by another person, except where due reference is made in the text of the thesis.

This thesis includes three original papers published, one paper accepted and available online, and two papers submitted to peer reviewed journals. The core theme of the thesis is structural mechanics. The ideas, development and writing up of all the papers in the thesis were the principal responsibility of myself, the student, working within the **Civil Engineering Department** under the supervision of **Dr. Amin Heidarpour**.

The inclusion of co-authors reflects the fact that the work came from active collaboration between researchers and acknowledges input into team-based research.
In the case of Chapters 2 to 7 my contribution to the work involved the following:

Thesis Chapter	Publication Title	Status *(published, in press, accepted or returned for revision, submitted)*	Nature and % of student contribution	Co-author names Nature and % of Co-author's contribution	Co-authors, Monash student Y/N
2	Mechanical properties of ultra-high strength (Grade 1200) steel tubes under cooling phase of a fire: An experimental investigation	*Published*	70%. Development of ideas; Establishing the methodology; Experimental work; Data analysis; Writing up and revisions.	1) Dr. A. Heidarpour (20%) Financial support; Input into manuscript; Revision 2) Prof. X.L. Zhao (5%) Financial support; Revision 3) Prof. C.R. Hutchinson (5%); Input into manuscript; Revision	No

3	Post-fire mechanical response of ultra-high strength (Grade 1200) steel under high temperatures: Linking thermal stability and microstructure	*Published*	70%. Development of ideas; Establishing the methodology; Experimental work; Data analysis; Writing up and revisions.	1) Dr. A. Heidarpour (20%) Financial support; Input into manuscript; Revision 2) Prof. X.L. Zhao (5%) Financial support; Revision 3) Prof. C.R. Hutchinson (5%); Input into manuscript; Revision	No
4	Effect of creep strain on mechanical behaviour of ultra-high strength (Grade 1200) steel subject to cooling phase of a fire	*Published*	70%. Development of ideas; Establishing the methodology; Experimental work; Data analysis; Writing up and revisions.	1) Dr. A. Heidarpour (20%) Financial support; Input into manuscript; Revision 2) Prof. X.L. Zhao (5%) Financial support; Revision 3) Prof. C.R. Hutchinson (5%); Input into manuscript; Revision	No
5	On the use of Bernstain-Bézier functions for modelling the post-fire stress-strain relationship of ultra-high strength steel (Grade 1200)	*Accepted*	75%. Development of ideas; Establishing the methodology; Experimental work; Data analysis; Writing up and revisions.	2) Dr. A. Heidarpour (20%) Financial support; Input into manuscript; Revision 3) Prof. X.L. Zhao (5%) Financial support; Revision	No
6	Mechanical response of ultra-high strength (Grade 1200) steel under extreme cooling conditions	*Published*	65%. Development of ideas; Establishing the methodology; Experimental work; Data analysis; Writing up and revisions.	1) A.A. Hossain Apon (15%) Experimental work; Data analysis 2) Dr. A. Heidarpour (10%) Financial support; Input into manuscript; Revision 3) Prof. X.L. Zhao (5%) Financial support; Revision 4) Prof. C.R. Hutchinson (5%); Input into manuscript; Revision	Yes No No No

7	The effect of manufacturing process on the post-fire mechanical response of thin-walled ultra-high strength steel (Grade 1200) tubes	*Accepted*	75%. Development of ideas; Establishing the methodology; Experimental work; Data analysis; Writing up and revisions.	2) Dr. A. Heidarpour (20%) Financial support; Input into manuscript; Revision 3) Prof. X.L. Zhao (5%) Financial support; Revision	No

I **have renumbered** sections of submitted or published papers in order to generate a consistent presentation within the thesis.

Student signature: *Fatemeh Azhari*  **Date:** 28/08/2018

The undersigned hereby certifies that the above declaration correctly reflects the nature and extent of the student's and co-authors' contributions to this work. In instances where I am not the responsible author I have consulted with the responsible author to agree on the respective contributions of the authors.

Main Supervisor signature:  **Date:** 28/08/2018

List of Publications

The results obtained from the research conducted by the candidate have been summarised and published in the journal and conference papers listed as follows. All the journal papers were published in ISI Quarter 1 (Q1) peer reviewed journals in the field of civil engineering and structural mechanics. The list also includes 2 other journal papers that are accepted for publication in ISI Q1 peer reviewed journals and are presented as the 5th and 7th chapter of this thesis and also 2 conference papers. The candidate is the lead author in all publications.

Peer reviewed journal papers:

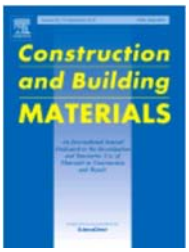

1. Mechanical properties of ultra-high strength (Grade 1200) steel tubes under cooling phase of a fire: An experimental investigation

Azhari F, Heidarpour A, Zhao X-L, Hutchinson CR,

Construction and Building Materials, 2015; Volume 93, Pages 841-50.

2. Post-fire mechanical response of ultra-high strength (Grade 1200) steel under high temperatures: Linking thermal stability and microstructure

Azhari F, Heidarpour A, Zhao X-L, Hutchinson CR,

Thin-Walled Structures, 2017; Volume 119, Pages 114-25.

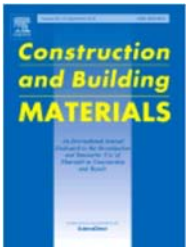

3. Effect of creep strain on mechanical behaviour of ultra-high strength (Grade 1200) steel subject to cooling phase of a fire

Azhari F, Heidarpour A, Zhao X-L, Hutchinson CR,

Construction and Building Materials, 2017; Volume 136, Pages 18-30.

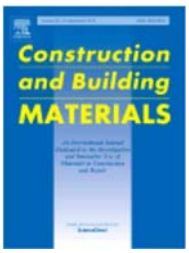

4. Mechanical response of ultra-high strength (Grade 1200) steel under extreme cooling conditions

Azhari F, A. A. Hossain Apon, Heidarpour A, Zhao X-L, Hutchinson CR,

Construction and Building Materials, 2018; Volume 175; Pages 790-803.

Journal papers accepted for publication:

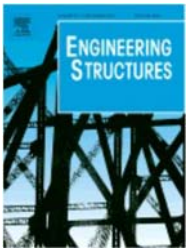

1. On the use of Bernstain-Bézier functions for modelling the post-fire stress-strain relationship of ultra-high strength steel (Grade 1200)

Azhari F, Heidarpour A, Zhao X-L,

Accepted for publication in Engineering Structures on 26 August 2018.

2. The effect of manufacturing process on the post-fire mechanical response of thin-walled ultra-high strength steel (Grade 1200) tubes

Azhari F, Heidarpour A, Zhao X-L,

Accepted for publication in Thin-Walled Structures

November 2018; Volume 132, Pages 16-24.

Peer reviewed conference papers:

1. Evaluating post-fire mechanical behaviour of ultra-high strength (Grade1200) steel tubes

Azhari F, Heidarpour A, Zhao X-L, Hutchinson CR,

Structures in Fire, Proceedings of the Ninth International Conference,

8-10 June 2016, Princeton University, USA.

2. Post-fire behaviour of cold-formed ultra-high strength steel tubular stub columns

Azhari F, Heidarpour A, Zhao X-L,

16th International Symposium on Tubular Structures (ISTS16),

4-6 December 2017, Melbourne, Australia.

Acknowledgement

I take this opportunity to extend my appreciation to all those who made this PhD thesis possible.

First and foremost, I would like to express my sincere gratitude to my main supervisor, Dr. Amin Heidarpour, for his patient supervision throughout my PhD candidature. His continuous guidance and academic support during my research allowed me to grow as a research scientist. I appreciate his creative ideas and valuable suggestions, which helped me to present the scientific results in an effective manner in this thesis.

I also sincerely thank my co-supervisor, Prof. Xiao-Ling Zhao for his kind support during the period of my candidature. His experience in the field truly improved the quality of my research. I would like to extend my special thanks to Prof. Christopher R. Hutchinson, who has been a truly dedicated mentor. Without his generous contribution to the microstructural evaluation part of my thesis, I would not have been able to perform such a multidisciplinary research work. I would like to acknowledge the technical staff of the Civil Engineering Laboratory, Mr. Long Goh, Mr. Mark Taylor, Mr. Philip Warnes, Mr. Zoltan Csaki and Mr. Peter Dunbar for their practical advice and help. My profound gratitude goes to Mrs. Jenny Manson and Mrs. Min Major for their kind support in their role as the research and postgraduate managers in the Civil Engineering Department. My special thanks goes to my colleagues and friends at Monash University for their encouragement and moral support throughout the years of my PhD.

During the last year of my PhD candidature, I had the chance to visit IBK (Institut für Baustatik und Konstruktion) at ETH Zürich for three months. This visit was supported by the Engineering Faculty, Monash University and IBK, ETH Zürich. I would like to thank Prof. Mario Fontana, Dr. Martin Neuenschwander and Dr. Elyas Ghafoori for their scientific support during this research travel.

I recognize that this research would have not been possible without the financial assistance of the Australian Research Council. I would also like to appreciate the financial support of Endeavour Scholarships and Fellowships by the Australian Government-Department of Education and my helpful case managers throughout the years. I appreciate the support of SSAB Corporation for providing the required material and

engineering services. I would like to acknowledge the use of facilities at Monash Centre for Electron Microscopy (MCEM).

Last but definitely not the least, I would like to express my utmost appreciation to my dear family: my loving husband, Hamidreza, who continuously supported me to maintain my enthusiasm and motivation throughout this whole time; my dear parents, my sisters and my brother who have always loved me unconditionally and supported me during this journey; my dear parents-in-law, sisters-in-law and brothers-in-law for their kind support; and my beautiful nieces and nephew for completing my life. They are the most important people in my world and I dedicate this thesis to them.

Table of Contents

List of Figures:

Chapter 1:

Chapter 2:

Chapter 3:

Chapter 4:

Chapter 5:

Chapter 6:

Chapter 7:

List of Tables

Chapter 1:

Chapter 2:

Chapter 3:

Chapter 4:

Chapter 5:

Chapter 6:

Chapter 7:

Chapter 1

Introduction

Table of Contents

1.1. Motivation

During the past decades, ultra-high strength steels (UHSS) with nominal yield strength of up to 1200 MPa have been offered by steel manufacturing companies. One of the most widespread applications of these materials is in the automotive industry [1-5]. The high specific strength and energy absorption of these materials lead to weight and cost reduction and improvement of road safety issues. Also, in the field of civil engineering, the unique characteristics of these materials can be highly beneficial for construction of sustainable and energy efficient structural members. The labour and transport costs can be considerably reduced as lighter equipment and fewer people are needed at the construction site. Considering these characteristics, innovative fabricated columns composed of Grade 1200 UHSS tubes have recently been proposed [6, 7]. The superior performance of these columns indicates their great potential to be used as a structural material.

In order to ensure the safety and durability of the structural members composed of UHSS material, it is necessary to evaluate the mechanical behaviour of this material under extreme loading conditions, such as fire, blast, etc. Fire is a common severe hazard that can damage the structural members and result in the failure of the whole structure during its service life [8-17]. A fire has two main phases of heat-up and cooling. In the heat-up phase, the temperature increases until it reaches its maximum and the fire is fully developed. In the cooling phase, the temperature reduces until the fire is fully extinguished. To perform a rational analysis of a structure subjected to fire, it is required to investigate the mechanical response of the construction materials under the two phases of fire. When a structural member is cooled to the ambient state after surviving the heat-up phase of a fire, its residual mechanical properties determine whether it can be reused in the structure. Therefore, in addition to the in-fire (elevated temperature) mechanical response of construction materials of a structure, their post-fire (ambient) mechanical response is of great importance. When a structure is subjected to fire, severe thermal changes are not the only reason for the changes in mechanical properties of the structural members. The sustaining loads, such as dead loads and live loads can also considerably affect their in-fire and post-fire mechanical response due to the thermal creep strain caused in the material during fire. Thus, in order to conduct a rational thermal analysis on the structural members cooled from fire temperatures, it is necessary

to develop a constitutive material model which is capable of considering the effect of both severe temperature changes and the thermal creep strain on the post-fire mechanical behaviour of the construction materials. Meanwhile, it is also important to investigate the effect of cooling rate of fire and manufacturing process of the material as important factors that can significantly change the microstructure of the material during cooling phase of a fire.

1.2. State of the art

To date, some researchers have focused on the in-fire and post-fire mechanical behaviour of structural steels [18-23]. They showed that there is a considerable change in the in-fire and post-fire mechanical properties of steel materials depending on their original yield strength, the maximum fire temperature, the cooling rate, etc. While most of this studies are focused on mild steel (MS) and high strength steel (HSS) materials, there is a scarcity of data on the in-fire and post-fire mechanical response of UHSS with nominal yield strength of 1200 MPa [24]. In this study, a novel set of experimental tests are designed to investigate the realistic in-fire and post-fire mechanical behaviour of Grade 1200 UHSS. While the main purpose of this study is evaluation of the post-fire mechanical response of UHSS, the in-fire mechanical behaviour of this material is examined for better understanding of the effect of cooling phase of a fire.

The first set of experiments focuses on the effect of severe temperature changes on the mechanical response of UHSS material subjected to fire. In these tests, standard dog-bone specimens are extracted from the UHSS tubes and tensile coupon tests are carried out on them at elevated temperatures (in-fire evaluation) and after cooling to room temperature (post-fire evaluation). Another set of experiments are designed to simulate realistic fire conditions by considering the effect of sustaining axial loads applied to the test specimen during fire in addition to the severe temperature changes. In this set of experiments, a sustained tensile axial load (F_s) is applied to the UHSS specimens during both heat-up and cooling phases of a fire and tensile coupon tests are subsequently conducted on the test specimens at room temperature. Again, to understand the effect of cooling phase of a fire, similar experiments are carried out on UHSS specimens at fire temperatures before cooling to the ambient state. A constitutive material model calibrated with the results of

the afore-mentioned experimental tests, is then proposed to take into consideration the realistic post-fire response of UHSS material.

From the results provided in the literature, it can be understood that after exposure to a certain temperature, the cooling rate of fire can significantly affect the post-fire mechanical response of steel materials [23, 25]. Therefore, in this study, the effect of cooling rate of fire on the post-fire mechanical behaviour of UHSS material is experimentally investigated. To achieve this, the post-fire mechanical properties of UHSS specimens cooled from fire temperatures with an extremely high cooling rate are compared to those of the air-cooled specimens. In addition, to simulate another extreme cooling condition, tensile coupon tests are carried out on UHSS cooled from the ambient state to harsh low temperatures (down to -80°C).

For comparison purposes, all the aforementioned experiments are also carried out on lower grades of structural steels, i.e. Grade 800 HSS and Grade 350 MS and the effect of steel grade is discussed. Moreover, using the optical and scanning electron microscopy (SEM) methods, and also the thermodynamic stability plots of the phases present in the tested materials, the mechanical properties obtained from the experimental tests are justified.

The literature shows that manufacturing process of steel materials can greatly affect their mechanical behaviour under fire conditions [18, 26]. UHSS materials attain their high strength by very fast quenching techniques either in water or oil. However, they lose ductility during the quenching process and different manufacturing companies use different methods to compensate this loss. Two very famous manufacturing techniques used for UHSS materials are the conventional quenching and tempering technique (QT), and the direct quenching technique (DQ). The UHSS material used in all stages of this study is manufactured by SSAB manufacturing company using the second method (i.e. DQ). In this study, to understand the effect of manufacturing process on the post-fire mechanical response of UHSS material, standard tensile coupon tests are conducted on direct-quenched, and quenched and tempered UHSS specimens (labelled as UHSS-DQ and UHSS-QT, respectively) at fire temperatures and after cooling to the ambient state. Afterwards, a finite element (FE) model is developed to compare the post-fire compression behaviour of tubular stub-columns made of UHSS-DQ and UHSS-QT

materials. For verification of the FE model, quasi-static compression tests are conducted on UHSS-QT tubular stub columns cooled from different fire temperatures to room temperature. It is shown that the manufacturing process substantially affects the mechanical properties of UHSS stub-columns under cooling phase of a fire.

1.3. Thesis objectives

1.3.1. Experimental investigations

In-fire/ Post-fire tensile mechanical properties of UHSS:

To perform a rational global analysis on a structure subjected to fire, it is important to understand the mechanical behaviour of the construction materials at elevated temperatures (in-fire evaluation) and after cooling to room temperature (post-fire evaluation). To this end, two sets of experimental tests are conducted in the in-fire (i.e. heat-up tests) and post-fire stages (i.e. cooling tests).

The nonlinear stress-strain curves obtained from the heat-up and cooling tests provide basic information representing the strength and ductility of the Grade 1200 UHSS tube specimens tested at fire temperatures and after cooling to room temperature. In order to investigate the effect of steel grade on the in-fire/post-fire mechanical behaviour of steel, the stress-strain response of Grade 800 HSS and Grade 350 MS tube specimens undergone similar experimental tests are compared to that of UHSS tube specimens. Considering that the main focus of this study are the cooling tests, the effect of the elevated temperature exposure on the microstructure of the specimens undergone these tests are examined using optical microscopy and SEM methods. In addition, the thermodynamic stability diagrams of the phases present in the tested materials are plotted. Based on the microstructural evaluation performed in this study, a recommendation is made for separating studies of the effect of elevated temperatures on the residual strength of steel into two classes of low and high fire temperatures. Therefore, in this thesis, evaluation of the in-fire/post-fire mechanical response of UHSS subjected to low and high fire temperature regimes are conducted in two separate chapters (chapters 2 and 3).

Effect of creep strain on the in-fire/post-fire tensile mechanical properties of UHSS:

As mentioned in the previous section, sustaining loads can seriously affect the mechanical properties of steel materials under fire. To investigate this, two sets of experimental tests are conducted: Creep-Heat-up tests and Creep-Cooling tests.

In the Creep-Heat-up tests the effect of creep on mechanical behaviour of UHSS (Grade 1200) at elevated temperatures is investigated. The mechanical properties of UHSS specimens heated up to elevated temperatures while subjected to the sustained tensile axial load of F_s were discussed. In these tests F_s is defined as: $F_s = \beta f_{u,T} S_0$, where, β is the sustained axial load ratio, $f_{u,T}$ is the ultimate tensile strength of the test material at elevated temperature T, and S_0 is the cross sectional area of the specimen. In the Creep-Cooling tests, which are the main focus of this study, a multi-phase evaluation of creep and cooling phase of a fire is performed. The test procedure is similar to the Creep-Heat-up tests except that after stabilisation of the temperature of the test specimen, it is air-cooled to room temperature under load control. Then, once the specimen reaches room temperature, tensile loading is continued under strain-controlled conditions until failure.

All these tests are conducted for different values of maximum fire temperature (T) and sustained axial load ratio (β). From the results obtained from the Creep-Heat-up and Creep-Cooling tests, the variation in creep strain, the stress-strain curves and the residual strength of the UHSS specimens are discussed.

Also, to evaluate the effect of steel grade, the Creep-Heat-up tests and Creep-Cooling tests with maximum fire temperature of T=700°C and $\beta = 0.8$ are conducted on Grade 800 HSS and Grade 350 MS tube specimens. In order to discuss the microstructural origin of accelerated softening in UHSS due to the creep strain, SEM method is used.

Tensile mechanical properties of UHSS under extreme cooling conditions:

In order to perform a comprehensive study, the mechanical behaviour of UHSS under extreme cooling conditions is also investigated in this thesis. These conditions are defined as cooling from fire temperatures with an extreme cooling rate, which is the main focus of this part of the study, and cooling from the ambient state to sub-zero temperatures.

For simulation of the extreme cooling rate, Grade 1200 UHSS standard dog-bone specimens are heated up to different fire temperatures (up to 800°C) and cooled to room temperature using water-quenching (WQ) technique. Thus, the effect of extreme cooling rate on the post-fire mechanical response of the tested materials is evaluated by comparing the residual mechanical properties of water-quenched specimens (~3500°C/min average cooling rate) to those of the air-cooled (AC) specimens (~20°C/min average cooling rate). To simulate extreme cooling temperatures, the test specimens are cooled to sub-zero temperatures of down to -80°C using Liquid Nitrogen (LN) injection. To understand the effect of steel grade on mechanical behaviour of steel under extreme cooling conditions, both set of experiments are carried out on Grade 800 HSS and Grade 350 MS structural steels. To interpret the microstructural changes occurred in the tested UHSS specimens, optical and SEM techniques are used.

The effect of manufacturing process on the post-fire mechanical response of UHSS tubes:

Following the significant effect of the manufacturing process on the residual mechanical properties of high strength steel materials [18, 26], this part of the research work aims to investigate this effect on Grade 1200 UHSS material. To achieve this, heat-up and cooling tests are conducted on standard specimens extracted from two UHSS tubes with different manufacturing processes, i.e. UHSS-QT and UHSS-DQ tubes. The results obtained for the in-fire/post-fire tensile behaviour of these materials are compared to each other. Considering the superior performance of UHSS tubes when used in innovative fabricated columns [6, 7], the effect of manufacturing process on post-fire compressive mechanical behaviour of UHSS tubular stub columns is also discussed. To this end, a numerical finite element (FE) model is developed to compare the post-fire behaviour of UHSS-QT and UHSS-DQ stub-columns. To verify the numerical model, quasi-static compression tests with displacement rate of 0.3 mm/min are carried out on UHSS-QT stub columns cooled from different fire temperatures (up to 800°C) to the ambient state. The load-axial deformation of the columns is recorded.

1.3.2. Numerical Modellings

Constitutive model for the post-fire tensile mechanical properties of UHSS:

From the experiments conducted in this thesis, it is resulted that the post-fire stress-strain response of UHSS is highly dependent on the maximum fire temperature and the creep strain caused due to the sustained axial loads applied to it during fire. In this thesis, first, using the modified compound Ramberg-Osgood equations, an empirical constitutive material model is developed, which takes into account the post-fire mechanical response of UHSS in terms of the maximum fire temperature. However, to perform a rational thermal analysis on a UHSS structural member cooled from fire temperatures, it is necessary to develop a post-fire material constitutive model, which in addition to the maximum fire temperature, considers the effect of creep strain. To achieve this, the Bernstain-Bézier functions are employed to present the relationship between the stress, strain, the maximum fire temperature and the sustained axial load ratio (β) for Grade 1200 UHSS cooled from fire temperatures to room temperature. In order to calibrate and validate the model, the results obtained from the experimental tests are used. The proposed model is capable of extrapolating the stress-strain curves out of the range of the available experimental tests data.

Moreover, the instantaneous stress-induced strain is extracted from the modelled stress-strain-temperature response of the UHSS tested at elevated temperatures. Consequently, knowing the instantaneous stress-induced strain from the model, and the total transient strain and the thermal strain of UHSS from the experimental tests, the thermal creep strain of UHSS subjected to different values of constant axial load during transient fire is obtained.

Finite element model for post-fire compressive mechanical response of thin-walled UHSS tubular stub columns:

In order to compare the post-fire compressive behaviour of UHSS-QT and UHSS-DQ tubular stub-columns, a numerical FE model is developed using ABAQUS FE package. The model is calibrated using the experimental quasi-static compression tests conducted on Grade 1200 UHSS-QT stub-columns cooled from various fire temperatures to room temperature. In this model, the realistic plastic models, nonlinear material and geometry, and most importantly, the changes of the material properties due to the fire temperature

exposures are taken into consideration for both UHSS-DQ and UHSS-QT materials. The model can be considered as a simulation tool for future research purposes.

The summary of the objectives mentioned in this section, is provided in Figure 1-1. In this figure, the in-fire and post-fire investigations are illustrated by red and blue colours, respectively.

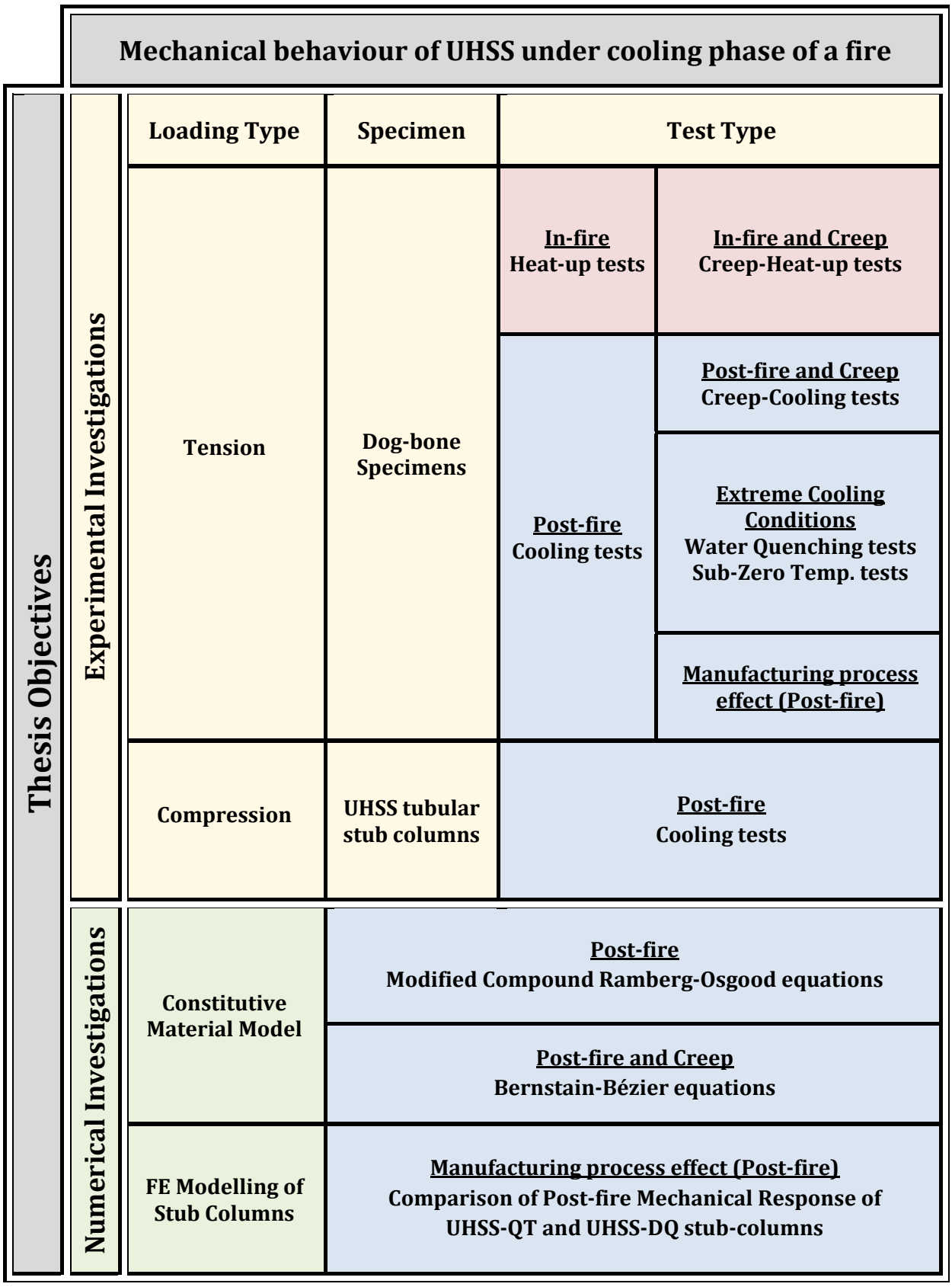

Figure 1-1. Thesis Objectives

1.4. Thesis Outline

An overall outline of each chapter and the structure of thesis chapters is presented in Table 1-1. The general structure of the thesis is in the format of thesis by publications. Chapters 2 to 4 and 6 are published journal papers (listed in page ix) and chapters 5 and 7 are currently under-review in international journals (listed in page x).

Table 1-1. The outline of the thesis

Chapter 1: Introduction
Chapter 2: Mechanical properties of ultra-high strength (Grade 1200) steel tubes under cooling phase of a fire: An experimental investigation
Chapter 3: Post-fire mechanical response of ultra-high strength (Grade 1200) steel under high temperatures: Linking thermal stability and microstructure
Chapter 4: Effect of creep strain on mechanical behaviour of ultra-high strength (Grade 1200) steel subject to cooling phase of a fire
Chapter 5: On the use of Bernstain-Bézier functions for modelling the post-fire stress-strain relationship of ultra-high strength steel (Grade 1200)
Chapter 6: Mechanical response of ultra-high strength (Grade 1200) steel under extreme cooling conditions
Chapter 7: The effect of manufacturing process on the post-fire mechanical response of ultra-high strength steel (Grade 1200) tubes
Chapter 8: Conclusions and future work

Chapter 1: Introduction

In this chapter a general overview of the thesis is given. This includes the motivation of the research, explanations on how the knowledge gaps are addressed, and the main objectives of the thesis. The objectives of the thesis are divided into two main sections, first being the experimental investigations and second the numerical modellings, all of which are addressed in Chapters 2 to 7 of this thesis.

Chapter 2: Mechanical properties of ultra-high strength (Grade 1200) steel tubes under cooling phase of a fire: An experimental investigation

This chapter investigates the post-fire tensile mechanical behaviour of Grade 1200 UHSS steel tubes after cooling from low fire temperatures (up to 600°C). This investigation is conducted experimentally through quasi-static tensile tests carried out on standard dog-bone specimens taken from UHSS tubes. The tensile tests are conducted at elevated temperatures (Heat-up tests) and after the specimens are cooled to room temperature (Cooling tests) to investigate the in-fire and post-fire mechanical properties of UHSS. Although the main focus of this study is the post-fire mechanical response of the UHSS material, the Heat-up tests are conducted to better understand the effect of cooling phase of a fire. Cooling rate effect is investigated using LN injection and by considering three different cooling rates. The effect of steel grade on post-fire mechanical response of steel is also evaluated by conducting the heat-up and cooling tests on Grade 350 MS and Grade 800 HSS. Microstructure examination of the tested specimens is preformed using optical and SEM methods. By calculating the thermodynamic stability of the ferrite and cementite phases in the tested materials and based on the phase changes occurring in the steel material during fire, a recommendation is made to separate the studies of the effect of fire temperature on the post-fire mechanical response of steel into two temperature regimes of low and high fire temperatures.

Chapter 3: Post-fire mechanical response of ultra-high strength (Grade 1200) steel under high temperatures: Linking thermal stability and microstructure

Following the recommendation made in Chapter 2 for separating the studies of the effect of simulated fire temperature on residual mechanical response of steel into low and high fire temperature regimes, this chapter examines the post-fire mechanical response of UHSS subjected to high fire temperatures (up to 800°C). Similar to Chapter 2, Heat-up and Cooling tests are conducted on UHSS specimens for investigation of the in-fire and post-fire mechanical behaviour of this material. However, the experimental test setup used in this chapter to simulate the high fire temperature exposure is different from that used for low fire temperatures in Chapter 2. A comparison study is performed by conducting the same experimental tests on Grade 800 HSS material. The microstructures of the tested specimens are examined using optical microscopy and SEM techniques and the thermal

stability of the phases present in the tested materials are linked with their microstructure. Finally, using the experimental tests results, an empirical constitutive model is developed to predict the post-fire stress-strain response of the UHSS materials cooled from fire temperatures of up to 800°C.

Chapter 4: Effect of creep strain on mechanical behaviour of ultra-high strength (Grade 1200) steel subject to cooling phase of a fire

In this chapter, the mechanical behaviour of Grade 1200 UHSS tube subject to a multi-phase loading scenario including fire and creep is investigated. Thus, for the first time, this study simulates a realistic fire condition, where in addition to severe temperature changes, the effect of the creep strain caused by the sustained axial loads applied to the specimens are taken into consideration. Standard dog-bone specimens extracted from UHSS tubes are undergone two sets of experiments, i.e. Creep-Heat-up tests and Creep-Cooling tests. These tests are designed to investigate the effect of creep strain on the in-fire and post-fire mechanical behaviour of UHSS, respectively. However, the main focus of this study is the Creep-Cooling tests. To investigate the effect of steel grade, the same set of tests are carried out on standard specimens taken from the Grade 800 HSS and Grade 350 MS tubes. Finally, similar to the previous chapters, SEM is used to discuss the physical origin of the softening occurs in the microstructure of the UHSS specimens subjected to creep during the simulated fire.

Chapter 5: On the use of Bernstain-Bézier functions for modelling the post-fire stress-strain relationship of ultra-high strength steel (Grade 1200)

This chapter employs Bernstain-Bézier functions and presents the relationship between the stress, strain, the maximum fire temperature and the sustained axial load ratio (β) for Grade 1200 UHSS cooled from different fire temperatures to room temperature. The proposed model is calibrated and validated using the experimental results obtained in Chapters 2 to 4 of this thesis. Also, the in-fire stress-strain-temperature response of the UHSS tested at elevated temperatures is obtained from the model and the instantaneous stress-induced strain of the UHSS under transient fire is predicted. Finally, knowing the strain components derived from the proposed model and the experimental tests results,

variation of the creep strain with temperature for UHSS subjected to different values of constant axial load during transient fire is obtained.

Chapter 6: Mechanical response of ultra-high strength (Grade 1200) steel under extreme cooling conditions

This chapter examines the mechanical properties of Grade 1200 UHSS under extreme cooling conditions, specified as extreme cooling rates or extreme cooling temperatures. However, the main focus of this research is the first condition (extreme cooling rates), which is simulated by heating standard dog-bone UHSS specimens to elevated temperatures (up to 800°C) and cooling them to the ambient state using the water-quenching (WQ) technique. In order to simulate the second condition (extreme cooling temperatures), LN injection is used to cool the test specimens to sub-zero temperatures of down to -80°C. To investigate the steel grade effect, both sets of experimental tests are conducted on standard dog-bone specimens extracted from Grade 800 HSS and Grade 350 MS tubes. Finally, using optical and SEM techniques, microstructure examination of the tested UHSS specimens is conducted.

Chapter 7: The effect of manufacturing process on the post-fire mechanical response of thin-walled ultra-high strength steel (Grade 1200) tubes

In this chapter, it is aimed to evaluate the manufacturing process effect on the residual mechanical properties of Grade 1200 UHSS cooled from fire temperatures to room temperature. To achieve this, a comparison study is conducted on the post-fire mechanical response of two Grade 1200 UHSS materials, one manufactured by direct quenching technique (UHSS-DQ) and one by the conventional quenching and tempering method (UHSS-QT); while they exhibit the same original room temperature stress-strain behaviour. For comparison of the in-fire and post-fire tensile mechanical response of these materials, cooling tests are carried out on them. In order to understand the effect of manufacturing process on the post-fire compressive behaviour of UHSS tubular stub-columns, a FE model is developed in ABAQUS FE package with precise modelling inputs. The post-fire mechanical behaviour of the stub-columns composed of these two UHSS materials are then compared for different maximum fire temperatures. To verify the model, compression tests are carried out on the UHSS stub-columns with length to

diameter ratio of 3 ($L/D = 3$) at room temperature after cooling from different fire temperatures. The FE model can be used as a verified simulation tool for future investigations.

Chapter 8: Conclusions and future work

This chapter summarises the objectives achieved in this research and provides an overview of the main outcomes of different stages of the thesis. In addition, recommendations are made for continuing this research work in future.

References

[1] K. Osawa, T. Shimomura, M. Kinoshita, K. Matsudo, K. Iwase, Development of high-strength cold-rolled steel sheets for automotive use by continuous annealing, SAE Technical Papers, (1983).
[2] C. Cazes, F. Ronin, Use of HSS1, VHSS2 and UHSS3 steels in the body in white: A panorama of the latest European vehicles, state of art and perspectives, SAE Technical Papers, (2002).
[3] T. Nonaka, H. Taniguchi, K. Goto, K. Yamazaki, Development of ultra-high-strength cold-rolled steel sheets for automotive use, Nippon Steel Technical Report, (2003) 13-15.
[4] Y. Mukai, Development of new high-strength steel sheets for automobiles, R and D: Research and Development Kobe Steel Engineering Reports, 55 (2005) 30-35.
[5] M. Aratani, Y. Ishiguro, Y. Hashimoto, S. Toyoda, H. Kimura, O. Sonobe, M. Gunji, Development of UTS 980 MPa grade steel tube with excellent formability for automotive body parts, in: Lecture Notes in Electrical Engineering, 2013, pp. 213-224.
[6] F. Javidan, A. Heidarpour, X.-L. Zhao, J. Minkkinen, Application of high strength and ultra-high strength steel tubes in long hybrid compressive members: Experimental and numerical investigation, Thin-Walled Structures, 102 (2016) 273-285.
[7] M. Nassirnia, A. Heidarpour, X.-L. Zhao, J. Minkkinen, Innovative hollow columns comprising corrugated plates and ultra high-strength steel tubes, Thin-Walled Structures, 101 (2016) 14-25.
[8] A. Heidarpour, S. Cevro, Q.-Y. Song, X.-L. Zhao, Behaviour of stub columns utilising mild-steel plates and VHS tubes under fire, Journal of Constructional Steel Research, 95 (2014) 220-229.
[9] Q.-Y. Song, A. Heidarpour, X.-L. Zhao, L.-H. Han, Post-earthquake fire behavior of welded steel I-beam to hollow column connections: An experimental investigation, Thin-Walled Structures, 98, Part A (2016) 143-153.
[10] M. Mirmomeni, A. Heidarpour, X.L. Zhao, C.R. Hutchinson, J.A. Packer, C. Wu, Mechanical properties of partially damaged structural steel induced by high strain rate loading at elevated temperatures - An experimental investigation, International Journal of Impact Engineering, 76 (2014) 178-188.
[11] S. Sinaie, A. Heidarpour, X.L. Zhao, Stress-strain-temperature relation for cyclically-damaged structural mild steel, Engineering Structures, 77 (2014) 84-94.
[12] S. Hosseini, A. Heidarpour, F. Collins, C.R. Hutchinson, Effect of strain ageing on the mechanical properties of partially damaged structural mild steel, Construction and Building Materials, 77 (2015) 83-93.
[13] S. Sinaie, A. Heidarpour, X.L. Zhao, Mechanical properties of cyclically-damaged structural mild steel at elevated temperatures, Construction and Building Materials, 52 (2014) 465-472.
[14] W. Li, X. Zhang, H. Kou, R. Wang, D. Fang, Theoretical prediction of temperature dependent yield strength for metallic materials, International Journal of Mechanical Sciences.
[15] T.J. Lin, Y.B. Yang, C.W. Huang, Inelastic nonlinear behavior of steel trusses cooled down from a heating stage, International Journal of Mechanical Sciences, 52 (2010) 982-992.
[16] S.L. Mannan, M. Valsan, High-temperature low cycle fatigue, creep–fatigue and thermomechanical fatigue of steels and their welds, International Journal of Mechanical Sciences, 48 (2006) 160-175.

[17] M. Sorine, C.H.M. Simha, I. van Riemsdijk, M.J. Worswick, Prediction of necking of high strength steel tubes during hydroforming—multi-axial loading, International Journal of Mechanical Sciences, 50 (2008) 1411-1422.
[18] S.P. Chiew, M.S. Zhao, C.K. Lee, Mechanical properties of heat-treated high strength steel under fire/post-fire conditions, Journal of Constructional Steel Research, 98 (2014) 12-19.
[19] S. Gunalan, M. Mahendran, Experimental investigation of post-fire mechanical properties of cold-formed steels, Thin-Walled Structures, 84 (2014) 241-254.
[20] J. Outinen, Mechanical properties of structural steel at elevated temperatures and after cooling down, in: 10th International Conference - Fire and Materials 2007.
[21] X. Qiang, F.S.K. Bijlaard, H. Kolstein, Post-fire mechanical properties of high strength structural steels S460 and S690, Engineering Structures, 35 (2012) 1-10.
[22] X. Qiang, F.S.K. Bijlaard, H. Kolstein, Post-fire performance of very high strength steel S960, Journal of Constructional Steel Research, 80 (2013) 235-242.
[23] W. Wang, T. Liu, J. Liu, Experimental study on post-fire mechanical properties of high strength Q460 steel, Journal of Constructional Steel Research, 114 (2015) 100-109.
[24] A. Heidarpour, N.S. Tofts, A.H. Korayem, X.L. Zhao, C.R. Hutchinson, Mechanical properties of very high strength steel at elevated temperatures, Fire Safety Journal, 64 (2014) 27-35.
[25] E.M. Aziz, V.K. Kodur, Effect of temperature and cooling regime on mechanical properties of high-strength low-alloy steel, Fire and Materials, 40 (2016) 926-939.
[26] S. Kesawan, M. Mahendran, Post-fire mechanical properties of cold-formed steel hollow sections, Construction and Building Materials, 161 (2018) 26-36.

Chapter 2

Mechanical properties of ultra-high strength (Grade 1200) steel tubes under cooling phase of a fire: An experimental investigation

This chapter has been published in the Journal of *Construction and Building Materials*, Volume 93, September 2015, Pages 841-50.

DOI: 10.1016/j.conbuildmat.2015.05.082

Reprinted here with the Author Rights granted by Elsevier.

Table of Contents

Abstract

There has recently been a growing trend towards using ultra-high strength steel (UHSS) in many engineering applications. However, few researches have focused on the mechanical properties of this kind of steel at elevated temperatures. In this study, the mechanical properties of UHSS at temperatures characteristic of fire and after cooling from fire temperatures, are studied experimentally. The specimens taken from UHSS tubes are subjected to fire temperatures of up to 600°C and tensile tests are carried out both at elevated temperatures and after the specimens were cooled to room temperature. As expected, the strength of the UHSS specimens decreases significantly when tested under fire temperatures of 450°C and 600°C. However, the strength of the UHSS is also considerably reduced after cooling down from high fire temperatures to room temperature. The stress–strain curves, strength and ductility of the UHSS tube specimens are discussed. Furthermore, in order to perform a comparison study, the stress–strain curves for three different grades of steel tubes including UHSS, high strength steel (HSS) and Mild steel (MS) tubes are presented and compared. It is shown that the reduction in the strength of the UHSS after cooling from fire temperatures of up to 600°C does not occur to the same extent for HSS and MS steels. The effect of the cooling rate after exposure to fire temperatures on the mechanical properties of UHSS tube specimens is also investigated. Micro-structure examination is conducted using optical and scanning electron microscopy (SEM) and the room temperature strength reduction in the UHSS after exposure to the fire temperatures is discussed in terms of the effect on the steel microstructure. A recommendation has been made for separating studies of the effect of simulated fire temperatures on the residual strength of steel into two classes (low and high temperature), depending on whether a critical maximum temperature (which depends on alloy composition) is exceeded and the science under-lying this recommendation has been discussed.

Key Words: ultra-high strength steel, fire, cooling, stress-strain curve, steel tube, cooling rate, micrograph

2.1. Introduction

During the past decades, ultra-high strength steel (UHSS) tubes with nominal yield strengths of up to 1200 MPa have been widely used in the automotive industry due to the increased tensile strength and high energy absorption which leads to the weight and cost reduction and improvement of road safety issues [1-5]. Presently, due to construction development, the demand for using high strength steel in civil engineering applications is also increasing [6-10]. However, due to the lack of relevant design codes of practice covering the behaviour of UHSS under extreme actions, limited application of this kind of steel is seen in construction industry around the world. In order to utilise UHSS tubes in civil engineering applications, their behaviour under various loading scenarios including fire, cyclic, impact, etc. must be investigated. This paper addresses the mechanical properties of UHSS tubes under the cooling phase of a fire.

When only partial damage or no damage occurs during an extreme action, it might be possible to reuse the structural member [11-17]. However, after a structure is cooled down from a fire temperature, residual stresses may be developed [18]. In order to develop a rational thermal analysis in which the effect of residual stresses are taken into account, investigating the mechanical properties of the material under cooling phase of fire is essential.

One of the primary models developed to describe the behaviour of structural members during the cooling phase of a fire was introduced by El-Rimawi et al. [19]. In this study, the available stress-strain curves for the steel materials at elevated temperatures were employed and by adopting a bi-linear unloading curve and applying some modifications, a simple model was developed to describe the cooling path of structural members. Bailey et al. [20] developed a model in which a curvilinear unloading path, instead of the bi-linear one proposed by El-Rimawi [19], was adopted. Furthermore, it was assumed that the cyclic loading of steel members in a fire does not occur which allows the definition of a unique and reversible unloading path. According to the results presented in [19], it can be observed that compared to El-Rimawi's model, Bailey's model results in a lower absolute value of the permanent strain and thus a greater recovery of displacement. However, neither of these two models were validated with experimental results. Wang et al. [21] developed a numerical model for steel structures during the cooling phase. They

provided a simple model describing the unloading path during the cooling phase by using a line and a half of the original stress-strain curve. The model was implemented into the authors' computer program and a steel truss was analysed using the presented model to demonstrate the residual deformations and stresses developed in the structures after a fire. However, due to the lack of experimental data on this topic, the results were only verified using ANSYS finite element software.

In order to investigate the remaining strength of steel structures exposed to fire, Outinen [22] carried out tensile tests on different grades of structural steel materials including S355, S460M, S350GD+Z, S355J2H and EN 1.4301. The tensile coupons were cooled to room temperature from fire temperatures of up to 1000°C. The stress-strain curves for the coupons taken from flat and corner regions of cold-formed steel tubes were presented by the author and their post-fire behaviour was discussed. Qiang et al. [23] performed a set of tests to investigate the behaviour of S460 steel under fire and post-fire conditions. In this research, in order to study the post-fire behaviour of the material, they heated the steel specimens to fire temperatures of up to 1000°C and then performed tensile tests at room temperature after cooling the specimens. The residual elastic modulus, yield strength and ultimate tensile strength of S460N steel after cooling down from fire temperatures were reported. It was shown that S460 steel regains at least 70% of its original mechanical properties. The same authors performed a similar study on high strength steel S960 [24]. The results indicated that post-fire behaviour of S960 steel is different to S460 steel. Comparing the results obtained for S460 and S960 steel specimens cooled from temperatures above 600°C to room temperature, a sharper reduction in residual yield strength and ultimate tensile strength of S960 was observed. Moreover, the mechanical properties of both S960 and S460 steel are only affected by the cooling phase when they are subjected to fire temperatures above 600°C.

The effect of cooling from fire temperatures on the mechanical properties of the steel connectors such as bolts has also been investigated. Hanus et al. [25] performed steady-state tests at various temperatures after heating Grade 8.8 bolts to 800°C and then cooling them at a rate of 10-30°C/min. They also developed an analytical model for the stress-strain behaviour of bolts during a natural fire which gives values of strength reduction factors for the cooling phase.

Research on the mechanical properties of ultra-high strength steels with nominal yield strengths above 960MPa at elevated temperatures is limited and the behaviour of UHSS tubes during the cooling phase of a fire has not so far been investigated. Heidarpour et al. [26] presented an experimental study on UHSS (Grade 1200) tubes subjected to elevated temperatures of up to 600°C and the changes in strength and ductility were discussed. The results showed a dramatic deterioration in strength of the UHSS after 300°C. They also proposed some equations to describe the reduction factors of 0.2% proof stress and ultimate tensile strength for UHSS tubes at fire temperature.

This paper addresses the mechanical properties of ultra-high strength steel during the cooling phase of a fire. Although the nominal tensile strength of UHSS studied by Heidarpour et al. [26] is close to that of the alloy used in this study, due to differences in chemical composition as well as manufacturing process, experimental tests at elevated temperatures are also carried out on the UHSS specimens in this study. Therefore, two sets of experimental tests are carried out. The first set of tests are heat-up tests where the specimens taken from UHSS tubes undergo strain-controlled tensile tests at elevated temperatures. The second set of tests, which forms the main focus of this study, includes the cooling tests where the tensile test is carried out at room temperature on UHSS specimens after being cooled down from fire temperatures. In these latter tests, the changes in strength and ductility of the material are discussed. In order to compare the change in the material properties of the UHSS tubes with those of high-strength steel (HSS) and Mild-steel (MS) tubes, experimental tests were also carried out on tensile coupons taken from HSS and MS tubes. In addition, the effect of cooling rate from simulated fire temperatures on the mechanical properties of UHSS tube specimens cooled down from 600ºC is also investigated. Finally, using the optical and scanning electron microscopy (SEM), microstructure examinations are performed on the bulk microstructures of the tested specimens and the relationship between the changes in microstructure and the changes in mechanical properties after fire temperature exposure are discussed.

2.2. Experimental tests

2.2.1. Test Specimens

The test specimens are taken from ultra-high strength steel (Grade 1200), high strength steel (Grade 800) and Mild-steel (Grade 350) cold-formed tubes with nominal diameter and wall thickness of 76.1 mm and 3.2 mm, respectively. The geometry of the test specimens is shown in Figure 2-1 and the samples are sectioned from the tubes using high pressure water jet cutting. The shape and dimensions of the specimens are determined in agreement with the limitations defined in ASTM E8 [27]. As shown in Figure 2-2, the specimens were taken from two strips located at right angles (90^0) to the tube weld line. For the sake of comparison, some tests are also performed on the UHSS specimens taken from the opposite face (180^0). In order to grip the end of the specimens for the tensile tests, they are mechanically flattened according to the instructions provided in AS1391 [28] .

It is worth noting that UHSS and HSS tubes are manufactured by a unique pro-cess developed by SSAB manufacturing company called direct quenching. Unlike the traditional quenching technique where the material is quenched in several stages, in direct quenching method the material is quenched only in one stage. The chemical compositions of the steels used in this study are shown in Table 2-1. Each test is performed at least twice. In case that the difference between the results obtained from two similar tests is more than 3%, an additional test is conducted. The cross sectional area of the specimens is calculated by [28]

$$S_0 = \frac{b}{4}(D^2 - b^2)^{\frac{1}{2}} + \frac{D^2}{4}\arcsin\frac{b}{D} - \frac{b}{4}\left[(D-2a)\ -b^2\right]^{\frac{1}{2}} - \left(\frac{D-2a}{2}\right)^2 \arcsin\frac{b}{D-2a} \qquad (2\text{-}1)$$

where D is the tube diameter, and b and a are the width and thickness of the cross section of gauge length shown in Figure 2-1, respectively.

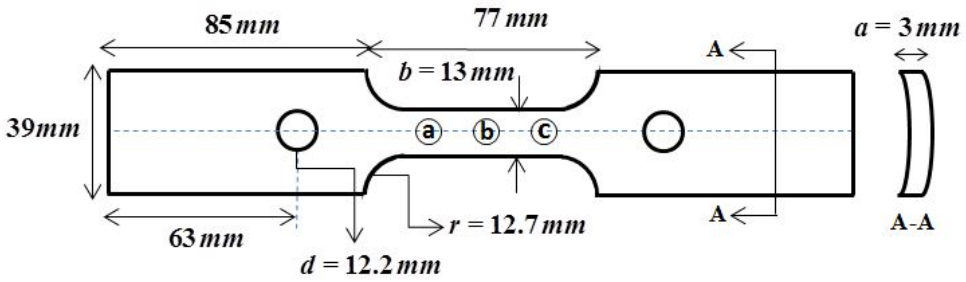

Figure 2-1. The test specimens geometry

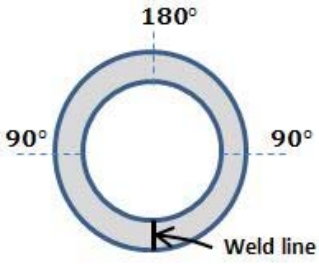

Figure 2-2. The tube section

Table 2-1. The chemical composition of test specimens (wt%)

Material	C	Si	Mn	P	S	Cr	Ni	Mo	B	Al
UHSS	0.230	0.800	1.700	0.025	0.015	1.500	1.00	0.500	0.005	
HSS	0.100	0.250	2.100	0.020	0.010					0.015
MS	0.230	0.400	1.350	0.040	0.050					

2.2.2. Testing Method

In order to investigate the mechanical properties of the steel materials at high temperatures, two types of tests are typically performed: either transient state tests, or steady state tests. In transient state tests, the specimens are subjected to a constant load and the temperature is increased with a specific rate. In the steady state tests, the specimens are held at a constant temperature and the load is increased to failure. Although the transient state tests describe a more realistic fire condition, the steady state tests provide the advantage that they directly give the stress-strain curve from the experimental data and the standards support this method [29]. The steady state tests are the testing method applied in this study. In this paper, the experimental tests are

conducted in two stages including the in-fire stage and the post-fire stage representing the heat-up tests and the cooling tests, respectively.

2.2.2.1. Heat-up tests

For heat-up tests, the specimen is positioned between the grips in the Instron Environmental chamber. Three thermocouples labelled as T_1, T_2 and T_3, are attached to three points a, b and c on the gauge length of the specimen (Figure 2-1) and the chamber is heated to fire temperatures of 150°C, 300°C, 450°C and 600°C, which is the maximum temperature capacity of the chamber. The heating rate in all tests is taken as $10°C/min$. The temperature throughout the specimen is stabilised when the difference between the temperature T_i of each thermocouple and the target temperature T_t is less than 2%, i.e. $|T_i - T_t| \leq 2\%$. Once the temperature is stable, the specimen is subjected to a strain-controlled tensile test with an applied strain rate of $0.005 \pm 0.002\,\text{min}^{-1}$ until failure. The tensile test is conducted using the Instron 5982 100kN testing machine. In order to record the axial strain during the test, an MTS non-contact laser extensometer is used to record the distance between two reflective stickers glued to the sample gauge length. The test setup is shown in Figure 2-3 .

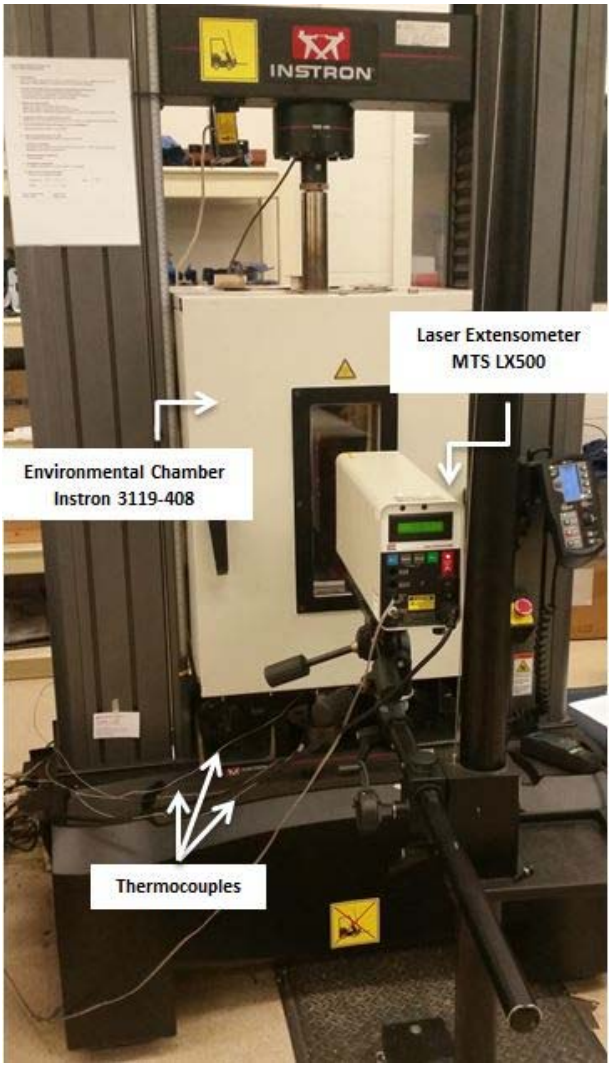

Figure 2-3. Test setup

2.2.2.2. Cooling tests

The main purpose of this study is to investigate the effect of the cooling stage of a fire on the mechanical properties of UHS steel tubes. To perform such experiments, the test specimens are first heated to the target fire temperatures using the procedure explained in the previous section. After being stabilised at the target temperature (T_t), the specimen is held at the temperature T_t for ~20 minutes. The specimen is then cooled to the room temperature by simply turning off the chamber. Finally, after reaching room temperature, the specimen is subjected to a strain controlled tensile test with an applied strain rate of $0.005 \pm 0.002\,\text{min}^{-1}$ until failure.

To attempt to rationalise the effect of the simulated fire temperature exposure on the subsequent room temperature mechanical properties, the microstructures of samples

were examined using a JEOL 7001F FEG scanning electron microscope (SEM). SEM obtains high resolution images using a focused beam of electrons. The specimens are examined in high vacuum condition. The acceleration voltages employed in emitting the electrons to the sample surface is 15kV and a working distance of 10mm was used.

2.3. Results and Discussions

2.3.1. Determination of Mechanical Properties

In this study, in order to investigate the behaviour of an UHSS subjected to the cooling phase of a fire, the 0.2% proof stress, ultimate tensile strength, total strain at 0.2% proof stress, strain at ultimate tensile strength and energy absorption are determined. The values of these parameters are illustrated in a typical stress-strain curve shown in Figure 2-4. As indicated in Figure 2-4, the values of 0.2% proof stress ($f_{0.2}$) and the total strain at 0.2% proof stress (ε_y) are obtained by finding the intersection of the curve with a line starting from the 0.2 % strain parallel to the elastic part of stress-strain curve. The maximum stress in the stress-strain curve and the strain corresponding to this stress represent the ultimate tensile strength (f_u) and the strain at ultimate tensile strength (ε_u), respectively. Finally, the energy absorption (U^*) is found by calculating the area under the stress-strain curve starting from zero strain to the strain at ultimate tensile strength (ε_u).

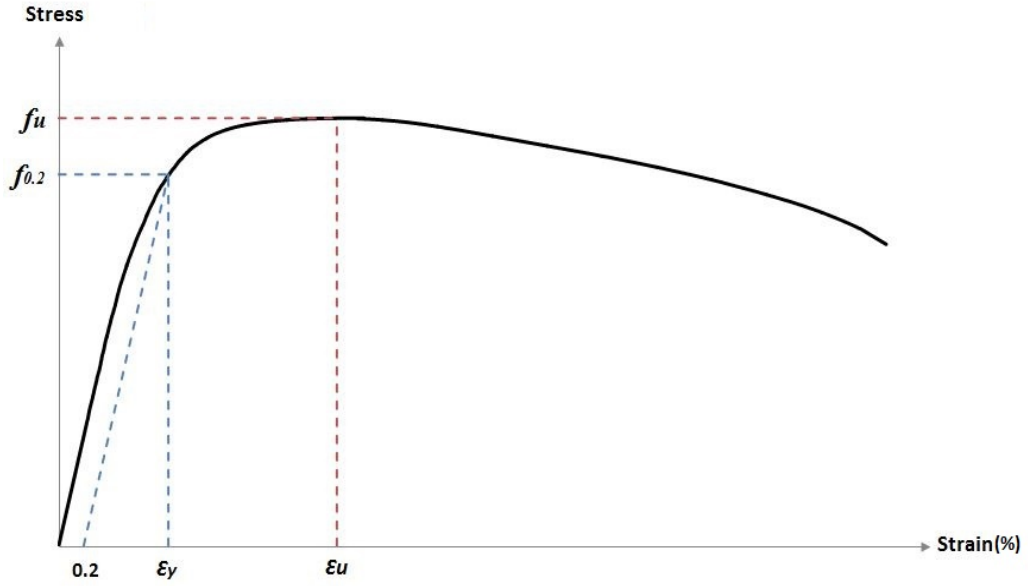

Figure 2-4. Definition of mechanical properties on a typical stress-strain curve

2.3.1.1. Stress-strain curves

To examine the behaviour of ultra-high strength steel (UHSS) tubes in and after fire, two sets of tests are conducted: heat-up tests and cooling tests.

Figure 2-5 shows the stress-strain curves of UHSS samples at elevated temperatures ranging from 150°C to 600°C. It is worth mentioning that the curves indicate the stress and strain values up to the maximum strength of material for which the necking region of steel material has not been depicted due to inaccurate strain readings in this region. In these curves, the stress-strain curve of the UHSS at temperature ***T*** is shown as UHSS-**H*T*** in which **H** and ***T*** represent heating and target temperature, respectively. For example, UHSS-H300 indicates a tensile test performed at T= 300°C. It can be seen from Figure 2-5 that although the strength of UHSS decreases considerably as the temperature is increased, the maximum strength fu even at 600°C, is still reasonably high and close to the Mild Steel (MS) tubes strength at room temperature.

The main purpose of this study is to discuss the effect of the cooling phase of a fire on the mechanical response of UHSS. The stress-strain curves of UHSS specimens which have been cooled to the room temperature from fire temperatures of up to 600°C are presented in Figure 2-6. The stress-strain curves for a UHSS specimen **c**ooled from the temperature ***T*** is shown as UHSS-**C*T***. For example, the stress-strain curve corresponding to UHSS-C450 represents the stress and strain values obtained from monotonic tensile tests at room temperature on a UHSS specimen which has been cooled from 450°C to room temperature. It can be seen from Figure 2-6 that the UHSS specimens do not regain their original strength after being cooled from fire temperatures above 450°C. This experimental result is not consistent with the strain reversal based model proposed by El-Rimawi et al. [19], in which the strength of the steel is fully regained after cooling from temperature T_1 to T_2 ($T_1 > T_2$). Considering T_1= 450°C or 600°C and T_2 to be room temperature, it can be seen from Figure 2-6 that El-Rimawi's model may not predict an accurate behaviour for UHSS material. Furthermore, it is evident that the strain at ultimate tensile strength increases when the heat-up temperature T increases. Unlike the tests at elevated temperatures where the modulus of elasticity decreases when the temperature increases (Figure 2-5), no significant change in the modulus of elasticity of UHSS specimens at room temperature after cooling tests is observed (Figure 2-6). In

other words, unlike the strength, the initial stiffness of the UHSS material is fully regained under the cooling phase. This conclusion supports the fact that similar to Mild steel, for UHSS specimens having experienced fire temperatures of up to 600°C, the elastic modulus is independent of the temperature history and only depends on the temperature in which the specimen is being tested [30].

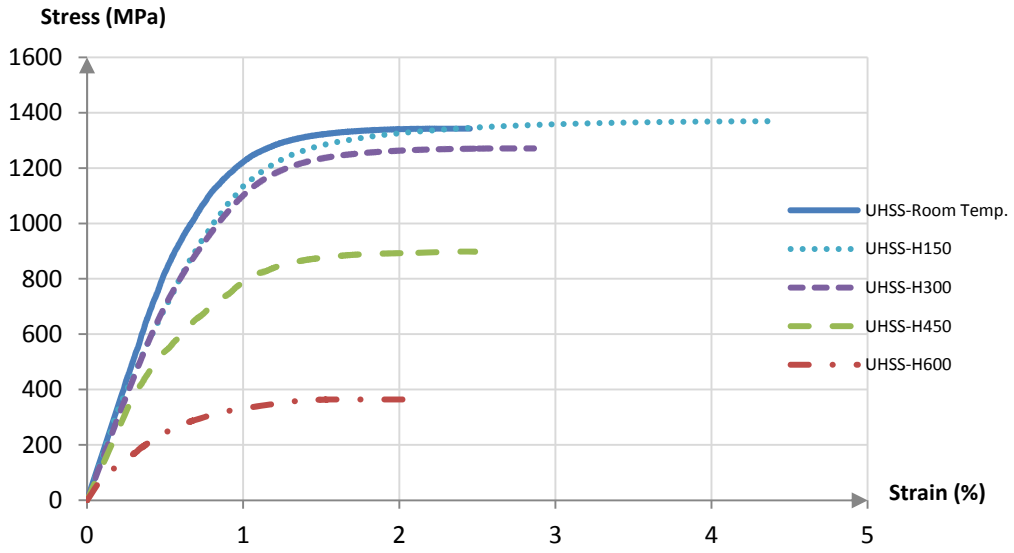

Figure 2-5. Stress-strain curves for UHSS specimens at elevated temperatures

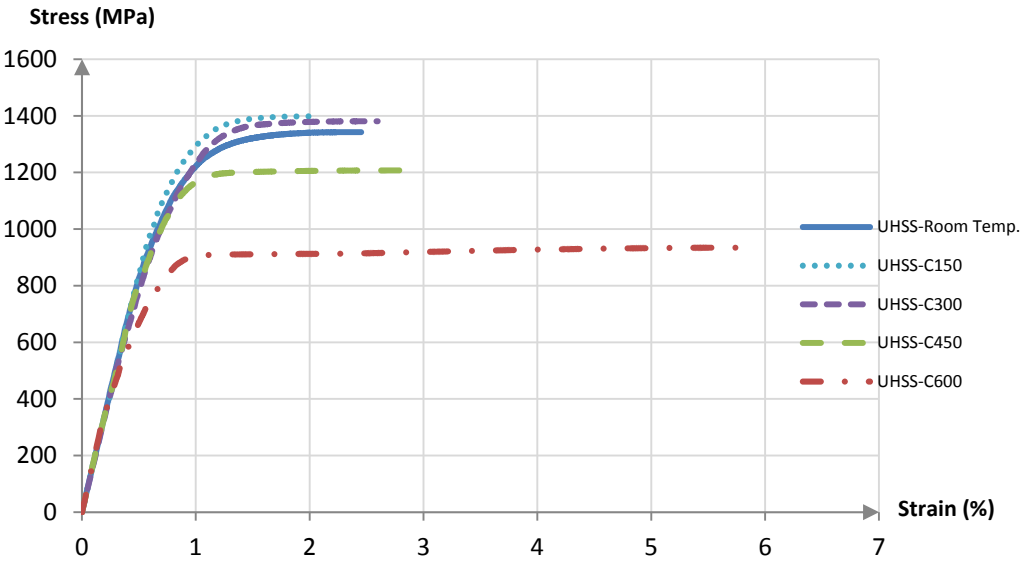

Figure 2-6. Stress-strain curves for UHSS specimens at room temperature after cooling down from the elevated temperature T to room temperature

2.3.1.2. 0.2% Proof stress and ultimate tensile strength

In this section, the variation of 0.2% proof stress and the ultimate tensile strength of the UHSS specimens during the cooling phase of a fire are discussed. The strength variation factors are defined by

$$R_{u,CT} = \frac{f_{u,CT}}{f_{u,RT}} \tag{2-2}$$

$$R_{p,CT} = \frac{f_{0.2,CT}}{f_{0.2,RT}} \tag{2-3}$$

where $f_{u,CT}$ and $f_{0.2,CT}$ denote the ultimate tensile strength and the 0.2% proof stress of UHSS specimens when they are cooled from temperature T to room temperature, respectively, while $f_{u,RT}$ and $f_{0.2,RT}$ represent the corresponding values for ultimate tensile strength and 0.2% proof stress of the virgin material at room temperature, respectively. The variations of $R_{u,CT}$ and $R_{p,CT}$ for fire temperatures of up to 600°C are presented in Table 2-2. It can be seen that for specimens having experienced temperatures up to 300°C, the strength of material is almost unchanged when cooled to the room temperature. However, for specimens exposed to fire temperatures of 450°C and 600°C only 90% and 70% of the strength is regained, respectively.

The strength variation factors are also calculated for specimens taken from the strips at opposite face (180^0) to the weld line of UHSS tubes (Figure 2-2). Although the values of $f_{u,CT}$, $f_{0.2,CT}$, $f_{u,RT}$ and $f_{0.2,RT}$ for UHSS specimens taken from 180^0 strip are higher than those taken from 90^0 strip, no difference in the values of variation factors ($R_{u,CT}$ and $R_{p,CT}$) of 180^0 strips with those obtained for 90^0 strips is observed.

Table 2-2. Variation of strength after cooling down from various fire temperatures

Temperature	150°C	300°C	450°C	600°C
$R_{u,CT}$	1.04	1.03	0.90	0.70
$R_{p,CT}$	1.09	1.00	0.94	0.68

2.3.1.3. Ductility and energy absorption

The energy absorption, or strain energy U^*, is the total mechanical energy per unit volume absorbed by the material in straining it to a given value of strain, ε, and is expressed by Eq. (2-4) [31] such that

$$U^* = \int_0^{\varepsilon} \sigma \, d\varepsilon \tag{2-4}$$

in which σ is stress. In this study, the energy absorbed in the material up to the onset of necking is considered so that the upper bound of the integral in Eq.(2-4) takes the value of the strain at ultimate tensile strength ε_u. The variation of energy absorption is quantified by normalizing the values of U^* with respect to that for the virgin material:

$$E_{CT} = \frac{U^*_{CT}}{U^*_{RT}} \tag{2-5}$$

in which U^*_{CT} is the strain energy for UHSS specimens tested at room temperature when they are cooled down from temperature T and U^*_{RT} is the strain energy for the virgin specimens tested in room temperature.

Another parameter indicating the ductility of a material is the ratio of the strain at ultimate tensile strength to the total strain at 0.2% proof stress ($\mu = \frac{\varepsilon_u}{\varepsilon_y}$). Similar to the strain energy, the variations of μ can be determined from

$$D_{CT} = \frac{\mu_{CT}}{\mu_{RT}} \tag{2-6}$$

where the CT and RT indices correspond to the μ values for UHSS specimen tested at room temperature after cooling from temperature T and that of virgin material tested at room temperature, respectively.

Table 2-3 presents the results for ductility factors (E_{CT} and D_{CT}), defined by Eqs. (2-5) and (2-6). It can be seen from this table that for UHSS specimens cooled down from a higher temperature, both ductility factors show an increasing tendency.

Table 2-3. Variation of ductility factors after cooling down from various fire temperatures

Temperature	**150**℃	**300**℃	**450**℃	**600**℃
E_{CT}	0.842	1.090	1.129	1.924
D_{CT}	0.788	1.063	1.234	3.197

2.3.2. Effect of Steel Grade on the Mechanical Properties

The mechanical behaviour of the steel material depends on the steel microstructure and the most important determinants of the microstructure are the alloy chemical composition and the manufacturing process. In this study, in order to investigate the effect of steel grade on the mechanical behaviour during the cooling stage of a fire, tensile coupons are taken from 3 different grades of steel tube, namely Grade 1200 (UHSS), Grade 800 (HSS) and Grade 350 (MS). Tensile tests were performed at room temperature, at fire temperature of 600°C and also after being cooled from 600°C to room temperature. The stress-strain curves of MS, HSS and UHSS for the different tests are illustrated in Figures 2-7 to 2-9. It can be seen from Figures 2-7 and 2-8 that no obvious strength reduction is observed when the MS and HSS specimens are cooled from 600°C. However, as discussed in the previous sections, a 30% reduction is observed for the corresponding UHSS specimens. Nevertheless, the residual strength of UHSS is still considerably higher than the MS strength at room temperature and is almost equal to that of HSS.

It may be seen from Figure 2-8 that a more pronounced upper and lower yield points occur in the MS-C600 and HSS-C600 steels after cooling from 600°C (Figure 2-8), than in the as received material (Figure 2-7) despite the strengths not being so different. The reason behind the occurrence of these yield points after exposure to 600°C is that the elevated temperature provides sufficient mobility to the carbon (C) atoms that they can segregate to dislocations at elevated temperatures and pin the dislocations. When a stress is then applied to the specimen at room temperature, it needs to first unpin the dislocations from the segregated C atoms before yielding may occur. Once the dislocations start to move, a lower stress is required to keep them moving. Therefore, the stress drops a little after deformation begins which results in the lower yield point in the stress-strain curve. However, in order to experimentally observe a lower yield point, the stress required to unpin the dislocation from the C segregation must be higher than the stress required to propagate the dislocation through the microstructure. In the case of Mild steel (MS), which is not very strong, the stress to unpin is significantly higher than the stress required to propagate the dislocations and thus a clear sharp yield point can be observed. For high strength steel (HSS), the stress required to propagate the dislocations through the microstructure and cause deformation is much higher than in MS; however this stress is still less than the stress required to unpin dislocations from

the segregated C. Therefore, the difference between the upper and lower yield points of HSS-C600 is not as obvious as that for the MS-C600. For the ultra-high strength steel (UHSS), the stress required to push dislocations through the microstructure is still expected to be higher than that required to unpin dislocations from segregated C, even after the changes taken place at 600°C. Therefore, no distinct yield point is observed at UHSS-C600.

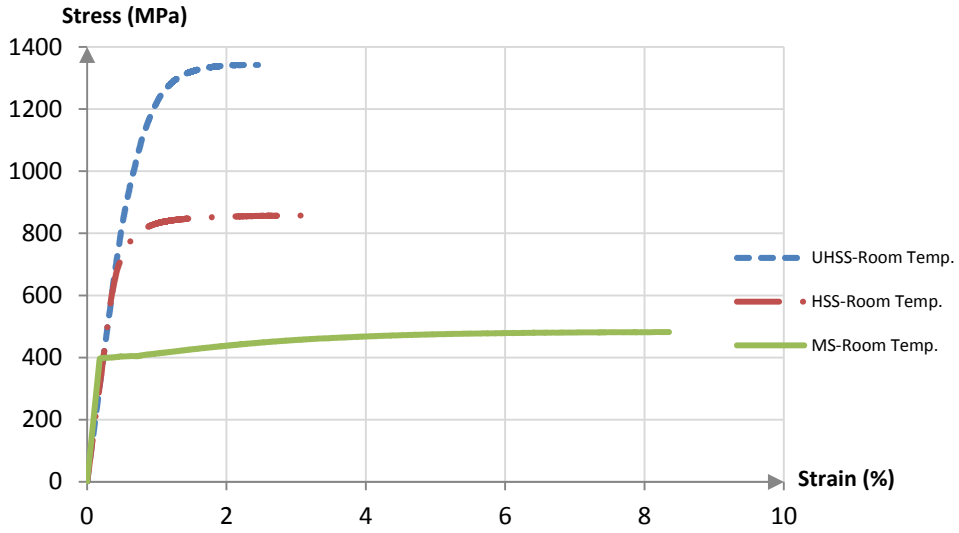

Figure 2-7. Stress-strain curves for different steel specimens at room temperature

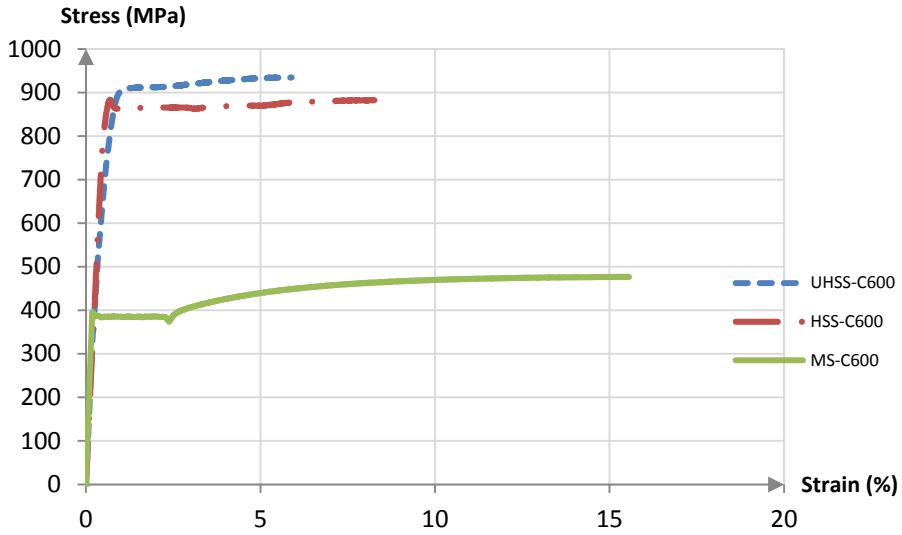

Figure 2-8. Stress-strain curves for different steel specimens cooled down from 600°C temperature

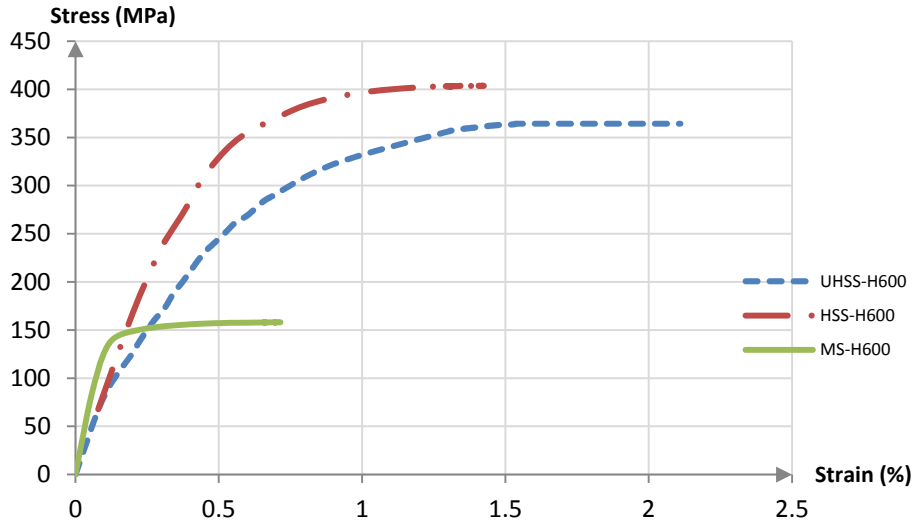

Figure 2-9. Stress-strain curves for different steel specimens heated up to 600°C temperature

2.3.3. Effect of Cooling Rate on the Mechanical Properties

In order to investigate the effect of cooling rate from the simulated fire temperatures on the mechanical properties of the UHSS tube specimens subjected to cooling stage of a fire, three different cooling rates were considered, and all other parameters are kept unchanged. In all the tests discussed in previous sections, the specimens were cooled simply by turning off the heating chamber connected to the Instron. In this section, in order to consider different cooling rates including r=10°C/min and r=20°C/min, liquid Nitrogen (LN) is injected into the chamber to control the speed of cooling (Figure 2-10).

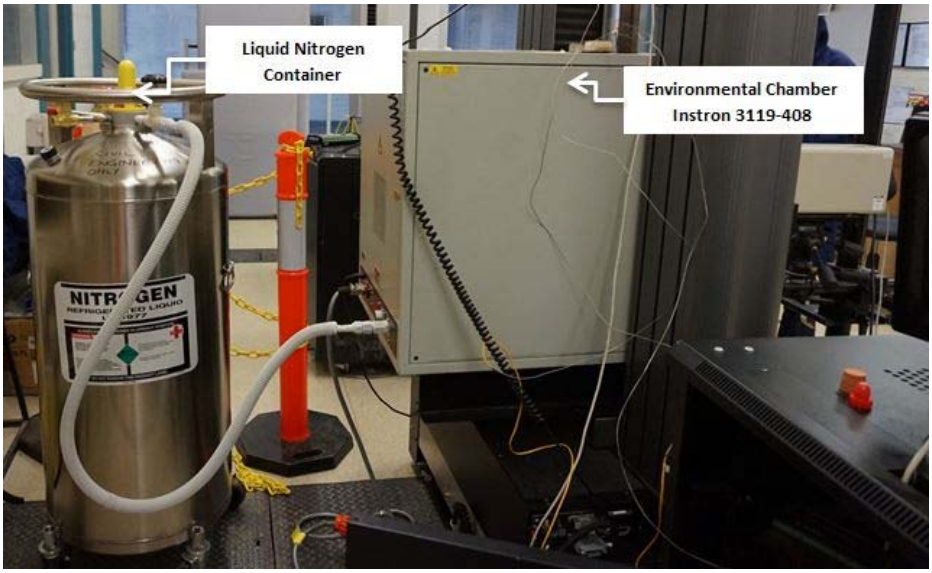

Figure 2-10. Test setup to study the effect of cooling rate on mechanical properties

The time-temperature curves recorded from the thermocouples attached to the middle of the UHSS specimen, i.e. T_2, are shown in Figure 2-11. Note that in this figure, the UHSS-C600 curve refers to the test in which the specimen is cooled down by turning off the chamber, and the UHSS-C600-r10 and UHSS-C600-r20 curves are related to the tests where the specimens are cooled down with cooling rates of 10°C/min and 20°C/min, respectively. The room temperature stress-strain curves for UHSS specimens subjected to the different time-temperature curves are shown in Figure 2-12. It can be observed that the curves for the three tests with different cooling rates are essentially the same, meaning that the mechanical properties of UHSS are not affected by the cooling rate in the range of cooling rates explored in this study.

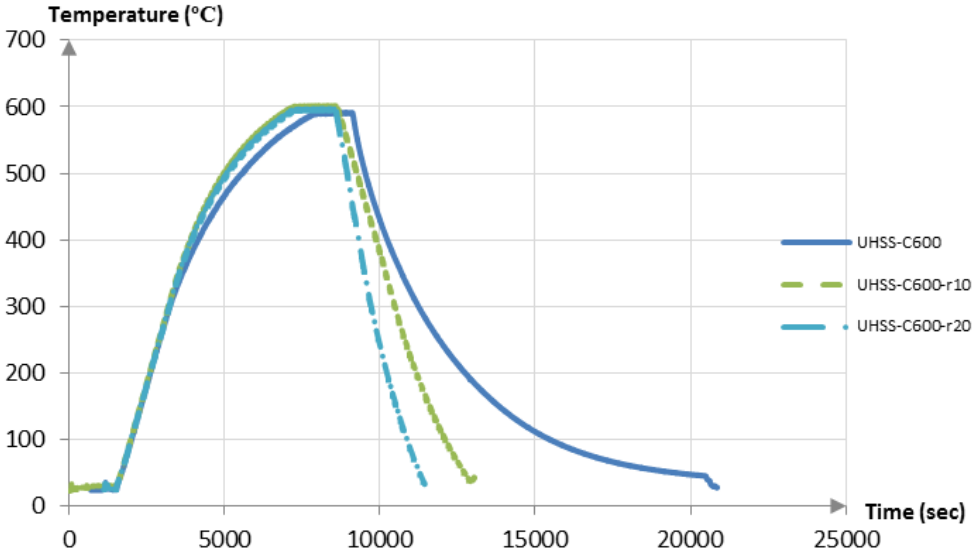

Figure 2-11. Time-temperature curves for UHSS specimens cooled down from 600°C with different cooling rates

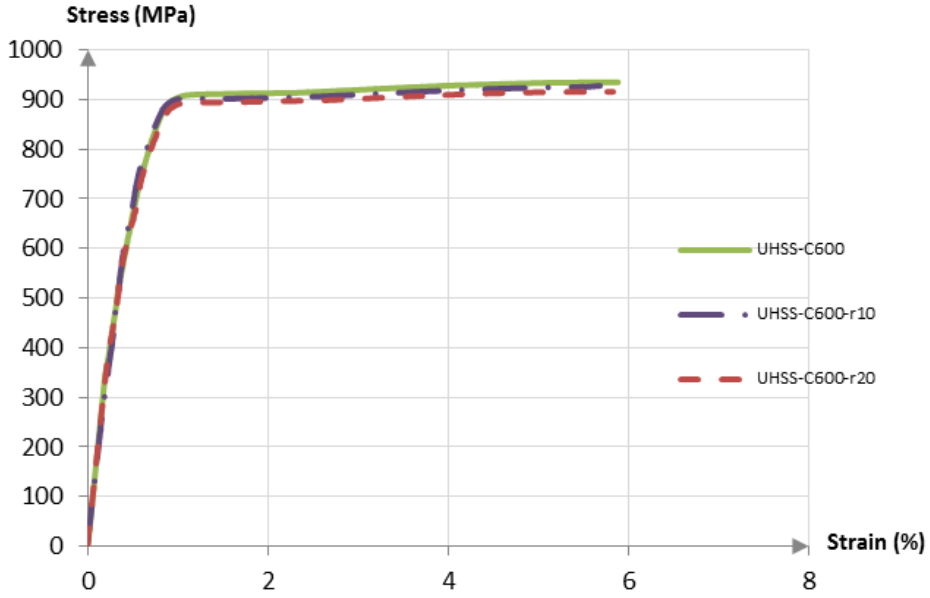

Figure 2-12. Stress-strain curves for UHSS specimens cooled down from 600°C with different cooling rates

2.4. Microstructure evaluation

The mechanical response of the different steels considered in this work is controlled by the microstructure. The effect on the room temperature mechanical properties from exposing the steels to simulated fire temperatures, depends on the effect of this elevated temperature exposure on the microstructure, and the dominant microstructural features that give the alloy its strength. To provide some insight in the effect of the simulated fire exposure on the resulting room temperature strength, the microstructures of each of the Mild Steel (MS), high strength steel (HSS) and ultra-high strength steel (UHSS) are examined before and after simulated fire exposure at 600°C.

Figure 2-13 shows optical micrographs obtained from the bulk microstructure of the MS specimen both in its original state (Figure 2-13a) and after being cooled from 600°C (Figure 2-13b). This is a typical ferritic microstructure of a low carbon steel [32]. The white regions are the ferrite grains delineated by black lines which represent the boundaries between the different grains. Some small black regions can also be observed and these represent a very small volume fraction of pearlite (consisting of a composite of ferrite and cementite). Since the MS alloy has very low carbon content, the microstructure is almost 100% polycrystalline ferrite and only a very small amount of the dark pearlite regions can be seen. The dominant mechanism controlling the strength of such Mild steels is 'grainsize strengthening' [32]. The strength is controlled by the size of ferrite grains and small grains lead to higher strengths. By comparing Figure 2-13a and b, it can be noticed that the ferrite grain size in the sample cooled from 600°C is slightly bigger than that of the as-received state. Since the grainsize in the as-received state is already around 8-10 microns, the increase to around 10-15 microns after heating does not lead to a very large effect on the yield strength of the steel. The expected change in strength from such a change in grain size can be estimated using the Hall-Petch law [33]: $\Delta\sigma = k\left(d_1^{-1/2} - d_2^{-1/2}\right)$, where k is the Hall-Petch coefficienct (0.74 MPa $m^{1/2}$) for Mild Steel [32], and d_1 and d_2 are the ferrite grainsizes before and after elevated temperature exposure. Using these numbers one obtains a predicted change in strength of only, $\Delta\sigma$=30MPa. This is a small value compared with the yield strength of the MS of ~400MPa and this is why the strength of MS is almost totally recovered after being cooled from 600°C to room temperature. The reason the ferrite grain size increases after holding at

600ºC is that the grain boundaries separating the individual ferrite grains (Figure 2-13) are thermodynamic defects and if the system is provided with sufficient thermal energy, the ferrite grains will grow so as to decrease the total area of grain boundaries per unit volume [34, 35]. This is a thermally activated process and occurs faster at higher temperatures. In this case, the ferrite grain growth is sufficiently slow at 600ºC, that a large effect on the strength is not observed. Holding the Mild steel for longer times at 600ºC, or at higher temperatures will lead to a greater reduction in strength as a result of further ferrite grain growth.

The microstructures of the HSS and UHSS are much finer than those of the MS and as a result, SEM was required to resolve them. In Figures 2-14 and 2-15, the SEM micrographs obtained from the bulk microstructures of the as-received HSS and UHSS specimens and those cooled from 600°C to room temperature are shown, respectively. In the SEM images shown in Figure 2-14, the dark regions are the ferrite grains and the brighter regions contain cementite (i.e. the same phases that are present in the Mild steel are also present in the HSS but they are distributed differently and also present with much smaller sizes). Looking at the images obtained from HSS bulk microstructure (Figure 2-14), it can be observed that the ferrite grain size is just slightly larger in the sample cooled from 600ºC to room temperature. This could lead to a decrease in the strength of HSS specimens after exposure at 600°C but like the Mild steel previously discussed, the change in grain size is small and it does not lead to a large change in the strength. However, holding for longer times at 600°C or at higher temperatures will definitely lead to a reduction in the residual strength of HSS after elevated temperature exposure.

The microstructures of the UHSS shown in Figure 2-15 are very different to those of the MS and HSS. These are typical martensitic microstructures [36]. Martensite is a non-equilibrium phase that is related to the ferrite in the Mild and HS steels except that it is much stronger, but also brittle. During the UHSS manufacturing process, in order to improve the ductility of the martensite so that it can be used for engineering applications, either in one stage or several stages, it is 'tempered' at specific temperatures. This results in the conversion of parts of the martensite to ferrite containing very small particles of cementite (these appear as white spots in Figure 2-15). The objective of the temperature treatment during processing is to retain as much of the strength as possible but to provide the alloy with some more ductility. When a UHSS specimen is heated to elevated

temperatures, if the fire temperature is in the 'tempering temperature range of martensite', the tempering process will continue and the strength will continue to be reduced. Unlike the cases for the MS and HSS where the evolution of the strength as a result of elevated temperature exposure is controlled by the kinetics of ferrite grain growth (which is relatively slow), the kinetics of tempering are controlled by C diffusion, which is extremely fast, and as a consequence the changes in the strength of the UHSS occur very quickly [37]. In Figure 2-15, it can be noticed that the 'lath' structure is greatly decreased after heating up to 600°C and the small white cementite particles in these images are more numerous and slightly larger in the alloy cooled from 600°C, meaning that more C has been removed from the solution making the martensite softer. This is the reason for the significant reduction in the strength of the UHSS after exposure at 600°C. Holding for longer times at 600°C, or at higher temperatures will result in a greater strength reduction.

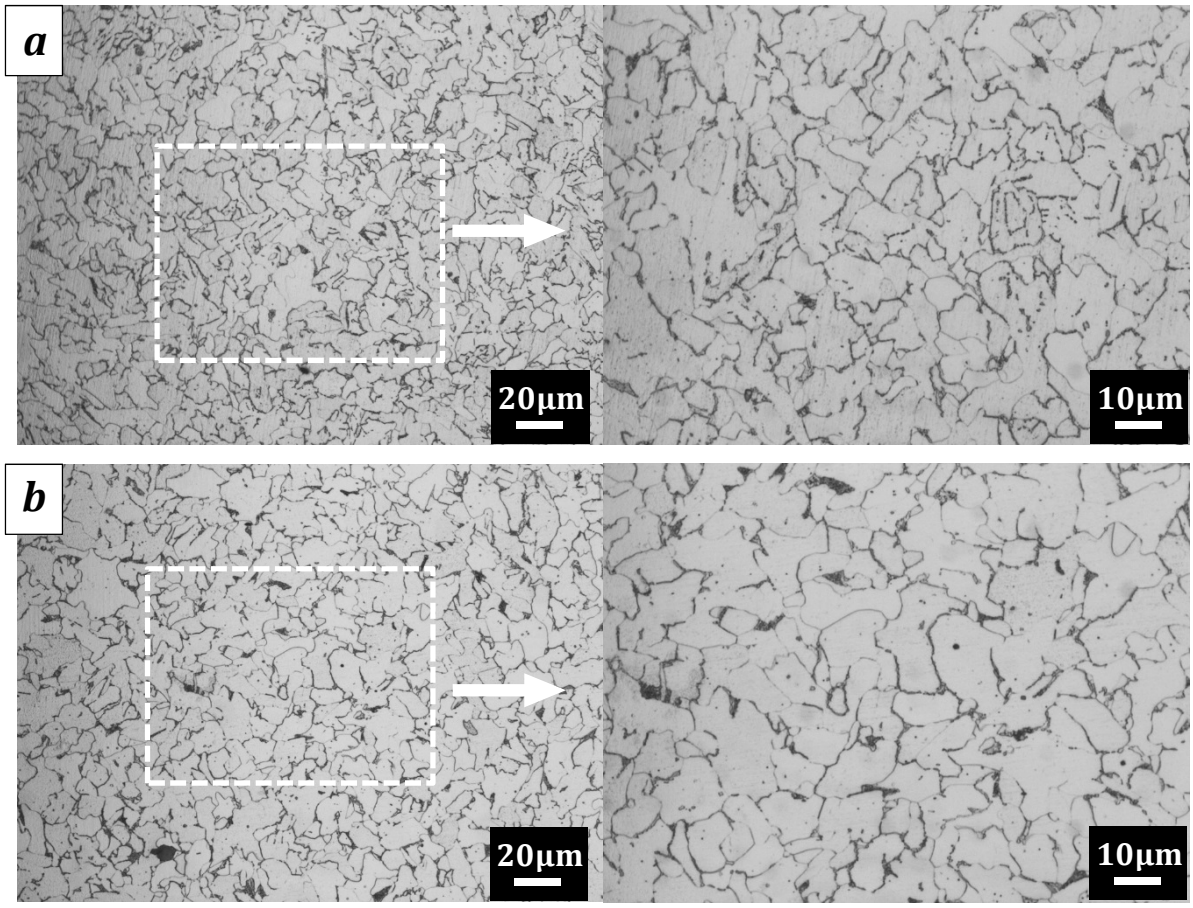

Figure 2-13. Optical micrographs of virgin MS specimens at (a) room temperature and (b) after cooled down from 600°C to the room temperature

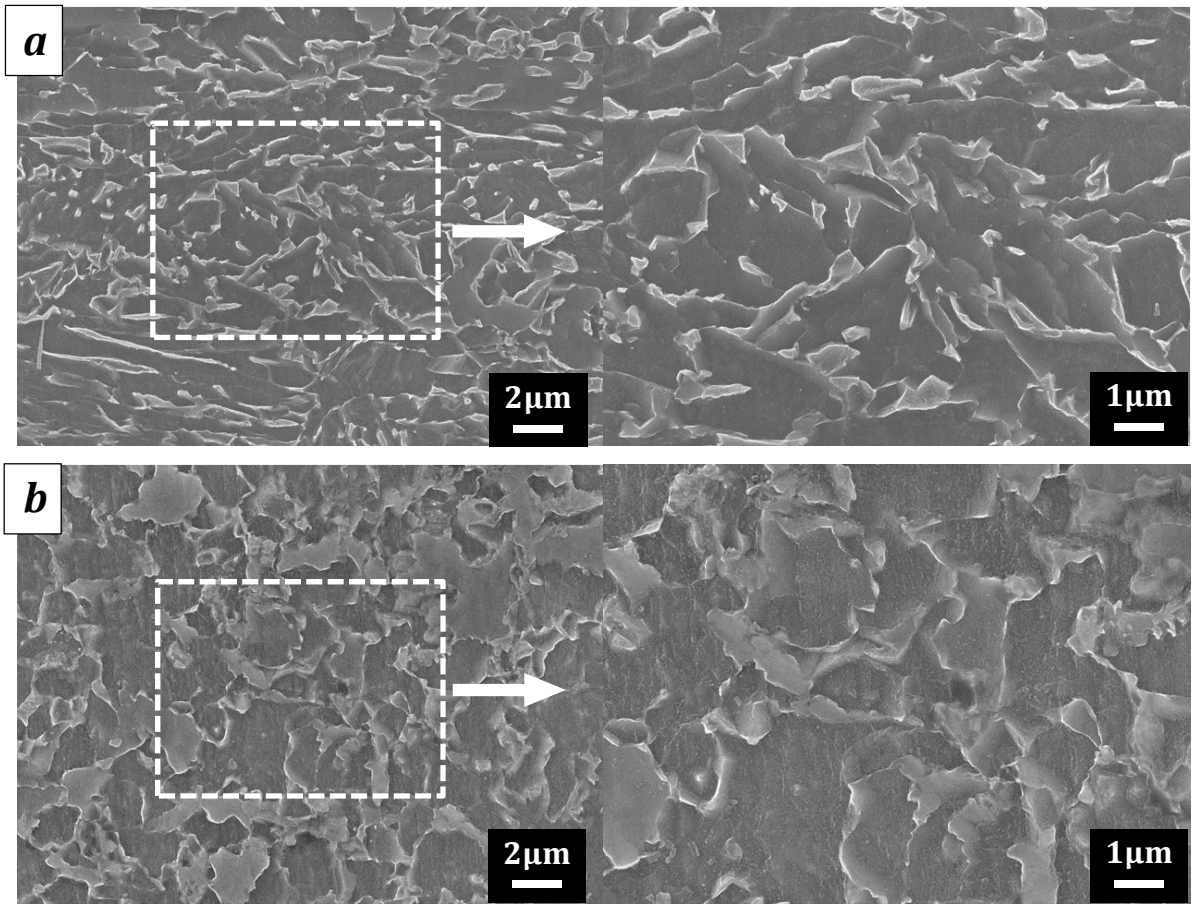

Figure 2-14. SEM images of virgin HSS specimens at (a) room temperature and (b) after cooled down from 600°C to the room temperature

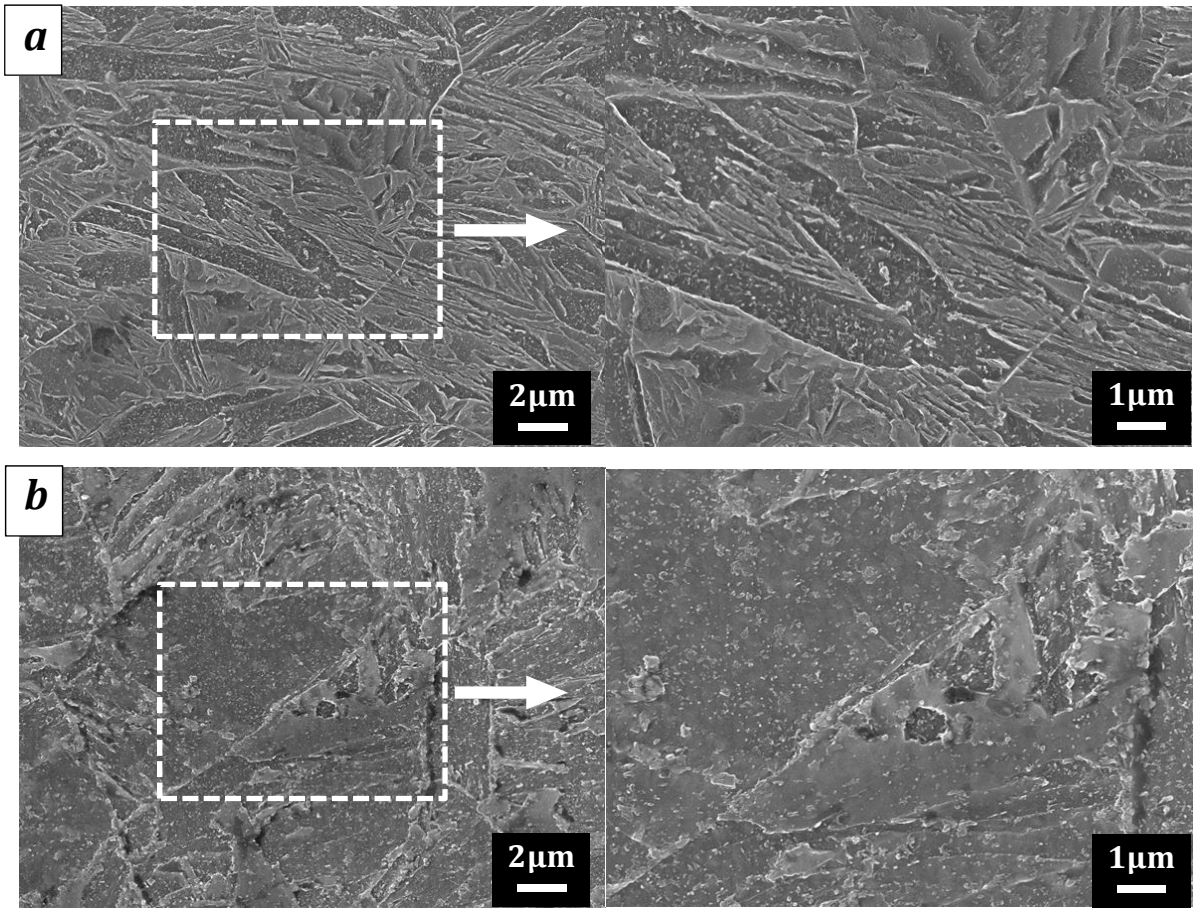

Figure 2-15. SEM images of virgin UHSS specimens at (a) room temperature and (b) after cooled down from 600°C to the room temperature

A key point should be made regarding the exposure of these steels to elevated temperatures and the effects this has on the microstructures and the resulting strength after cooling to room temperature from simulated fire conditions. In each of the cases discussed above, the phases or features contained within the microstructures (ferrite and cementite – martensite is a form of ferrite) did not change in identity and only their sizes changed. These changes can be predicted for arbitrary thermal exposures and hence the effect on the strength can be described using tools developed in the field of Materials Science and Engineering. However, this is only true whilst the phases present in the microstructure remain the same and this is not true if the thermal exposure of the alloy exceeds a certain temperature.

Figure 2-16 contains calculated plots of the thermodynamic stability of the ferrite and cementite phases in each of the alloy chemistries considered in this study. These plots

have been calculated using computational thermodynamics using the program Thermo-Calc [38] and the most up to date steel database, TCFe7.

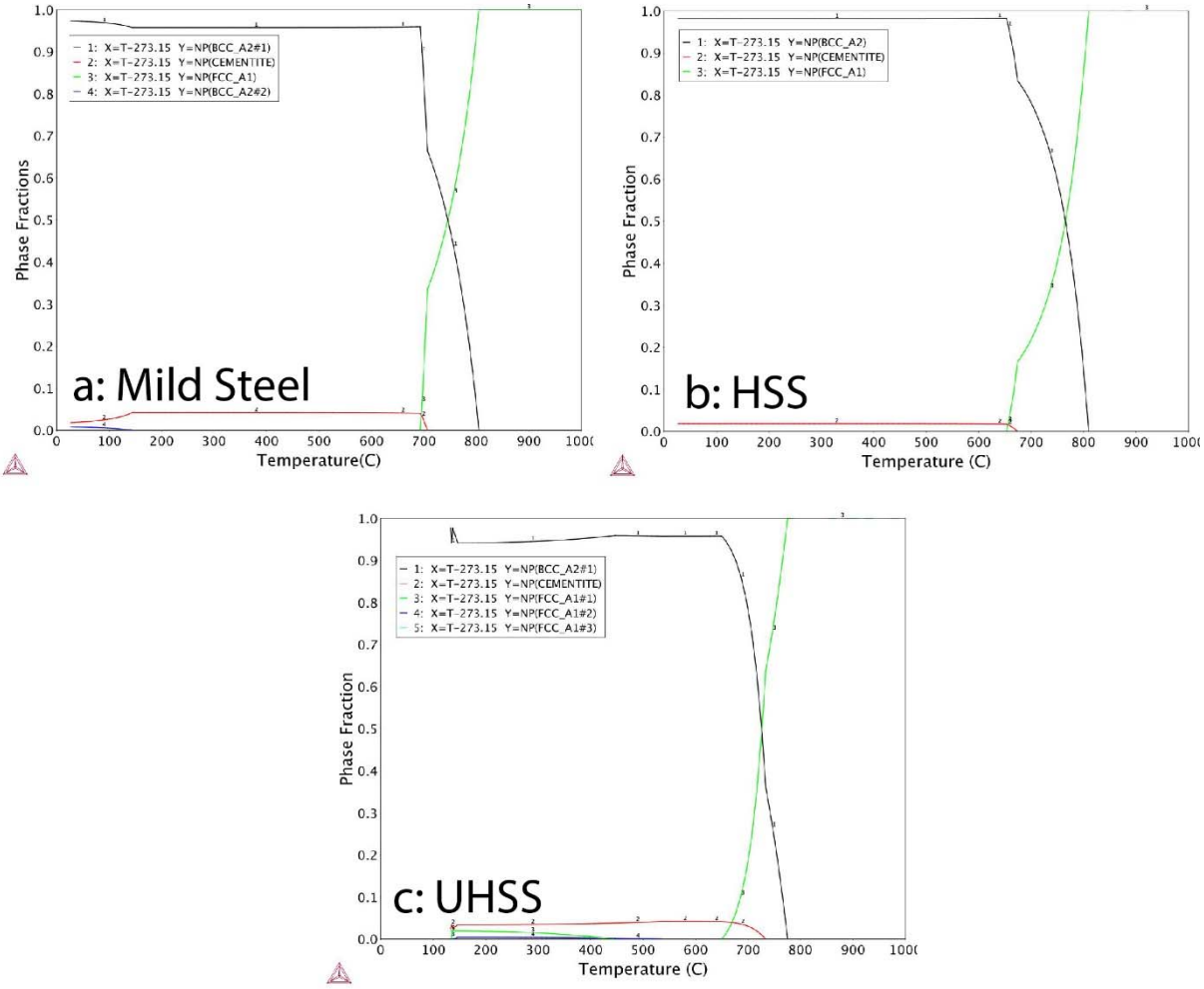

Figure 2-16. Calculated plots of the thermal stability of ferrite (BCC), cementite and austenite (FCC) in each of the alloy chemistries considered in this study as a function of temperature using the software package, Thermo-Calc.

In each case, one may notice that the phases present at temperatures up to 600ºC are ferrite and cementite, consistent with the experimental observations of microstructure made above. However, continued heating to temperatures above 700ºC for the Mild steel, and ~650ºC for the HSS and UHSS would lead to the formation of a new phase, austenite. Exposure to temperatures above 800ºC leads to a 100% austenite microstructure. Subsequent cooling from these high temperatures will lead to the austenite transforming back into ferrite and cementite but it will not create the nice, well controlled microstructures that are generated by controlled cooling in the manufacturing process to

give the initial properties of the as-received materials. One may expect a substantial deterioration in the mechanical properties of materials cooled from temperatures above ~800°C for these alloy compositions and the resulting properties will be a strong function of the cooling rate.

From a metallurgical point of view, one should separate the effects of simulated fire exposures on the strengths of steel into two classes: low temperature class, where the maximum temperature reached does not lead to changes in the identities of the phases in the microstructures, and a high temperature class where austenite is formed. Predictions of the evolution of the strength in the low temperature class can be made from Materials Science and Engineering, but the residual mechanical properties in the high temperature class depend mostly on the cooling rate and are more difficult to predict. Of course, the separation between the low temperature and high temperature class is alloy composition specific.

2.5. Conclusion

In this paper, an experimental study was performed to examine the mechanical properties of ultra-high strength steel (UHSS) tubes during the cooling phase of a fire. According to the experiments, the strength of UHSS tube specimens after being cooled to room temperature from fire temperatures of 450°C and 600°C, was considerably reduced. This behaviour is not consistent with the models previously proposed for stress-strain curves of Mild steel when cooling from elevated temperatures. Therefore, new models must be introduced to take into account the strength reduction of UHSS in the cooling phase of fire. The ductility of UHSS tube specimens cooled from elevated temperatures was also examined. The results indicate that the higher temperature the specimens have experienced, the more ductility is recovered. Furthermore, the results for the UHSS tube specimens were compared to those obtained for Mild steel (MS) and high strength steel (HSS) tube specimens. It was shown that contrary to UHSS, MS and HSS do not experience significant strength reduction after being cooled from fire temperatures of up to 600°C. In addition, it was concluded that the cooling rate of fire has no significant effect on mechanical properties of UHSS specimens cooled from fire temperatures of up to 600°C. To elaborate deeper into the changes occurred in the mechanical properties of MS, HSS and UHSS tube specimens subjected to cooling phase of a fire, micrographs from the bulk

microstructure of these materials both in their original sate and after being cooled from 600ºC were obtained and the microstructural reason for the resulted strength of specimens subjected to cooling phase of fire was explained. An attempt has been made to emphasise that in considerations of the effect of elevated temperature exposures on the residual strengths of steels, one should consider two regimes of behaviour depending on the maximum temperature reached. The effect of the temperature on the steel microstructure (and hence the residual mechanical properties) is very different in the two regimes: in the low temperature regime (up to ~650-700ºC for the steels examined in this study), the changes in strength depend strongly on the maximum temperature reached and also (but less strongly) on the time at elevated temperature, but are relatively insensitive to the cooling rate. In the high temperature regime, the time and maximum temperature reached are relatively unimportant (so long as the temperature is above the limit separating the high and low temperature regimes) and the residual steel strength will depend strongly on the cooling rate from elevated temperature.

Acknowledgement

The research work presented in this paper was supported by the Australian Government-Department of Education and also by Australian Research Council through a Discovery Project (DP130100181) awarded to the second and third authors. The authors would like to thank the Monash Civil Engineering Workshop staff for their support in fabricating the tests specimens. The authors acknowledge the use of facilities at Monash Centre for Electron Microscopy. We also thank SSAB Corporation for providing ultra-high strength and high strength steel tubes.

References

[1] K. Osawa, T. Shimomura, M. Kinoshita, K. Matsudo, K. Iwase, Development of high-strength cold-rolled steel sheets for automotive use by continuous annealing, SAE Technical Papers, (1983).
[2] C. Cazes, F. Ronin, Use of HSS1, VHSS2 and UHSS3 steels in the body in white: A panorama of the latest European vehicles, state of art and perspectives, SAE Technical Papers, (2002).
[3] T. Nonaka, H. Taniguchi, K. Goto, K. Yamazaki, Development of ultra-high-strength cold-rolled steel sheets for automotive use, Nippon Steel Technical Report, (2003) 13-15.
[4] Y. Mukai, Development of new high-strength steel sheets for automobiles, R and D: Research and Development Kobe Steel Engineering Reports, 55 (2005) 30-35.
[5] M. Aratani, Y. Ishiguro, Y. Hashimoto, S. Toyoda, H. Kimura, O. Sonobe, M. Gunji, Development of UTS 980 MPa grade steel tube with excellent formability for automotive body parts, in: Lecture Notes in Electrical Engineering, 2013, pp. 213-224.
[6] M.A. Bradford, H. Ban, Buckling of high-strength steel beams, in: European conference on steel and composite structures (Eurosteel 2014), Naples, Italy, 2014.
[7] V.L. Hoang, J.P. Jaspart, J.F. Demonceau, Circular tube columns in high strength steel: Economical solutions for building frames, in: Proceeding of the 7th European conference on steel and composite structures (Eurosteel 2014), Naples, Italy, 2014.
[8] F. Javidan, A. Heidarpour, X.L. Zhao, J. Minkkinen, Compressive Behavior of Innovative Hollow Long Fabricated Columns with High Strength and Ultra-High Strength tubes, in: 15th International Symposium on Tubular Structures, Rio de Janeiro, Brazil., 2015.
[9] M. Nassirnia, A. Heidarpour, X.L. Zhao, J. Minkkinen, Innovative Corrugated Hollow Columns utilizing Ultra High Strength Steel Tubes, in: 15th International Symposium on Tubular Structures, Rio de Janeiro, Brazil., 2015.
[10] F. Javidan, A. Heidarpour, X.L. Zhao, J. Minkkinen, Performance of innovative fabricated long hollow columns under axial compression, Journal of Constructional Steel Research, 106 (2015) 99-109.
[11] M. Mirmomeni, A. Heidarpour, X.L. Zhao, C.R. Hutchinson, J.A. Packer, C. Wu, Mechanical properties of partially damaged structural steel induced by high strain rate loading at elevated temperatures - An experimental investigation, International Journal of Impact Engineering, 76 (2014) 178-188.
[12] S. Sinaie, A. Heidarpour, X.L. Zhao, Stress-strain-temperature relation for cyclically-damaged structural mild steel, Engineering Structures, 77 (2014) 84-94.
[13] S. Sinaie, A. Heidarpour, X.L. Zhao, A multi-objective optimization approach to the parameter determination of constitutive plasticity models for the simulation of multi-phase load histories, Computers and Structures, 138 (2014) 112-132.
[14] S. Sinaie, A. Heidarpour, X.L. Zhao, Mechanical properties of cyclically-damaged structural mild steel at elevated temperatures, Construction and Building Materials, 52 (2014) 465-472.
[15] Q.Y. Song, A. Heidarpour, X.L. Zhao, L.H. Han, Performance of Unstiffened Welded Steel I-Beam to Hollow Tubular Column Connections Under Seismic Loading, International Journal of Structural Stability and Dynamics, (2014).
[16] S. Hosseini, A. Heidarpour, F. Collins, C.R. Hutchinson, Effect of strain ageing on the mechanical properties of partially damaged structural mild steel, Construction and Building Materials, 77 (2015) 83-93.

[17] A. Heidarpour, S. Cevro, Q.Y. Song, X.L. Zhao, Behaviour of stub columns utilising mild-steel plates and VHS tubes under fire, Journal of Constructional Steel Research, 95 (2014) 220-229.
[18] A. Heidarpour, An innovation beam-column element for nonlinear analysis of steel members under cooling phase of a fire, in: European conference on steel and composite structures (Eurosteel 2014), Naples, Italy.
[19] J.A. El-Rimawi, I.W. Burgess, R.J. Plank, The treatment of strain reversal in structural members during the cooling phase of a fire, Journal of Constructional Steel Research, 37 (1996) 115-135.
[20] C.G. Bailey, I.W. Burgess, R.J. Plank, Computer simulation of a full-scale structural fire test, Structural Engineer, 74 (1996) 93-100.
[21] P. Wang, G. Li, S. Guo, Effects of the cooling phase of a fire on steel structures, Fire Safety Journal, 43 (2008) 451-458.
[22] J. Outinen, Mechanical properties of structural steel at elevated temperatures and after cooling down, in: 10th International Conference - Fire and Materials 2007.
[23] X. Qiang, F.S.K. Bijlaard, H. Kolstein, R. Xia, Experimental study on high strength structural steel S460 in fire and after cooling down, IES Journal Part A: Civil and Structural Engineering, 6 (2013) 104-111.
[24] X. Qiang, F.S.K. Bijlaard, H. Kolstein, Post-fire performance of very high strength steel S960, Journal of Constructional Steel Research, 80 (2013) 235-242.
[25] F. Hanus, G. Zilli, J.M. Franssen, Experimental investigations and analytical model for the behavior of grade 8.8 bolts and butt welds under heating and subsequent cooling, in: Structures in Fire - Proceedings of the Sixth International Conference, SiF'10, 2010, pp. 638-645.
[26] A. Heidarpour, N.S. Tofts, A.H. Korayem, X.L. Zhao, C.R. Hutchinson, Mechanical properties of very high strength steel at elevated temperatures, Fire Safety Journal, 64 (2014) 27-35.
[27] ASTM Standard E8/E8M, in: Standard Test Methods for Tension Testing of Methallic Materials, ASTM International, West Conshohocken, PA: USA, 2011.
[28] American Institution of Steel Construction (AISC), Specification for Structural Steel Buildings, ANSI/AISC, in, Chicago, 2010.
[29] Australian Standard AS2291, in: Metallic materials—Tensile testing at elevated temperatures, Standards Australia, GPO Box 476, Sydney, NSW 2001, Australia, 2007.
[30] H.J. Frost, M.F. Ashby, Chapter 5-The B.C.C. transition metals: W, V, Cr, Nb, Mo, Ta and α-Fe in: Deformation-mechanism maps : the plasticity and creep of metals and ceramics, Pergamon Press, Oxford [Oxfordshire]; New York, 1982, pp. 30-42.
[31] D. Roylance, Stress-strain curves, Massachusetts Institute of Technology study, Cambridge, (2001).
[32] H.K.D.H. Bhadeshia, S.R. Honeycombe, Chapter 2 - The Strengthening of Iron and its Alloys, in: H.K.D.H.B.R. Honeycombe (Ed.) Steels (Third Edition)-Microstructure and Properties, Butterworth-Heinemann, Oxford, 2006, pp. 17-38.
[33] W.D. Callister, Fundamentals of Materials Science and Engineering (Second Edition).
[34] R.D.D. J. W. Martin, B. Cantor, Chapter 5-Microstructural instability due to interfaces, in: Stability of microstructure in metallic systems (Second Edition), Cambridge University Press, 1997.
[35] F.J. Humphreys, M. Hatherly, Chapter 11 - Grain Growth Following Recrystallization, in: F.J.H. Hatherly (Ed.) Recrystallization and Related Annealing Phenomena (Second Edition), Elsevier, Oxford, 2004, pp. 333-378.

[36] H.K.D.H. Bhadeshia, S.R. Honeycombe, Chapter 5 - Formation of Martensite, in: H.K.D.H.B.R. Honeycombe (Ed.) Steels (Third Edition)-Microstructure and Properties, Butterworth-Heinemann, Oxford, 2006, pp. 95-128.
[37] H.K.D.H. Bhadeshia, S.R. Honeycombe, Chapter 9 - The Tempering of Martensite, in: H.K.D.H.B.R. Honeycombe (Ed.) Steels (Third Edition)-Microstructure and Properties, Butterworth-Heinemann, Oxford, 2006, pp. 183-208.
[38] Thermo-Calc Software. [ONLINE] Available at: http://www.thermocalc.com/contact-us/thermo-calc-offices/, in, Foundation of Computational Thermodynamics, 1995.

Chapter 3

Post-fire mechanical response of ultra-high strength (Grade 1200) steel under high temperatures: linking thermal stability and microstructure

This chapter has been published in the Journal of *Thin-Walled Structures*, Volume 119, October 2017, Pages 114-125.

DOI: 10.1016/j.tws.2017.05.030

Reprinted here with the Author Rights granted by Elsevier.

Table of Contents

Abstract

Recently, ultra-high strength steel (UHSS) tubes with nominal yield strengths of up to 1200 MPa have attracted attention for applications in engineering fields. While many studies have focused on the mechanical behaviour of mild carbon steel at elevated temperatures, there is a scarcity of data for the in-fire and post-fire mechanical response of the UHSS material. In this study, the tensile mechanical properties of the UHSS tube under fire and after cooling from fire temperatures of up to 800°C to room temperature are studied. The stress-strain curves, strength and ductility of the UHSS material are discussed. It is shown that the in-fire strength of the UHSS tube starts to deteriorate when the specimens are exposed to fire temperatures above 300°C and is almost dis-appeared when tested at 800°C. There is also a major reduction in the strength of the UHSS tube specimens cooled from fire temperatures above 470°C to room temperature. To investigate the effect of steel grade on the in-fire and post fire mechanical behaviour of steel materials, the stress-strain curves of Grade 800 high strength steel (HSS) tube specimens are presented and compared with those obtained for Grade 1200 UHSS tube. In order to interpret the experimental results, microstructural examination on the UHSS is conducted using optical and scanning electron microscopy (SEM). The plots of the thermodynamic stability of the ferrite and cementite phases in the UHSS and HSS are calculated and the phase changes occurring during each fire temperature exposure are discussed. Based on the results obtained from experimental tests, an empirical constitutive model which takes into account the post-fire behaviour of UHSS material is developed. The constitutive model can be implemented into commercial finite element packages to carry out a rational thermal analysis and perform fire safety design and evaluation.

Key Words: ultra-high strength steel; fire; cooling; stress-strain curve; micrograph; empirical model

3.1. Introduction

In recent years, ultra-high strength structural steels (UHSS) have been offered by steel manufacturing companies. Due to the high specific strength of these materials, their application in the automotive industry has been increasing to reduce the weight of automobiles [1-3]. Recent research conducted on UHSS indicates that this type of steel has also a great potential to be introduced as a structural material in civil engineering applications [4-10]. Using UHSS in structural engineering can lead to savings in engineering work, labour and transport costs since lighter lifting equipment and fewer people may be needed at the construction site. Moreover, UHSS may enable the structures to be constructed considerably lighter than usual. Although UHSS with nominal yield strength of 1200 MPa has promising properties for civil engineering applications, there is still lack of knowledge about the behaviour of this material under extreme structural loadings such as fire, earthquake, impact and blast. Fire is considered to be one of the severe hazards which may occur individually, or followed by another extreme action [11-15], and can significantly damage the structure during its service life. In order to perform a rational analysis on the steel structural members made of UHSS subjected to fire temperatures, understanding their constitutive material behaviour after exposure to elevated temperatures is necessary.

A number of researchers have focused on the in-fire and post-fire mechanical behaviour of structural steels [7, 16-22]. Outinen [18] investigated the in-fire and post-fire mechanical properties of S355 cold-formed steel. The results showed that even after the steel specimens are cooled from fire temperatures of up to 700°C, their yield strength is still the same as that of the virgin material. Qiang et al. [19, 20] performed a set of experimental tests to investigate the behaviour of S460, S690 and S960 steels under fire and post-fire conditions. In order to study the post-fire behaviour of these three steel grades, the specimens were heated to fire temperatures of up to 1000°C and then performed quasi-static tensile tests at room temperature after cooling the specimens. The changes in the yield strength and ultimate strength of test specimens after cooling down from fire temperatures were studied. Their results showed that the aforementioned mechanical properties are only affected by the cooling phase when they are subjected to fire temperatures above 600°C. Moreover, the stronger the tested steel was, the more deterioration in its mechanical properties occurred when cooled from elevated

temperatures. Chiew et al. [16] studied the in-fire and post-fire mechanical properties of the reheated, quenched and tempered high strength S690 steel plate (RQT-HSS-S690). They studied the changes in the 0.2% proof stress, 2.0% stress and ultimate strength of the RQT-S690 HSS plate at elevated temperatures of up to 1000 °C and after being cooled to room temperature. According to their results, the residual strength properties of the RQT-S690 HSS specimens after being cooled from temperatures above 400°C are considerably reduced. Wang et al. [21] evaluated the ultimate strength, elongation and the elastic modulus of the high strength Q460 steel (HSS-Q460) after being cooled from fire temperatures of up to 900°C to room temperature. In order to cool down the test specimens, they applied two cooling methods: natural air cooling and cooling by water. Their results showed that when the HSS-Q460 specimens are cooled from temperatures below 700°C, their mechanical properties are almost unchanged. However, for specimens cooled from higher temperature exposures, up to 30% reduction in strength results was observed. In addition, they concluded that the cooling method has a significant influence on the ultimate strength and elongation of the HSS-Q460. Heidarpour et al. [23] investigated the in-fire mechanical properties of the UHSS (Grade 1200) tubes subjected to elevated temperatures of up to 600°C. Their results showed that the strength of the UHSS is considerably deteriorated when tested at temperatures above 300°C. Using the experimental results, they proposed a set of predictive equations describing the reduction factors of 0.2% proof stress and ultimate tensile strength for the UHSS tubes at fire temperature of up to 600°C.

From the literature review it can be understood that in all studies focusing on the post-fire mechanical behaviour of steel materials, depending on the grade of the tested steel, the effect of cooling phase of a fire is significant when temperature increases above a critical temperature. This phenomenon was discussed by Azhari et al. for different grades of steels [7]. Based on the plots of the thermodynamic stability of the phases present in the microstructure of the UHSS and HSS, the fire temperature exposures are classified in two groups: Low fire temperatures and high fire temperatures. Considering that temperatures below 600°C are classified as low fire temperatures category for the ultra-high strength steel (UHSS), an experimental study was performed on the UHSS (Grade 1200) tubes subjected to low fire temperatures and the changes occurred in their strength and ductility at elevated temperatures of up to 600°C and after being cooled to

room temperature were discussed [7]. The results showed that while there is a significant reduction in the strength of the UHSS specimens tested under fire temperatures of 450°C and 600°C, the residual strength of the UHSS is also considerably reduced after cooling from these temperatures.

Although studies have been conducted on the post-fire mechanical behaviour of mild steel (MS) and high strength steel (HSS), the effect of cooling phase of a fire on mechanical properties of the Grade 1200 ultra-high strength steel (UHSS) subject to high fire temperatures (i.e. above 600°C) has not been investigated. This paper addresses the in-fire and post-fire mechanical properties of the UHSS (Grade 1200) tube specimens subjected to fire temperatures of up to 800°C.

Two sets of experimental tests are carried out in this work. The first set includes heat-up tests where the specimens from the UHSS tubes are subjected to tensile tests at fire temperatures of up to 800°C. The second set includes the cooling tests where the quasi-static tensile test is carried out at room temperature on the UHSS specimens after being cooled from fire temperatures. The changes occurring in the mechanical properties of the material, including strength and ductility, in these two sets of tests are discussed. In order to investigate the effect of steel grade on the in-fire and post-fire mechanical properties of steel, the same tests are also conducted on specimens taken from high strength steel (HSS) tubes with nominal yield strength of 800MPa. The effect of the elevated temperature exposure on the microstructure of the specimens cooled from temperatures above 700°C (high fire temperatures) is evaluated using optical microscopy and scanning electron microscopy (SEM) methods and the microstructural reason for the mechanical tests results are explained. The thermodynamic stability of the ferrite and cementite phases in the UHSS and HSS obtained by the authors [7] is studied and the reason behind the residual strength reductions are explained based on the phase changes occurring in the steel material during fire. Finally, based on the data obtained from the experimental tests, an empirical constitutive description is developed to predict the stress-strain response of the UHSS materials cooled from fire temperatures of up to 800°C to room temperature.

3.2. Experimental tests

The work recently performed by the authors [7] was limited to the investigation of the in-fire/post-fire mechanical behaviour of Grade 1200 ultra-high strength steel (UHSS) subjected to fire temperatures up to 600°C. Since it is expected that the residual mechanical properties of UHSS should exhibit a discontinuous alteration after exposure to temperatures above ~700°C, in this paper experimental tests are per-formed to evaluate the mechanical behaviour of UHSS tubes at fire temperatures above 600°C, known as high fire temperatures, and after being cooled to room temperature. For comparison purposes, the experimental tests are also carried out on Grade 800 high strength steel (HSS) tube material.

3.2.1. Test Specimens

The chemical compositions of Grade 1200 and Grade 800 steels considered in this paper and their manufacturing process are similar to those presented in Ref. [7]. The test specimens were sectioned from the UHSS and HSS tubes using high pressure water jet cutting with nominal external diameter of 76.1 mm and wall thickness of 3.2 mm. As shown in Figure 3-1, the shape and dimensions of the specimens are determined in accordance with ASTM E8 [24]. The specimens are cut from two strips located at right angles (90º) to the tube weld line as indicated in Figure 3-2.

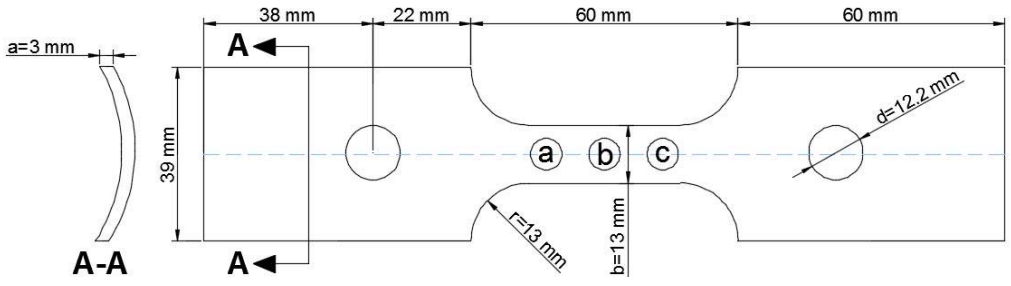

Figure 3-1. Dimensions of test specimens

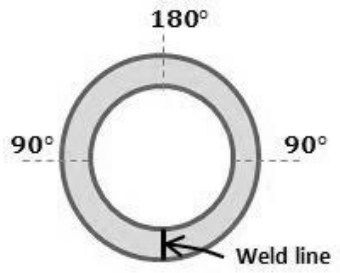

Figure 3-2. The tube section

In order to fit the samples into the grips for the tensile tests, they are mechanically flattened based on the instructions given in AS1391 [25]. Each test is repeated until the results obtained from two similar tests have a difference of less than 3%. The cross sectional area of the gauge length of the test specimens is determined according to AS1391 [25].

3.2.2. Testing Method

3.2.2.1. Heat-up tests

For the heat-up tests, the SF-16 split furnace shown in Figure 3-3 is installed on the Instron 5982 100kN testing machine. In this furnace, a resistance wire is wound on to a recrystallised alumina tube in three independent zones to form the furnace element. This three-zone format allows the user to modify the furnace temperature gradient, creating a uniform central zone. The furnace can heat the specimen up to 900ºC at a rate of ~20ºC/min.

As illustrated in Figure 3-3c, three thermocouples labelled as T_1, T_2 and T_3 are attached to three points (a, b and c) on the gauge length of the tensile coupon shown in Figure 3-1 to record its real time-temperature profile. Nine different target temperatures are considered in this study, i.e. room temperature (RT), 300ºC, 470ºC, 540ºC, 600ºC, 650ºC, 700ºC, 750ºC and 800ºC. It is worth mentioning that the tests under fire temperatures below 600ºC have been already conducted by the authors [7] for the same UHSS tube material. However, the device employed in the previous study to heat up the specimens was an environmental chamber which uses a different heating mechanism from the furnace used in the present study. The environmental chamber uses forced convection heat transfer method to provide an optimum temperature distribution. Forced

convection stands for the transfer of heat by motion of a fluid which is instigated by application of an external motive force [26]. In an environmental chamber, the fluid transferring the heat is the air and the external force moving the air is generated by the chamber's fan. However, in model SF-16 split furnace, the specimen gripped inside this furnace is heated through a combination of convection and radiation, dependant on the test temperature. Thermal radiation is the transfer of heat by means of the emission of photons in electromagnetic waves which carry the heat energy away from the source to the surrounding objects.

It is well-known that temperature measurements in heating devices that use radiation to transfer the heat to the specimen can be affected by radiation errors. From the literature [27, 28], it was concluded that the main factor controlling the radiation errors is the thermal inertia of the furnace wall lining material. Harada et al. [28] investigated the reproducibility of the fire tests data for two commonly used wall lining materials, i.e. fire brick and ceramic fibre. According to their results, due to small thermal inertia of ceramic fibre, the range of data scatter in the ceramic fibre wall furnaces was considerably lower than that in the fire brick wall furnaces. In the furnace used for this study, high-performance ceramic fibre insulation is used to reduce heat losses and provide fast heating rates.

In order to obtain a uniform set of data, all fire temperatures ranging from 300°C to 800°C are considered in this study. Since both UHSS and HSS tube specimens lose ~97% of their strength at temperatures above 800°C, the maximum temperature studied in this re-search does not exceed 800°C. When the difference between the temperature T_i of each thermocouple and the target temperature T_t is less than 2%, i.e. $|T_i - T_t| \leq 2\%$, it is assumed that the thermal profile is uniform throughout the specimen and the quasi-static tensile test can be started. Hence, by using the Instron 5982 100kN testing machine, a strain-controlled tensile test with an applied strain rate of $0.005 \pm 0.002\,\text{min}^{-1}$ [24] is carried out on the specimen until failure. As for strain measurement of the specimen during the tensile test, the model 3448 High Temperature Contact Extensometer with approximate gauge length of 25mm is used. As shown in Figure 3-3b, the front cut-out of the furnace allows the extensometer to enter inside the furnace and be in contact with the specimen gripped inside the furnace.

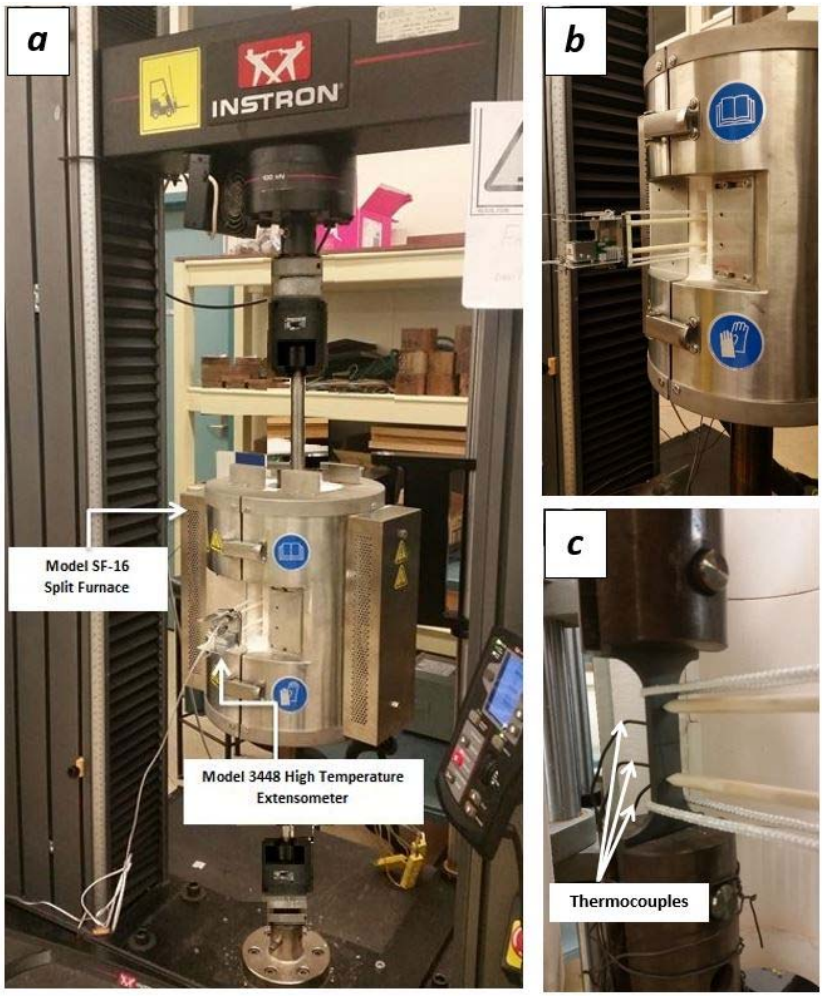

Figure 3-3. a and b) Test setup from different views, c) inside the furnace

3.2.2.2. Cooling tests

In order to evaluate the post-fire mechanical response of the UHSS and HSS tubes after cooling from fire temperatures of up to 800°C, the test specimens are heated up to the target temperature as explained in the previous section. Once the temperatures shown by the three thermocouples attached to the specimen are stabilised at the target temperature (T_t), the temperature is held constant for 20 mins. The specimen is then allowed to air cool at its own rate by turning off the furnace and opening the door as shown in Figure 3-4. The strain-controlled tensile test with an applied strain rate of $0.005 \pm 0.002\,\text{min}^{-1}$ is then conducted on the test specimen once it reaches room temperature.

Figure 3-4. The cooling test setup for the post-fire stage (T_t=800°C)

Finally, in order to help interpret the results obtained from the cooling tests, microstructural examination of the UHSS materials cooled from some very high fire temperatures is conducted using optical and scanning electron microscopy (SEM).

3.3. Results and Discussion

3.3.1. General Descriptions

In order to investigate the effect of high temperature exposure on mechanical properties of the tested steels, the stress-strain curves, characteristic tensile strengths, strain values and energy absorption are determined. Since the stress-strain curves do not exhibit a pronounced yield point, the tensile strength at different strain levels including 0.2%, 0.5%, 1.5% and 2.0% strains and also the ultimate tensile strength are reported as characteristic tensile strengths. The values of these parameters are illustrated in a typical stress-strain curve shown in Figure 3-5. As indicated in Figure 3-5, the values of 0.2% proof stress ($f_{0.2}$) and 0.5% stress ($f_{0.5}$) are determined by finding the intersection of the stress-strain curve with a line starting from the 0.2% and 0.5% strains, respectively, parallel to the elastic part of the curve. The strain corresponding to the 0.2% proof stress denotes the proof strain (ε_y). It is worth noting that in most research works, the value of $f_{0.5}$ is calculated by simply finding the stress at 0.5% strain level [16, 17]. However, since in the stress strain curves obtained in this research, the 0.5% strain is usually within the

yield stage, the $f_{0.5}$ value is found by the aforementioned method. As shown in Figure 3-5, in order to find the strength values at 1.5% and 2.0% strains, i.e. $f_{1.5}$ and $f_{2.0}$, the conventional method is applied. The maximum stress value in the engineering stress–engineering strain curve denotes the ultimate tensile strength (f_u) and the corresponding strain value is the uniform elongation (ε_u). Finally, the area under the stress-strain curve starting from zero strain to the uniform elongation (ε_u) represents the energy absorption (U^*).

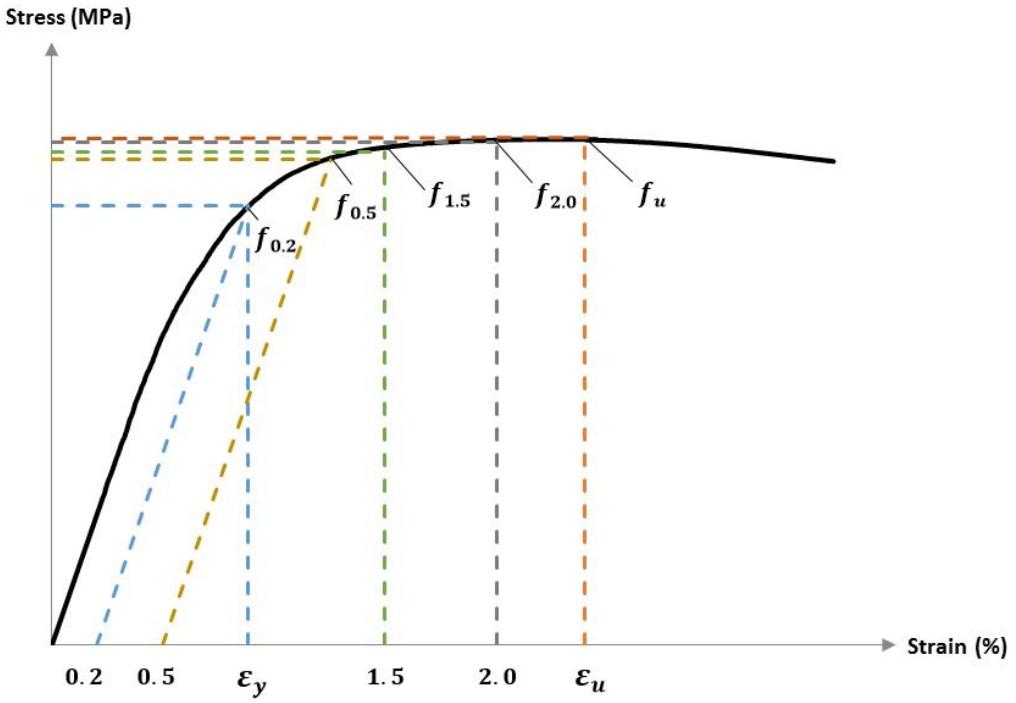

Figure 3-5. Definition of characteristic strengths and strains on a typical stress-strain curve

3.3.2. Stress-strain curves

Figure 3-6 shows the elevated temperature stress-strain curves resulting from the heat-up tests. Due to the changes that occur in the cross section of the specimens during necking and the fact that the cross-section geometry during necking depends on specimen size [29], the strains are no longer uniform once necking starts such that readings of the strain values are not accurate. In spite of that, the tensile tests are not terminated and the full engineering stress-strain curves are plotted up to the failure of the material. However, the onset of necking is signified by a black cross sign (**X**) on the

plotted curves. In this study, the UHSS specimen tested at elevated temperature ***T*** is shown as UHSS-**H*T***, where **H** represents the **H**eat-up test. For example, the stress-strain curve of the UHSS specimen tested at 800°C is labelled as UHSS-H800. Also, the UHSS-RT represents the stress-strain curve of the virgin UHSS at room temperature (**RT**). As illustrated in Figure 3-6, the strength of UHSS is reduced as the maximum temperature increases. In addition, a considerable drop in strength is observed when the temperature exceeds 600ºC.

The stress-strain curves of the UHSS specimens under strain-controlled tensile test at room temperature after being cooled from different fire temperatures are presented in Figure 3-7. Similar to the curve labelling system explained for the heat-up tests, the stress-strain curve of the UHSS specimens tested at room temperature after **c**ooling from the elevated temperature ***T*** are labelled as UHSS-**C*T***. For example, UHSS-C800 represents the stress-strain curve of the UHSS specimen cooled from 800°C to room temperature. It is evident from the curves shown in Figure 3-7 that the strength of UHSS is not regained after cooled from temperatures at or above 470ºC. However, according to [19, 20], the post-fire mechanical properties of S460, S690 and S960 steels are not affected until they are exposed to fire temperatures above 600°C. It is clear that the thermal response of the UHSS is fundamentally different to these previously studies steels. It can be also interpreted that the residual strength of UHSS is significantly reduced after being cooled from fire temperatures above 700°C. More detailed explanations about this phenomenon are provided in the Microstructure characterization section of this paper. In addition, it is curious that the UHSS-C750 and UHSS-C800 curves are almost the same and seemingly the variation of the residual strength of the UHSS with temperature is stabilised when subjected to fire temperatures above 750ºC. The reason behind this phenomenon is also explained in the Microstructure characterization section.

It is evident that the higher temperature the UHSS specimens have experienced, the more residual uniform elongation they experience when tested after being cooled to room temperature. The time-temperature curves of the UHSS specimens after being cooled from different fire temperatures are summarised in Figure 3-8. It can be seen that in most of the cooling tests, the approximate time at which the specimen reached its maximum temperature is around 90 min. This is consistent with real fire conditions in which during a certain time, different parts of the structure are heated up to different fire temperatures.

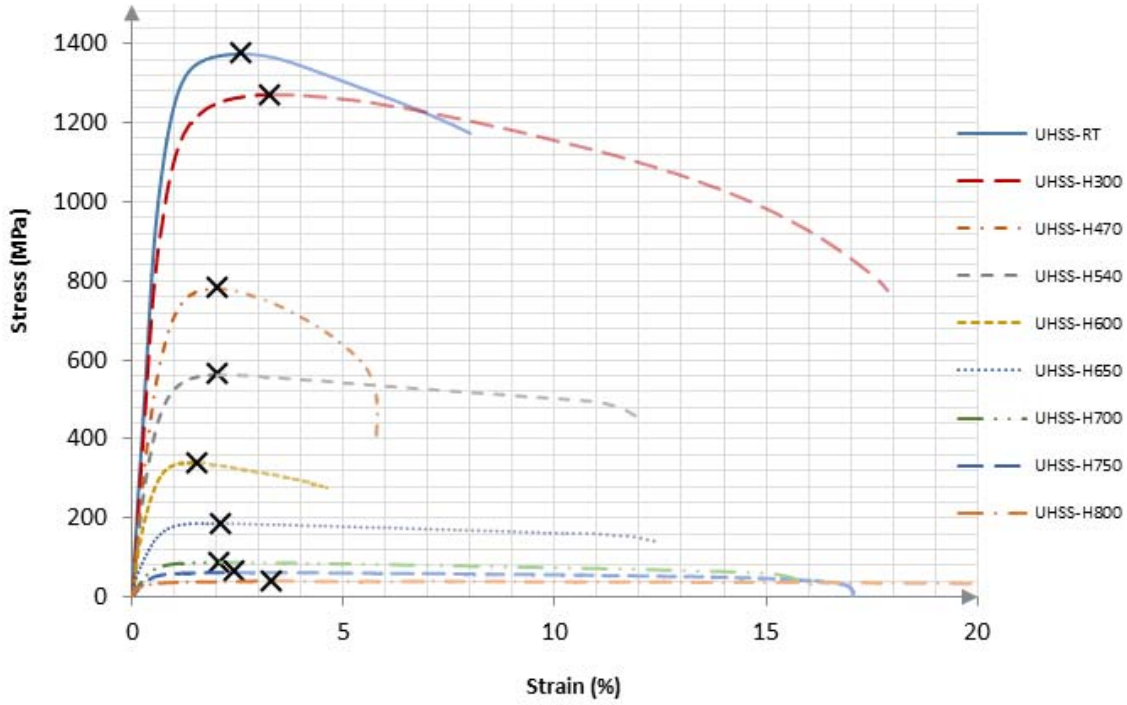

Figure 3-6. Stress-strain curves for UHSS specimens at elevated temperatures ranging from 300°C to 800°C

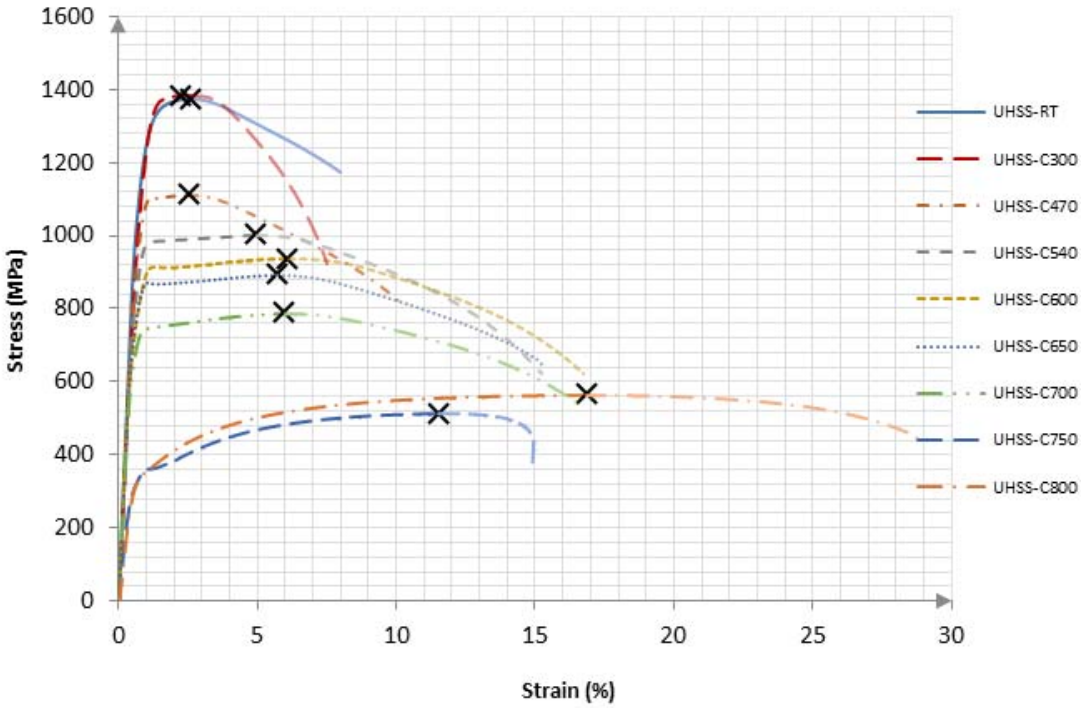

Figure 3-7. Stress-strain curves of UHSS specimens at room temperature after cooling from the elevated temperatures ranging from 300°C to 800°C

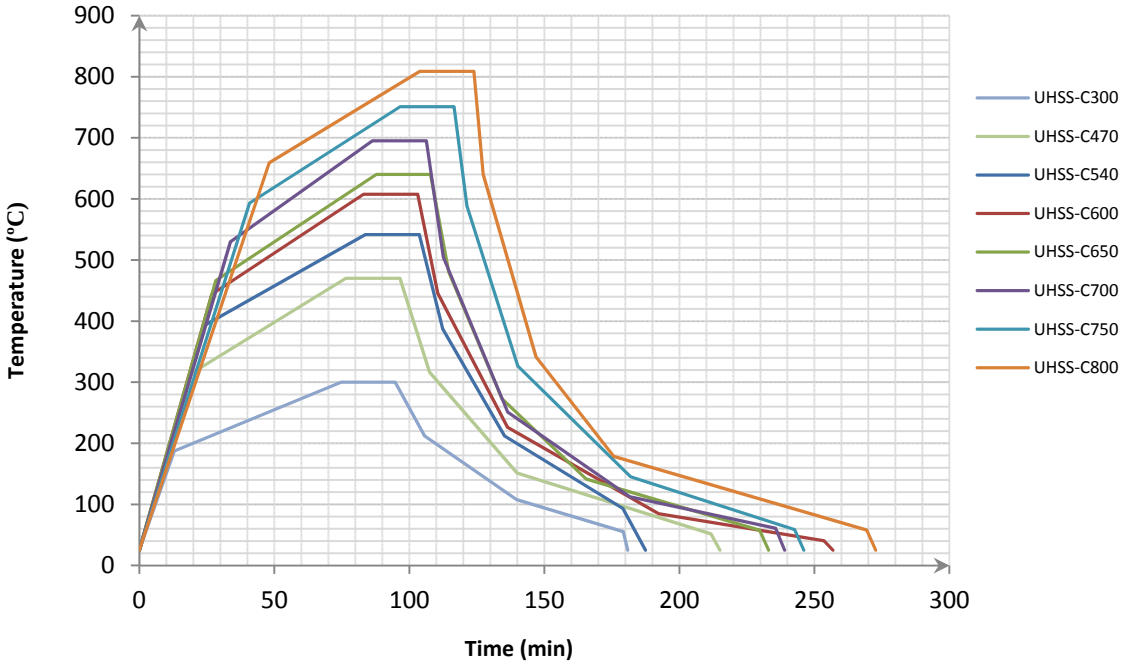

Figure 3-8. Temperature-time profile of UHSS specimens cooled from the elevated temperature T to room temperature

3.3.3. Strength

In order to discuss the variation of characteristic strengths with temperature of the steel specimens in both heat-up and cooling tests, reduction factors have been calculated as the ratio of the strength values at elevated temperatures and after cooling to room temperature to the corresponding strength values of virgin material at room temperature. The characteristic strength reduction factors for the heat-up tests and cooling tests are presented in Tables 3-1 and 3-2. In these Tables, T and CT indices correspond to the strength values for UHSS specimens tested at elevated temperature T and after cooling from temperature T to room temperature, respectively. Also, the RT index refers to the strength values of the virgin material tested at Room Temperature. For some heat-up tests, since the 1.5% and 2.0% strains are within the post-necking part of the stress-strain curve of the specimen, the reduction factors of their corresponding strengths, i.e. $f_{1.5,T}/f_{1.5,RT}$ and $f_{2.0,T}/f_{2.0,RT}$, are not reported in Table 3-1. Based on the data shown in Table 3-1, the UHSS specimens tested at temperatures above 700°C lose more

than 94% of their strength. The reduction of the values of $f_{0.2}$, $f_{0.5}$ and f_u occurs to the same extent.

As can be seen from the results shown in Table 3-2, the characteristic strength reduction factors obtained from the cooling tests have a decreasing trend with increasing temperature. There is a significant drop in the reduction factors of the specimens cooled from 750°C and above. Since the strength reduction factors of UHSS specimens after cooling from 750°C and 800°C are almost the same, it can be concluded that they have been stabilised such that they will not experience any higher reduction in their strength when they are cooled from higher fire temperatures. This phenomenon is rationalised in the Microstructure characterization section based on the plots of the thermodynamic stability of the phases present in the UHSS microstructure. Elaborating deeper into the results shown in Table 3-2, it can be seen that for specimens cooled from 750°C and 800°C to room temperature, the values of ultimate tensile strength are not reduced to the same extent as other characteristic strengths. The higher values of the ultimate tensile strength for the UHSS specimens cooled from these two temperatures show that the post-yield part of the UHSS-C750 and UHSS-C800 stress-strain curves has a more rounded shape compared to that of other curves as shown in Figure 3-7. This is a signature of a major microstructural change in the steel leading to a structure capable of exhibiting significantly more strain hardening capacity than the virgin material.

Table 3-1. Reduction factors of characteristic strengths for UHSS under various fire temperatures

Temperature	**300°C**	**470°C**	**540°C**	**600°C**	**650°C**	**700°C**	**750°C**	**800°C**
$\frac{f_{0.2,T}}{f_{0.2,RT}}$	0.889	0.496	0.368	0.222	0.091	0.041	0.032	0.025
$\frac{f_{0.5,T}}{f_{0.5,RT}}$	0.897	0.550	0.397	0.248	0.123	0.057	0.043	0.026
$\frac{f_{1.5,T}}{f_{1.5,RT}}$	0.896	0.570	0.411	0.252				
$\frac{f_{2.0,T}}{f_{2.0,RT}}$	0.912	0.569	0.409					
$\frac{f_{u,T}}{f_{u,RT}}$	0.925	0.568	0.410	0.247	0.134	0.064	0.047	0.030

Table 3-2. Reduction factors of characteristic strengths for UHSS after cooling from various fire temperatures

Temperature	300°C	470°C	540°C	600°C	650°C	700°C	750°C	800°C
$\frac{f_{0.2,CT}}{f_{0.2,RT}}$	1.00	0.850	0.774	0.650	0.665	0.575	0.264	0.258
$\frac{f_{0.5,CT}}{f_{0.5,RT}}$	1.00	0.840	0.750	0.687	0.664	0.565	0.271	0.269
$\frac{f_{1.5,CT}}{f_{1.5,RT}}$	1.02	0.818	0.730	0.676	0.650	0.558	0.273	0.285
$\frac{f_{2.0,CT}}{f_{2.0,RT}}$	1.02	0.808	0.723	0.667	0.645	0.553	0.281	0.301
$\frac{f_{u,CT}}{f_{u,RT}}$	1.03	0.809	0.729	0.681	0.653	0.574	0.372	0.411

In order to illustrate the effect of cooling phase of a fire on the UHSS's strength, the reduction factors of the 0.2% proof stress ($f_{0.2}/f_{0.2,RT}$) and the ultimate tensile strength ($f_u/f_{u,RT}$) for both heat-up and cooling tests are plotted in Figures 3-6 and 3-7 with respect to the maximum temperature the specimens have experienced. For the purposes of comparison, the values provided by the AS4100 [30] and AISC [31] standards for the 0.2% proof strength and the ultimate tensile strength reduction factors of mild steel at elevated temperatures are presented. The vertical distance between the curves obtained from the heat-up and cooling tests represents the strength recovered (compared to the elevated temperature strength) during the cooling phase of a fire.

As shown in Figures 3-6 and 3-7, using the values given by the standards to predict the tensile mechanical behaviour of UHSS structural members at fire temperatures may lead to an unsafe design. On the other hand, there is no provision in the building codes for the UHSS materials under cooling phase of a fire. In order to predict the in-fire and post-fire behaviour of the UHSS structural members, a new set of strength design formulations must be proposed.

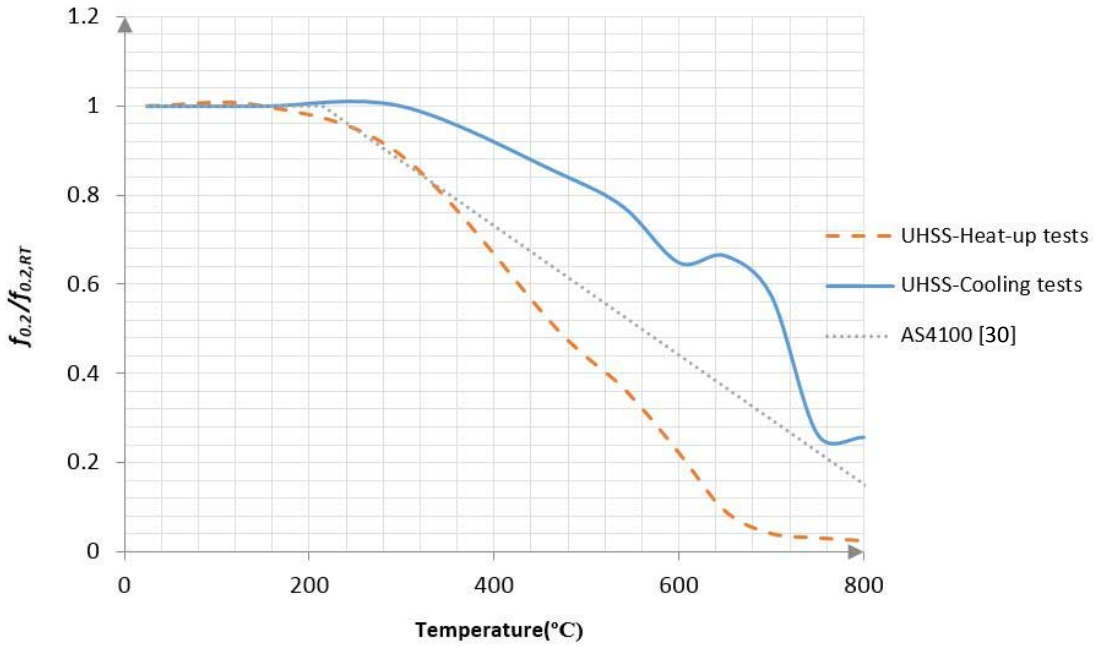

Figure 3-9. Variation of 0.2% proof stress reduction factor for UHSS under in-fire and post-fire conditions

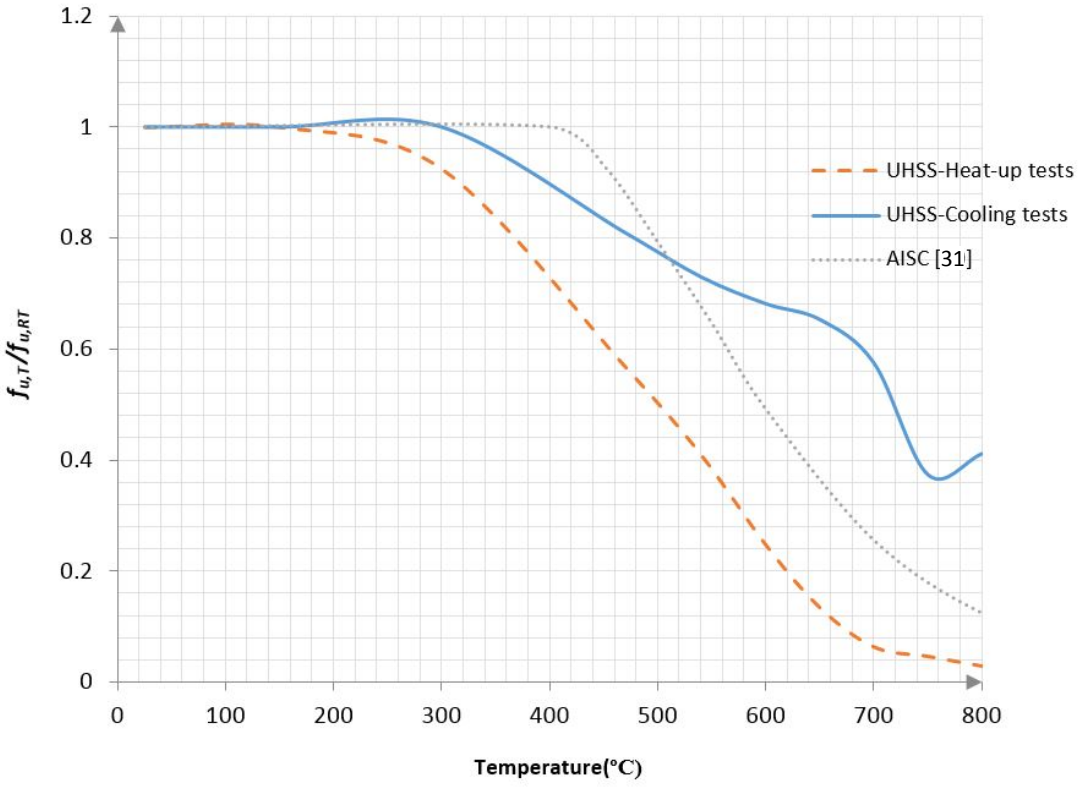

Figure 3-10. Variation of ultimate tensile strength reduction factors for UHSS under in-fire and post-fire conditions

3.3.4. Ductility

Several parameters can be calculated to discuss the ductility of a material under fire conditions. In this paper, the first parameter used to indicate the in-fire/post-fire ductility of the UHSS is the ratio of the uniform elongation ($\mathcal{E}_u$) of the UHSS specimens obtained from both heat-up and cooling tests to that of the virgin UHSS tested at room temperature ($\mathcal{E}_{u,RT}$). In Figure 3-11, the variation of $\mathcal{E}_u$ / $\mathcal{E}_{u,RT}$ ratios with respect to the maximum temperature the material has experienced are plotted. The results show that the variation of uniform elongation of the UHSS specimens tested at elevated temperatures do not share the same trend with those of the UHSS specimens tested after being cooled to room temperature. While the values of $\mathcal{E}_u$/ $\mathcal{E}_{u,RT}$ ratio for the UHSS specimens under cooling tests increase up to 6.5 as the temperature reaches 800ºC, their maximum value for the UHSS specimens under heat-up tests is only 1.27. The elongation of a material depends strongly on the strain hardening capacity of its structure and the rapid increases in the elongation after cooling from temperatures above 700°C again signifies a major change in the structure of these steels when heated above ~700°C.

Another parameter characterising the ductility or the energy ab-sorption of the material is the strain energy U^* absorbed by the material. Since the engineering stress and strain values are calculated based on the original dimensions of the tested specimen, they do not take into account the changes in the cross section area of the specimen during the tensile test [32]. Therefore, evaluation of the exact energy absorption up to the fracture of the tested specimens cannot be conducted based on the engineering stress-strain curves. Considering that the accurate determination of the true stress-strain curve during necking of the specimens is still under investigation [33-35] and the fact that response before necking is size-independent, in this paper, the energy absorption is calculated up to the onset of necking just as an indicator for the specimen's capability to absorb energy, which is defined by:

$$U^* = \int_0^{\varepsilon_u} \sigma \, d\varepsilon \tag{3-1}$$

where σ and ε are the engineering stress and strain of the material, respectively. The values of U^* obtained from the heat-up tests and cooling tests are normalised with respect

to that of the virgin UHSS tested at room temperature ($U^*_{,RT}$) and the variation of $U^*/U^*_{,RT}$ ratios with respect to the maximum temperature of the UHSS specimens are shown in Figure 3-12. It can be seen that for the UHSS specimens under cooling tests, $U^*/U^*_{,RT}$ ratio generally increases as the maximum temperature increases (although this shows a local maximum in the temperature range 600°C-700°C). However, for the UHSS specimens under heat-up tests, the ratio of $U^*/U^*_{,RT}$ considerably decreases as the maximum temperature increases. The reason behind this phenomenon is that in addition to the values of strain, the strength has also a considerable contribution to the magnitude of energy absorption. Therefore, the calculated energy absorption for the UHSS tested at 800°C is decreased to ~3% of that of the virgin UHSS tested at room temperature.

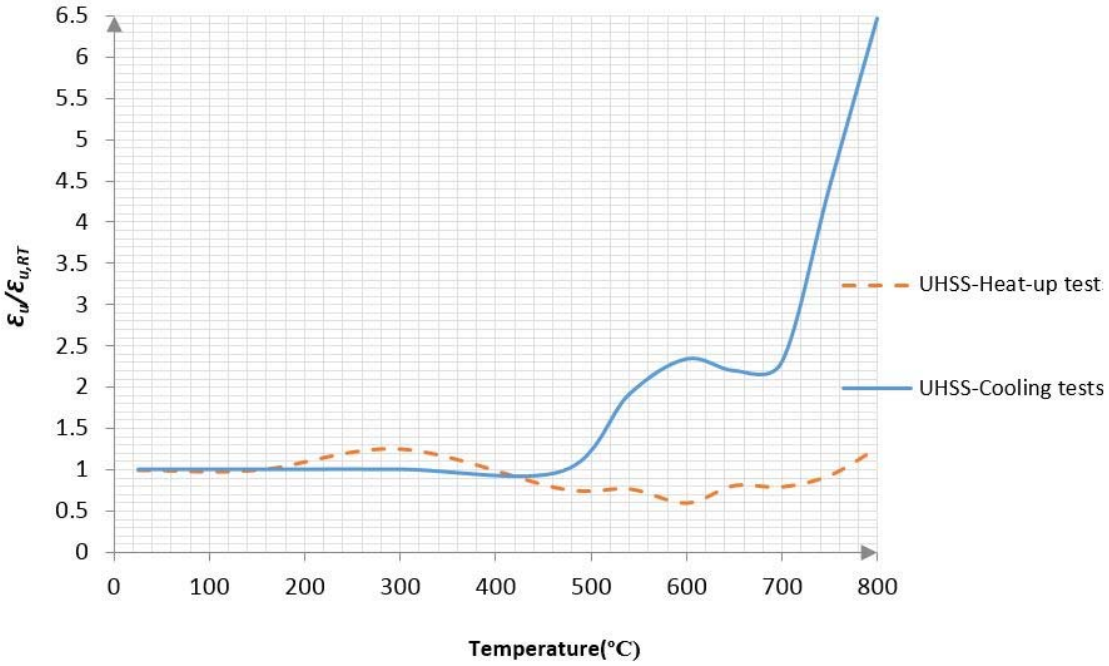

Figure 3-11. Variation of uniform elongation reduction factors for UHSS under in-fire and post-fire conditions

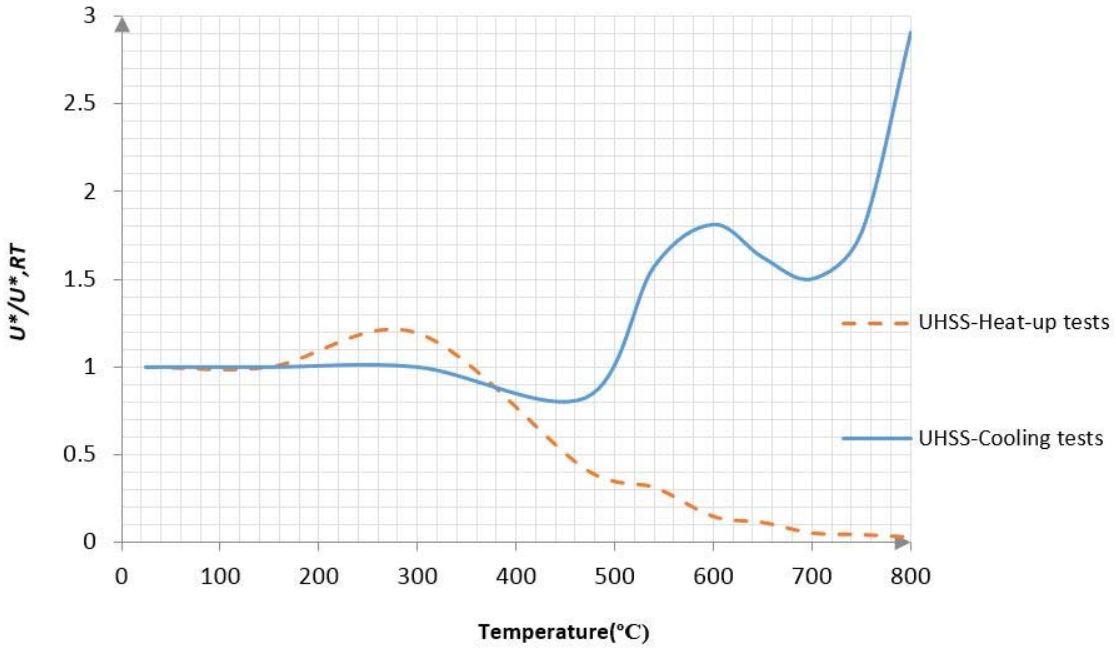

Figure 3-12. Variation of energy absorption reduction factors for UHSS under in-fire and post-fire conditions

The ductility of a structure is an important parameter to determine whether or not sufficient plastic deformation can be developed. Among a number of requirements recommended by the codes of practice such as AS4100 [30], AS/NZS 4600 [36] and Eurocode 3 [37] to determine whether the plastic analysis can be applied, the ratios of $f_u/f_{0.2}$, which has been addressed by all the aforementioned standards, and $\varepsilon_u/\varepsilon_y$ recommended by Eurocode 3 [37] are discussed in this study. According to AS4100 [30] and Eurocode 3 [37], the ratio of $f_u/f_{0.2}$ must be equal to or greater than 1.2, while AS/NZS 4600 [36] recommends a limit of 1.08 for this ratio. Moreover, $\varepsilon_u/\varepsilon_y$ must be equal to or greater than 20 as suggested by Eurocode 3 [37].

Tables 3-3 and 3-4 present the variations of $f_u/f_{0.2}$ and $\varepsilon_u/\varepsilon_y$ for the UHSS specimens tested at elevated temperature and after cooling from different fire temperatures. It can be seen that while the values obtained for the ratio of $f_u/f_{0.2}$ from the heat-up tests for temperatures equal to or greater than 300°C are within the acceptable limits recommended by the standards, those obtained for the UHSS specimens cooled from fire temperatures to room temperature do not meet the requirements of AS4100 [30] and Eurocode 3 [37] for all temperatures. However, they are still within the acceptable limit

suggested by AS/NZS 4600 [36]. In addition, according to the results shown in the second row of Tables 3-3 and 3-4, the values of $\varepsilon_u/\varepsilon_y$ do not meet the requirement of Eurocode 3 [37] for all temperature exposures, meaning that it may have to be modified to take into account the higher strength steel grades, the fire temperature exposure and the cooling phase.

Table 3-3. Variation of the ratios of $f_u/f_{0.2}$ and $\varepsilon_u/\varepsilon_y$ at various fire temperatures

Temperature	**RT**	**300°C**	**470°C**	**540°C**	**600°C**	**650°C**	**700°C**	**750°C**	**800°C**
$f_u/f_{0.2}$	1.174	1.221	1.345	1.309	1.306	1.724	1.827	1.743	1.398
$\varepsilon_u/\varepsilon_y$	3.106	3.892	3.153	3.514	3.255	6.551	7.767	9.231	12.565

Table 3-4. Variation of the ratios of $f_u/f_{0.2}$ and $\varepsilon_u/\varepsilon_y$ after cooling down from various fire temperatures

Temperature	**RT**	**300°C**	**470°C**	**540°C**	**600°C**	**650°C**	**700°C**	**750°C**	**800°C**
$f_u/f_{0.2}$	1.174	1.170	1.117	1.106	1.231	1.152	1.171	1.653	1.867
$\varepsilon_u/\varepsilon_y$	3.106	3.100	3.341	6.806	9.939	8.963	10.391	20.613	30.963

3.3.5. Comparison with Grade 800 high strength steel (HSS)

In order to investigate the effect of steel grade on the changes occurring in the mechanical behaviour of steel under fire conditions, the stress-strain curves of the HSS (Grade 800) tube specimens subjected to strain-controlled quasi-static tensile test at high fire temperatures and after cooling to room temperature are summarised in Figures 3-10 and 3-11, respectively. According to the results shown by the authors in Ref. [7] for the same HSS material, the strength of the HSS tube specimens cooled from fire temperatures below 600°C to room temperature are fully recovered. Therefore, in this study, to investigate the effect of steel grade on the residual mechanical properties of steel, only temperatures above 700°C are considered. In Figures 3-10 and 3-11, similar to the labelling system used for the UHSS specimens, the HSS-**H*T*** and HSS-**C*T*** curves represent the stress-strain curves of the HSS specimens tested at temperature ***T*** and at room temperature after being **c**ooled from temperature ***T***, respectively. Also, the stress-strain curve of the virgin HSS specimen tested at **R**oom **T**emperature is labelled as HSS-**RT**. As

shown in Figure 3-13, the strength and ductility of the HSS specimens tested at temperatures above 700ºC are considerably reduced. In addition, it can be seen from Figure 3-14 that while the strength of HSS is almost fully regained when cooled from 700ºC to room temperature, there is a significant reduction in the strength of the HSS tube specimens cooled from temperatures above 700ºC.

In order to better compare the effect of cooling phase of a fire on the strength and ductility of UHSS and HSS, the variations of the ultimate tensile strength and the uniform elongation with the maximum fire temperature are plotted in Figures 3-12 and 3-13. It can be seen that while the ultimate strength of the HSS specimen cooled from 800°C to room temperature is reduced to ~66% of that of the virgin HSS specimen at room temperature, the corresponding reduction factor for the UHSS (Grade 1200) is 41% (Figure 3-15). It may be noted that the ultimate stresses of the UHSS and the HSS, after cooling from 800°C are basically the same ~500MPa. This indicates that the special processing that is per-formed to give these two steels their room temperature properties is completely undone by heating to 800°C and the structure generated upon cooling back to room temperature is similar, and much weaker, in both steels. Also, the ductility of the HSS specimens tested after being cooled from 800°C to room temperature is 3 times its value for the virgin HSS tested at room temperature; however, the UHSS specimen cooled from 800°C experiences a uniform elongation of 6.5 times its original value (Figure 3-16). Thus, the UHSS loses its strength quicker than HSS while the rate of ductility increase in HSS subject to cooling phase of a fire is lower than that of UHSS. These results indicate the higher sensitivity of the UHSS to the temperature history of the material.

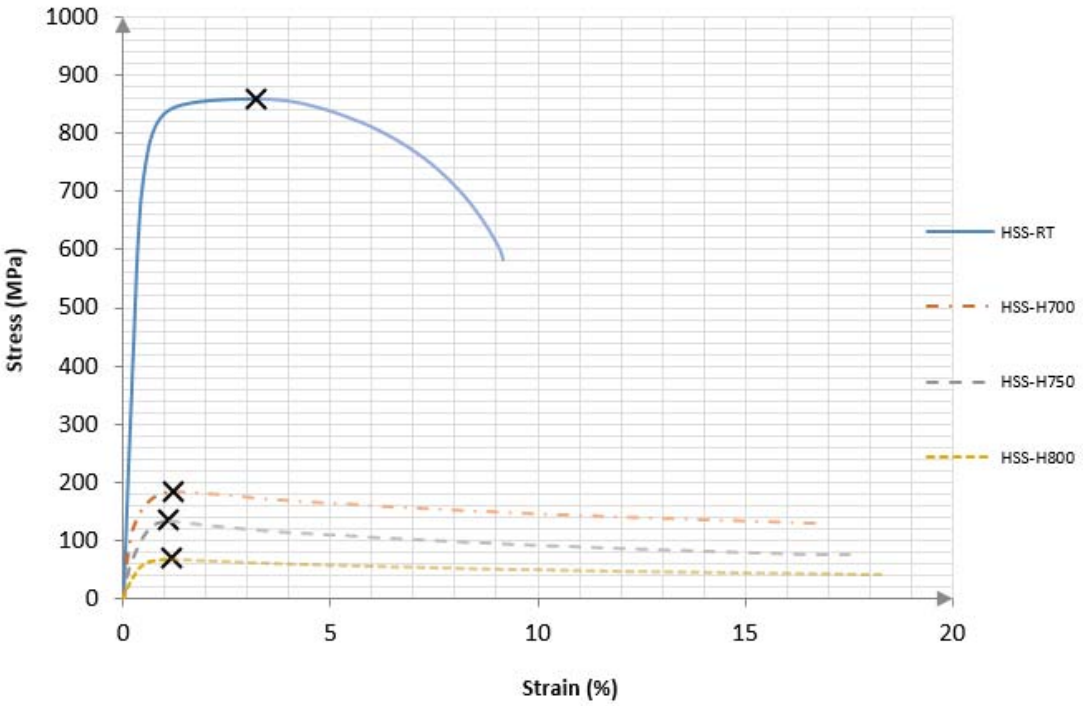

Figure 3-13. Stress-strain curves for the HSS specimens at high fire temperatures

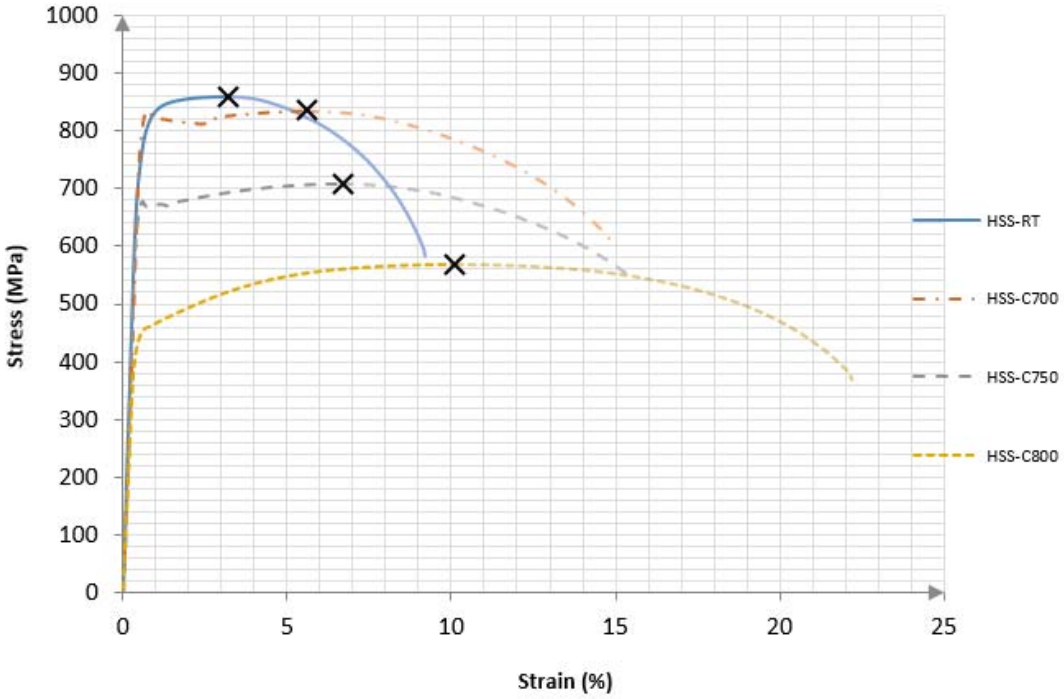

Figure 3-14. Stress-strain curves for the HSS specimens at room temperature after cooling from high fire temperatures

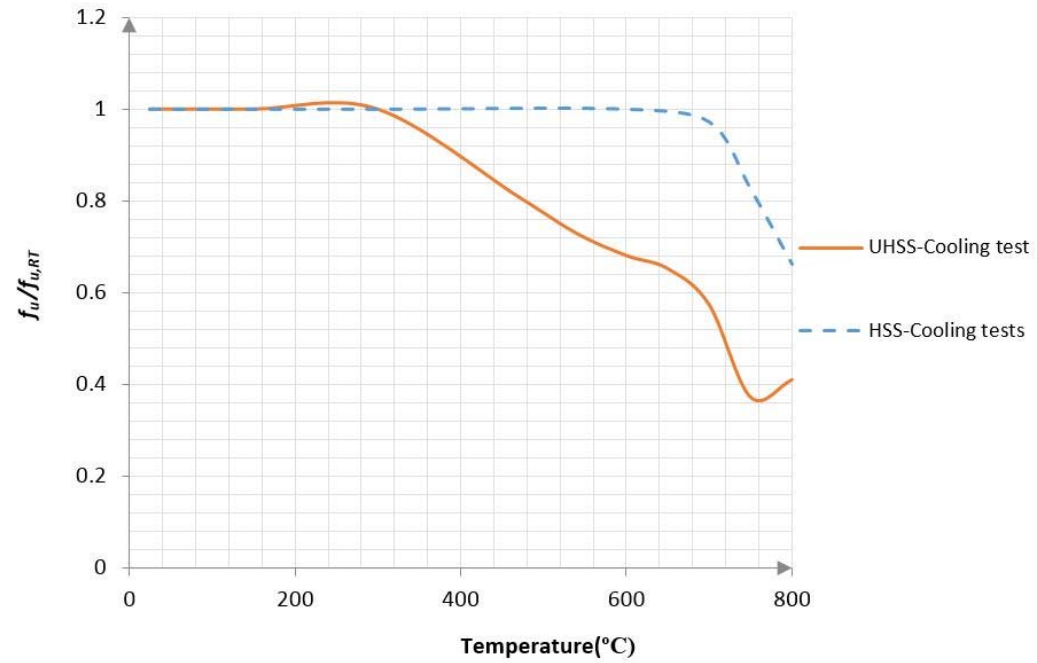

Figure 3-15. Variation of ultimate tensile strength of HSS and UHSS specimens after cooling from various fire temperatures

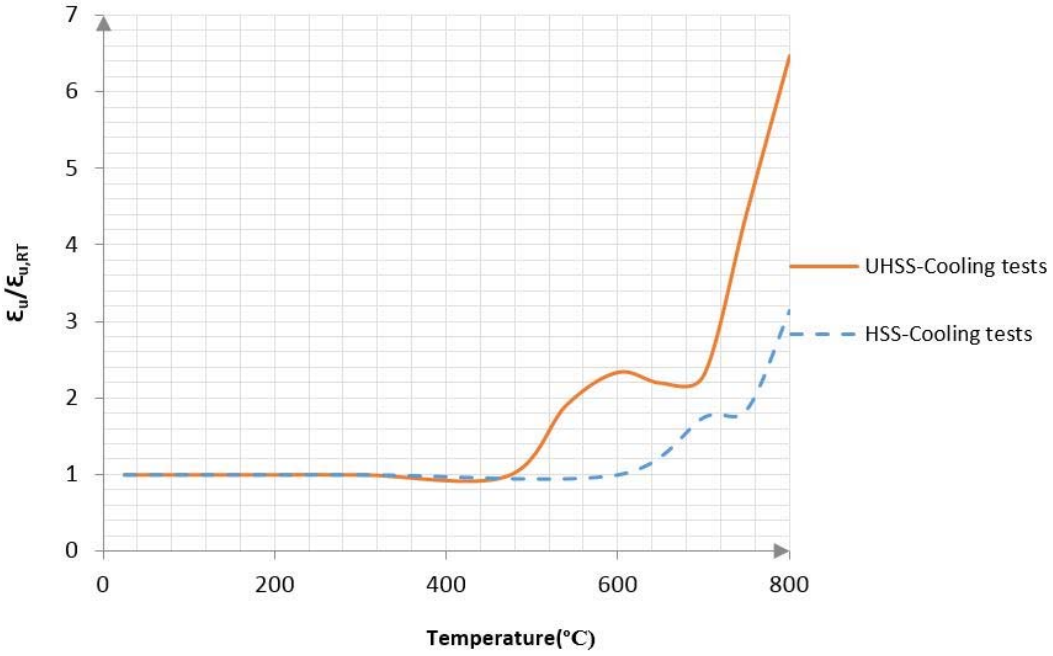

Figure 3-16. Variation of uniform elongation of HSS and UHSS specimens after cooling from various fire temperatures

3.4. Microstructure characterization

The mechanical behaviour of steel after being cooled from fire temperatures to room temperature is strongly dependant on the effect of the elevated temperature exposure on its microstructure.

In order to rationalise the microstructural changes occurring in the UHSS specimens during cooling phase of a fire, micrographs were obtained from the bulk microstructure of the UHSS in its original state (Figure 3-17a) and after being cooled from fire temperatures of 700ºC (Figure 3-17b), 750ºC (Figure 3-17c) and 800ºC (Figure 3-17d) to room temperature. Note that for the as-received UHSS material, due to its fine microstructure, Scanning Electron Microscopy (SEM) was used to resolve the structure. The microstructure of the remaining materials are coarse enough to be imaged using optical microscopy.

The UHSS considered in this study derives its strength from a tempered martensitic microstructure [38]. Martensite is a non-equilibrium phase that is very strong but also brittle. The ductility of martensite is improved by tempering the material at specific (relatively low) temperatures. This tempering leads to precipitation of cementite and the subsequent removal of C from the matrix which results in a better ductility but also lower strength. The white spots shown in Figure 3-17a are the cementite precipitates (Fe_3C) appearing as a result of tempering of martensite. In steels with martensitic microstructures, the strength is mainly controlled by the concentration of carbon remaining in solid solution (i.e. not present in the cementite). When a UHSS specimen is subjected to elevated temperatures, if the fire temperature coincide with the 'tempering temperature range of martensite', the tempering process and the subsequent C diffusion and removal from solid solution will continue resulting in significant strength reduction of the material.

As can be seen in Figure 3-17b, although there are some small equiaxed white grains which are the ferrite grains resulted from tempering of martensite, the lath shaped grains representing the tempered martensite structure are still present in the UHSS material cooled from 700ºC to room temperature. However, for the UHSS material cooled from 750ºC to room temperature (Figure 3-17c), the majority of the grains inside the microstructure are large equiaxed ferrite grains and only a few lath shaped grains

(tempered martensite) remain within the microstructure. As can be seen from Figure 3-17d, almost the entire microstructure of the UHSS material cooled from 800°C to room temperature consists of large ferrite grains and there is no sign of the lath morphology of the original martensitic structure. In the ferritic microstructures, the strength is mainly controlled by the size of the ferrite grains and larger ferrite grains lead to lower strength. The ferrite grains in the UHSS cooled from 750°C and 800°C are almost of the same size. Therefore, as shown in Figure 3-7, the strength reduction for the UHSS cooled from 750°C and 800°C are almost the same.

To better explain the changes occurring in the microstructure after the exposure of the steel materials to fire temperatures, plots of the thermodynamic stability of the ferrite and cementite phases in the UHSS and HSS are calculated using the Thermo-Calc program [13] and the most up to date steel database, TCFe7 (Figure 3-18). These are computational thermodynamic calculations and tell us which phases will be present as a function of temperature.

From the phase diagrams obtained for the UHSS, it can be concluded that after exposure to temperatures below 650°C, the UHSS will remain a tempered martensite/ferrite and the phases present in the microstructure of the material (ferrite/martensite and cementite) do not change in identity and only their sizes change. For these temperatures, known as low fire temperatures, the factors controlling the strength after cooling are the maximum temperature and the time the material experiences at that temperature. However, heating the UHSS to temperatures above 650°C leads to the formation of a new phase called austenite (the green curve in Figure 3-18b). The austenite is a high temperature phase of steel and will not exist at room temperature in the types of steel compositions considered in this study. Depending on how fast the UHSS is cooled from these high temperatures, different percentage of austenite is converted to ferrite or pearlite. If the cooling rate is very fast (i.e. quenching in water or oil), then the original martensite microstructure may be recreated and no reduction in strength may be observed. The residual mechanical properties in steels subjected to high fire temperatures (i.e. above 700°C) are not very sensitive to the upper temperature reached (up to temperatures of ~1400°C) and depend mostly on the cooling rate from the fire temperature. These residual properties are much more difficult to predict because they require an understanding of the decomposition of the austenite phase as the temperature

is lowered and this is a strong function of both the steel composition and the cooling rate. This one question represents a whole field of research in the domain of Materials Science and Engineering [39-43].

For the UHSS heated up to temperatures above ~770°C, the steel phase is 100% austenite. The mechanical properties of the UHSS after cooling from temperatures above this would be basically the same. From the results obtained from the cooling tests performed on the UHSS (Figure 3-7), it can be seen that the stress-strain curves obtained for the UHSS specimens cooled from 750°C and 800°C to room temperature, almost match each other. It is important to note that cooling from these temperatures would lead to the austenite transforming back into ferrite and cementite. However, the nice and well controlled microstructures that are generated by controlled cooling in the manufacturing process of the as-received materials are not created.

From the phase diagrams calculated for the HSS material (Figure 3-18a), it can be seen that after exposure of the HSS to fire temperatures below ~680°C the phases present within its microstructure do not change. However, it is expected from these curves that for the HSS specimens cooled from temperatures between 700°C to 800°C, considerable strength reduction occurs. As can be seen from the curves shown in Figure 3-14, this prediction is consistent with the strength reduction resulted from the cooling tests conducted on the HSS specimens. Also, for the HSS specimens cooled from fire temperatures above ~800°C, 100% austenite is formed which means the residual stress-strain curves for these temperature exposures would be the same.

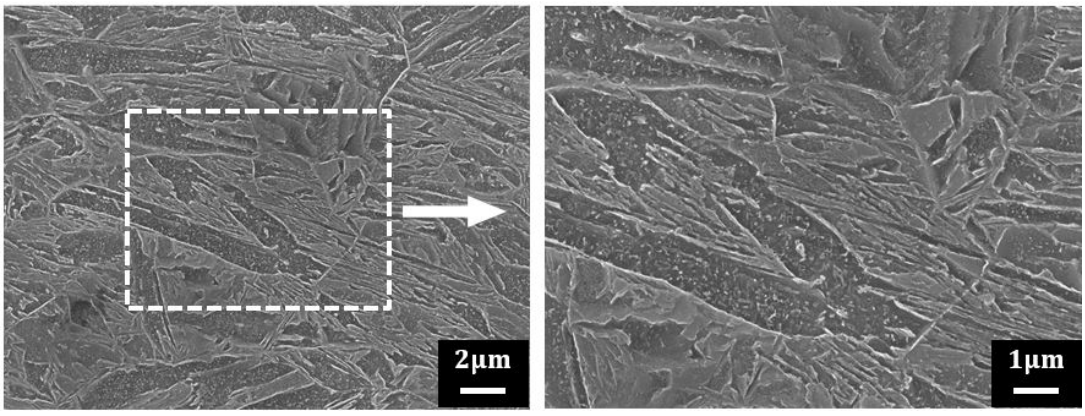

(a)

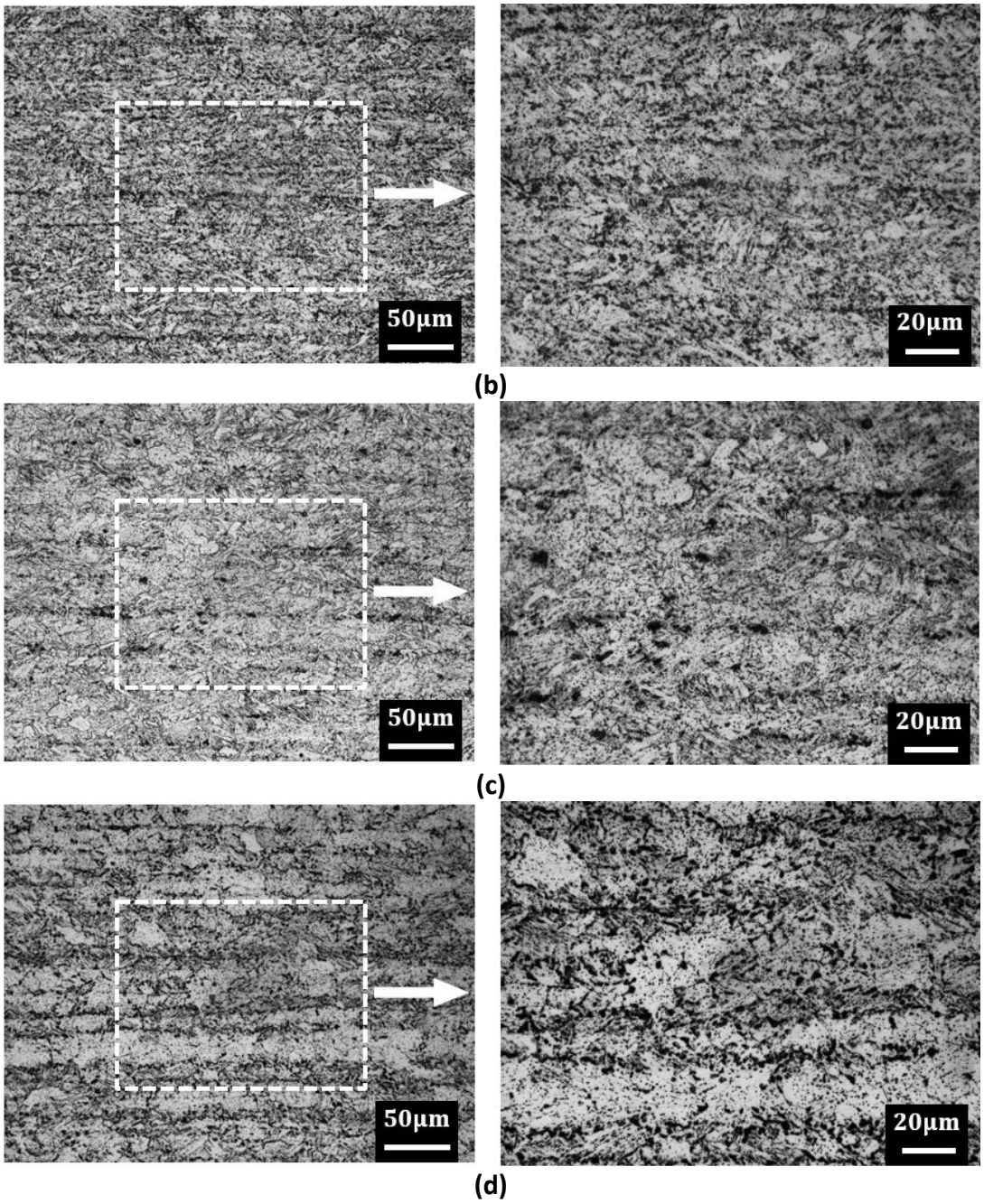

Figure 3-17. Micrographs of virgin UHSS specimens a) at room temperature (Scanning Electron Microscopy) and after cooled from b) 700°C, c) 750°C and d) 800°C to room temperature (Optical Microscopy)

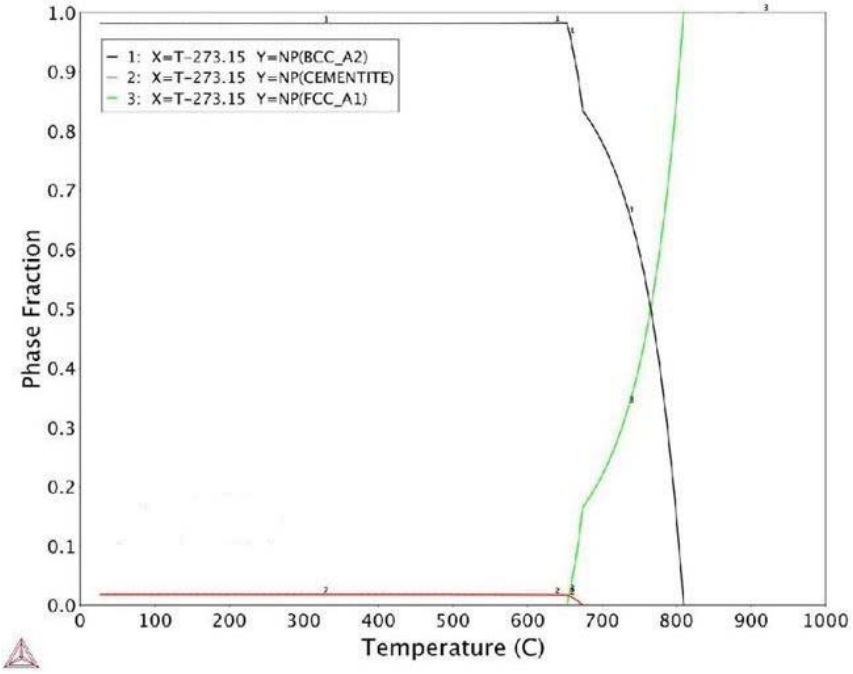

(a)

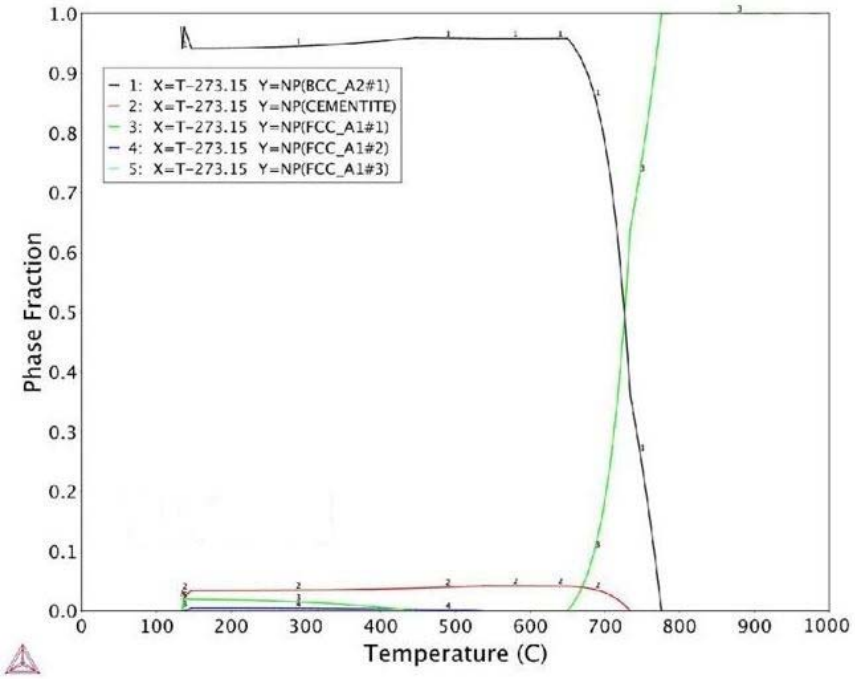

(b)

Figure 3-18. Calculated plots of the thermal stability of ferrite (BCC), cementite and austenite (FCC) in a)HSS and b)UHSS as a function of temperature using the software package, Thermo-Calc [13].

3.5. Predictive equations

In this section, the aim is to develop empirical equations for the stress-strain response of the UHSS material cooled from different fire temperatures to room temperature. According to Figure 3-7, the post-fire stress-strain curves obtained for the UHSS tube materials do not exhibit a pronounced yield point. The rounded and extended elasto-plastic transition observed for the UHSS is typical of advanced high strength steels and can also be observed in the stress-strain curves obtained for stainless steel specimens [44-46]. The sharp yield point is a feature especially characteristic of mild steels. In this study, the model used to predict the stress-strain response of the UHSS tube cooled from fire temperatures T to room temperature is based on the compound Ramberg-Osgood material model [45, 46] such that:

$$\varepsilon = \frac{\sigma}{E_{CT}} + 0.002\left(\frac{\sigma}{f_{0.2,CT}}\right)^{n_{CT}} \quad \text{for} \quad \sigma \le f_{0.2,CT}$$

$$\varepsilon = \frac{\sigma - f_{0.2,CT}}{E_{0.2,CT}} + \left(\varepsilon_{u,CT} - \varepsilon_{y,CT} - \frac{f_{u,CT} - f_{0.2,CT}}{E_{0.2,CT}}\right)\left(\frac{\sigma - f_{0.2,CT}}{f_{u,CT} - f_{0.2,CT}}\right)^{n'_{CT}} + \varepsilon_{y,CT} \qquad (3\text{-}2)$$

$$\text{for} \quad f_{0.2,CT} \le \sigma \le f_{u,CT}$$

where

$$E_{0.2,CT} = \frac{E_{CT}}{1 + 0.002 n_{CT} \dfrac{E_{CT}}{f_{0.2,\,CT}}} \qquad (3\text{-}3)$$

In the relations given in Eqs. (3-2) and (3-3), ε and σ are the engineering strain and stress, respectively, and the *CT* index is used for the properties of UHSS tube specimens tested after cooling from temperature *T* to room temperature. Also, n and n' are the exponential coefficients to take the material nonlinearity into consideration, whilst E and $E_{0.2}$ are the material's Young modulus and the tangent modulus at 0.2% proof stress, respectively. The definition of the remaining parameters used in Eq. (3-2) are illustrated in the schematic stress-strain curve shown in Figure 3-5.

By using the experimental results presented in the previous sections and finding the polynomials that have the best fit to the series of data points, the following predictive equations are obtained for the values of $f_{0.2,CT}$, $f_{u,CT}$ and $\varepsilon_{u,CT}$ in terms of the maximum

temperature T the UHSS specimens have experienced and also the corresponding parameter of the virgin material at room temperature.

$$\frac{f_{0.2,CT}}{f_{0.2,RT}}=\begin{cases}1 & 25 \le T \le 300\\ (118.15100-1.48514\,T+7.64380\cdot10^{-3}\,T^2-2.04374\cdot10^{-5}T^3+2.99481\cdot10^{-8}\,T^4 & \\ -2.28328\cdot10^{-11}\,T^5+7.08474\cdot10^{-15}\,T^6) & 300<T\le 800\end{cases} \quad (3\text{-}4)$$

$$\frac{f_{u,CT}}{f_{u,RT}}=\begin{cases}1 & 25 \le T \le 300\\ (73.04820-9.05365\cdot10^{-1}\,T+4.63958\cdot10^{-3}\,T^2-1.24018\cdot10^{-5}T^3 & \\ +1.82209\cdot10^{-8}\,T^4-1.39579\cdot10^{-11}\,T^5+4.35813\cdot10^{-15}\,T^6) & 300<T\le 800\end{cases} \quad (3\text{-}5)$$

$$\frac{\varepsilon_{u,CT}}{\varepsilon_{u,RT}}=\begin{cases}1 & 25 \le T \le 300\\ (33.31250-2.49832\cdot10^{-1}\,T+6.27862\cdot10^{-4}T^2-4.49286\cdot10^{-7}\,T^3 & \\ -3.33432\cdot10^{-10}\,T^4+4.2094\cdot10^{-13}\,T^5) & 300<T\le 800\end{cases} \quad (3\text{-}6)$$

where the *RT* index represents the virgin UHSS tube material tested at room temperature. It is worth noting that E and $E_{0.2}$ are independent of the temperature history of the UHSS tube specimens and are assumed to be constant, i.e. $E_{RT}=E_{CT}$ and $E_{0.2,RT}=E_{0.2,CT}$.

Also, according to Figure 3-5, $\varepsilon_{y,CT}$ can be determined from

$$\varepsilon_{y,CT}=\frac{f_{0.2,CT}}{E_{RT}}+0.002 \quad (3\text{-}7)$$

In order to find the values of the exponential coefficients n_{CT} and n'_{CT} in terms of the maximum fire temperature (*T*) the specimens have experienced, a nonlinear regression analysis is performed using the stress-strain curves shown in Figure 3-7 and Eq. (3-2). Hence, the following equations are derived:

$$n_{CT}=\begin{cases}6.4 & 25 \le T \le 300\\ (-125.43100+1.09094\,T-3.21568\cdot10^{-3}\,T^2+4.02685\cdot10^{-6}\,T^3 & \\ -1.82703\cdot10^{-9}\,T^4) & 300<T\le 800\end{cases} \quad (3\text{-}8)$$

$$n'_{CT}=\begin{cases}13.3 & 25 \le T \le 300\\ -138.73300+9.71289\cdot10^{-1}\,T-1.88696\cdot10^{-3}\,T^2+1.12958\cdot10^{-6}\,T^3 & 300<T\le 800\end{cases} \quad (3\text{-}9)$$

In order to validate the proposed material model shown in Eq. (3-2), the stress-strain curves obtained from the model and the experimental tests for the UHSS tube specimens cooled from different fire temperatures are depicted in Figure 3-19. Similar to the

labelling system used in Figure 3-7, the stress-strain curves of the UHSS **c**ooled from fire temperature ***T*** to room temperature obtained from the experiment and the proposed model are shown as UHSS-**C*T*** and UHSS-**C*T***-Model, respectively. Also, the stress-strain curves of the virgin UHSS material at room temperature obtained from the experiment and the proposed model are displayed as UHSS-**RT** and UHSS-**RT**-Model, respectively. Figure 3-19 indicates that a good accuracy is resulted from the stress-strain curves predicted by the proposed material model for the UHSS throughout the entire range of fire temperatures. It is worth noting that the main advantage of the model is that it is only taking the basic parameters of the UHSS at room temperatures, i.e. E_{RT} , $f_{0.2,RT}$, $f_{u,RT}$, $\varepsilon_{u,RT}$, and the maximum fire temperature T as input data. These parameters are usually known by the engineers and are commonly provided in the material data sheet by the steel manufacturing companies. Therefore, although using only $f_{0.2,RT}$ and $f_{u,RT}$ as input characteristic strength values have led to a gap between the 0.2% proof stress and the flat plastic region of UHSS-C800 and UHSS-C800-Model curves, the accuracy of the proposed model is still good enough to be applied for the engineering problems.

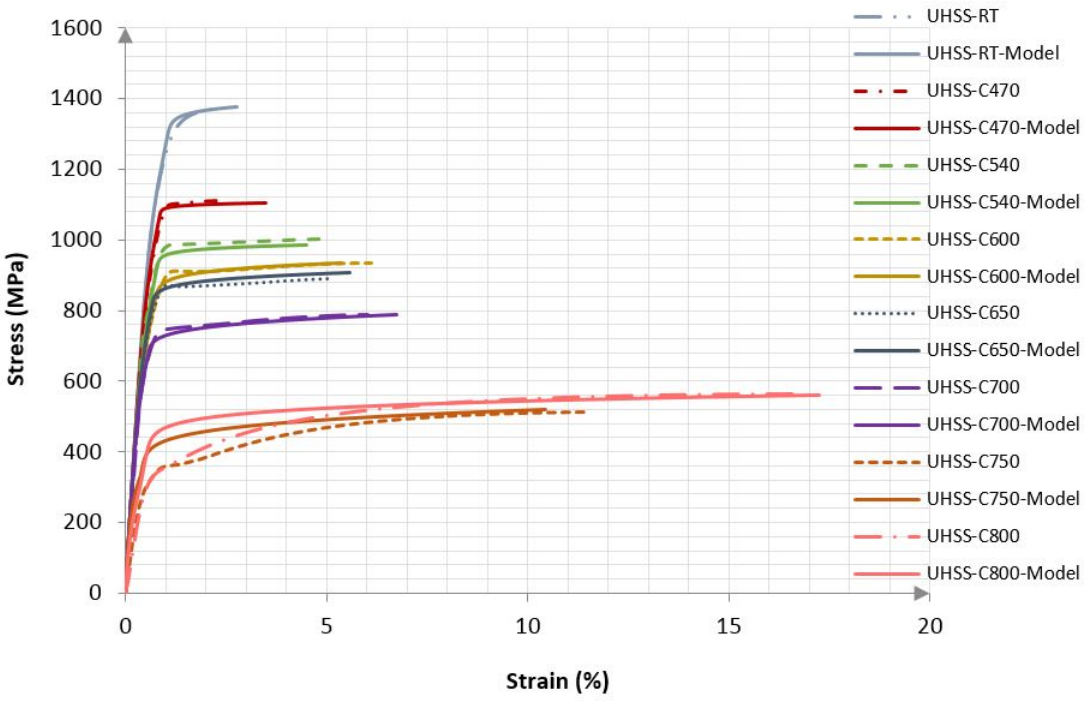

Figure 3-19. Comparison of Stress-strain curves of the test data and the proposed model for the UHSS tube specimens cooled from different elevated temperatures to room temperature

3.6. Conclusion

In this paper, the in-fire and post-fire mechanical behaviour of the Grade 1200 ultra-high strength steel (UHSS) tube subjected to fire temperatures ranging from 300°C to 800 °C were studied. According to the results obtained from the tensile tests conducted on the UHSS tube specimens at elevated temperatures, there is a considerable reduction in the strength of the specimens subjected to fire temperatures above 300°C, such that at fire temperatures as high as 800°C, the material becomes so soft that most of its strength is deteriorated. As for investigation of the post-fire mechanical behaviour of the UHSS tube, the strain-controlled tensile tests were conducted on the UHSS tube specimens at room temperature after being cooled from different fire temperatures. The results showed that although the deterioration in the strength of the UHSS tube starts after exposure to temperatures above 470°C, the most significant reduction in the residual strength can be observed when the material is cooled from fire temperatures above 600°C. However, once the UHSS is cooled from fire temperatures above ~750°C, the strength reduction becomes stabilised such that no more strength reduction is predicted if the specimens are cooled from fire temperatures higher than 750°C. In order to investigate the effect of steel grade on the in-fire and post-fire mechanical behaviour of steel, similar tests were conducted on the Grade 800 high strength steel (HSS) tube specimens. It was shown that there is a significant change in the post-fire stress-strain curves of the HSS tube specimens subjected to fire temperatures above 700°C. These conclusions were rationalised by considering the thermodynamic stability of the phases present in the microstructure of the UHSS and HSS materials and how these change when heating above ~700°C.

Using optical micrographs taken from the bulk microstructure of the UHSS specimens cooled from fire temperatures above 700°C and comparing them to SEM images taken from that of the UHSS specimen in its original state, the microstructural reason for the results obtained from the mechanical tests were explained. An empirical material model was finally proposed for the post-fire behaviour of the UHSS. The empirical model has a potential to be incorporated in the civil engineering codes of practice as well as

commercial finite element packages where rational fire safety design and evaluation are required.

Acknowledgement

The research work presented in this paper was supported by the Australian Government-Department of Education and also by Australian Research Council through a Discovery Project (DP150100442) awarded to the second and third authors. The authors acknowledge the use of facilities at Monash Centre for Electron Microscopy. The authors thank SSAB Corporation for providing ultra-high strength and high strength steel tubes.

References

[1] P. Beardmore, The potential for high strength steels in the U.S. automotive industry, Materials & Design, 2 (1981) 250-259.
[2] Y. Mukai, Development of new high-strength steel sheets for automobiles, R and D: Research and Development Kobe Steel Engineering Reports, 55 (2005) 30-35.
[3] T. Nonaka, H. Taniguchi, K. Goto, K. Yamazaki, Development of ultra-high-strength cold-rolled steel sheets for automotive use, Nippon Steel Technical Report, (2003) 13-15.
[4] M.A. Bradford, X.P. Liu, Flexural-torsional buckling of high-strength steel beams, Journal of Constructional Steel Research, 124 (2016) 122-131.
[5] M. Nassirnia, A. Heidarpour, X.-L. Zhao, J. Minkkinen, Innovative hollow corrugated columns: A fundamental study, Engineering Structures, 94 (2015) 43-53.
[6] F. Javidan, A. Heidarpour, X.L. Zhao, J. Minkkinen, Performance of innovative fabricated long hollow columns under axial compression, Journal of Constructional Steel Research, 106 (2015) 99-109.
[7] F. Azhari, A. Heidarpour, X.-L. Zhao, C.R. Hutchinson, Mechanical properties of ultra-high strength (Grade 1200) steel tubes under cooling phase of a fire: An experimental investigation, Construction and Building Materials, 93 (2015) 841-850.
[8] A. Heidarpour, S. Cevro, Q.-Y. Song, X.-L. Zhao, Behaviour of stub columns utilising mild-steel plates and VHS tubes under fire, Journal of Constructional Steel Research, 95 (2014) 220-229.
[9] N. Sadeghi, A. Heidarpour, X.L. Zhao, R. Al-Mahaidi, Numerical investigation of innovative modular beam-to-fabricated column connections under monotonic loading, in: Insights and Innovations in Structural Engineering, Mechanics and Computation - Proceedings of the 6th International Conference on Structural Engineering, Mechanics and Computation, SEMC 2016, 2016, pp. 1247-1252.
[10] M. Farahi, A. Heidarpour, X.-L. Zhao, R. Al-Mahaidi, Parametric study on the static compressive behaviour of concrete-filled double-skin sections consisting of corrugated plates, Thin-Walled Structures, 107 (2016) 526-542.
[11] Q.-Y. Song, A. Heidarpour, X.-L. Zhao, L.-H. Han, Post-earthquake fire behavior of welded steel I-beam to hollow column connections: An experimental investigation, Thin-Walled Structures, 98, Part A (2016) 143-153.
[12] M. Mirmomeni, A. Heidarpour, X.L. Zhao, C.R. Hutchinson, J.A. Packer, C. Wu, Mechanical properties of partially damaged structural steel induced by high strain rate loading at elevated temperatures - An experimental investigation, International Journal of Impact Engineering, 76 (2014) 178-188.
[13] S. Sinaie, A. Heidarpour, X.L. Zhao, Stress-strain-temperature relation for cyclically-damaged structural mild steel, Engineering Structures, 77 (2014) 84-94.
[14] S. Hosseini, A. Heidarpour, F. Collins, C.R. Hutchinson, Effect of strain ageing on the mechanical properties of partially damaged structural mild steel, Construction and Building Materials, 77 (2015) 83-93.
[15] S. Sinaie, A. Heidarpour, X.L. Zhao, Mechanical properties of cyclically-damaged structural mild steel at elevated temperatures, Construction and Building Materials, 52 (2014) 465-472.
[16] S.P. Chiew, M.S. Zhao, C.K. Lee, Mechanical properties of heat-treated high strength steel under fire/post-fire conditions, Journal of Constructional Steel Research, 98 (2014) 12-19.

[17] S. Gunalan, M. Mahendran, Experimental investigation of post-fire mechanical properties of cold-formed steels, Thin-Walled Structures, 84 (2014) 241-254.
[18] J. Outinen, Mechanical properties of structural steel at elevated temperatures and after cooling down, in: 10th International Conference - Fire and Materials 2007.
[19] X. Qiang, F.S.K. Bijlaard, H. Kolstein, Post-fire mechanical properties of high strength structural steels S460 and S690, Engineering Structures, 35 (2012) 1-10.
[20] X. Qiang, F.S.K. Bijlaard, H. Kolstein, Post-fire performance of very high strength steel S960, Journal of Constructional Steel Research, 80 (2013) 235-242.
[21] W. Wang, T. Liu, J. Liu, Experimental study on post-fire mechanical properties of high strength Q460 steel, Journal of Constructional Steel Research, 114 (2015) 100-109.
[22] M. Amraei, T. Skriko, T. Björk, X.-L. Zhao, Plastic strain characteristics of butt-welded ultra-high strength steel (UHSS), Thin-Walled Structures, 109 (2016) 227-241.
[23] A. Heidarpour, N.S. Tofts, A.H. Korayem, X.L. Zhao, C.R. Hutchinson, Mechanical properties of very high strength steel at elevated temperatures, Fire Safety Journal, 64 (2014) 27-35.
[24] ASTM Standard E8/E8M, in: Standard Test Methods for Tension Testing of Methallic Materials, ASTM International, West Conshohocken, PA: USA, 2011.
[25] Australian Standard AS1391, in: Methods for tensile testing of metals, Standards Australia, 1 the Crescent, Homebush, NSW 2140, Australia, 1991.
[26] V.A. Narang, Heat transfer analysis in steel structures, in, Worcester Polytechnic Institute, 2005.
[27] S. Brohez, C. Delvosalle, G. Marlair, A two-thermocouples probe for radiation corrections of measured temperatures in compartment fires, Fire Safety Journal, 39 (2004) 399-411.
[28] K. Harada, Y. Yabuki, T. Terai, A Theoretical Consideration On Heat Transfer In Fire Resistance Furnaces For Furnace Harmonization, Fire Safety Science 5(1997) 1033-1044.
[29] Y. Ling, Uniaxial True Stress-Strain after Necking, AMP Journal of Technology 5(June, 1996).
[30] Australia Standards AS4100, Steel structures, Sydney, Australia, 1998.
[31] American Institution of Steel Construction (AISC), Specification for Structural Steel Buildings, ANSI/AISC, in, Chicago, 2010.
[32] ASM, Atlas of Stress-Strain Curves, 2nd Edition, ASM International, 2002.
[33] R. Fonseca, I. Dario, Correction of the post -necking true stress - strain data using instrumented nanoindentation, in, The University of North Carolina at Charlotte, 2014.
[34] L. Wang, W. Tong, Identification of post-necking strain hardening behavior of thin sheet metals from image-based surface strain data in uniaxial tension tests, International Journal of Solids and Structures, 75–76 (2015) 12-31.
[35] K. Zhao, L. Wang, Y. Chang, J. Yan, Identification of post-necking stress–strain curve for sheet metals by inverse method, Mechanics of Materials, 92 (2016) 107-118.
[36] Australian/New Zealand Standard AS/NZS 4600, Cold-Formed Steel Structures, Standards Australia, Sydney, Australia and Standards New Zealand, Wellington, New Zealand, 2005.
[37] European Code 3,Eurocode 3: Design of Steel Structures, European Committee for Standardization, Brussels, Belgium, 2010.
[38] H.K.D.H. Bhadeshia, S.R. Honeycombe, Chapter 5 - Formation of Martensite, in: H.K.D.H.B.R. Honeycombe (Ed.) Steels (Third Edition)-Microstructure and Properties, Butterworth-Heinemann, Oxford, 2006, pp. 95-128.

[39] M. Gouné, F. Danoix, J. Ågren, Y. Bréchet, C.R. Hutchinson, M. Militzer, G. Purdy, S. van der Zwaag, H. Zurob, Overview of the current issues in austenite to ferrite transformation and the role of migrating interfaces therein for low alloyed steels, Materials Science and Engineering: R: Reports, 92 (2015) 1-38.
[40] D. Panahi, H. Van Landeghem, C.R. Hutchinson, G. Purdy, H.S. Zurob, New insights into the limit for non-partitioning ferrite growth, Acta Materialia, 86 (2015) 286-294.
[41] C. Qiu, H.S. Zurob, C.R. Hutchinson, The coupled solute drag effect during ferrite growth in Fe–C–Mn–Si alloys using controlled decarburization, Acta Materialia, 100 (2015) 333-343.
[42] C. Qiu, H.S. Zurob, D. Panahi, Y. Brechet, G.R. Purdy, C.R. Hutchinson, Quantifying the solute drag effect on ferrite growth in Fe-C-X alloys using controlled decarburization experiments, Metallurgical Transactions A, 44 (2013) 3472-3483.
[43] H.S. Zurob, D. Panahi, C.R. Hutchinson, Y. Brechet, G.R. Purdy, Self-Consistent Model for Planar Ferrite Growth in Fe-C-X Alloys, Metallurgical Transactions A, 44 (2013) 3456-3471.
[44] I. Arrayago, E. Real, L. Gardner, Description of stress–strain curves for stainless steel alloys, Materials & Design, 87 (2015) 540-552.
[45] E. Mirambell, E. Real, On the calculation of deflections in structural stainless steel beams: an experimental and numerical investigation, Journal of Constructional Steel Research, 54 (2000) 109-133.
[46] K.J.R. Rasmussen, Full-range stress–strain curves for stainless steel alloys, Journal of Constructional Steel Research, 59 (2003) 47-61.

Chapter 4

Post-fire Effect of creep strain on mechanical behaviour of ultra-high strength (Grade 1200) steel subject to cooling phase of a fire

This chapter has been published in the Journal of *Construction and Building Materials*, Volume 136, April 2017, Pages 18-30.

DOI: 10.1016/j.conbuildmat.2017.01.025

Reprinted here with the Author Rights granted by Elsevier.

Table of Contents

Abstract

This paper evaluates the mechanical behaviour of Grade 1200 ultra-high strength steel (UHSS) tube under a multi-phase loading scenario including fire and creep. To achieve this, two sets of experiments are performed on standard dog-bone specimens taken from UHSS tubes. In the first set of experiments, termed Creep-Heat-up tests, the specimens are axially loaded to a specific stress level, f_s. Whilst the axial load is maintained, the samples are heated to elevated temperatures of up to 700°C and a tensile test is performed on them at elevated temperature. The second set of experiments, which are the main focus of this study, are termed Creep-Cooling tests and are similar to the first set except that the specimens are tested to failure after being cooled to room temperature. The axial load in this set of tests is maintained during both heat-up and cooling phases of a fire. The stress-strain curves, the creep strain the specimens experience due to the sustained axial load during fire, and the residual strength of the test specimens are discussed. In order to investigate the effect of steel grade, Grade 800 high strength steel (HSS) and Grade 350 mild steel (MS) specimens are also tested and the results are compared. Finally, the microstructural origin of accelerated softening in UHSS due to creep strain is discussed.

Key Words: ultra-high strength steel, fire, creep, cooling, stress-strain curve, sustained load

4.1. Introduction

During the past decades, the high strength and energy absorption characteristics of ultra-high strength steels (UHSS) have made steel manufacturing companies interested in offering these materials to the automotive industry. The high strength to weight ratio of UHSS means they may also have some potential to be used in structures to produce energy efficient members. Innovative fabricated columns composed of ultra-high strength steel (UHSS) tubes with nominal yield strength of 1200MPa have recently been proposed [1-3]. The superior mechanical properties of these columns show the potential of UHSS to be used as a structural material.

The behaviour of steel structures under different loading scenarios have been widely investigated, e.g. [4, 5]. Nevertheless, to ensure the safety and durability of the structure, it is also necessary to understand the behaviour of construction materials under extreme events such as fire [6]. However, there is currently a lack of relevant design codes accounting for the behaviour of Grade 1200 UHSS under fire conditions in the available steel standards.

A fire has two main phases: the heat-up phase where the temperature reaches its peak, and the cooling phase, where the fire enters its decay stage and the temperature reduces to ambient. In order to analyse a structure subjected to fire, it is necessary to understand the behaviour of the construction material under both heat-up and cooling phases. When a structural member survives the heat-up phase of a fire and is cooled to room temperature, its residual strength determines whether or not it is reusable. In recent years, there has been a great focus on evaluating the mechanical behaviour of steel at elevated temperatures [7-12]. Comparatively fewer works have focused on the behaviour of steels after being cooled from fire temperatures [13-17]. Regarding the mechanical behaviour of UHSS under fire conditions, an experimental study on coupons taken from UHSS (Grade 1200) tubes subjected to low fire temperatures (up to 600°C) [18] as well as high fire temperatures (up to 800°C) [19] has recently been performed. The changes occurring in the tensile mechanical properties of UHSS at elevated temperatures and after being cooled to room temperature were discussed.

When a fire hazard occurs in a structure, in addition to the severe changes of the structural members due to thermal loading, the sustaining loads (such as dead loads, live

loads, etc.) may also affect the in-fire (elevated temperature) and post-fire (ambient) mechanical response of the structural material. In order to simulate fire loading of the steel, the mechanical loads present during the fire must also be considered. In other words, during a real fire in a structure, the temperature is increasing to its peak and decreasing to room temperature while the structural member is subjected to mechanical loads. This may cause creep in which the strain in a structural member varies under load [20]. Consequently, assuming that during the heat-up and cooling phases of fire, the load applied to the structural members are sustained, a study of the thermal creep of the material along with its effect on the mechanical response under temperature variations is necessary to simulate a real fire situation.

Many researchers have investigated the creep failure of steel subjected to elevated temperatures [21-27]. Morovat et al. investigated the creep behaviour of ASTM A992 steel at elevated temperatures [27]. They reported that creep is significantly dependant on the temperature and stress level of the material during fire. Brnic et al. evaluated the creep behaviour of high-strength low-alloy steel at elevated temperatures. They carried out uniaxial creep tests for different elevated temperatures and different loads [22]. The same authors performed an experimental study on the behaviour of heat-resistant austenitic steel subjected to uniaxial stress at elevated temperatures of up to 800°C and investigated its creep resistance at different temperatures for different loads [21].

In the present work, in order to simulate the behaviour of UHSS (Grade 1200) during the cooling phase of a fire, tensile coupons taken from UHSS tube specimens are subjected to a sustained tensile axial load (F_s) during both heat-up and cooling phases of fire and strain-controlled tensile tests are subsequently performed. Unlike the previously mentioned researches where the steel material was subjected to creep failure at elevated temperatures, in the present study, the UHSS is not subjected to creep failure. Although creep occurs in the UHSS during the heat-up and cooling phases of fire, the material is failed by performing tensile tests of the test specimens so that the residual strength after creep can be quantified. Similar multi-phase studies were conducted on concrete filled steel tube and reinforced concrete under compression loads [28, 29]. In these works, they applied different constant loads to the specimens and increased the temperature while the load was maintained, then performed compression tests on test specimens until failure.

In the present study, two sets of tests are performed: Creep-Heat-up tests and Creep-Cooling tests. The Creep-Heat-up tests investigate the effect of creep on mechanical behaviour of UHSS (Grade 1200) at elevated temperatures. The Creep-Cooling tests, which are the main focus of this work, evaluate the effect of creep on mechanical behaviour of UHSS subject to cooling phase of a fire. The variation in creep strain, the stress-strain curves obtained from the tensile tests and the residual strength of the UHSS specimens after different tests are calculated and discussed.

In order to evaluate the effect of steel grade, the same tests are performed on samples of Grade 800 high strength steel (HSS) and Grade 350 mild steel (MS) tube specimens and the results are compared with those of UHSS specimens. For the HSS and MS materials, after being cooled from temperatures of up to 600°C to room temperature their strength remain relatively unchanged [18]. Therefore, the maximum fire temperature considered for them is 700°C. The microstructural origin of the accelerated softening in UHSS due to the creep strain occurring during elevated temperature loading is characterised using Scanning Electron Microscopy (SEM) and the physical origin of the softening is discussed.

4.2. Experimental tests

4.2.1. Test Specimens

Three grades of steel tubes are considered in this study: Grade 1200 ultra-high strength steel (UHSS), Grade 800 high strength steel (HSS) and Grade 350 mild steel (MS). The chemical compositions of these materials are shown in Table 4-1. Due to the lack of knowledge about the behaviour of UHSS under fire and creep, and also its high sensitivity to elevated temperature exposures [18], this steel is the main focus of this study and the HSS and MS tubes are tested for the purpose of comparison. Standard dog-bone test specimens are extracted from the steel tubes using water-jet cutting. The nominal diameter and wall thickness of all tubes are 76.1mm and 3.2mm, respectively. The geometry and location of the specimens sectioned from the steel tubes are illustrated in Figure 4-1.

Table 4-1. The chemical compositions of tested materials (wt %)

Material	C	Si	Mn	P	S	Cr	Ni	Mo	B	Al
UHSS	0.230	0.800	1.700	0.025	0.015	1.500	1.000	0.500	0.005	
HSS	0.100	0.250	2.100	0.020	0.010					0.015
MS	0.230	0.400	1.350	0.040	0.050					

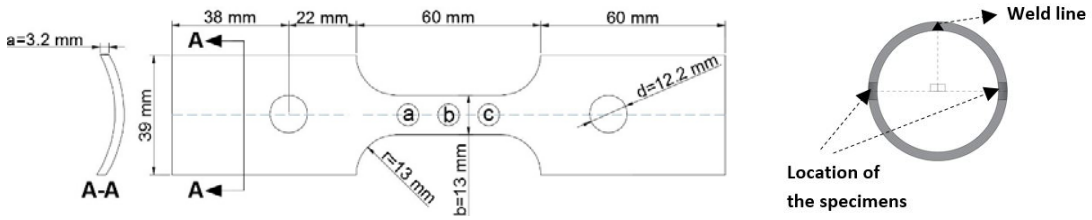

(a) **(b)**

Figure 4-1. a) Geometry and b) location of test specimens sectioned from the steel tubes

Using the instructions provided in AS1391 [30], the ends of the test specimens are mechanically flattened to be gripped for the tensile test. The cross section area (S_0) of the gauge length of the test specimens is calculated by [30]:

$$S_0 = \frac{b}{4}(D^2 - b^2)^{\frac{1}{2}} + \frac{D^2}{4}\arcsin\frac{b}{D} - \frac{b}{4}[(D-2a) - b^2]^{\frac{1}{2}} - (\frac{D-2a}{2})^2 \arcsin\frac{b}{D-2a} \qquad (4\text{-}1)$$

in which, *b* and *a* are the width and thickness of the specimen gauge length (Figure 4-1.a) and *D* is the tube diameter.

4.2.2. Test Method

Two sets of experimental tests, Creep-Heat-up tests and Creep-Cooling tests are performed to investigate the mechanical behaviour of UHSS under the multi-phase loading scenario of creep and fire.

4.2.2.1. Creep-Heat-up tests

In this set of tests, the test specimen is first loaded to the tensile load of F_s using the Instron 5982 100kN testing machine on which a SF-16 split furnace is installed (Figure

4-2). F_s is defined as the sustained axial load applied to the specimen and is obtained from $F_s = f_s S_0$, where S_0 is the cross sectional area of the specimen (Eq. (4-1)) and f_s is determined by

$$f_s = \beta f_{u,T} \tag{4-2}$$

In Eq.(2), $f_{u,T}$ is the ultimate tensile strength of the test material at elevated temperature T and β is the sustained axial load ratio.

The furnace is subsequently set to the target fire temperature T and is switched on. During the heat up, the testing machine is operating under load control so that the upper jaw of the machine could displace to accommodate the thermal expansion of the specimen while the load remains constant at F_s. Once the temperatures of the three thermocouples attached to three points *a*, *b* and *c* on the specimen's gauge length (Figure 4-1) are stabilised at the target temperature *T*, the temperature is held constant for 20 mins. Subsequently, the tensile loading is continued under strain-controlled conditions with an applied strain rate of $0.005 \pm 0.002\,\text{min}^{-1}$[31] until failure. The strain rate is remained constant by the movement of the cross-head of the testing machine. In order to monitor the creep strain during the heat-up phase and the 20min elevated temperature hold, and also the strain variation during the tensile test, the model 3448 High Temperature Contact Extensometer with approximate gauge length of 25mm is used. The test setup is illustrated in Figure 4-2.

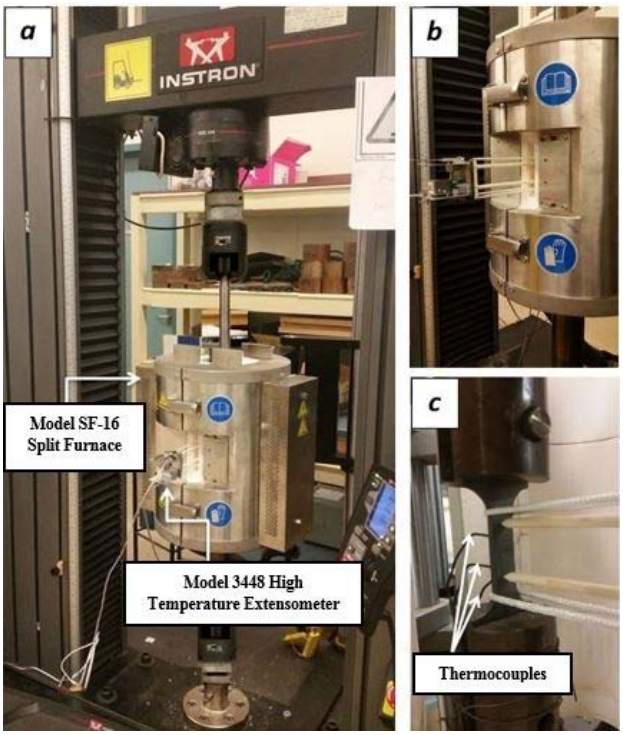

Figure 4-2. Testing apparatus including (a) Instron 100kN machine; (b) furnace, and (c) high temperature contact extensometer

4.2.2.2. Creep-Cooling tests

This set of tests are designed to perform a multi-phase evaluation of creep and cooling phase of a fire. The test procedure is similar to the Creep-Heat-up tests except that once the temperature of the test specimen is stabilised at the target temperature for 20min, the furnace is switched off and allowed to cool to room temperature under load control. Once the specimen reaches room temperature, tensile loading is continued under strain-controlled conditions until failure. The test procedure can be divided into 4 stages:

Stage I: Loading the test specimen to $F_s = f_s S_0$;

Stage II: Heating up the test specimen to fire temperature T while subjected to $F_s = f_s S_0$ until the temperatures of all three thermocouples are stabilised;

Stage III: Cooling the test specimen from temperature T to room temperature (RT) while subjected to $F_s = f_s S_0$;

Stage IV: Performing tensile test on the test specimen until failure

The schematic representation of the last situation of the specimen at each of the above-mentioned stages is illustrated in Figure 4-3. The grey and red colours in this figure denote the stages at which the final temperature is the room temperature (*RT*) and the target fire temperature (*T*), respectively.

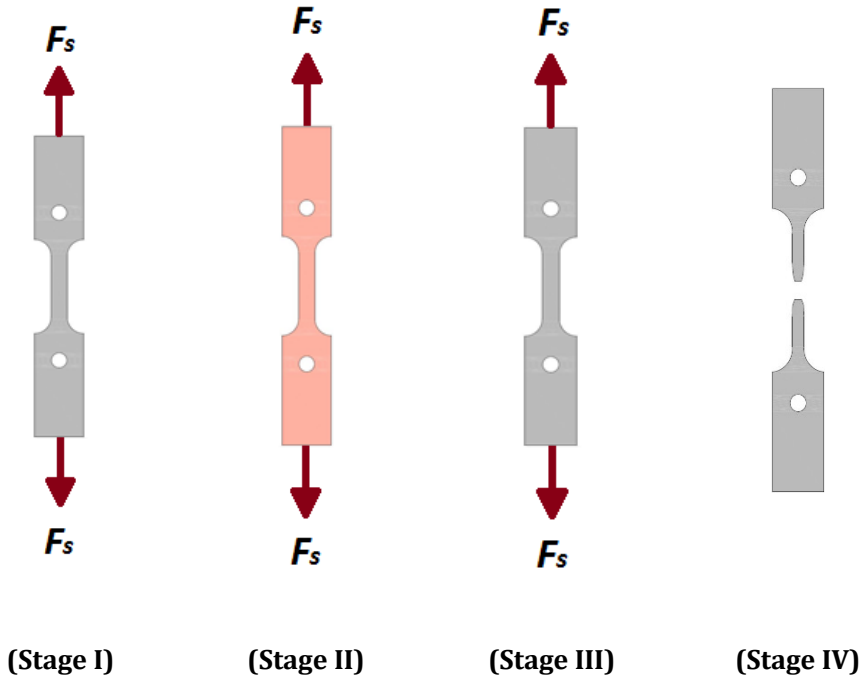

Figure 4-3. Schematic representation of the Creep-Cooling test procedure divided into 4 stages

4.3. Results and Discussions

4.3.1. Definition of mechanical properties

To investigate the mechanical properties of the test materials under creep and cooling phase of a fire, the stress-strain curves, the creep strain values, characteristic tensile strengths and ductility parameters are extracted from experimental tests. To better understand the test procedure and the evolution of the creep strain during a Creep-Cooling test, the variation of temperature with respect to axial strain during a typical Creep-Cooling test is demonstrated in Figure 4-4.a. The stage number defined in the previous section corresponding to different parts of this graph as well as the strain values at different stages of the test are indicated in this figure. In Figure 4-4.b, the strain values

and characteristic tensile strengths on a typical stress-strain curve are illustrated. Note that all values depicted in these figures are engineering values in which the original cross-section area and gauge length are used.

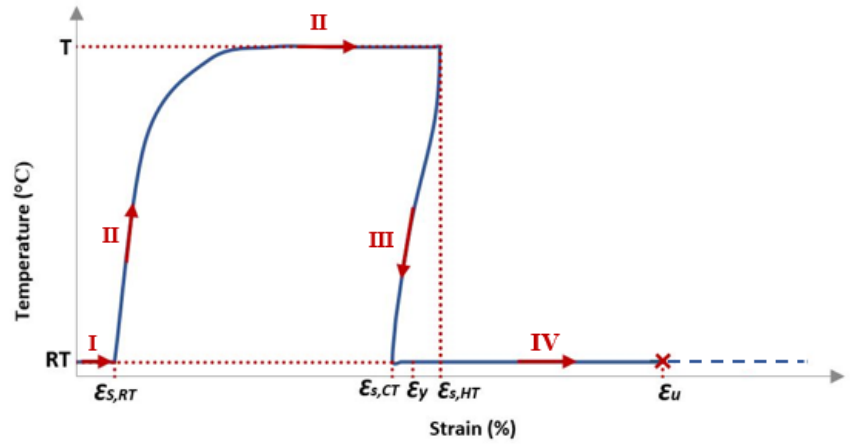

(a)

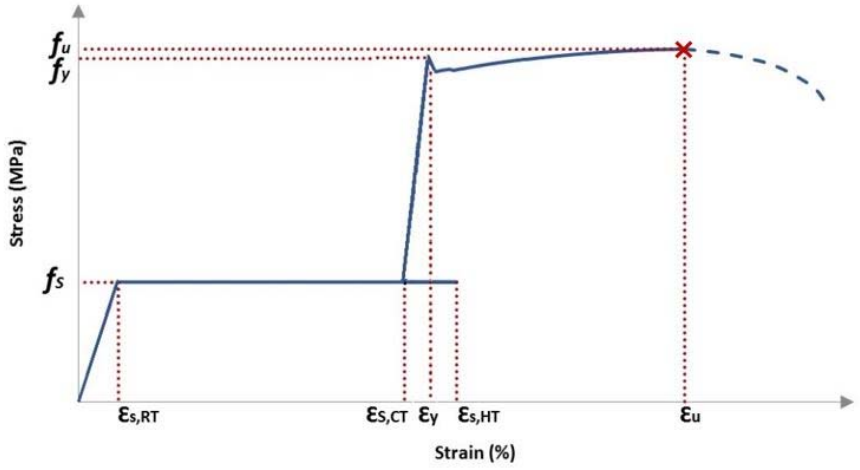

(b)

Figure 4-4. Definition of mechanical properties on typical a) temperature-strain and b) stress-strain curves for a Creep-Cooling test

The creep strain is defined as:

$$\Delta\varepsilon_{cr} = \varepsilon_{s,CT} - \varepsilon_{s,RT} \tag{4-3}$$

where $\Delta\varepsilon_{cr}$ is the net creep strain the test specimen experiences during the test. As illustrated in Figure 4-4.b, $\varepsilon_{s,RT}$ and $\varepsilon_{s,CT}$ are the strain values under **s**ustained axial load before the heat-up stage at **r**oom **t**emperature and after being **c**ooled from elevated temperature ***T*** to room temperature, respectively.

The strain occurring in the material due to the **th**ermal expansion of the specimen heated to temperature *T* is called thermal strain ($\Delta\varepsilon_{th}$) and is calculated by:

$$\Delta\varepsilon_{th} = \varepsilon_{s,HT} - \varepsilon_{s,CT} \tag{4-4}$$

where, $\varepsilon_{s,HT}$ is the strain value of the test specimen under **s**ustained axial load at the end of the **h**eat-up stage (Stage II) at elevated temperature ***T***. As can be observed from Figure 4-4.a, since after cooling the specimen under the sustained axial load from temperature *T* to room temperature, $\Delta\varepsilon_{th}$ is recovered in the material, it is concluded that this strain difference between the end of stages II and III is due to the thermal expansion of the material.

The tensile yield stress (f_y) and the ultimate tensile strength (f_u) are calculated from the experiments performed. As shown in Figure 4-4.b, f_y represents the upper pronounced yield point and f_u refers to the maximum tensile strength in the stress-strain curve.

The sustained axial load applied to the specimen is determined by $F_s = f_s S_0$, where S_0 and f_s are defined in Eqs. (4-1) and (4-2), respectively. In Eq. (4-2), the values of $f_{u,T}$ for different temperatures *T* are obtained from Ref. [19] and are summarised in Table 4-2. The values of the sustained axial load ratio β should be determined such that the material does not fail at the end of stage II, i.e. $\beta < 1$. Based on the limit states requirement for steel members subjected to tension provided in Australian standards, the capacity factor to be considered for a safe design should not exceed 0.9 [32]. Therefore, the range of β considered in this study is $0.6 \le \beta \le 0.85$ so that plastic strain develops in the test specimen during stage II, while it also satisfies the safe design recommended by the standards. Since the test material loses the majority of its strength at temperatures above

700°C, in order to apply 0.85% of its strength at the elevated temperature, i.e. $f_s = 0.85 f_{u,T}$, loads lower than 2kN would be applied to the test specimen. This low load is in the bottom 10% of the load cell capacity for our machine which is the regime where the force readings are less precise. Although in Ref. [19] heat-up tests were conducted on steel materials at elevated temperatures up to 800°C, in this study 700°C is considered as the maximum fire temperature so as to be operating in that range of the Instron load cell where we may have the best confidence in the force measurements.

Table 4-2. Variation of the ultimate tensile strength of the UHSS tube specimens undergone strain-controlled tensile test at elevated temperature T ($f_{u,T}$)[19]

T	**300°C**	**470°C**	**540°C**	**600°C**	**700°C**
$f_{u,T}\,(MPa)$	1270	780	563	340	119

The strain values corresponding to f_y and f_u represent the yield strain (ε_y) and the uniform elongation (ε_u), respectively. Since the material begins to neck at the uniform elongation (ε_u), the strain readings after ε_u are inaccurate. In this paper, the stress-strain curves prior to necking of the specimens, i.e. up to ε_u, are reported and the post-necking behaviour (shown by broken lines in Figure 4-4) is not investigated. Although ε_y can be calculated from the values of f_y and the elastic modulus of the material (E), due to the importance of variation of ε_y for different applications in civil engineering, the values of this parameter are also reported in this paper.

4.3.2. Stress-strain curves

To understand the behaviour of UHSS under a multi-phase loading scenario including creep and fire, the in-fire and post-fire mechanical behaviour of the UHSS specimens subjected to creep with a constant sustained axial load ratio of $\beta = 0.8$ are investigated for different fire temperature exposures. The stress-strain curves of the UHSS specimens subjected to Creep-**C**ooling tests (UHSS-**C*T***-0.8) and Creep-**H**eat-up tests (UHSS-**H*T***-0.8) with $\beta = 0.8$ and different maximum fire temperatures $\boldsymbol{T}$ ($300°C \le T \le 700°C$) are presented in Figure 4-5.a-e. To facilitate comparison and better illustrate the effect of

creep during fire, the stress-strain curves for the UHSS specimens tested when **h**eated-up to elevated temperature ***T*** and after being **c**ooled to room temperature without sustained axial load ($\beta = 0$) [19] are also included in these figures. These curves are labelled UHSS-**H*T*** and UHSS-**C*T***, respectively. For example, in Figure 4-5.a, the UHSS-C300 and UHSS-C300-0.8 stress-strain curves are obtained from strain-controlled tensile tests performed on UHSS specimens after cooling from 300°C to room temperature without being subjected to any axial load, i.e. $\beta = 0$, and when subjected to 80% of the ultimate tensile strength of UHSS at 300°C, i.e. $f_s = 0.8 f_{u,300}$ or $\beta = 0.8$, during the heat-up and cooling phases, respectively. Similarly, the UHSS-H300 and UHSS-H300-0.8 stress-strain curves represent tensile tests performed on UHSS specimens at 300°C without any axial load ($\beta = 0$) and while subjected to axial load ratio of $\beta = 0.8$ during the heat-up phase, respectively. By looking at the stress-strain curve shown in Figure 4-4 for a typical Creep-Cooling test and Eq. (4-4), it can be understood that the difference between the lengths of the horizontal lines in the middle of UHSS-C300-0.8 and UHSS-H300-0.8 stress-strain curves represent the thermal strain ($\Delta\varepsilon_{th}$) indicating the thermal expansion of the UHSS that was recovered when cooling to room temperature.

It can be observed from Figure 4-5.a-e that the creep strain experienced by the UHSS specimens during fire increases significantly for fire temperatures above 470°C. By comparing UHSS-H*T* and UHSS-C*T* curves with the corresponding UHSS-C*T*-0.8 and UHSS-H*T*-0.8 ones, it can be concluded that although the creep strain does not have a strong influence on the in-fire (elevated temperature) strength of UHSS specimens, for $T \geq 470°C$, it results in a considerable reduction in the post-fire (ambient temperature) strength of these specimens. It is also apparent from these curves that the higher the maximum fire temperature, the larger creep strain observed and the greater the reduction in ambient temperature strength of the materials. Although for all the Creep-Cooling tests of Figure 4-5 β is constant at 0.8, greater creep strain occurs in the specimens exposed to higher fire temperatures. As expected, it can be understood from UHSS-H*T*-0.8 and UHSS-C*T*-0.8 curves that the maximum creep strain ($\Delta\varepsilon_{cr} + \Delta\varepsilon_{th}$) experienced by the specimens is almost equal for those subjected to both Creep-Heat-up and Creep-Cooling tests with the same maximum fire temperature *T*. However, there is

no thermal creep strain recovery for the specimens subjected to Creep-Heat-up tests so $\Delta\varepsilon_{th} = 0$.

The occurrence of creep in the UHSS specimens during fire, results in a pronounced yield point in their post-fire stress-strain curves. This is especially obvious in Figures 4-1.c-e. After UHSS specimens are exposed to elevated temperatures, the carbon (C) atoms find sufficient mobility to segregate to dislocations at elevated temperatures and pin them. When a cooled specimen is then subjected to a tensile test, the stress applied to the specimen must first unpin the dislocations to yield the material. This stress to unpin at room temperature is usually greater than the stress to subsequently propagate dislocations through the microstructure during deformation and as a result, a sharp yield point is observed. This phenomena has been discussed in [18].

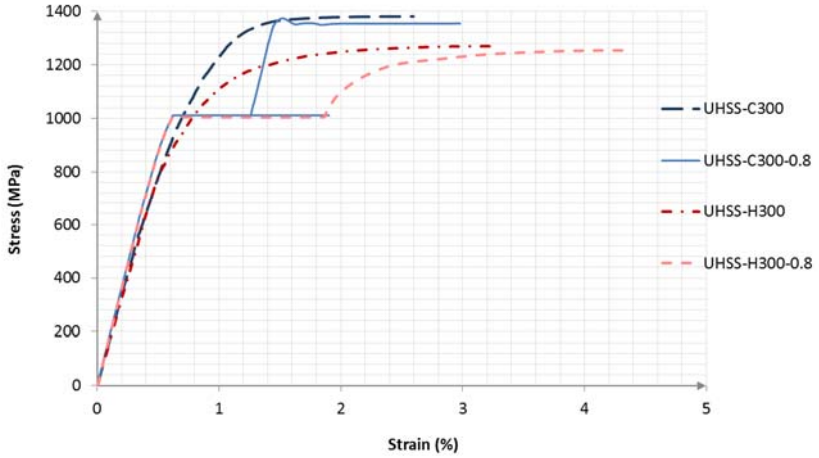

(a)

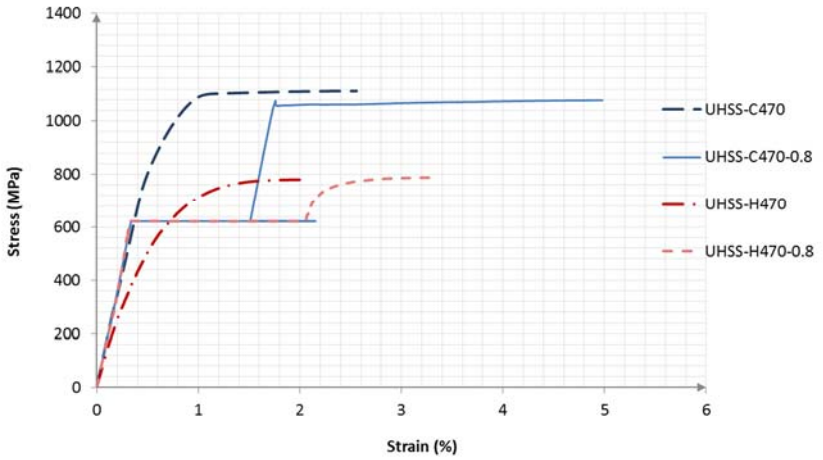
Stress (MPa)
Strain (%)
UHSS-C470
UHSS-C470-0.8
UHSS-H470
UHSS-H470-0.8

(b)

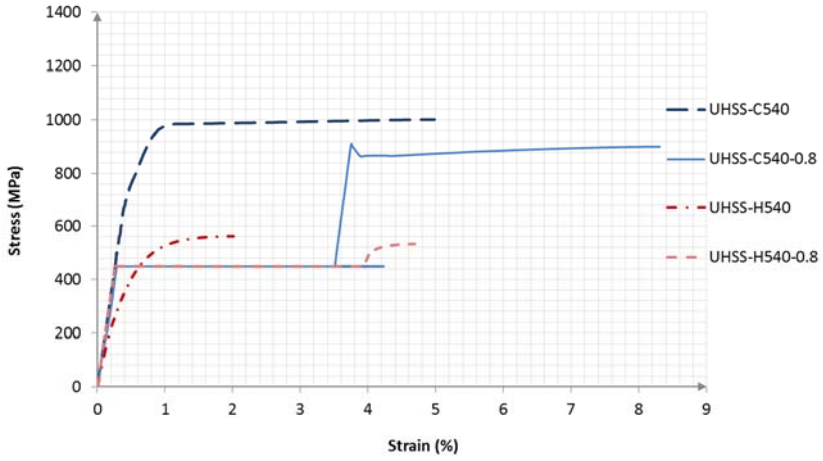
Stress (MPa)
Strain (%)
UHSS-C540
UHSS-C540-0.8
UHSS-H540
UHSS-H540-0.8

(c)

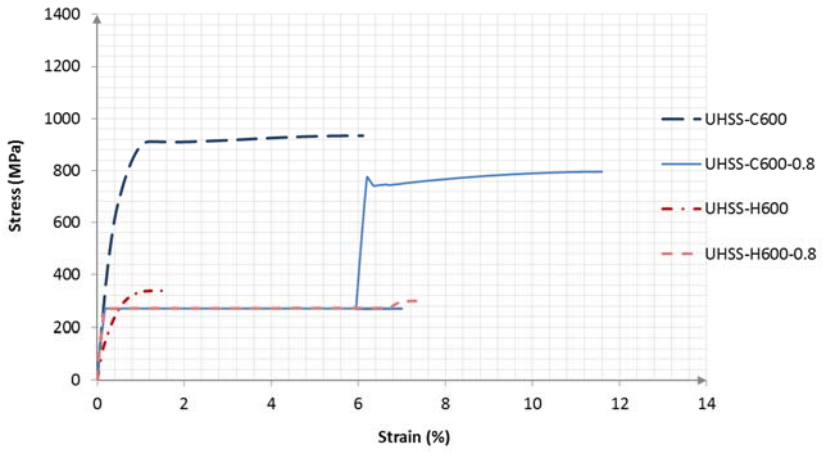
Stress (MPa)
Strain (%)
UHSS-C600
UHSS-C600-0.8
UHSS-H600
UHSS-H600-0.8

(d)

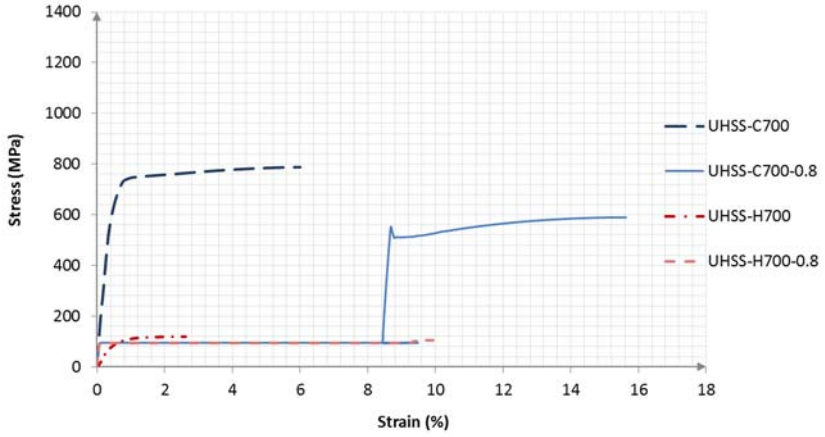

(e)

Figure 4-5. Stress-strain curves for UHSS specimens at a) 300°C b) 470°C, c) 540°C, d) 600°C and e) 700°C and after being cooled to room temperature while subjected to sustained axial load ratio of β=0.8

In order to evaluate the effect of the sustained axial load ratio, β, in a creep-fire multi-phase loading scenario, the stress-strain curves of the UHSS specimens subjected to different values of β ($0.6 \le \beta \le 0.85$) and cooled from 600°C to room temperature are shown in Figure 4-6. By comparing the stress-strain curves of UHSS-C600 and UHSS-C600-0.6, where the value of the sustained axial load is 60% of the ultimate strength of the UHSS tested at 600°C, a negligible strength difference is observed under the conditions of a 20min elevated temperature hold employed in this study. However, for larger values of β, i.e. $\beta > 0.6$, the difference between the ultimate strength of UHSS-C600 and UHSS-C600-β curves becomes significant. This implies that the sustained axial load does not significantly affect the strength of the UHSS specimens tested after being cooled from a 20min hold at 600°C, unless the value of the sustained axial load (F_s) is larger than 60% of the ultimate strength of UHSS at 600°C. The higher values of β also lead to larger values of creep strain for the UHSS specimens subjected to tensile tests after being cooled from 600°C to room temperature. By increasing β from 0.75 to 0.8, a considerable reduction in strength is observed. This means there exists a critical axial load ratio, i.e. $\beta = 0.8$, above which increasing the load becomes more critical and affects the creep and strength reduction more seriously. As can be seen from Figure 4-6,

increasing the value of F_s up to 85% of the ultimate strength of UHSS at 600°C, leads to a large creep strain and a significant reduction in the strength of the UHSS cooled to room temperature. These results can be used to determine the true value of the allowable sustained axial load which can be applied to the structural members made of UHSS material during a fire hazard.

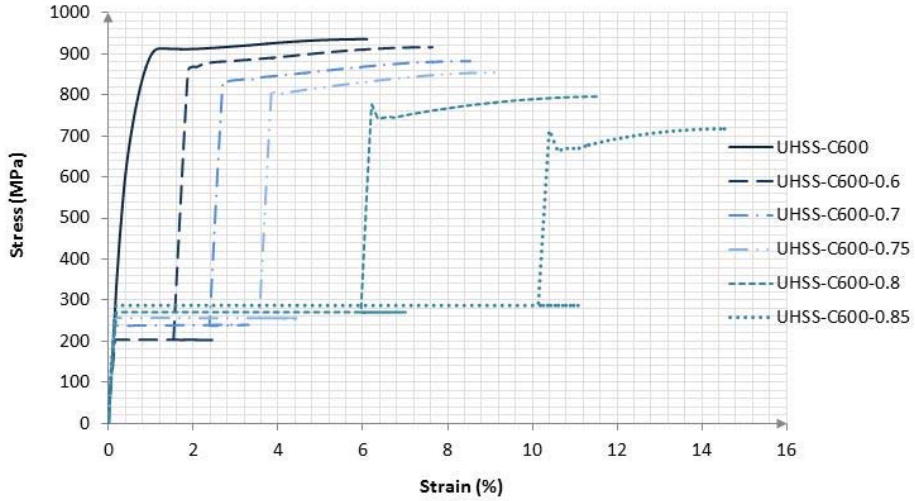

Figure 4-6. Stress-strain curves for UHSS specimens after cooling down from 600°C to room temperature subjected to different sustained axial load ratios (β)

4.3.3. Creep strain

In this section, the variation of creep strain is discussed for the UHSS specimens subjected to the multi-phase loading scenario considered in this paper. Calculation of the net creep strain ($\Delta\varepsilon_{cr}$) and the thermal strain ($\Delta\varepsilon_{th}$) from the stress-strain curves was explained in section 4.3.1. In Table 4-3, the values of $\Delta\varepsilon_{cr}$ and $\Delta\varepsilon_{th}$ for the UHSS-C***T***-0.8 curves ($300°C \le T \le 700°C$) are presented, where $\Delta\varepsilon_{cr,CT,\beta}$ and $\Delta\varepsilon_{th,CT,\beta}$ refer to the $\Delta\varepsilon_{cr}$ and $\Delta\varepsilon_{th}$ values of the specimens subjected to Creep-**C**ooling tests with the maximum fire temperature ***T*** and sustained axial load ratio of β. Looking at the variation of the values of the net creep strain with the maximum fire temperature *T*, it is evident that a considerable increase in $\Delta\varepsilon_{cr,CT,0.8}$ starts from *T*=540°C, i.e. $\Delta\varepsilon_{cr,C540,0.8} = 3.22\%$. As *T* increases above 540°C, the value of creep strain grows larger such that for *T*=700°C,

$\Delta\varepsilon_{cr,C700,0.8}$ reaches 8.35%. As expected, the variation of $\Delta\varepsilon_{th,CT,0.8}$ with *T*, is much less considerable compared to $\Delta\varepsilon_{cr,CT,0.8}$.

Table 4-3. Variation of the creep strain and thermal strain for UHSS specimens cooled from various fire temperatures under sustained axial load ratio of β=0.8

T	300°C	470°C	540°C	600°C	700°C
$\Delta\varepsilon_{cr,CT,0.8}$ (%)	0.64	1.18	3.22	5.77	8.35
$\Delta\varepsilon_{th,CT,0.8}$ (%)	0.63	0.64	0.72	0.90	1.04

In Table 4-4, the values of $\Delta\varepsilon_{cr}$ and $\Delta\varepsilon_{th}$ for the UHSS-C600-β curves, where β varies from 0.6 to 0.85 are presented. The values of $\Delta\varepsilon_{cr,C600,\beta}$ clearly illustrate the abrupt increase in the creep strain when β is larger than 0.75: $\Delta\varepsilon_{cr,C600,\beta}$ is almost doubled with every 0.5 increment in β. For $\beta = 0.85$, ~10% net creep strain is experienced by the UHSS specimen cooled from 600°C to room temperature. These results also explain the reason for selecting $\beta = 0.8$ as a critical sustained axial load ratio to study the effect of temperature in the Creep-Cooling and Creep-Heat-up tests (Figure 4-5 and Table 4-3). Of course, it is expected that the values of $\Delta\varepsilon_{th,C600,\beta}$ are constant for all β values, which supports the fact that thermal expansion is only a function of the maximum temperature T and is a representative of the creep percentage occurring due to the change in temperature and not the mechanical loading.

It is important to note that the variation of $\Delta\varepsilon_{cr,CT,\beta}$ with β for other maximum fire temperatures may be different from those obtained for *T*=600°C. In Ref. [18] the authors concluded from the thermal stability diagram of material phases that *T*=600°C is a critical maximum fire temperature for the UHSS material. In the current study, in order to study the effect of β, this temperature has been considered. If the constant temperature is considered as *T*=700°C, due to the small value of the ultimate strength at this temperature, considering β values of 0.6 or 0.7 would have led to a very small values of F_s which are less than the accuracy of the testing machine.

Another important point about the results obtained in this study is that other than the values of the sustained axial load ratio β, the absolute magnitude of the load may also affect the values of creep during a fire. In order to study the variation of the values of $\Delta\varepsilon_{cr}$ and $\Delta\varepsilon_{th}$ with the maximum temperature while the magnitude of the sustained axial load (F_s) is constant, a constant magnitude of F_s should be more than ~70% of the ultimate load capacity of UHSS at different fire temperatures ($F_{u,T} = f_{u,T}S_0$), i.e. $F_s \geq 0.7F_{u,T}$. Since there is a considerable difference between the values of $F_{u,T}$ for different maximum temperatures *T*, selecting a constant F_s which satisfies the condition of $F_s \geq 0.7F_{u,T}$ for all temperatures, is not possible.

Table 4-4. Variation of the creep strain for UHSS specimens cooled from 600°C under various sustained axial load ratios (β)

β	**0.6**	**0.7**	**0.75**	**0.8**	**0.85**
$\Delta\varepsilon_{cr,C600,\beta}$ (%)	1.39	2.25	3.39	5.77	9.96
$\Delta\varepsilon_{th,C600,\beta}$ (%)	0.86	0.85	0.86	0.90	0.88

Furthermore, it can be interpreted from Figure 4-5 that in order to calculate the values of net creep strain for the Creep-**H**eat-up tests, i.e. $\Delta\varepsilon_{cr,HT,\beta}$, the following relation can be simply used:

$$\Delta\varepsilon_{cr,HT,\beta} = \Delta\varepsilon_{cr,CT,\beta} + \Delta\varepsilon_{th,CT,\beta} \quad (4\text{-}5)$$

where the values of $\Delta\varepsilon_{cr,CT,\beta}$ and $\Delta\varepsilon_{th,CT,\beta}$ can be taken from Tables 4-3 and 4-4.

4.3.4. Strength and Ductility

The changes in the strength and ductility of UHSS specimens subjected to the multi-hazard loading schemes are also studied. The yield strength and the ultimate tensile strength values resulting from the Creep-**C**ooling tests with axial load ratio of β and the maximum fire temperature *T* denoted as $f_{y,CT,\beta}$ and $f_{u,CT,\beta}$, respectively, are calculated. The reduction in the values of $f_{u,CT,\beta}$ with respect to those reported in Ref. [19] for the

UHSS specimens cooled from different fire temperatures *T* without sustained axial load, i.e. $f_{u,CT}$, is defined as:

$$R_{u,CT,\beta}(\%) = (1 - \frac{f_{u,CT,\beta}}{f_{u,CT}}) \times 100 \quad (4\text{-}6)$$

Since in the stress-strain curves obtained for the UHSS specimens cooled from fire temperatures *T* to room temperature, i.e. UHSS-C***T*** curves shown in Figure 4-5, there is no such pronounced upper yield point, only the values of $f_{y,CT,\beta}$ are presented and no reduction factor is defined for them.

The strength values for the UHSS specimens subjected to Creep-Cooling tests with a constant axial load ratio of $\beta = 0.8$ and different maximum temperatures *T* and also those obtained from the tests with different values of β and a constant maximum temperature of *T*=600°C are presented in Tables 4-5 and 4-6, respectively. With increasing maximum fire temperature, it is shown that the values of $f_{y,CT,0.8}$ and $f_{u,CT,0.8}$ decrease significantly. A part of this strength reduction is due to the elevated temperature exposure and a part of it is due to the existence of sustained axial load and the consequent creep strain that changes the microstructure of the material in a direction that decreases its strength. In order to understand the latter part, values of the ultimate strength reduction factor defined in Eq. (4-6), i.e. $R_{u,CT,0.8}$, may be evaluated. As shown in Table 4-5, for the UHSS specimens cooled from temperatures of up to 470°C, the maximum reduction in the strength due to existence of creep is ~3% which is negligible. However, for the UHSS specimens subjected to Creep-Cooling tests with axial load ratio of $\beta = 0.8$ and maximum fire temperatures above 470°C, the ultimate strength reduces by 10 to 25% with respect to the same material cooled from the corresponding fire temperatures with $\beta = 0$. Therefore, in the design of UHSS structural members, neglecting the sustained load on the structure means disregarding a significant amount of strength reduction which may lead to an unsafe design.

From the results derived from the Creep-Cooling tests with maximum fire temperature of *T*=600°C and different β values (Table 4-6), it can be seen that the effect of sustained axial load and the consequential creep strain becomes significant when $\beta \geq 0.7$. As β

increases from 0.7 to 0.85, the reduction in ultimate tensile strength of the UHSS specimens cooled from 600°C to room temperature, i.e. $R_{u,C600,\beta}$, increases up to ~23% which is a considerable strength loss. For all the UHSS specimens cooled from 600°C while subjected to different sustained axial load ratios, the ultimate tensile strength ($f_{u,C600,\beta}$) is well above the corresponding yield stress ($f_{y,C600,\beta}$). This indicates that after the material yields, strain hardening occurs and strength increases such that prior to the necking of the sample, it can experience a higher stress level compared to the yield stress. The microstructural origin of the strength reduction of UHSS due to the creep loading during fire is explained in Section 4.4.

Table 4-5. Variation of strength for UHSS specimens cooled from various fire temperatures under sustained axial load ratio of β=0.8

Temperature	**300°C**	**470°C**	**540°C**	**600°C**	**700°C**
$f_{y,CT,0.8}\,(MPa)$	1373	1076	911	777	553
$f_{u,CT,0.8}\,(MPa)$	1354	1078	900	797	590
$R_{u,CT,0.8}(\%)$	1.4	3	10.2	14.8	25.2

Table 4-6. Variation of strength for UHSS specimens cooled from 600°C under various axial load ratios (β)

β	**0.6**	**0.7**	**0.75**	**0.8**	**0.85**
$f_{y,C600,\beta}\,(MPa)$	866	830	816	777	713
$f_{u,C600,\beta}\,(MPa)$	917	883	854	797	717
$R_{u,C600,\beta}(\%)$	2	5.7	8.7	14.8	23.4

To evaluate the ductility of the tested specimens, the values of yield strain (ε_y) and uniform elongation (ε_u) have been extracted from the tensile test results. ε_y and ε_u values resulting from the Creep-**C**ooling tests with axial load ratio of β and the maximum fire temperature *T*, shown as $\varepsilon_{y,CT,\beta}$ and $\varepsilon_{u,CT,\beta}$, respectively, are presented in Tables 4-7 and 4-8. It can be seen from Table 4-7 that for a constant axial load ratio, i.e. $\beta = 0.8$, as the maximum temperature the UHSS specimens have experienced increases, more

ductility is observed. The results shown in Table 4-8 indicate that for a constant fire temperature, i.e. T=600°C, increasing the axial load ratio (β) from 0.6 to 0.85 yields to a significant increase in ductility. This increase in ductility is a natural consequence of the decreasing ultimate strength which means necking (defining the uniform elongation) is postponed to larger strains (Considère criterion [33]). By comparing the variation of ductility values shown in Tables 4-7 and 4-8, it can be concluded that for the Creep-Cooling tests with β=0.8, ε_y and ε_u values are both increased by ~5 to 6 times when T increases from 300°C to 700°C. However, for Creep-Cooling tests with T=600°C, while increasing the values of β from 0.6 to 0.85 leads to increase of ε_y by ~5.5 times, ε_u values are only increased by ~2 times. This means that although increasing the axial load ratio (β) for Creep-Cooling tests with T=600°C results in a larger creep strain, it shortens the plastic plateau of the stress strain curves.

Table 4-7. Variation of ductility parameters for UHSS specimens cooled from various fire temperatures under sustained axial load ratio of β=0.8

Temperature	**300°C**	**470°C**	**540°C**	**600°C**	**700°C**
$\varepsilon_{y,CT,0.8}$ (%)	1.522	1.759	3.751	6.202	8.686
$\varepsilon_{u,CT,0.8}$ (%)	2.980	4.978	8.307	11.598	15.631

Table 4-8. Variation of ductility parameters for UHSS specimens cooled from 600°C under various axial load ratios (β)

β	**0.6**	**0.7**	**0.75**	**0.8**	**0.85**
$\varepsilon_{y,C600,\beta}$ (%)	1.896	2.696	3.855	6.202	10.394
$\varepsilon_{u,C600,\beta}$ (%)	7.640	8.542	9.150	11.598	14.596

4.3.5. Comparison with other steel grades

To evaluate the effect of steel grade on the mechanical behaviour of steel under the multi-phase loading scenario defined in this paper, the stress-strain curves of Grade 800 High Strength Steel (HSS) and Grade 350 Mild Steel (MS) tubes are also presented for a couple of tests. In Figure 4-7, the stress-strain curves of the virgin UHSS, HSS and MS tube

specimens tested at room temperature (RT) are presented. There is a considerable difference between the uniform elongation of the MS material compared to that of the UHSS and HSS. In Ref. [18], it was shown that unlike UHSS, there is no significant change in the strength of the HSS and MS specimens cooled from temperatures of up to 600°C (low fire temperatures) compared to their as-received strength. For these two materials, focus is placed on the maximum fire temperature of T=700°C. The stress-strain curves of the HSS and MS tube specimens subjected to Creep-Cooling test with maximum fire temperature of T=700°C and sustained axial load ratio of $\beta = 0.8$ are shown in Figures 4-8 and 4-9, respectively. The stress-strain curves of the HSS and MS specimens tested at 700°C, i.e. HSS-H700 and MS-H700, and after being cooled to room temperature, i.e. HSS-C700 and MS-C700, without being subjected to any sustained axial load are also included in these figures. To have a better comparison between the results of these three grades of steel, all the post-fire stress-strain curves are plotted in Figure 4-10.

By comparing the results of HSS-C700 and HSS-C700-0.8, it is evident that the HSS subjected to both creep and cooling phase of a fire experiences $\sim$6% strength reduction compared to that experiencing the cooling phase of a fire alone. This result shows that HSS is quite a resistant material to creep loading under fire conditions. From the MS-H700-0.8 curve, it can be concluded that the when the tensile test is carried out on the MS tube specimen at 700°C which was subjected to load ratio of $\beta = 0.8$ during the heat-up stage, the specimen can no longer bear any tensile load and is softened immediately after the start of the test which is displayed by a red triangle on this curve. However, it can be seen from MS-C700-0.8 curve that if this specimen is cooled to room temperature after reaching 700°C, part of its strength is recovered and the MS subjected to creep and cooling phases of a fire can harden up to 380MPa stress. Nevertheless, the fact that the in-fire strength of MS material, which is commonly used in structural engineering, is fully deteriorated when creep occurs prior to the loading at elevated temperature, makes the fire design of structures made of this material a critical issue. Comparing the stress-strain curves obtained for these three grades of steel, it can be concluded that while HSS is the most resistant material to creep under fire conditions, MS and UHSS are sensitive materials under multi-phase loading scenarios including both creep and elevated temperature exposures. Although there is a considerable reduction in the strength of UHSS materials subjected to creep and fire loadings, the residual strength of UHSS after

being subjected to the multi-phase loading scenario considered in this study is still close to the strength of the virgin MS material. Therefore, when designing UHSS structural members, if the effect of creep on the residual strength of these members after cooling from fire is taken into account, using UHSS material may still be a cost-efficient option.

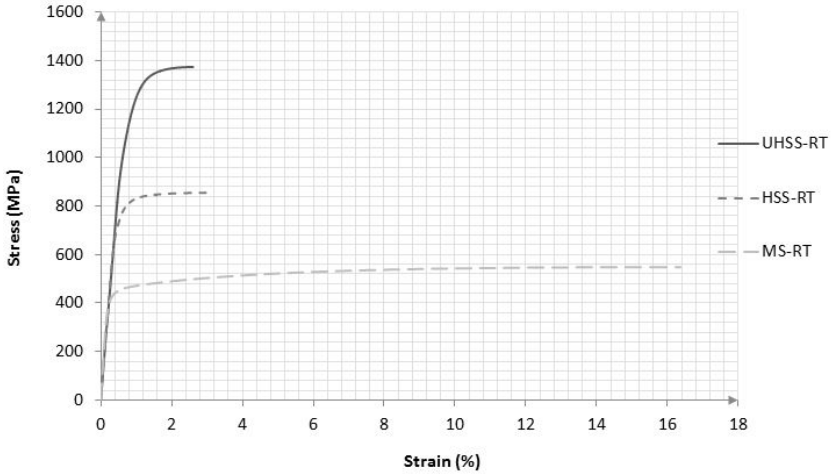

Figure 4-7. Stress-strain curves of MS, HSS and UHSS specimens at room temperature

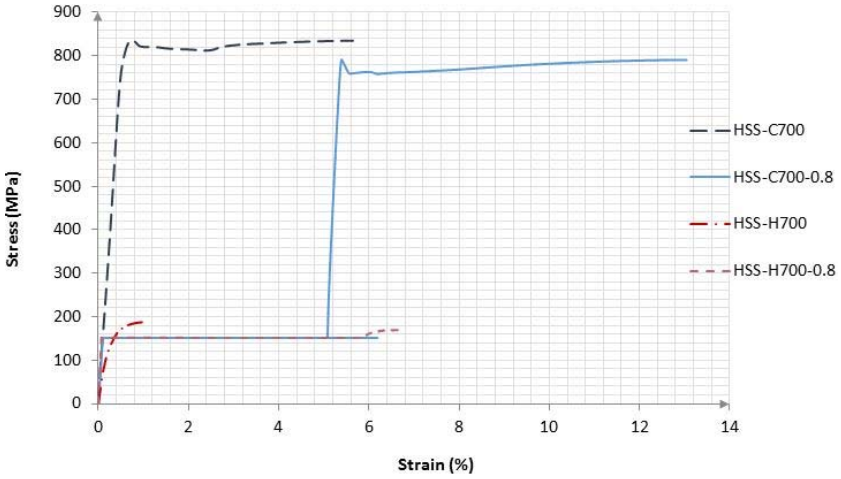

Figure 4-8. Stress-strain curves for HSS specimens at 700°C and after being cooled to room temperature with and without sustained axial load

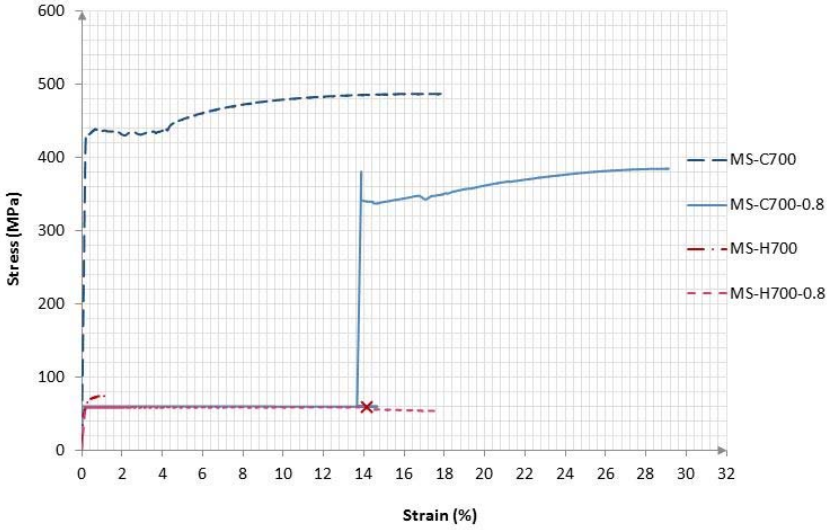

Figure 4-9. Stress-strain curves for MS specimens at 700°C and after being cooled to room temperature with and without sustained axial load

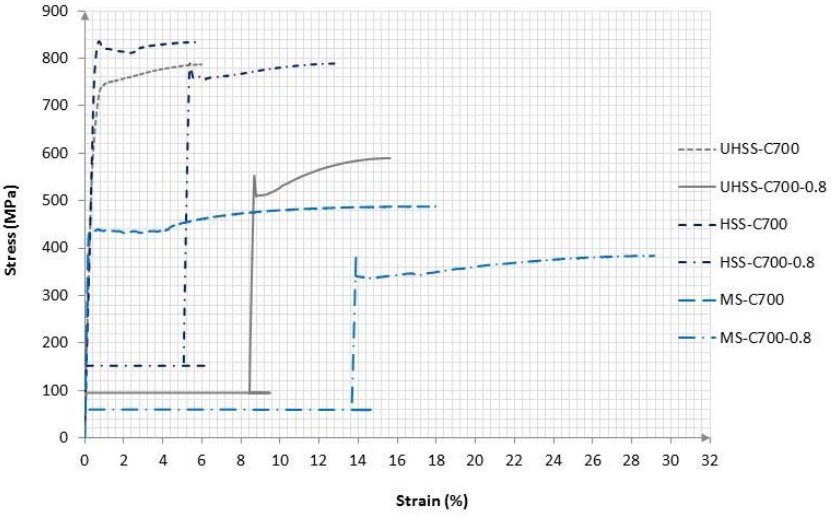

Figure 4-10. Comparison of Stress-strain curves for UHSS, HSS and MS specimens after being cooled from 700°C to room temperature with and without sustained axial load

4.4. Microstructural origin of accelerated softening due to creep strain

The high strength of the UHSS considered in this study is derived from a tempered martensitic microstructure [34]. Martensite is very strong but also brittle microstructure and in order to make it ductile so that it is applicable for engineering purposes, it is tempered. The tempering involves an elevated temperature hold at temperatures ranging from 300°C to 600°C. Tempering of martensite leads to precipitation of cementite particles and the removal of carbon from solid solution. This has the effect of decreasing the strength of the martensite, but also providing the necessary ductility and toughness for it to be useful in engineering applications. To have a better understanding of the phases present in this material, the SEM images taken from the bulk microstructure of the as-received UHSS material obtained in Ref. [18] are shown in Figure 4-11. The lath microstructure shown in these SEM images represents the martensitic microstructure, the dark regions and the small white particles represent the ferrite and cementite phases, respectively.

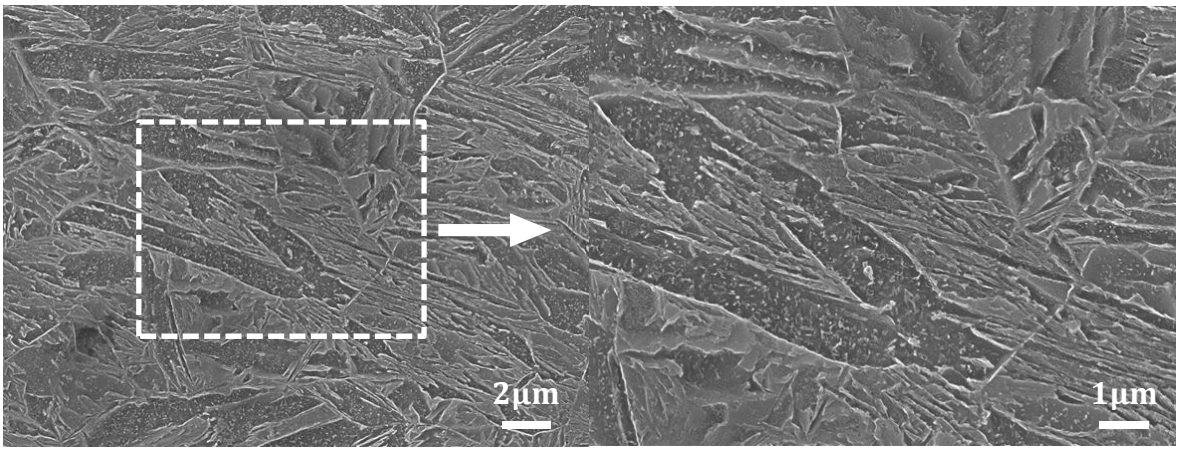

Figure 4-11. SEM micrographs of the bulk microstructure of the as-received UHSS specimen at room temperature [18]

When a UHSS is heated to fire temperatures, the tempering process of martensite effectively continues which leads to further softening of the material and the reduction in its strength. It was shown in Ref. [18] that after the UHSS material is cooled from 600°C, which is considered a low fire temperature, the lath microstructure of UHSS is partly deteriorated. However, the phases present in UHSS do not change in identity and only the size and configuration of the microstructural grains change.

When a UHSS material is subjected to the multi-phase loading scenario of creep and fire at the types of temperatures considered in this study, the tempering process is further accelerated and the UHSS will soften even more quickly. During the precipitation of cementite that occurs during tempering of the UHSS, the cementite particles will grow and coarsen. As they increase in average size, the strength of the martensite will decrease. This process is controlled by the diffusion of carbon and is a thermally activated process – this is why tempering occurs faster at higher temperatures and why softening will proceed with longer exposures at elevated temperature.

However, the UHSS examined in this study was subjected to both elevated temperature exposure and concurrent creep strain. The creep strain process involves the movement of dislocations in the microstructure. These dislocations can provide additional short circuit paths for carbon diffusion and further accelerate the tempering process. This leads to acceleration of the growth of the average precipitate size during straining at elevated temperature and accelerated softening of the UHSS.

To demonstrate the microstructural origin of the accelerated softening due to creep strain, the most extreme condition which is the maximum fire temperature of 700°C and the sustained axial load ratio of $\beta = 0.8$ is considered. Using scanning electron microscopy (SEM), micrographs have been obtained from two parts of a tensile specimen after cooling from 700°C to room temperature while subjected to the sustained axial load ratio of $\beta = 0.8$ during heat-up and cooling phases. To demonstrate the effect of only the elevated temperature exposure, SEM images are taken from the grip area of the UHSS specimen. To demonstrate the effect of concurrent elevated temperature exposure and creep strain SEM images are taken from the gauge area of the same UHSS specimen ensuring the comparison is between material that has experienced exactly the same thermal history and the only difference being part of it has sustained an additional creep strain. Figure 4-12 shows the low and high magnification SEM micrographs of the bulk microstructure of the UHSS specimen cooled from 700°C to room temperature without experiencing creep strain (Figure 4-12.a and c), and with the creep strain caused by sustained axial load ratio of $\beta = 0.8$ (Figure 4-12.b and d). By looking at the low magnification SEM images (Figure 4-12.a and b), it can be seen that the lath microstructure is still remained within both microstructures. However, by comparing the high magnification SEM images (Figure 4-12.d and c), it can be observed that the average

size of the white cementite precipitates in Figure 4-12.c is smaller than that of the SEM image shown in Figure 4-12.d. This is the direct demonstration of the acceleration of cementite growth due to the creep strain leading to coarsening of the carbide precipitates in the microstructure, and consequently a decrease in the strength of the UHSS. This strain-induced acceleration of precipitation processes is well known in the field of Materials Science and Engineering [35] and is exploited in the processing of many engineering alloys.

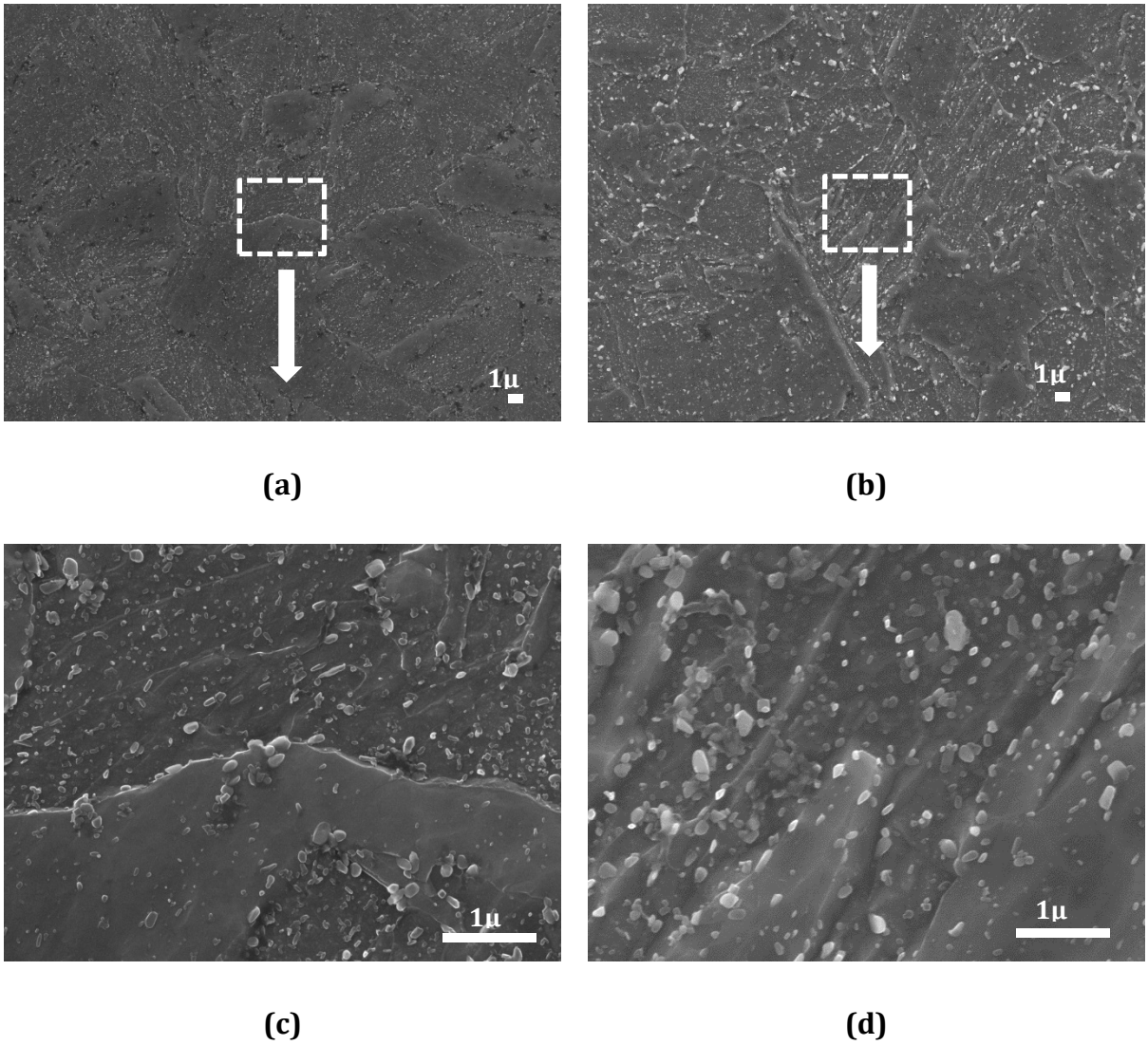

Figure 4-12. Low and high magnification SEM micrographs of the bulk microstructure of the UHSS specimen cooled from 700°C to room temperature a and c)without experiencing creep strain, and b and d)with creep strain caused by axial load ratio of β=0.8 during heat-up and cooling phases.

In order to quantitatively demonstrate the accelerated cementite precipitate growth caused by creep strain during fire, the size distribution of different precipitate sizes inside the microstructures of the UHSS specimens cooled from 700°C to room temperature without and with experiencing the creep strain caused due to the axial load ratio of $\beta = 0.8$ are illustrated in Figure 4-13 and labelled UHSS-C700 and UHSS-C700-0.8, respectively. It can be seen that for small size precipitates, i.e. precipitate diameter<1μm, the frequency of the particles for the UHSS specimen cooled 700°C without any axial load (UHSS-C700) is more than that experienced creep during fire (UHSS-C700-0.8). However, as the diameter of the precipitate increases above 1μm, the number of precipitates for the strained specimen (UHSS-C700-0.8) becomes more; such that the maximum precipitate diameter size in the strained specimen is larger than 0.4 μm, while for the UHSS specimen cooled from 700°C without experiencing creep, this value is less than 0.3 μm.

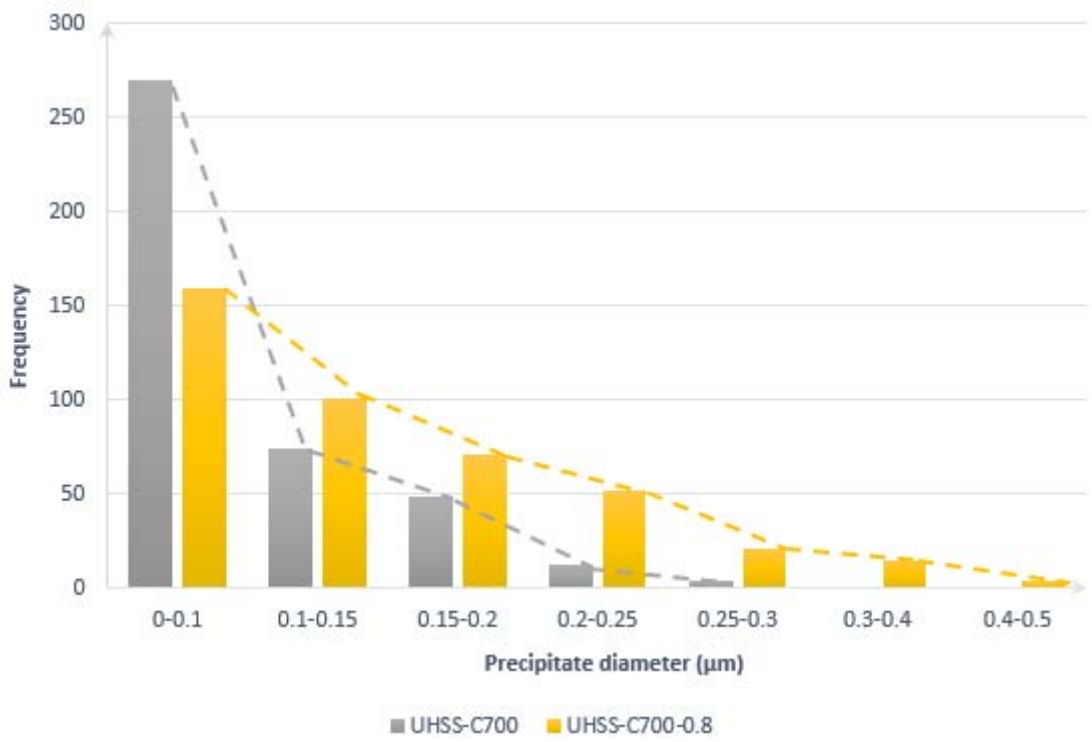

Figure 4-13. Distribution of the precipitate diameters for the UHSS specimens cooled from 700°C to room temperature without experiencing creep as compared to that subjected to sustained axial load of β=0.8 during heat-up and cooling phases.

As a result of the discussion made in this section, since tempering of martensite is controlled by C diffusion, it can be expected that as the maximum temperature the UHSS

experiences during fire increases, faster martensite tempering and consequently, faster softening is resulted. We may also expect that as the time the material is held at elevated temperature increases, the degree of softening will also increase. Furthermore, by increasing the value of axial load ratio β, due to the additional effect from the plasticity that occurs during the subsequent creep deformation, the martensite softening will further accelerate. Therefore, it was observed from the results shown in Figures 4-5 and 4-6 that increasing the maximum fire temperature and β may lead to a considerable reduction in strength of UHSS.

4.5. Conclusion

In this paper, experiments were performed to evaluate the mechanical behaviour of Grade 1200 ultra-high strength steel (UHSS) tube under a multi-phase loading scenario including creep and fire. Tensile tests were carried out on UHSS tube specimens cooled from fire temperatures ranging from 300°C to 700°C to room temperature while subjected to a sustained axial load during the heat-up and cooling phases of fire. The sustained axial load led to a creep strain in the test specimens cooled from fire. For comparison purposes, the test specimens subjected to the sustained axial load were also tested at elevated temperatures to evaluate the effect of cooling phase of fire. The stress-strain curves obtained from the experimental tests indicated that for a constant value of sustained axial load ratio β as the maximum temperature the specimens had experienced during fire was increased, the specimens experienced larger creep strains and consequently, the strength reduction became more significant. Also, for a constant maximum fire temperature, increasing the values of β up to 0.85 led to a considerable increase in the creep strain and a significant reduction in the strength of the UHSS specimens compared to the case where they had not experienced creep during fire. It is evident from the obtained results that the creep strain, which is resulted from the existence of sustained axial load on the specimens during fire, and the strength reduction have a direct relationship. Also, when a UHSS structural member is cooled from a fire, both the maximum fire temperature and the sustained loads applied to the member control its residual strength. To evaluate the effect of steel grade, the Creep-Heat-up tests and Creep-Cooling tests for maximum fire temperature of 700°C and $\beta = 0.8$ were also conducted on Grade 800 high strength steel (HSS) and Grade 350 mild steel (MS) tube

specimens. The results showed that while the HSS was the most resistant material to creep, the UHSS and MS experienced a significant creep strain during fire. Even though the UHSS was the most sensitive material to the existence of sustained axial load during fire, the residual strength was almost the same as that of the virgin MS at room temperature, which confirms the potential of this material to be used in structural engineering field. Using the scanning electron microscopy (SEM), the microstructural origin of accelerated softening in UHSS due to creep strain was discussed. It was shown that the creep strain during fire accelerated the cementite growth in the microstructure leading to a decrease in the strength of the UHSS.

Acknowledgement

This research work was supported by the Australian Government-Department of Education and also by Australian Research Council through a Discovery Project (DP130100181) awarded to the second and third authors. The authors would like to thank SSAB Corporation for providing high strength and ultra-high strength steel tubes. We also acknowledge the Monash Civil Engineering Workshop staff for their support in fabricating the tests specimens.

References

[1] F. Javidan, A. Heidarpour, X.-L. Zhao, J. Minkkinen, Performance of innovative fabricated long hollow columns under axial compression, Journal of Constructional Steel Research, 106 (2015) 99-109.
[2] M. Nassirnia, A. Heidarpour, X.L. Zhao, J. Minkkinen, Innovative hollow columns comprising corrugated plates and ultra high-strength steel tubes, Thin-Walled Structures, 101 (2016) 14-25.
[3] A. Heidarpour, S. Cevro, Q.-Y. Song, X.-L. Zhao, Behaviour of stub columns utilising mild-steel plates and VHS tubes under fire, Journal of Constructional Steel Research, 95 (2014) 220-229.
[4] M. Farahi, A. Heidarpour, X.-L. Zhao, R. Al-Mahaidi, Compressive behaviour of concrete-filled double-skin sections consisting of corrugated plates, Engineering Structures, 111 (2016) 467-477.
[5] S. Hosseini, A. Heidarpour, F. Collins, C.R. Hutchinson, Effect of strain ageing on the mechanical properties of partially damaged structural mild steel, Construction and Building Materials, 77 (2015) 83-93.
[6] Q.-Y. Song, A. Heidarpour, X.-L. Zhao, L.-H. Han, Post-earthquake fire behavior of welded steel I-beam to hollow column connections: An experimental investigation, Thin-Walled Structures, 98, Part A (2016) 143-153.
[7] J. Outinen, Mechanical properties of structural steel at elevated temperatures and after cooling down, in: 10th International Conference - Fire and Materials 2007.
[8] L. Gardner, A. Insausti, K.T. Ng, M. Ashraf, Elevated temperature material properties of stainless steel alloys, Journal of Constructional Steel Research, 66 (2010) 634-647.
[9] A. Heidarpour, N.S. Tofts, A.H. Korayem, X.L. Zhao, C.R. Hutchinson, Mechanical properties of very high strength steel at elevated temperatures, Fire Safety Journal, 64 (2014) 27-35.
[10] M. Mirmomeni, A. Heidarpour, X.L. Zhao, C.R. Hutchinson, J.A. Packer, C. Wu, Mechanical properties of partially damaged structural steel induced by high strain rate loading at elevated temperatures - An experimental investigation, International Journal of Impact Engineering, 76 (2014) 178-188.
[11] S. Sinaie, A. Heidarpour, X.L. Zhao, Mechanical properties of cyclically-damaged structural mild steel at elevated temperatures, Construction and Building Materials, 52 (2014) 465-472.
[12] L. Gardner, Y. Bu, P. Francis, N.R. Baddoo, K.A. Cashell, F. McCann, Elevated temperature material properties of stainless steel reinforcing bar, Construction and Building Materials, 114 (2016) 977-997.
[13] X. Qiang, F.S.K. Bijlaard, H. Kolstein, Post-fire performance of very high strength steel S960, Journal of Constructional Steel Research, 80 (2013) 235-242.
[14] S.P. Chiew, M.S. Zhao, C.K. Lee, Mechanical properties of heat-treated high strength steel under fire/post-fire conditions, Journal of Constructional Steel Research, 98 (2014) 12-19.
[15] X. Qiang, X. Jiang, F.S.K. Bijlaard, H. Kolstein, Y. Luo, Post-fire behaviour of high strength steel endplate connections — Part 1: Experimental study, Journal of Constructional Steel Research, 108 (2015) 82-93.
[16] X. Qiang, F.S.K. Bijlaard, H. Kolstein, R. Xia, Experimental study on high strength structural steel S460 in fire and after cooling down, IES Journal Part A: Civil and Structural Engineering, 6 (2013) 104-111.

[17] W. Wang, T. Liu, J. Liu, Experimental study on post-fire mechanical properties of high strength Q460 steel, Journal of Constructional Steel Research, 114 (2015) 100-109.
[18] F. Azhari, A. Heidarpour, X.-L. Zhao, C.R. Hutchinson, Mechanical properties of ultra-high strength (Grade 1200) steel tubes under cooling phase of a fire: An experimental investigation, Construction and Building Materials, 93 (2015) 841-850.
[19] F. Azhari, A. Heidarpour, X.-L. Zhao, C.R. Hutchinson, Post-fire mechanical response of ultra-high strength (Grade 1200) steel tubes subjected to temperatures of up to 800°C: linking thermal stability and microstructure, International Journal of Mechanical Sciences (Submitted in 15.Feb.2016, Under review).
[20] R. Solecki, P.R. Conant, Advanced mechanics of materials, Oxford University Press; 2003, New York.
[21] J. Brnic, G. Turkalj, M. Canadija, S. Krscanski, M. Brcic, D. Lanc, Deformation behaviour and material properties of austenitic heat-resistant steel X15CrNiSi25-20 subjected to high temperatures and creep, Materials & Design, 69 (2015) 219-229.
[22] J. Brnic, G. Turkalj, M. Canadija, D. Lanc, Creep behavior of high-strength low-alloy steel at elevated temperatures, Materials Science and Engineering: A, 499 (2009) 23-27.
[23] M. Cowan, K. Khandelwal, Modeling of high temperature creep in ASTM A992 structural steels, Engineering Structures, 80 (2014) 426-434.
[24] D.-B. Park, S.-M. Hong, K.-H. Lee, M.-Y. Huh, J.-Y. Suh, S.-C. Lee, W.-S. Jung, High-temperature creep behavior and microstructural evolution of an 18Cr9Ni3CuNbVN austenitic stainless steel, Materials Characterization, 93 (2014) 52-61.
[25] A.G.d. Reis, D.A.P. Reis, A.J. Abdalla, J. Otubo, High-temperature creep resistance and effects on the austenite reversion and precipitation of 18 Ni (300) maraging steel, Materials Characterization, 107 (2015) 350-357.
[26] Q. Yang, T. Zheng, D. Zhang, F. Bu, X. Qiu, X. Liu, J. Meng, Creep behavior of high-pressure die-cast Mg-4Al-4La-0.4Mn alloy under medium stresses and at intermediate temperatures, Materials Science and Engineering: A, 650 (2016) 190-196.
[27] A. Morovat, J. Lee, M. Engelhardt, E. Taleff, T. Helwig, V. Segrest, Creep Properties of ASTM A992 Steel at Elevated Temperatures, Proceedings, Second International Conference on Structures and Building Materials, 446-449 (2012).
[28] J. Huo, G. Huang, Y. Xiao, Effects of sustained axial load and cooling phase on post-fire behaviour of concrete-filled steel tubular stub columns, Journal of Constructional Steel Research, 65 (2009) 1664-1676.
[29] J. Huo, J. Zhang, Z. Wang, Y. Xiao, Effects of sustained axial load and cooling phase on post-fire behaviour of reinforced concrete stub columns, Fire Safety Journal, 59 (2013) 76-87.
[30] American Institution of Steel Construction (AISC), Specification for Structural Steel Buildings, ANSI/AISC, in, Chicago, 2010.
[31] ASTM Standard E8/E8M, in: Standard Test Methods for Tension Testing of Methallic Materials, ASTM International, West Conshohocken, PA: USA, 2011.
[32] Australia Standards AS4100, Steel structures, Sydney, Australia, 1998.
[33] A. Considère, Annales des ponts et chaussées I sem, (1885) 574.
[34] H.K.D.H. Bhadeshia, S.R. Honeycombe, Chapter 5 - Formation of Martensite, in: H.K.D.H.B.R. Honeycombe (Ed.) Steels (Third Edition)-Microstructure and Properties, Butterworth-Heinemann, Oxford, 2006, pp. 95-128.
[35] A. Deschamps, G. Fribourg, Y. Bréchet, J.L. Chemin, C.R. Hutchinson, In situ evaluation of dynamic precipitation during plastic straining of an Al–Zn–Mg–Cu alloy, Acta Materialia, 60 (2012) 1905-1916.

Chapter 5

On the use of Bernstain-Bézier functions for modelling the post-fire stress-strain relationship of ultra-high strength steel (Grade 1200)

This chapter has been accepted for publication in the Journal of *Engineering Structures* on 26 August 2018.

Reprinted here with the Author Rights granted by Elsevier.

Table of Contents

Abstract

Ultra-high strength steels (UHSS) have significant potential applications in the engineering fields due to their unique specifications. In recent years, it has been experimentally shown that the post-fire stress-strain response of this material is highly dependent on the maximum steel temperature and the sustained load applied to it during fire. This paper employs the Bernstain-Bézier functions to present the relationship between the stress, strain, the maximum fire temperature and the sustained axial load ratio (β) for Grade 1200 UHSS cooled for fire temperatures to room temperature. The experimental results are used to verify and validate the proposed model throughout the paper. The model showed to be capable of not only interpolating the stress-strain curves, but also extrapolating them out of the range of the available experimental tests data. Also, taking advantage of the stress-strain-temperature response of the UHSS tested at elevated temperatures, the instantaneous stress-induced strain and consequently the creep strain of UHSS subjected to different constant sustained load values during transient fire are obtained.

Key Words: ultra-high strength steel; fire; cooling; Bernstain-Bézier functions; sustained axial load

5.1. Introduction

Fire is one of the most common hazards that can severely damage steel structures. After the cooling phase of a fire, the residual strength and ductility of the structural members determine whether or not they can be reused. To perform a rational structural analysis, it is necessary to evaluate the post-fire stress-strain response of the steel materials used in the structure. Several studies have been conducted to evaluate the residual stress-strain relationship of different grades of steel cooled from fire temperatures [1-11]. While ultra-high strength steels (UHSS) with yield strength of up to 1200 MPa have shown a great potential to be used as cost-effective construction materials in structural members [12-17], a few researchers have focused on their in-fire and post-fire mechanical response.

In recent years, Azhari et al. [6, 8, 9] investigated the realistic mechanical response of Grade 1200 UHSS at fire temperatures and after cooling from elevated temperatures to room temperature through extensive experimental tests. It was shown that contrary to the assumptions made in the primary models of the post-fire stress-strain response of mild steel [18, 19], the residual strength of UHSS significantly reduces when cooled from fire temperatures above 450°C [6, 8]. The reason for this greater strength loss of UHSS compared to mild steel lies behind their different microstructures and thermodynamic stability phase diagrams, which has deeply been elaborated by authors in Refs. [6, 8]. In Ref.[8], the compound Ramberg Osgood material model was modified and an empirical stress-strain model was developed in terms of the maximum fire temperature for the UHSS cooled from fire temperatures to room temperature. Although the proposed model can accurately predict the post-fire stress-strain response of UHSS cooled from different elevated temperatures, it does not take into account the effect of creep strain caused by the sustained loads resulted from dead and live loads exerted on the UHSS specimens. Thus, in Ref. [9], the in-fire and post-fire mechanical response of UHSS subjected to different sustained load values were discussed and the effect of the consequent transient creep strain was experimentally evaluated. However, a stress-strain model that in addition to the maximum fire temperature, takes into account the effect of sustained axial load, cannot be easily developed by modifying the empirical model proposed in Ref.[8].

In this paper, Bernstain-Bézier functions [20] are employed to present the relationship between the post-fire stress and strain, the maximum fire temperature and the sustained axial load applied to UHSS specimens during heat-up and cooling phases of fire. Thus, using the Cooling and Creep-Cooling test results obtained in Refs. [8, 9], Bernstain-Bézier surfaces taking into account the aforementioned variables are developed. In addition, the same model is developed for the UHSS tested at fire temperatures. Thus, from the Bernstain-Bézier surface created using the experimental results of the heat-up tests (Ref. [8]), the instantaneous stress-induced strain (ε_{σ}) of the UHSS subjected to different constant stress values during transient fire is extracted. Finally, by subtracting the free thermal strain (ε_{th}) and the ε_{σ} strain of UHSS from the total strain (ε_{total}) values obtained from the heat-up phase of the Creep-Cooling tests carried out on UHSS (Ref. [9]), the variation of the transient creep strain (ε_{cr}) with the fire temperature is obtained for different constant stress levels. The obtained transient creep strain can be used for practical applications by fire engineers in modelling the response of structural components composed of UHSS under creep/fire multi-phase loading scenarios.

5.2. Experimental program

In order to develop and calibrate a model representing the relationship between the post-fire stress-strain curves, the maximum fire temperature and the sustained axial load inserted on UHSS specimens during fire, experimental tests simulating the fire conditions are required. This section briefly explains the procedure of the following sets of experimental tests conducted in Refs. [6, 8, 9] and used in this paper including: Heat-up tests, Cooling tests and Creep-Cooling tests. The last state of the standard dog-bone coupons at each stage of these experimental sets are schematically described in Figure 5-1 (a-c). In this figure, the red and grey colours represent the elevated temperature and room temperature, respectively. The temperature changes at each stage of the tests are illustrated above them; where RT represents room temperature, and T_t denotes the target temperature (maximum steel temperature). It is important to note that each test was conducted at least twice. An additional test was conducted unless the difference between the results obtained from two similar tests is less than 3%.

Heat-up tests (Figure 5-1a): The UHSS tensile coupons were first heated up to different elevated temperatures (Stage I), and once the temperature of the specimen was stabled

for ~20 minutes (based on [5]), strain-controlled tensile test was carried out on the specimen until failure (Stage II). As it will be explained later in Section 5.4.3, the purpose of using this set of tests in this paper is to extract the instantaneous stress-induced transient strain (ε_{σ}) of UHSS for calculation of the creep strain (ε_{cr}).

Cooling tests (Figure 5-1b): The UHSS specimens were heated up to different elevated temperatures (Stage I), and after stabilization of the temperature for ~20 minutes, they were air cooled to room temperature (Stage II). Then, strain controlled tensile tests were performed until the specimens failed (Stage III).

Creep-Cooling tests (Figure 5-1c): This test was simulated at the same conditions as the Cooling tests, except that the effect of the creep strain caused by the sustained axial loads exerted on the specimens during fire was taken into account. Thus, an axial tensile load of $F_s = \beta.f_{u,T}.S$ (axial stress of $f_s = \beta.f_{u,T}$) was first applied to the UHSS specimen (Stage I), where β is the axial load ratio, $f_{u,T}$ is the ultimate tensile strength of UHSS at elevated temperature *T*, and *S* is the cross section area of the specimen. Then, while this axial load was constantly kept on the specimen, it was heated up to an elevated temperature *T* (Stage II) and after the temperature was stable for ~20 minutes, it was air cooled to room temperature (Stage III). In the last stage of the Creep-Cooling tests, the UHSS specimen was undergone strain-controlled tensile test at room temperature until failure. It is worth noting that the Cooling tests are a specific version of the Creep-Cooling tests with $\beta = 0$. More details about these experiments can be found in the recent papers published by the authors [6, 8, 9].

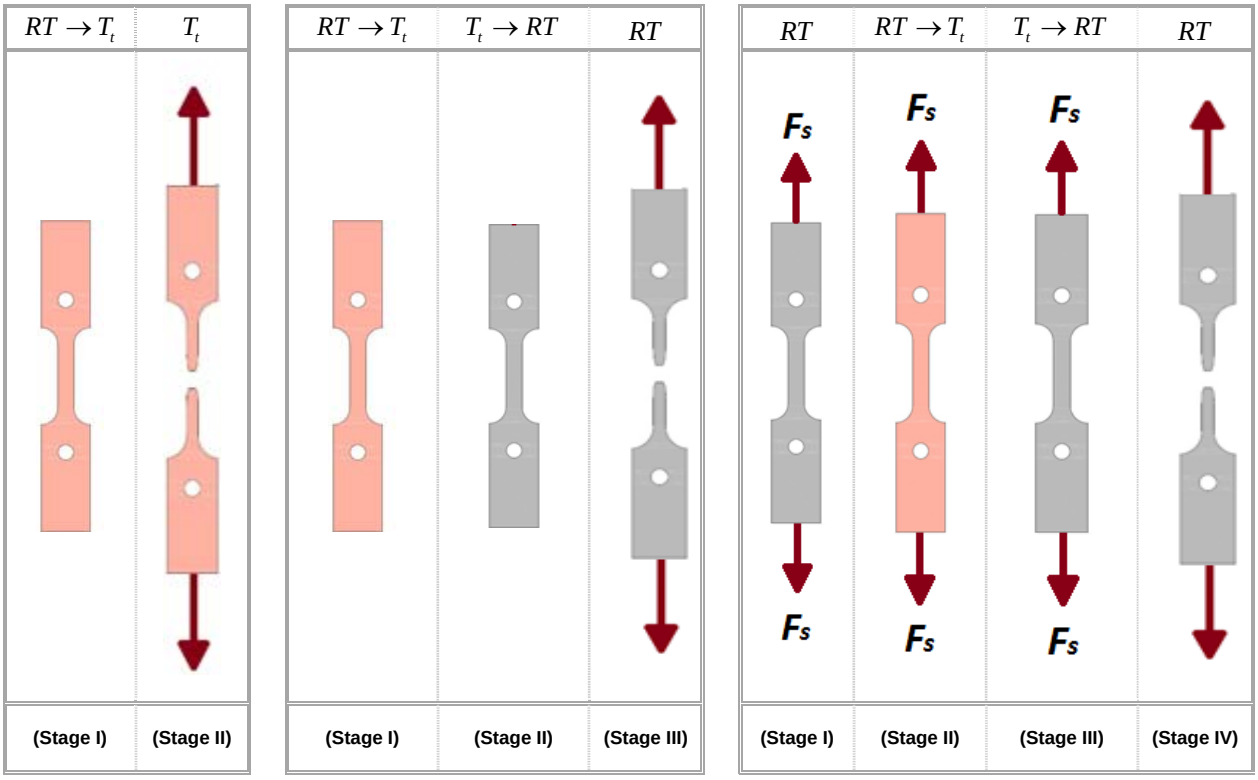

Figure 5-1. Schematic representation of the experimental stages of a) Heat-up tests, b) Cooling tests and c) Creep-Cooling tests.

5.3. Post-fire stress-strain response

5.3.1. Existing models

A few researchers focusing on the post-fire mechanical response of high strength steels (HSS) with grades of up to 960 [2, 3, 5] have proposed temperature dependent predictive equations for the elastic modulus, yield strength and in some cases the ultimate tensile strength of HSS cooled from fire temperatures to room temperature. However, in the literature, there is no material model representing a continuous stress-strain relationship taking into account the realistic post-fire behaviour of steel materials. In recent years, for the first time, the authors of this paper proposed an empirical model for Grade 1200 UHSS representing its full post-fire stress-strain curve up to the onset of necking (ultimate tensile stress, f_u) with a single set of parameters [8]. In this model, using the compound

Ramberg-Osgood equations [21], the following post-fire stress-strain relationship was developed in terms of the maximum fire temperature *T*:

$$\varepsilon = \frac{\sigma}{E_{CT}} + 0.002\left(\frac{\sigma}{f_{0.2,CT}}\right)^{n_{CT}} \quad \text{for} \quad \sigma \le f_{0.2,CT}$$

$$\varepsilon = \frac{\sigma - f_{0.2,CT}}{E_{0.2,CT}} + \left(\varepsilon_{u,CT} - \varepsilon_{y,CT} - \frac{f_{u,CT} - f_{0.2,CT}}{E_{0.2,CT}}\right)\left(\frac{\sigma - f_{0.2,CT}}{f_{u,CT} - f_{0.2,CT}}\right)^{n'_{CT}} + \varepsilon_{y,CT} \quad \text{for} \quad f_{0.2,CT} \le \sigma \le f_{u,CT} \tag{5-1}$$

where

$$E_{0.2,CT} = \frac{E_{CT}}{1 + 0.002 n_{CT} \frac{E_{CT}}{f_{0.2,CT}}} \tag{5-2}$$

In Eqs. (5-1) and (5-2), ε and σ are the engineering strain and stress values, respectively. The *CT* index represents the parameters of UHSS specimens obtained after **c**ooling from temperature ***T*** to room temperature. The exponential coefficients n and n' are introduced to take the material nonlinearity into consideration. $f_{0.2}$ and f_u are the 0.2% proof stress and ultimate tensile stress, respectively; and ε_y and ε_u are their corresponding strain values. E and $E_{0.2}$ are the Young's modulus and the tangent modulus of the material at 0.2% proof stress, respectively. All these parameters are defined in terms of the corresponding values at room temperature (with *RT* index) and the maximum fire temperature (*T*) in Ref. [8]. The model has shown to be capable of accurately and robustly predicting the post-fire stress-strain curve of UHSS cooled from different fire temperatures and was validated against experimental test results. In spite of that, this model has the following shortcomings:

1. Combining nonlinear equations in one single relation is computationally expensive;
2. Introducing new parameters like the sustained axial load ratio (β) to the existing models cannot be easily done;
3. While interpolating the stress-strain curves for fire temperatures (or β values) inside the range of those used in the experimental tests can be performed with these models, extrapolating the curves for a temperature (or β values) outside the tested range is usually not possible;

4. Modifying the relations from stress based (strain defined in terms of stress) to strain based (stress defined in terms of strain) is very difficult due to the complexity of the arithmetic equations in these models.

Therefore, it is necessary to develop a material model which overcomes these issues; especially when the material is subjected to multi-phase loading scenarios, in which multiple parameters identifying the loading scenario must be taken into consideration. In this regard, using Bernstein-Bézier equations, Sinaie et al. [22] proposed a material model for cyclically damaged mild steels subjected to fire and took into account the effect of damage along with the elevated temperature in their model. In this paper, using the same technique, it is attempted to develop a material model for the post-fire behaviour of UHSS which takes into account both maximum fire temperature (T) and the sustained axial load ratio (β).

5.3.2. Proposed model

In this study, the stress-strain curves are broken to several pieces, each of which are represented by a 2nd order Bernstein-Bézier curve. The main advantages of this approach compared to the case where the entire curve is represented by a higher order Bernstein-Bézier curve are higher robustness and simplicity. In the following section, the Bernstein-Bézier equations, which are the basis of the proposed model, are briefly explained.

5.3.2.1. Bernstein-Bézier equations

The Bernstein-Bézier objects of n^{th} order are constructed with the n^{th} order Bernstein interpolating polynomials which are defined as:

$$B_i^n(s) = C_n^i s^i (1-s)^{n-i} \tag{5-3}$$

where $0 \le i \le n$, $0 \le s \le 1$ and C_n^i, is the binomial function defined as $C_n^i = \frac{n!}{i!(n-i)!}$.

Figure 5-2 presents the 2nd order Bernstein functions, i.e. n=2, which are used in this study. It can be seen that with $0 \le s \le 1$, the values of $B_i^2(s)$ are also bounded between 0 and 1.

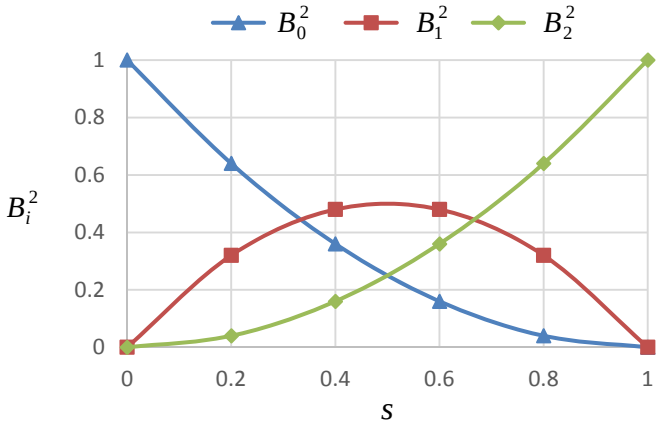

Figure 5-2. Plots of the 2nd order Bernstein polynomials

Using the Bernstein interpolating polynomial function (Eq. (5-3)) and *n+1* control points in a two-dimensional (2D) space, a 2D Bernstein-Bézier curve of degree *n* can be expressed as:

$$\mathbf{P}(s) = (P_x(s), P_y(s)) = \sum_{i=0}^{n} B_i^n(s)\mathbf{P}_i, \qquad s \in [0;1] \tag{5-4}$$

where $\mathbf{P}_i = (P_{ix}, P_{iy})$ are the control points with coordinates being expressed with respect to the conventional orthogonal reference frame.

In Figure 5-3, a 2nd order Bernstein-Bézier curve created with three control points in a 2D space is illustrated. A noteworthy fact that can be also seen from this figure is that these curves always pass through the end control points ($\mathbf{P}_0$ and $\mathbf{P}_2$), but not necessarily the intermediate control points ($\mathbf{P}_1$). The intermediate control point $\mathbf{P}_1$ can be found from the intersection of the tangent lines passing through the end control points. Therefore, knowing the coordinates of the end control point and the slope of the tangent lines at those points, a unique 2nd order Bernstein-Bézier curve can be constructed.

One of the main advantages of these curves comes from the fact that $P_x(s)$ and $P_y(s)$ are indirectly related to each other with an intermediate variable, *s*. Therefore, assuming $P_x(s)$ as the engineering strain (ε) and $P_y(s)$ as the engineering stress (σ), with a minor computational cost, the strain-based formulation ($\sigma = f(\varepsilon)$) can be easily converted to a stress-based one ($\varepsilon = f(\sigma)$). This characteristic is highly beneficial for finding the transient stress-induced strain, which is applied in Section 5.4.3 of this paper.

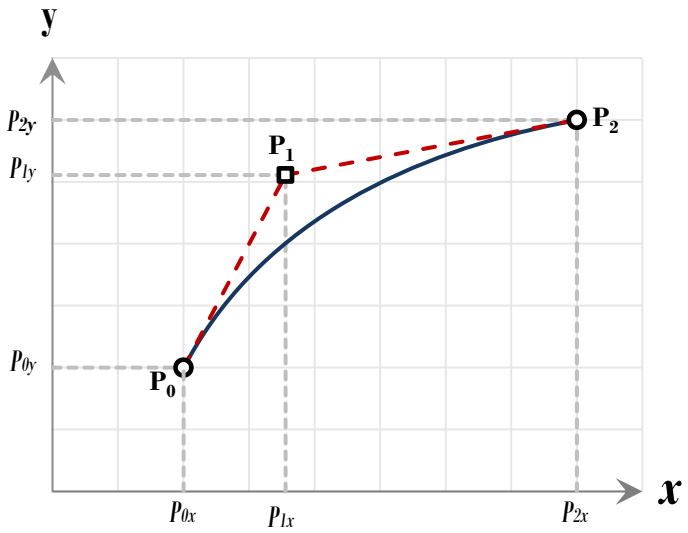

Figure 5-3. Illustration of the 2nd order Bézier curve created with three control points: P_0, P_1 and P_2

The Bernstein–Bézier equations are also capable of predicting the curve outside the range of the dataset used for calibration of the model. The method of data extrapolation is illustrated in Figure 5-4. In this method, assuming that the Bernstein–Bézier curve constructed by $\mathbf{P}_0$, $\mathbf{P}_1$ and $\mathbf{P}_2$ control points is known, the curve outside the range is constructed by $\mathbf{Q}_0$, $\mathbf{Q}_1$ and $\mathbf{Q}_2$ extrapolated control points. The known curve and the extrapolated one intersect at $\mathbf{P}_2$, thus $\mathbf{Q}_0 = \mathbf{P}_2$, and have equal tangents at this point. The $\mathbf{Q}_1$ intermediate control point is located on the extension of $\mathbf{P}_1\mathbf{P}_2$ vector in such a way that the length of $\mathbf{P}_1\mathbf{P}_2$ is equal to that of $\mathbf{P}_2\mathbf{Q}_1$ (or $\mathbf{Q}_0\mathbf{Q}_1$). Finally the end control point $\mathbf{Q}_2$ is determined by first, finding the $\mathbf{X}$ point located on the extension of $\mathbf{P}_0\mathbf{P}_1$ vector so that the length of $\mathbf{P}_0\mathbf{P}_1$ is equal to that of $\mathbf{P}_1\mathbf{X}$. Then, $\mathbf{Q}_2$ is found by extending the $\mathbf{XQ}_1$ vector in a way that the length of $\mathbf{XQ}_1$ is equal to that of $\mathbf{Q}_1\mathbf{Q}_2$. The extrapolated control points can also be derived by the algorithm given in Ref. [22] based on vector arithmetic. It is obvious that this data extrapolation method works provided that the data change outside the range continues with the same trend as that inside the data range. Thus, when using this method in this paper, it is assumed that outside the range of the curves used for calibration of the model, the stress-strain curves will continue changing with a similar trend and no unexpected variation of mechanical properties is occurred.

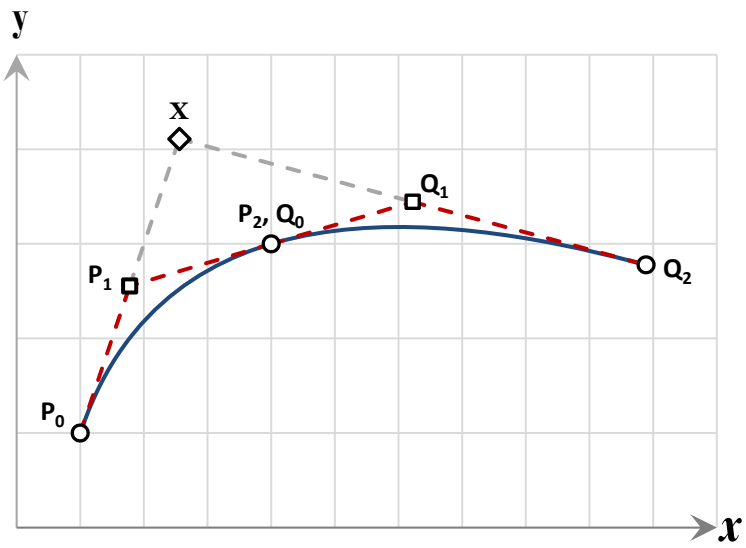

Figure 5-4. Illustration of data extrapolation technique by the 2nd order Bézier curve

Bézier curves can be naturally extended to higher dimensions. A 3D Bernstein–Bézier surface can be constructed using *m+1* by *n+1* control points in a 3D space as:

$$\mathbf{P}(s_1,s_2)=(P_x(s_1,s_2),P_y(s_1,s_2),P_z(s_1,s_2))=\sum_{i=0}^{n}\sum_{j=0}^{m}B_i^n(s_1)B_j^m(s_2)\mathbf{P}_{ij},\qquad s_1\ \&\ s_2\in[0;1]\quad (5\text{-}5)$$

in which, $\mathbf{P}_{ij}=(P_{ijx},P_{ijy},P_{ijz})$ are the control points and the Bernstein interpolating polynomials can be calculated from Eq. (5-3).

An example of a 2nd order 3D Bernstein–Bézier surface created with 9 control points is depicted in Figure 5-5. The end and intermediate control points are represented by circle and square markers, respectively. Similar to the 2D curves presented in Figure 5-3, the intermediate control points determine the slope of the surface at end control points in different directions.

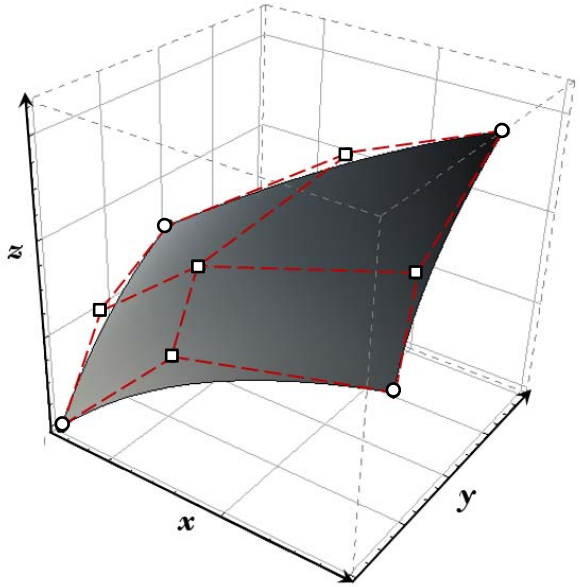

Figure 5-5. Illustration of the 2nd order Bézier surface in 3D space created with nine control points

5.3.2.2. Stress-strain curves

In Figure 5-6, typical stress-strain curves obtained from the Creep-Cooling experimental tests ($\beta > 0$) and Cooling tests ($\beta = 0$) are presented. The description of the parameters shown on these curves are given in Refs. [8, 9] in details. It is noteworthy that in Figure 5-6a ($\beta > 0$), because of the limited space of the plot area, f_{yup} and f_u are close to each other and do not necessarily have the same values. In this study, the full stress-strain curves of the Creep-Cooling tests and the Cooling tests starting from the zero stress ($\sigma = 0, \varepsilon = 0$) to the ultimate tensile stress ($\sigma = f_u, \varepsilon = \varepsilon_u$) are divided to 6 and 4 parts, respectively. These parts are separated by the end control points of **N1**$_{CC}$ to **N6**$_{CC}$ on the stress-strain curves of **C**reep-**C**ooling tests and **N1**$_{C}$ to **N4**$_{C}$ on the curves of the **C**ooling tests. Each part is then modelled by a 2nd order Bernstein-Bézier curve. An alternative approach could be modelling the full stress-strain curve with a higher order Bernstein-Bézier curve; however, to maintain simplicity and have a higher robustness, only 2nd order curves are taken in this study.

The main difference between the procedure of the Creep-Cooling tests ($\beta > 0$) and Cooling tests ($\beta = 0$) is that the creep strain caused by the sustained axial load in the Creep-Cooling tests is not generated in the material during the Cooling tests. Therefore,

in the Cooling tests both f_s and $\Delta\varepsilon_{cr}$ are equal to zero. To check whether the stress-strain curve of Figure 5-6a can be considered as a general curve type for the proposed model, these changes (i.e. $f_s = 0$ and $\Delta\varepsilon_{cr} = 0$) were applied to this curve. In the resulted curve, **N1**$_{CC}$ and **N2**$_{CC}$ are eliminated and the only remaining difference from the stress-strain curve of Figure 5-6b would be the pronounced sharp yield point. If in the case of $\beta = 0$, it is assumed that the stress at **N3**$_{CC}$ is equal to f_p ($f_{y,top}$ is replaced by f_p) and the one at **N4**$_{CC}$ is equal to $f_{0.2}$ ($f_{y,bot}$ is replaced by $f_{0.2}$), the sharp yield point is eliminated and the stress-strain curve of Figure 5-6a can represent both Creep-Cooling tests and Cooling tests. Thus, for the case of $\beta = 0$, considering these assumptions, it can be concluded that in the curves of Figure 5-6, **N1**$_{C}$ =**N3**$_{CC}$ and **N2**$_{C}$ =**N4**$_{CC}$, while **N1**$_{CC}$ and **N2**$_{CC}$ are eliminated.

For a better clarification of the parameters involved in the proposed model, the stress, strain and tangent modulus values at different end control points on the post-fire stress-strain curve of Figure 5-6a (as a general curve) are defined in Table 5-1 for all β ranges ($\beta > 0$ and $\beta = 0$). As shown in Figure 5-3, the tangent modulus parameters given in the table for different end control points determine the slope of the curve at these points. Thus, using the values of stress, strain and tangent modulus at the end control points of **N1**$_{CC}$ to **N6**$_{CC}$, six 2nd order Bernstein-Bézier curves can be constructed and connected to each other to form the stress-strain curve of Figure 5-6a ($\beta > 0$). However, for construction of the stress-strain curve of Figure 5-6b ($\beta = 0$), since **N1**$_{CC}$ and **N2**$_{CC}$ are eliminated, four 2nd order Bernstein-Bézier curves are needed. In the last two rows of Table 5-1, the independent variables are extracted for both cases of $\beta > 0$ and $\beta = 0$. It can be inferred that 13 independent parameters are needed for definition of the post-fire stress-strain curve of UHSS subjected to sustained axial loads during the heat-up and cooling phases of fire ($\beta > 0$). However, for the case where no axial load is inserted on the specimens ($\beta = 0$), the number of independent variables is reduced to 8. The reason for this reduction is elimination of **N1**$_{CC}$ and **N2**$_{CC}$ control points, and also the fact that ε_p and ε_y strains are dependent variables which are defined in terms of the elastic modulus (E) and their corresponding stresses, f_p and $f_{0.2}$, respectively. In Figure 5-6, all dependant and independent variables except for the tangent modulus ones are illustrated and the independent variables are underlined.

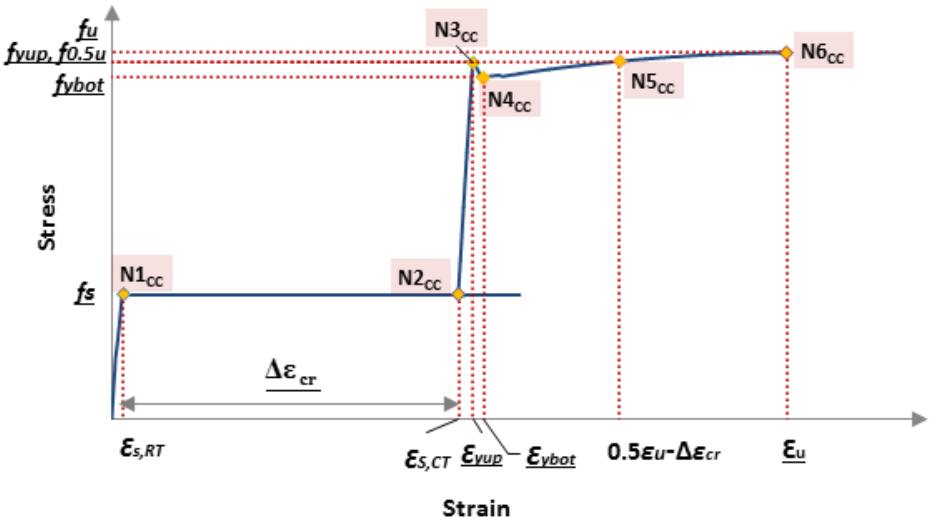

(a)

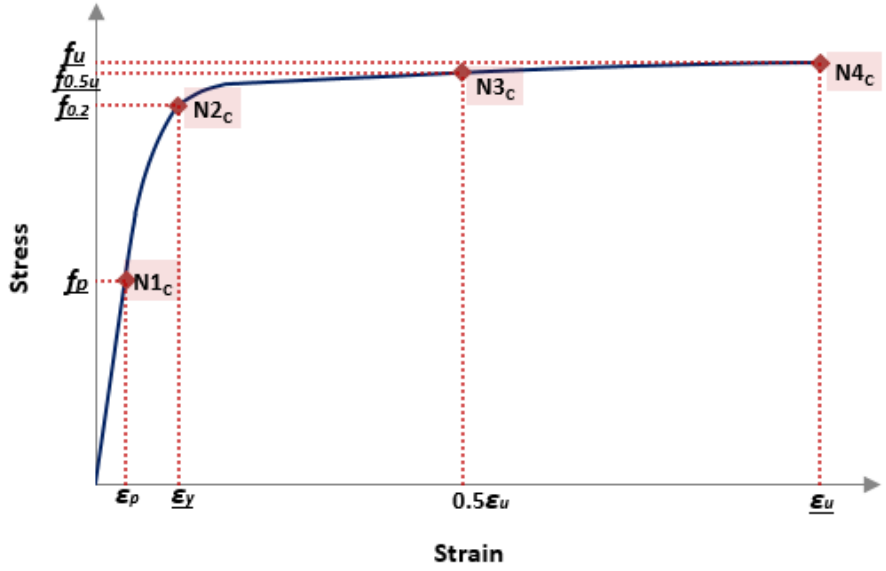

(b)

Figure 5-6.Illustration of the main control points on the stress-strain curve of a UHSS a)with (β>0) and b)without axial load (β=0)

Table 5-1. The dependent and independent parameters involved in the stress-strain model

Node label of the End Control Points		N1cc	N2cc	N3cc	N4cc	N5cc	N6cc
Stress	$\beta > 0$	f_s	f_s	f_{yup}	f_{ybot}	$f_{0.5u}$	f_u
	$\beta = 0$	0	0	f_p	$f_{0.2}$	$f_{0.5u}$	f_u
Strain	$\beta > 0$	$\varepsilon_{s,RT} = \frac{f_s}{E}$	$\varepsilon_{s,CT} = \varepsilon_{s,RT} + \Delta\varepsilon_{cr}$	ε_{yup}	ε_{ybot}	$0.5\varepsilon_u - \Delta\varepsilon_{cr}$	ε_u
	$\beta = 0$	0	0	$\varepsilon_p = \frac{f_p}{E}$	$\varepsilon_y = 0.002 + \frac{f_{0.2}}{E}$	$0.5\varepsilon_u$	ε_u
Tangent Modulus	$\beta > 0$	E	0	E_{yup}	E_{ybot}	$E_{0.5u}$	0
	$\beta = 0$	0	0	E	$E_{0.2}$	$E_{0.5u}$	0
Independent Variables	$\beta > 0$	f_s , E	$\Delta\varepsilon_{cr}$	ε_{yup} , f_{yup} , E_{yup}	ε_{ybot} , f_{ybot} , E_{ybot}	$f_{0.5u}$, $E_{0.5u}$	ε_u , f_u
	$\beta = 0$	**None**	**None**	f_p , E	$f_{0.2}$, $E_{0.2}$	$f_{0.5u}$, $E_{0.5u}$	ε_u , f_u

5.4. Results and Discussion

5.4.1. Comparison with the experimental stress-strain curves

In this section, the stress-strain curves predicted by the proposed model for the UHSS cooled from different fire temperatures to room temperature while subjected to different values of sustained axial load ratio, i.e. $\beta = 0$, $\beta = 0.7$ and $\beta = 0.8$, are presented. These curves are illustrated in Figure 5-7 and compared to the curves obtained from the experimental tests in Refs. [8, 9]. It is important to note that according to the results obtained by the authors in Ref. [9], it was shown that lower axial load ratios does not have a considerable effect on the in-fire/post-fire response of UHSS and the amount of creep strain induced in the specimens during fire is not significant. However, for load ratios above 0.7, a small change (e.g. changing from 0.7 to 0.75 or from 0.75 to 0.8) has a considerable effect on the in-fire/post-fire response of UHSS. In Figure 5-7, the stress-strain curves of the UHSS **c**ooled from fire temperature ***T*** to room temperature with sustained axial load ratio of $\boldsymbol{\beta}$ obtained from the experimental tests and the proposed model are shown as UHSS-**C*T*-$\boldsymbol{\beta}$**-Exp and UHSS-**C*T*-$\boldsymbol{\beta}$**-Model, respectively. In case of $\beta = 0$

, $\boldsymbol{\beta}$ is simply removed from UHSS-**C*T*-$\boldsymbol{\beta}$**-Exp and UHSS-**C*T*-$\boldsymbol{\beta}$**-Model labels. Also, the stress-strain curves of the virgin UHSS tested at room temperature obtained from the experiment and the proposed model are displayed as UHSS-**RT**-Exp and UHSS-**RT**-Model, respectively. From the 3 sets of plots illustrated in Figure 5-7 for $\beta = 0$, $\beta = 0.7$ and $\beta = 0.8$, it can be observed that the stress-strain curves obtained from the proposed model are in a very good agreement with those of the experimental tests. It is worth noting that the strain reversal observed in the horizontal plateau of the stress-strain curves with $\beta > 0$ (denoted as $\Delta\varepsilon_{th}$ in Ref. [9]) is occurred in the material due to the thermal expansion of the specimen heated to temperature *T*. The variation of $\Delta\varepsilon_{th}$ with temperature is known from the experiments regardless of the β values and is not taken into account by the proposed model. Nevertheless, variation of the thermal strain with temperature is discussed in Section 5.4.3 of this paper.

In Figure 5-7a ($\beta = 0$), to validate the model, the stress-strain curves of the UHSS cooled from 540°C and 650°C to room temperature are also obtained from the proposed model and represented by UHSS-C540-Model-Validation and UHSS-C650-Model-Validation labels. The reason for considering these two curves for validation is that they were not used for calibration of the model. The good agreement between these curves with the stress-strain curves of the corresponding experimental curves, i.e. UHSS-C540-Exp and UHSS-C650-Exp, shows that the model is capable of predicting the post-fire stress-strain response of UHSS for different maximum fire temperatures of up to 800°C.

Furthermore, since the sustained axial stress values corresponding to $\beta = 0.7$ and $\beta = 0.8$ ratios, i.e. $f_s = 0.8 f_{u,800}$ and $f_s = 0.7 f_{u,800}$, have very small values, the UHSS-C800-0.8-Exp and UHSS-C800-0.7-Exp tests could not be conducted experimentally as the accuracy of the loading machine was lower than these values [9]. However, as shown in Figure 5-7b and c, the stress-strain curves of the UHSS cooled from 800°C to room temperature with sustained axial load ratios of $\beta = 0.7$ and $\beta = 0.8$ are predicted by the proposed model and represented by UHSS-C800-0.7-Model-Prediction and UHSS-C800-0.8-Model-Prediction, respectively. The control points on these stress-strain curves are predicted using the data extrapolation technique shown in Figure 5-4. The curves are then constructed with 2nd order Bernstein-Bézier curves by the piecewise methodology depicted in Figure 5-6. As mentioned before, the predicted stress-strain curves are

reliable provided that the mechanical properties on these curves are changed with the same trend as those of UHSS cooled from lower temperatures. Also, the very sharp pronounced yield point of UHSS-C800-0.7-Model-Prediction curve in Figure 5-7b is because the UHSS-C700-0.7-Exp curve has a more pronounced yield point compared to the UHSS-C*T*-0.7-Exp curves with lower maximum fire temperatures (*T*). Therefore, following the same trend, the model predicted a pronounced yield point for UHSS-C800-0.7-Model-Prediction curve. However, as can be seen from Figure 5-7c, since the shape of the yield point on UHSS-C*T*-0.8-Exp curves does not change dramatically as *T* increases, the yield point of UHSS-C800-0.8-Model-Prediction curve is not very different from the other curves of this figure.

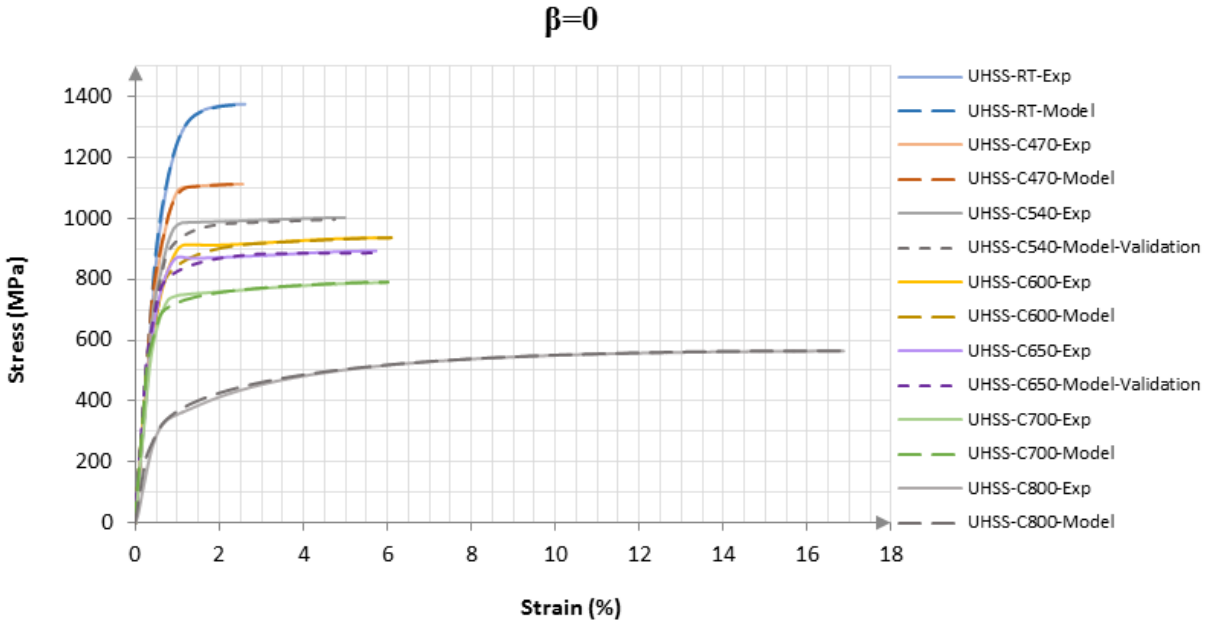

(a)

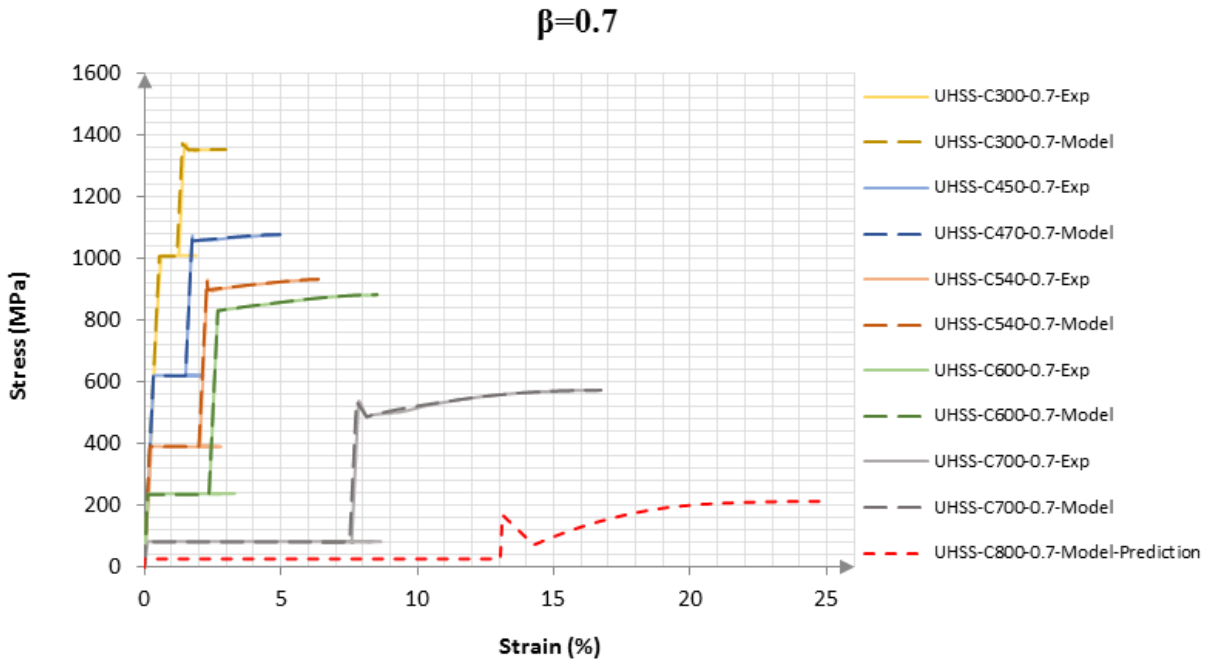

(b)

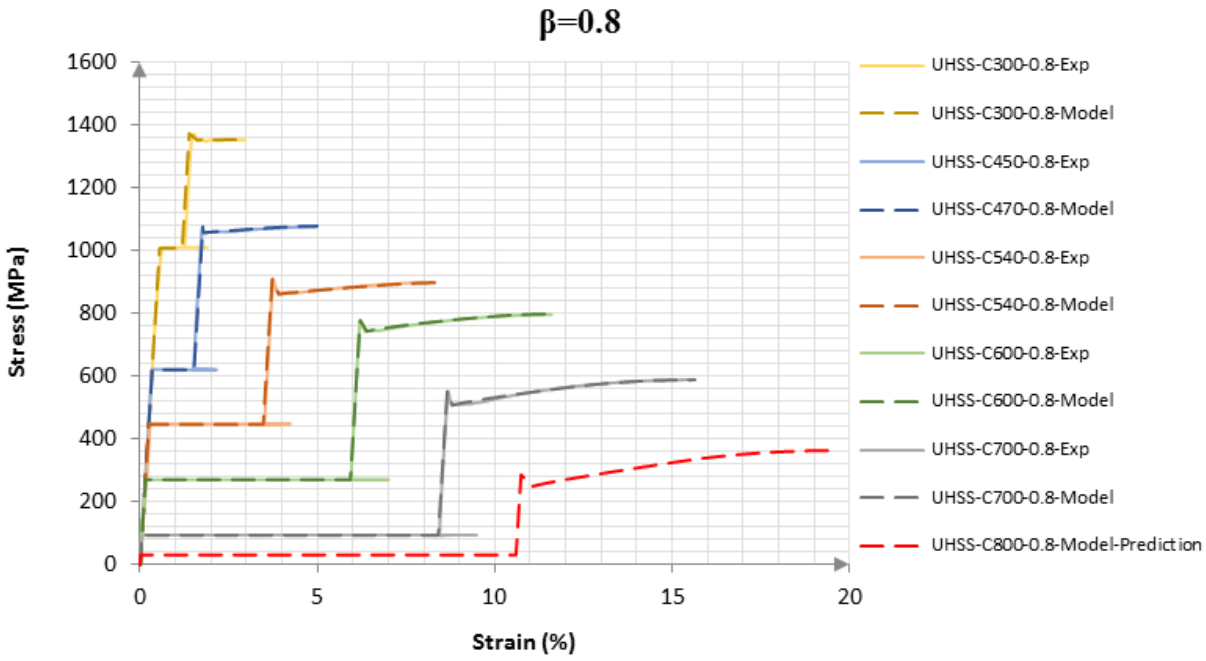

(c)

Figure 5-7. Comparison of stress-strain curves of the proposed model and the test data for the UHSS cooled from different fire temperatures a) without axial load (β=0) and with axial load ratios of b) β=0.7 and c) β=0.8

In order to illustrate the 2D stress-strain curves presented in Figure 5-7 in such a way that maximum information is presented in a single plot, 2nd order Bernstein-Bézier equations in 3D space are employed. Thus, using these equations, Figure 5-8 depicts the 3D stress-strain-temperature surfaces of UHSS cooled from fire temperatures while subjected to different values of sustained axial load ratio during heat-up and cooling phases, i.e. $\beta = 0$, $\beta = 0.7$ and $\beta = 0.8$. The temperature (T) shown on these plots is the maximum fire temperature the specimens experienced during fire. Also, for construction of these surfaces, stress has been considered as a dependant variable in terms of the independent variables of strain, maximum fire temperature (T) and the axial load ratio β. Similar to the method used for construction of 2D stress-strain curves (Figure 5-6), a piecewise approach is employed for these surfaces. The contours shown on the surfaces of Figure 5-8 divide them into different 2nd order Bernstein-Bézier surfaces (Figure 5-5) modelled between different end control points.

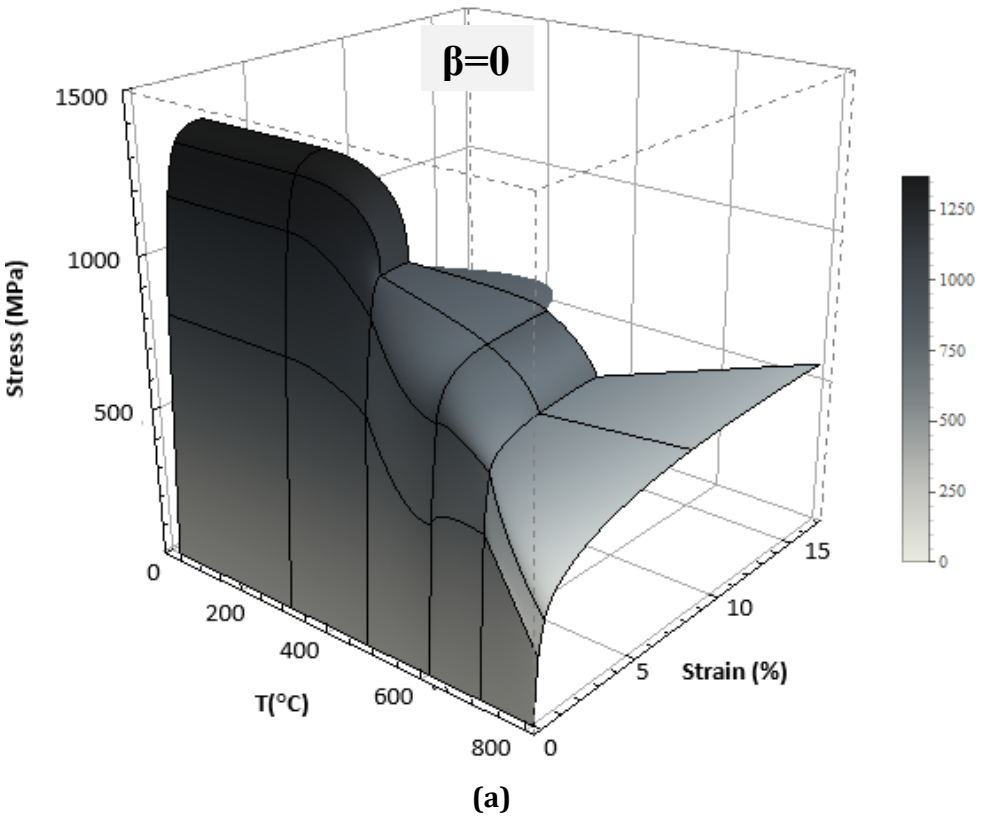

(a)

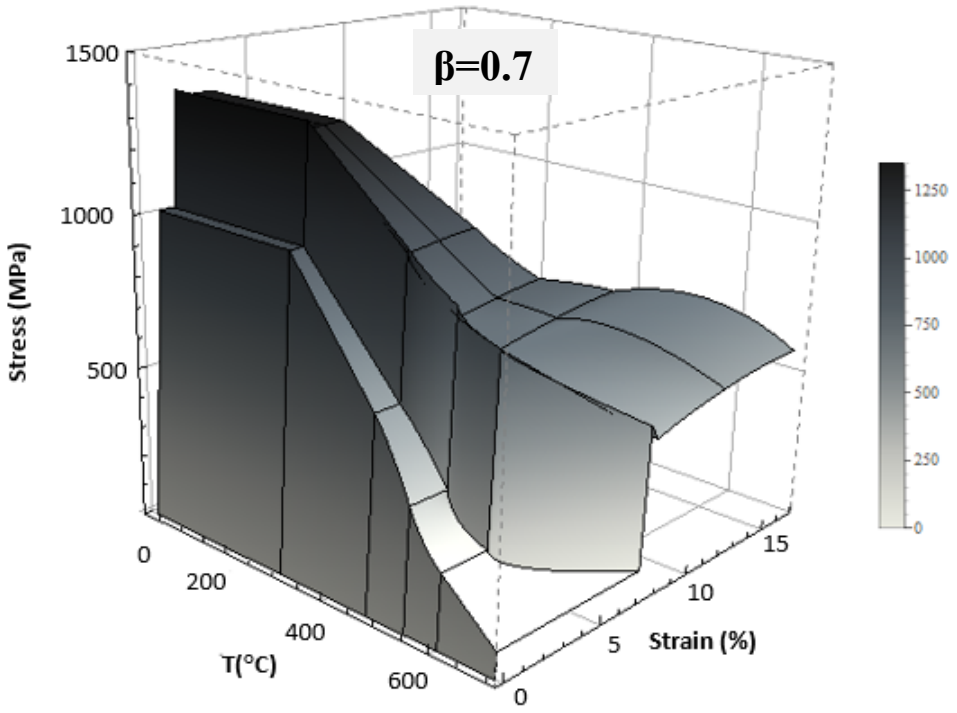

(b)

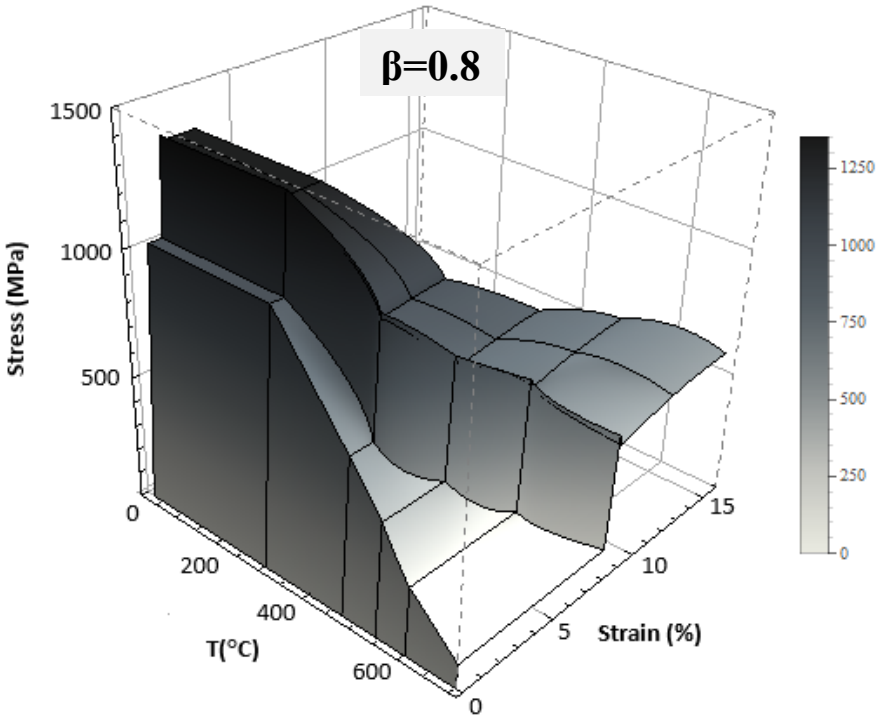

(c)

Figure 5-8. Stress-strain-temperature surfaces obtained from the proposed model for UHSS cooled from different fire temperatures, a) without axial load (β=0) and with axial load ratios of b) β=0.7 and c) β=0.8.

5.4.2. Mechanical Properties

In this section, to better demonstrate the accuracy of the proposed model, variation of some important post-fire mechanical properties with the maximum fire temperature (T) obtained from the experimental tests and the proposed model are compared. Figure 5-9 illustrates the variation of the yield stress (f_y), the yield strain (ε_y), the ultimate tensile stress (f_u) and the uniform elongation (ε_u) with the maximum fire temperature (T) for UHSS cooled from fire to room temperature without any sustained axial load ($\beta = 0$). In this figure, in addition to the mechanical properties obtained from the Model (**Model** data series), the experimental test results (called as **Experiment** data series) are also shown on each plot to show the accuracy of the model. It can be seen that for most maximum fire temperatures, the Experiments data series are in a good agreement with the modelled mechanical properties variation. However, for the UHSS cooled from 750°C to room temperature, while the ε_y and ε_u strains predicted by the proposed model match the experimental data, the modelled f_y and f_u stresses for this temperature do not accurately overlap with those obtained from the experiments. As explained in Ref. [8], when UHSS is subjected to ~750°C, phase transformation is stabilised and the material experiences no more strength reduction when cooled from temperatures above ~750°C. Since this behaviour depends on the chemical composition of the material, it was expected that the model cannot predict it.

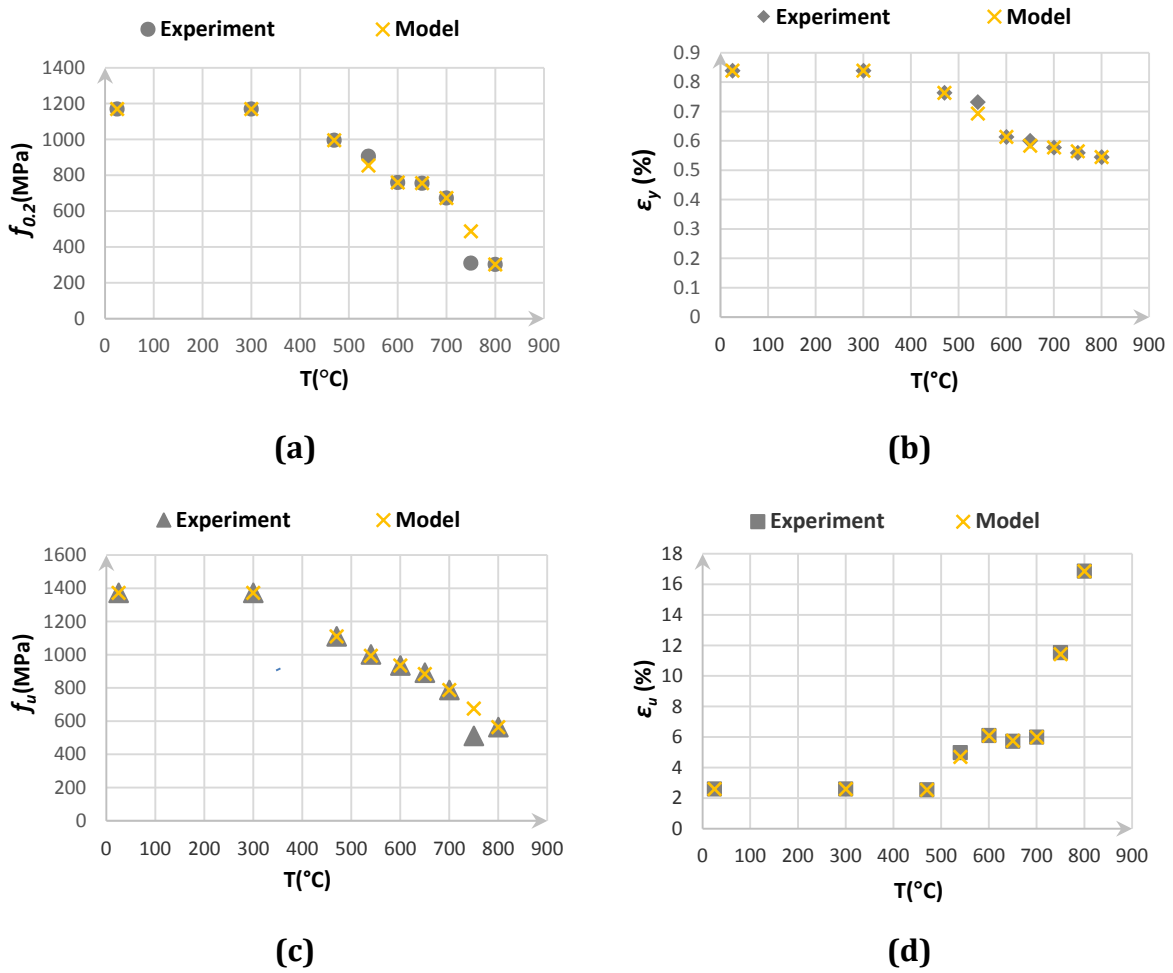

Figure 5-9. Variation of the a) yield stress (f_y), b) yield strain (ε_y), c) ultimate tensile stress (f_u) and d) uniform elongation (ε_u) of UHSS cooled from different fire temperatures without axial load (β=0) obtained from the Model compared with those resulted from experimental tests

As another set of examples showing the variation of the mechanical properties modelled by the proposed method, variation of the lower yield stress (f_{ybot}), the lower yield strain (ε_{ybot}), the ultimate tensile stress (f_u) and the uniform elongation (ε_u) with the maximum fire temperature for the UHSS cooled from different fire temperatures with sustained axial load ratio of $\beta = 0.8$ are depicted in Figure 5-10. The mechanical properties obtained from the experimental tests performed in Ref. [9] (**Experiment** data series) are also illustrated to verify the model. It is important to note that the model assumes no variation in the mechanical properties of UHSS cooled from temperatures below 300°C to room temperature while subjected to axial load ratio of $\beta = 0.8$. This assumption is made based on the fact that there is no strength reduction due to maximum fire temperature for UHSS cooled from temperatures equal and below 300°C and so there

is no change in the transient creep strain which is the main reason for the variation of the mechanical properties during the Creep-Cooling tests. Thus, as mentioned in Ref. [9], the stress-strain curve of UHSS cooled from 300°C to room temperature with $\beta = 0.8$, does not have a considerable difference with those cooled from lower temperatures with the same axial load ratio.

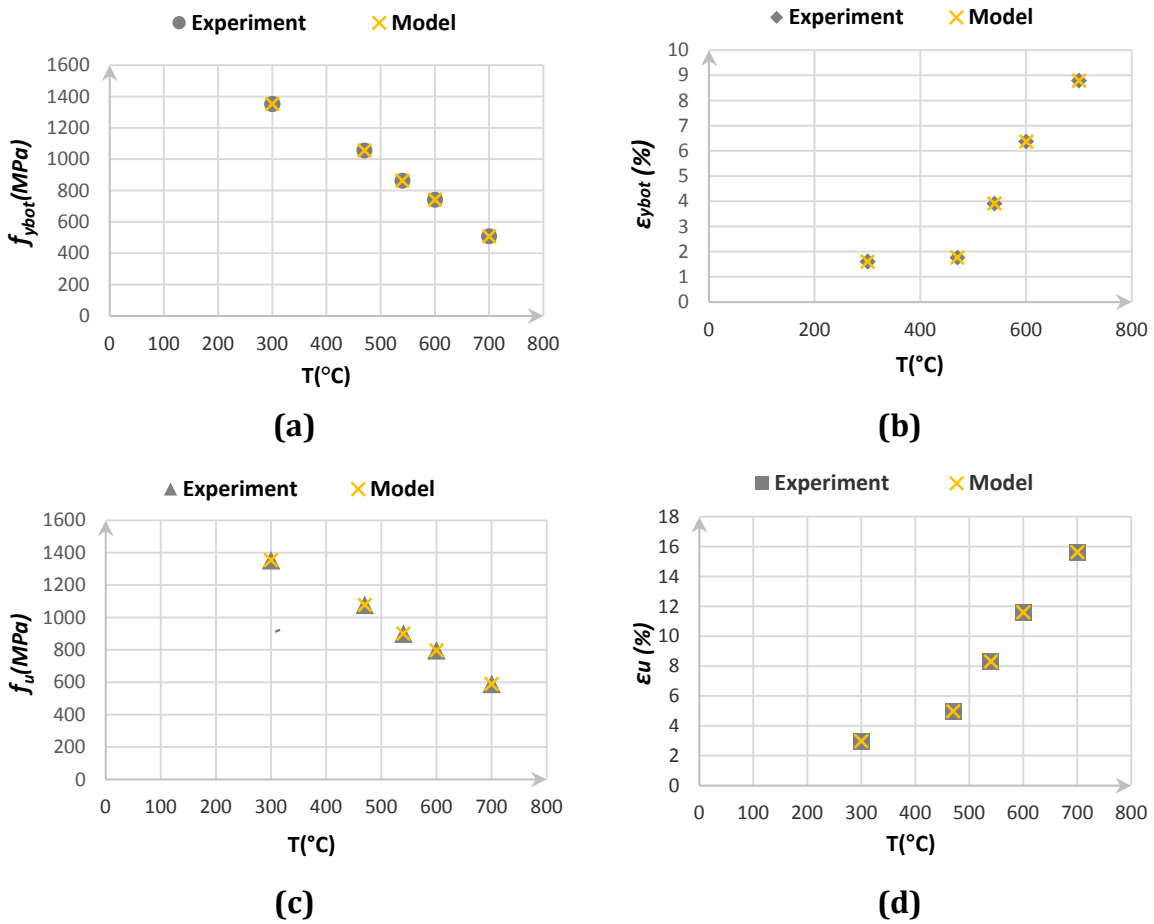

Figure 5-10. Variation of the a) lower yield stress (f_{ybot}), b) lower yield strain (ε_{ybot}), c) ultimate tensile stress (f_u) and d) uniform elongation (ε_u) of UHSS cooled from different fire temperatures with sustained axial load ratio of β=0.8 obtained from the Model compared with those resulted from the experimental tests

5.4.3. Derivation of creep strain

When a material is subjected to a constant stress during a simulated fire, the total strain experienced by the material is a mixture of different strain components. Thus, it is not possible to extract the variation of the pure creep strain (ε_{cr}) it has experienced with the fire temperature from the pure experimental tests data. In this study, it is attempted to derive the ε_{cr} strain of the UHSS subjected to different constant stress levels during a

transient fire using the experimental tests results and the capabilities of the proposed model.

The total strain (ε_{total}) of a material at elevated temperatures includes three general parts: the free thermal strain (ε_{th}), the stress-induced strain (ε_{σ}) and the creep strain (ε_{cr}) as shown in the following expression:

$$\varepsilon_{total}(\sigma,T)=\varepsilon_{th}(T)+\varepsilon_{\sigma}(\sigma,T)+\varepsilon_{cr}(\sigma,T) \quad (5\text{-}6)$$

in which, ε_{th} is only a function of temperature (T), while ε_{σ} and ε_{cr} are functions of both stress (σ) and temperature (T). Derivation of these strain components are explained in the following sections.

Thermal strain (ε_{th}):

In order to derive the thermal strain (ε_{th}) of Grade 1200 UHSS during a transient fire, the total strain recorded during the heat-up phase (Stage I of Figure 5-1a) with maximum fire temperature of 700°C, i.e. UHSS-H700, is used. During the heat-up phase, since the testing machine operated under load control while the load remained constant at zero, the recorded strain represents the ε_{th} strain of UHSS. In other words, considering the total strain (ε_{total}) defined in Eq. (5-6), since the stress level is set to zero, ε_{σ} and ε_{cr} strains are obviously disappeared and as a result: $\varepsilon_{total}=\varepsilon_{th}$.

In Figure 5-11, the variation of the thermal strain (ε_{th}) of Grade 1200 UHSS with temperature is illustrated. In this figure, the thermal strain of the UHSS material used in this study is also compared to some other steel types including the carbon mild steel and stainless steels from the available references, i.e. Eurocode 3 [23] and [24]. It can be seen that while the thermal strain of UHSS is very close to that of high chromium content stainless steel (AISI 430) [24], it is lower than that of the carbon mild steel (Eurocode 3 [23]) and has a considerable difference with that of the austenitic stainless steel reported in Eurocode 3 [23].

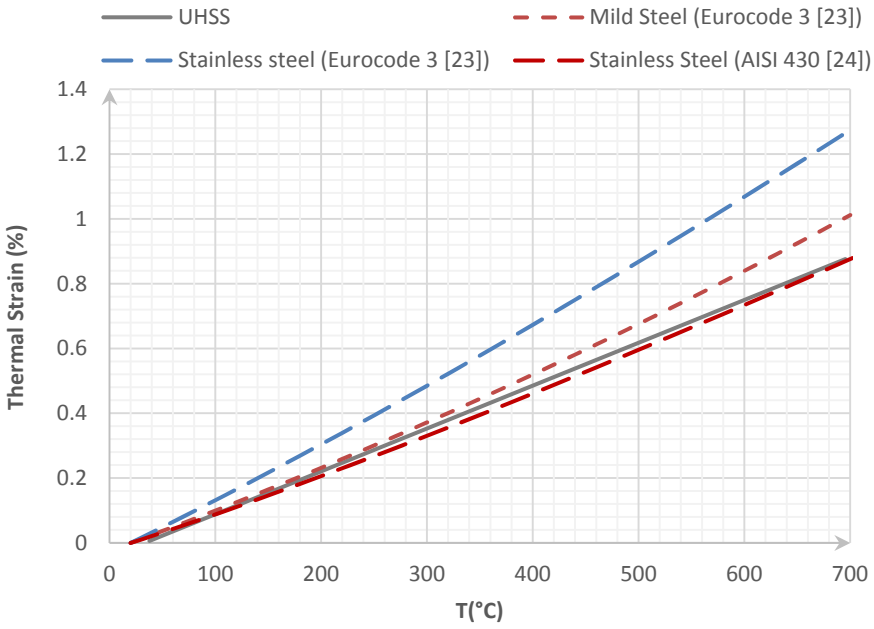

Figure 5-11. Thermal strain of UHSS compared to mild steel and stainless steels

Stress-induced strain (ε_σ):

One of the main advantages of constructing stress-strain-temperature surfaces is that by cutting planes with specific conditions through these surfaces, the interface curves satisfy those conditions. These planes can be horizontal planes specifying different constant stress levels while the interface curves show the variation of strain with the fire temperature at those stress levels. This is equivalent to the stress-induced strain response (ε_σ) in a transient fire test, in which the temperature of the material increases while the stress is kept constant. However, in order to have a meaningful strain-temperature curve, instead of the post-fire stress-strain-temperature surfaces shown in Figure 5-8, that of UHSS tested at fire temperatures and shown in Figure 5-12 is used. Then, the interface curves resulted from the intersection of horizontal planes with this surface represent the strain-temperature response of UHSS in transient fire under different constant stress levels. Alternatively, these curves can be simply obtained by considering the strain as the dependant variable and finding it in terms of the independent variables of stress and temperature. Noting that previously, the stress was considered as the dependant variable, while here the stress is assumed to have a constant value.

In Figure 5-13, the stress-induced strain-temperature ($\varepsilon_\sigma - T$) responses obtained from the present model for 4 different constant stress values including $\sigma = 94\,\text{MPa}$, $\sigma = 272\,\text{MPa}$, $\sigma = 449\,\text{MPa}$ and $\sigma = 624\,\text{MPa}$ are illustrated. These stress values are equivalent to $0.8\,f_{u,700}$ (or $0.08\,f_{0.2,RT}$), $0.8\,f_{u,600}$ (or $0.23\,f_{0.2,RT}$), $0.8\,f_{u,540}$ (or $0.38\,f_{0.2,RT}$) and $0.8\,f_{u,470}$ (or $0.53\,f_{0.2,RT}$), respectively.

Creep strain (ε_{cr}):

From the heat-up stage of the Creep-Cooling tests with $\beta = 0.8$ [9], variation of the total strains of UHSS with temperature in a transient fire under these constant stress values are obtained. If the thermal strain of UHSS shown in Figure 5-11 is subtracted from the total strains, based on Eq. (5-6), the resulted strains can be written as: $(\varepsilon_{total} - \varepsilon_{th}) = (\varepsilon_\sigma + \varepsilon_{cr})$. In Figure 5-13, the $(\varepsilon_{total} - \varepsilon_{th})$ strain values for the 4 constant stress values obtained from the experiments are also plotted. By comparing the curves obtained from the model with those obtained from the experiments, it can be seen that while they match well up to a certain temperature, after that temperature they diverge. The strain-temperature curves derived from the experimental tests include the stress-induced strain and the creep strain, i.e. $(\varepsilon_\sigma + \varepsilon_{cr})$. However, since the thermal strain has been removed from the stress-strain curves of the UHSS specimens tested at different elevated temperatures (they start from zero strain and zero stress), the strain-temperature curves obtained from the model represent only the stress-induced strain (ε_σ). Thus, this difference between the curves in each plot represents the creep strain (ε_{cr}) experienced by the material during fire due to the existence of constant axial load. In Figure 5-14, the values of ε_σ obtained from the model are subtracted from the curves of $(\varepsilon_{total} - \varepsilon_{th}) = (\varepsilon_\sigma + \varepsilon_{cr})$ obtained from the experiments. As a result, this figure shows the variation of ε_{cr} with temperature for the UHSS subjected to transient fire under different constant stress values. It can be seen from the curves of this figure that below ~450°C, for all constant stress values, the creep strain (ε_{cr}) induced in the UHSS under transient fire is almost zero. However, for fire temperatures above ~450°C, the value of ε_{cr} depends on the magnitude of the stress applied to the specimen. For instance, considering T=470°C temperature, the value of ε_{cr} is only considerable for the case of $\sigma = 624\text{MPa}$,

where the stress is equivalent to 80% of the capacity of UHSS at 470°C, i.e. $0.8 f_{u,470}$. For lower stress values, since they are well below the value of $f_{u,470}$ for UHSS, negligible ε_{cr} is induced in the material. Similarly, at T=540°C, the ε_{cr} caused by stress values below $\sigma = 449\,\text{MPa}$ (or $0.8 f_{u,540}$), are considerably lower than that induced in the UHSS in the case of $\sigma = 449\,\text{MPa}$. Noting that the UHSS subjected to $\sigma = 624\text{MPa}$ during fire, is already failed at T=540°C, as this stress value is higher than the ultimate capacity of UHSS at 540°C ($f_{u,540}$). Same reasoning is repeated for other fire temperatures. Also, it can be seen from Figure 5-14 that as the fire temperature (T) increases up to 700°C, the ε_{cr} values induced in the UHSS under $\sigma = 0.8 f_{u,T}$, are amplified up to 10 times.

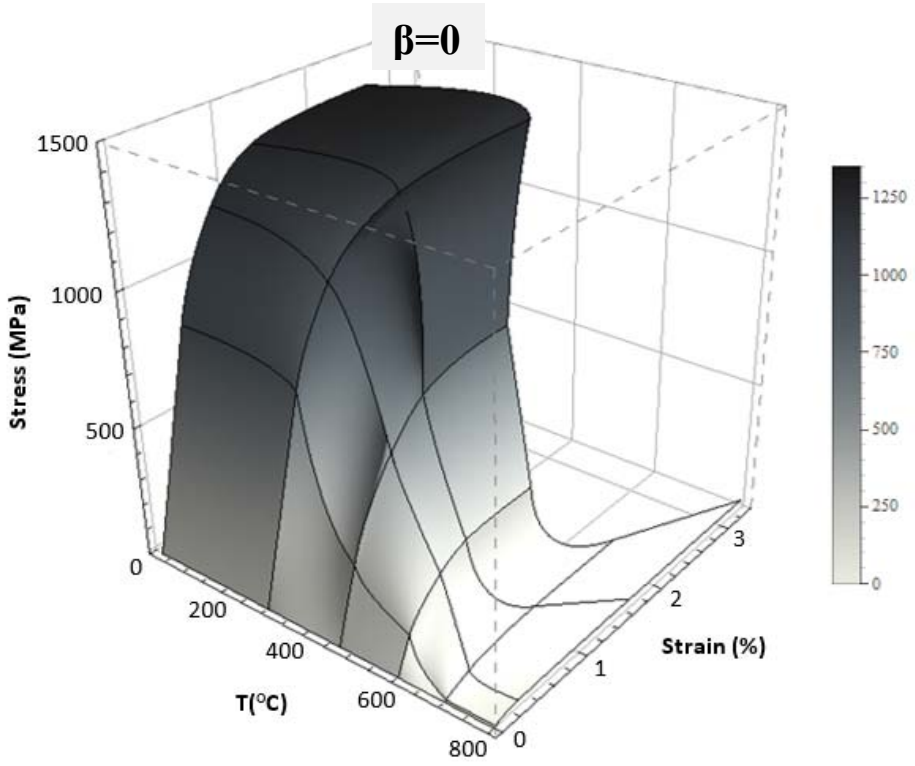

Figure 5-12. Stress-strain-temperature surfaces obtained by the proposed model for UHSS at different fire temperatures without axial load (β=0)

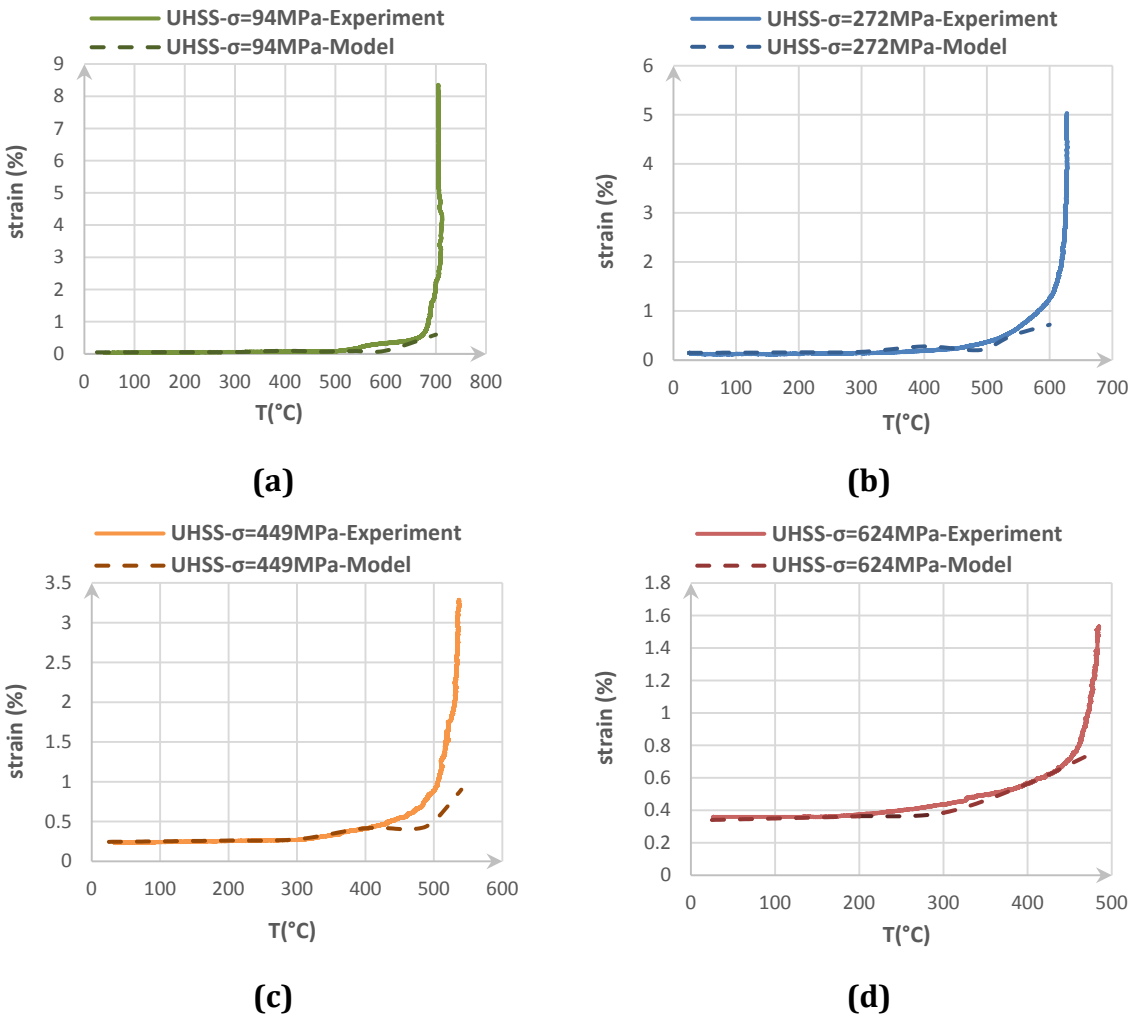

Figure 5-13.Comparison of the $(\varepsilon_\sigma + \varepsilon_{cr})$ strain in transient fire obtained from the experiments with the instantaneous stress-induced strain (ε_σ) predicted from the proposed model, for UHSS under different constant stress levels including: a)94MPa, b)272MPa, c)449MPa and d)624MPa

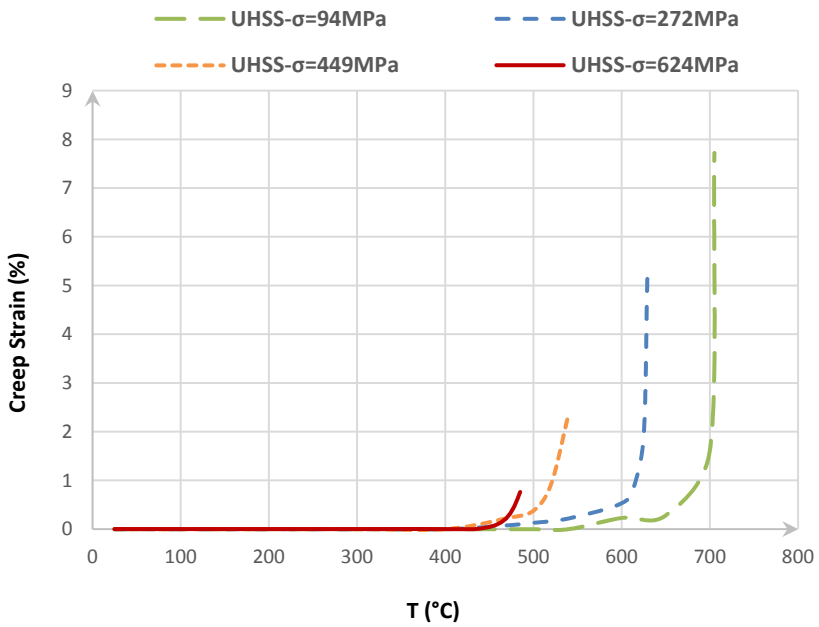

Figure 5-14. The creep strain (ε_{cr}) obtained from the proposed model and the experiments of Ref. [9] for UHSS subjected to different constant stress levels in transient fire

5.5. Conclusion

In this paper, Bernstain-Bézier functions were used to present the relationship between the stress, strain, the maximum fire temperature and the sustained axial load ratio for the UHSS tested at room temperature after cooling from different fire temperatures. The model was calibrated and validated with the experimental test results recently obtained by the authors of this paper in Refs. [6, 8, 9]. The model has the following main features:

1) It is capable of both interpolating and extrapolating the post-fire stress-strain curves.
2) It relates the post-fire stress-strain curves with both the maximum fire temperature and the axial load ratio.
3) By finding the interface curve between the $\sigma = \text{constant}$ surface and the in-fire stress-strain-temperature surface or switching the dependent variable from stress to strain, it can predict the instantaneous stress-induced strain (ε_{σ}) of the UHSS subjected to $\sigma = \text{constant}$ in a transient fire.

Therefore, although the proposed model may not seem as user friendly as other empirical models, due to its simple nature and not having nonlinear exponents, interchanging parameters can be easily conducted. This is highly beneficial in multi-phase loading scenarios for derivation of the creep strain as a very critical parameter required for the thermal analysis of steel structures; whereas in the available empirical models (i.e. Ramberg-Osgood, etc.), one cannot get the creep strain from the explicit relations. In this paper, knowing ε_{σ} in terms of the stress and temperature from the proposed model, the free thermal strain (ε_{th}) of UHSS as a function of fire temperature and the total strain (ε_{total}) obtained from the experimental test results obtained in Ref. [9], the variation of creep strain (ε_{cr}) of UHSS with the fire temperature for different constant stress levels were obtained. In all cases, a good agreement was achieved between the results predicted by the model and those obtained from the experimental tests. Obviously, for using the model for other types of steels (with different chemical compositions and manufacturing processes), similar to any other constitutive model (Ramberg-Osgood, etc.), calibration against a certain number of experimental tests must be conducted.

This paper provides the necessary inputs for modelling a structural component composed of UHSS material under fire/creep multi-phase loading scenario. Thus, it is a powerful model which can be used in research particularly aligned with finite element commercial packages such as ABAQUS, ANSYS, etc. The methodology can be extended to more and more applications like those included in Ref. [22]. Using the dataset provided in this paper together with those reported in the previous publications [6, 8, 9], the authors are now developing design recommendations for UHSS tubes under in-fire/post-fire conditions which is expected to be included in future publications.

Acknowledgement

The research work presented in this paper was supported by the Australian Government-Department of Education and also by Australian Research Council through a Discovery Project (DP150100442) awarded to the second and third authors.

References

[1] J. Outinen, Mechanical properties of structural steel at elevated temperatures and after cooling down, in: 10th International Conference - Fire and Materials 2007.
[2] X. Qiang, F.S.K. Bijlaard, H. Kolstein, Post-fire mechanical properties of high strength structural steels S460 and S690, Engineering Structures, 35 (2012) 1-10.
[3] X. Qiang, F.S.K. Bijlaard, H. Kolstein, Post-fire performance of very high strength steel S960, Journal of Constructional Steel Research, 80 (2013) 235-242.
[4] S. Gunalan, M. Mahendran, Experimental investigation of post-fire mechanical properties of cold-formed steels, Thin-Walled Structures, 84 (2014) 241-254.
[5] W. Wang, T. Liu, J. Liu, Experimental study on post-fire mechanical properties of high strength Q460 steel, Journal of Constructional Steel Research, 114 (2015) 100-109.
[6] F. Azhari, A. Heidarpour, X.-L. Zhao, C.R. Hutchinson, Mechanical properties of ultra-high strength (Grade 1200) steel tubes under cooling phase of a fire: An experimental investigation, Construction and Building Materials, 93 (2015) 841-850.
[7] M. Amraei, T. Skriko, T. Björk, X.-L. Zhao, Plastic strain characteristics of butt-welded ultra-high strength steel (UHSS), Thin-Walled Structures, 109 (2016) 227-241.
[8] F. Azhari, A. Heidarpour, X.-L. Zhao, C.R. Hutchinson, Post-fire mechanical response of ultra-high strength (Grade 1200) steel under high temperatures: Linking thermal stability and microstructure, Thin-Walled Structures, 119 (2017) 114-125.
[9] F. Azhari, A. Heidarpour, X.-L. Zhao, C.R. Hutchinson, Effect of creep strain on mechanical behaviour of ultra-high strength (Grade 1200) steel subject to cooling phase of a fire, Construction and Building Materials, 136 (2017) 18-30.
[10] J. Lu, H. Liu, Z. Chen, L. Bisby, Experimental investigation of the residual mechanical properties of cast steels after exposure to elevated temperature, Construction and Building Materials, 143 (2017) 259-271.
[11] S. Chen, S. Jiang, H. Guo, H. Cao, Y. Luo, K. Lan, Mechanical and ductile fracture performances of high strength structural steel Q690 after a fire: experimental investigation, Procedia Engineering, 210 (2017) 496-503.
[12] M.A. Bradford, X.P. Liu, Flexural-torsional buckling of high-strength steel beams, Journal of Constructional Steel Research, 124 (2016) 122-131.
[13] F. Javidan, A. Heidarpour, X.-L. Zhao, J. Minkkinen, Application of high strength and ultra-high strength steel tubes in long hybrid compressive members: Experimental and numerical investigation, Thin-Walled Structures, 102 (2016) 273-285.
[14] M. Nassirnia, A. Heidarpour, X.-L. Zhao, J. Minkkinen, Innovative hollow columns comprising corrugated plates and ultra high-strength steel tubes, Thin-Walled Structures, 101 (2016) 14-25.
[15] F. Javidan, A. Heidarpour, X.-L. Zhao, H. Fallahi, Fundamental behaviour of high strength and ultra-high strength steel subjected to low cycle structural damage, Engineering Structures, 143 (2017) 427-440.
[16] M. Farahi, A. Heidarpour, X.-L. Zhao, R. Al-Mahaidi, 08.35: Compressive behavior of concrete filled double skin sections consisting of corrugated plates and ultra-high strength steel corner tubes, ce/papers, 1 (2017) 2120-2127.
[17] S.N. Sadeghi, A. Heidarpour, X.-L. Zhao, R. Al-Mahaidi, An innovative I-beam to hybrid fabricated column connection: Experimental investigation, Engineering Structures, 148 (2017) 907-923.
[18] C.G. Bailey, I.W. Burgess, R.J. Plank, Computer simulation of a full-scale structural fire test, Structural Engineer, 74 (1996) 93-100.

[19] J.A. El-Rimawi, I.W. Burgess, R.J. Plank, The treatment of strain reversal in structural members during the cooling phase of a fire, Journal of Constructional Steel Research, 37 (1996) 115-135.
[20] G. Farin, 5 - The Bernstein Form of a Bézier Curve, in: Curves and Surfaces for CAGD (Fifth Edition), Morgan Kaufmann, San Francisco, 2002, pp. 57-79.
[21] E. Mirambell, E. Real, On the calculation of deflections in structural stainless steel beams: an experimental and numerical investigation, Journal of Constructional Steel Research, 54 (2000) 109-133.
[22] S. Sinaie, A. Heidarpour, X.L. Zhao, Stress-strain-temperature relation for cyclically-damaged structural mild steel, Engineering Structures, 77 (2014) 84-94.
[23] EN 1993-1-2, Eurocode 3: Design of steel structures - Part 1-2: General rules - Structural fire design, in, CEN, Brussels, , 2005.
[24] P.D. Desai, C.Y. Ho, Thermal Linear Expansion of Nine Selected AISI Stainless Steels, Defense Technical Information Center, 1978.

Chapter 6

Mechanical response of ultra-high strength (Grade 1200) steel under extreme cooling conditions

This chapter has been published in the Journal of *Construction and Building Materials*, Volume 175, June 2018, Pages 790-803.

DOI: 10.1016/j.conbuildmat.2018.04.191

Reprinted here with the Author Rights granted by Elsevier.

Table of Contents

Abstract

Ultra-high strength steels (UHSS) with nominal yield strength of up to 1200MPa have many potential applications in engineering fields. However, due to inadequate knowledge on the mechanical behaviour of these materials under extreme loading conditions (e.g. severe temperature changes), their extent of application in civil construction has remained restricted. This paper characterises the mechanical properties of Grade 1200 UHSS under extreme cooling conditions, which is defined as cooling from fire temperatures with an extreme cooling rate or cooling from ambient state to sub-zero temperatures. In order to simulate the extreme cooling rate, UHSS standard dog-bone specimens are heated up to different fire temperatures and cooled to room temperature using water-quenching (WQ) technique. To evaluate the effect of extreme cooling rate on the post-fire mechanical response of the tested materials, the residual mechanical properties of water-quenched specimens are compared to the air-cooled (AC) ones for different fire temperature exposures. For simulation of extreme cooling temperatures, the test specimens are cooled to sub-zero temperatures using Liquid Nitrogen (LN) injection. The changes in the mechanical properties of the tested specimens are then quantified and discussed. In both set of experiments, the mechanical behaviour of UHSS under extreme cooling conditions is compared to the common structural steels. Microstructural evaluation of UHSS tested specimens are also presented using optical and scanning electron microscopy (SEM) techniques.

Key Words: ultra-high strength steel; fire; cooling rate; water quenching; sub-zero temperature

6.1. Introduction

In order to minimise the weight of the structures and optimise the labour and transportation costs, ultra-high strength structural steels (UHSS) have recently been introduced as a promising construction material for energy efficient structural members [1-4]. In order to safely use these materials in civil engineering applications, their mechanical behaviour under different loading scenarios must be accurately known [5-13]. Considering fire as a common extreme loading scenario that can significantly damage the structure, understanding the behaviour of any construction material during this hazard is necessary.

In recent years, to investigate the effect of different parameters including maximum fire temperature, creep strain, steel grade, etc., on the mechanical properties of Grade 1200 UHSS material during fire and after cooling to room temperature, extensive experimental tests have been performed [3, 14-17]. With the main focus of these tests being on the residual mechanical properties of UHSS after cooling from fire to room temperature, it was concluded that the primary models proposed for the post-fire mechanical behaviour of mild steel [18, 19] are not applicable for all grades of steel and for all temperature ranges . It was also shown that there is a considerable reduction in the residual strength of UHSS cooled from fire temperatures of above 450°C [3, 14, 16]. In these studies, based on the thermodynamic stability of the phases present in UHSS, it was discussed that the mechanical behaviour of this material is very different in the two temperature regimes: the low temperature regime (up to ~700°C), and the high temperature regime (above 700°C). Based on the obtained results, it was observed that in low temperatures, while the changes in the post-fire residual strength of UHSS mostly depends on the maximum temperature reached, they are almost insensitive to the cooling rate. However, in the high temperature regime, it was predicted that the UHSS residual strength will be highly dependent on the cooling rate from elevated temperatures. The reason behind these conclusions were explained based on the phase diagrams, where in low temperatures, the identities of the phases present in the microstructures of the UHSS reached fire are not changed, and only the configuration and size of the microstructural grains are changed. However, due to formation of a new phase at high fire temperatures, depending on how fast the UHSS cools from fire, the residual strength of the material can significantly change. Some researchers in the field of civil engineering have so far

investigated the effect of cooling rate on the residual mechanical properties of steel materials after being cooled form different temperature regimes [20, 21]. Wang et al. [21] investigated the post-fire mechanical properties of high strength Q460 steel (HSS-Q460), including the yield strength, ultimate strength, uniform elongation and the elastic modulus, after exposure to fire temperatures of up to 900°C. In their study, two cooling methods of natural air-cooling and water-quenching were considered. They concluded that while the cooling method does not have a considerable effect on the yield strength and elastic modulus of the HSS-Q460 specimens cooled from fire to room temperature, it has a major effect on the ultimate tensile strength and uniform elongation of the HSS-Q460. According to their results, the ultimate tensile strength of the HSS-Q460 specimen water-quenched from 900°C to room temperature, is ~34% higher than the air-cooled one. However, the uniform elongation of the same water-quenched specimen is ~51% lower than the air-cooled one, meaning that the material becomes less ductile when cooled from fire with an extreme cooling rate. It was finally concluded that the effects of cooling method and even the maximum fire temperature on the residual mechanical properties of HSS-Q460 are only significant for temperatures above 700°C. In 2016, Aziz et al. [20] performed a similar study and evaluated the effect of fire temperature and cooling method on residual mechanical properties of ASTM A572 steel (high strength low alloy steel with original yield strength of 450MPa) after exposure to fire temperatures of up to 1000°C. According to their results, regardless of the method of cooling, the A572 steel cooled from fire temperatures of up to 600°C, recovers almost 100% of its original room temperature yield strength and ultimate tensile strength. However, this material loses ~40% of its yield strength when air-cooled from 800°C to room temperature and ~25% when water-quenched. In addition, the ultimate strength of A572 steel, only reduces when air-cooled from temperatures above 600°C and does not change when water-quenched from these temperatures. Similar to the results obtained in Ref. [21], the elastic modulus of A572 is fully reversible for all temperatures and both cooling methods. This result was quite expected as the elastic modulus of steel only depends on the temperature at which the material is tested [22].

From the literature, it is understood that the effect of cooling rate on residual mechanical behaviour of steel materials (especially high-strength steels) becomes significant after exposure to a certain temperature, which is the start of the high fire temperatures range.

This paper mainly aims to investigate the effect of extreme cooling rate on post-fire mechanical behaviour of Grade 1200 ultra-high strength steel (UHSS) cooled from high fire temperatures. To this end, the UHSS standard dog-bone coupons extracted from cold-formed welded UHSS tubes are heated up to different fire temperatures and cooled to room temperature using water-quenching and their residual mechanical properties including stress-strain curves, strength and ductility are compared to those of naturally air-cooled samples obtained in Ref. [16]. Similar tests are carried out on Grade 800 high strength steel (HSS) and Grade 350 mild steel (MS) and the effect of steel grade is discussed. For a more clear justification of the obtained results, a microstructural evaluation is performed on the bulk microstructure of some air-cooled and water-quenched materials.

In line with the purpose of simulating the extreme cooling conditions, this paper also investigates the mechanical behaviour of UHSS (as the main purpose), HSS and MS (for comparison purposes) cooled from room temperature to harsh low temperatures, i.e. sub-zero temperatures. As a common application of this goal of the study, it can be referred to the safety of critical offshore structures such as oil platforms, which require steel capable of exhibiting high load capacity while maintain structural integrity at very low temperature [23]. Although the general qualitative behaviour of these materials at sub-zero temperatures are quite predictable without performing experimental tests, quantifying the exact mechanical properties of them under harsh low temperatures is necessary for the design of offshore structures. It is noted that the design codes such as NORSOK standards only provide limited guidance on the requirements for steels at temperatures of down to -14°C [24].

In this paper standard dog-bone UHSS, HSS and MS steels are cooled to sub-zero temperatures of as low as -80°C and after conducting quasi-static tensile tests on them, their mechanical properties are measured and compared to the original room temperature values.

6.2. Experimental tests

6.2.1. Test Specimens

The chemical compositions of the three grades of steel studied in this paper, i.e. Grade 1200 UHSS, Grade 800 HSS and Grade 350 MS, are presented in Table 6-1. To conduct quasi-static tensile tests on the specimens, standard dog-bone specimens are extracted from the steel tubes using water-jet cutting. The nominal diameter and wall thickness of steel tubes are 76.1mm and 3.2mm, respectively. Figure 6-1 shows the geometry, dimensions and location of the specimens extracted from the tubes. It is important to note that all the steel tubes used in this study are cold-formed welded tubes. Also, the UHSS and HSS tubes are manufactured by the unique direct quenching method developed by SSAB manufacturing company, in which the material is quenched only in one stage [3, 14, 16].

Table 6-1. The chemical compositions of tested materials (wt %)

Material	C	Si	Mn	P	S	Cr	Ni	Mo	B	Al
UHSS	0.230	0.800	1.700	0.025	0.015	1.500	1.000	0.500	0.005	
HSS	0.100	0.250	2.100	0.020	0.010					0.015
MS	0.230	0.400	1.350	0.040	0.050					

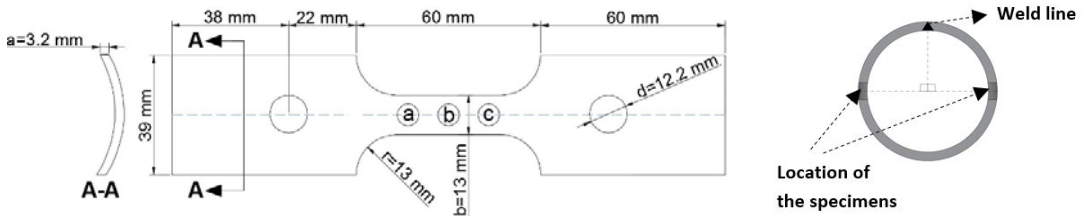

(a) **(b)**

Figure 6-1. a) Geometry and b) location of test specimens sectioned from the steel tubes

6.2.2. Testing Method

The extreme cooling conditions are defined as: 1) the case where the material cools from fire temperatures with an extremely high cooling rate compared to the natural air-cooling; and 2) the case where the material cools from the ambient state to sub-zero

temperatures. Two sets of tests are designed to simulate the aforementioned conditions, respectively, including: 1) water-quenching cooling tests, and 2) sub-zero temperature tests. Each test is conducted at least twice. However, if the difference between the results obtained from two similar tests is more than 3%, additional tests are conducted.

6.2.2.1 Water-quenching cooling tests

This set of tests are designed to simulate the extreme cooling rate from fire temperatures to room temperature. First, the specimen is located inside the SF-16 split furnace installed on the Instron 5982 100kN testing machine which heats the specimen up to 900°C at a rate of ~20°C/min. Three thermocouples are attached to three points (a, b and c) on the gauge length of the dog-bone specimen (Figure 6-1) to record the temperature of the specimen during fire. In order to attach the thermocouples to the specimen, a heat-resistant wire is wrapped around them on the grips of the loading machine in a way that the axial movement of the specimen is not limited. The temperature of the specimen is stabilised once the thermocouples' temperature remains constant for ~20 min. The door of the furnace is then opened and using a long heat-resistant plier, the heated specimen is taken out of the furnace and is subsequently quenched into the water inside a metal bucket such that its temperature drops very quickly to room temperature. This procedure from the time the door of the furnace is opened to the time the specimen is soaked into the water takes ~13 seconds. Thus, the simulated cooling rate from different fire temperatures is ~54-62 °C/sec (~3240-3720 °C/min). Note that the average rate for the natural air-cooling is about ~20°C/min. After accurately measuring the dimensions of the cooled specimen, it is subjected to strain controlled quasi-static tensile test using Instron 5982 100kN testing machine with an applied strain rate of $0.005 \pm 0.002\,\mathrm{min}^{-1}$ [25] until failure. The strain of the specimen during the tensile test is recorded using the contact extensometer. The main components of the apparatus of this set of tests (the furnace, testing machine, thermocouples and the extensometer), are the same as those used in Ref. [16] for the natural air-cooling tests.

6.2.2.2 Sub-zero temperature tests

Sub-zero temperature tests are performed to simulate extremely low temperature exposures on the UHSS specimens. After accurately measuring the dimensions of the

specimen, it is gripped inside Instron environmental chamber mounted on the Instron 5982 100kN testing machine. Similar to the water quenching cooling tests, thermocouples are attached to the back of the gauge length of the specimen while a strain gauge is attached to the middle of the specimen's gauge length to monitor and record the strain. The temperature inside the environmental chamber is then dropped at a rate of 10°C/min by injecting liquid nitrogen into the insulated chamber. The Instron environment chamber comes with an automated built in temperature controlling system that is used to control the inflow of liquid nitrogen and hence the temperature. During the cooling of the specimen, the testing machine is operating under load control so that its upper jaw could displace to accommodate the shrinkage of the specimen due to temperature reduction while the load is remained close to 0 kN. Upon reaching the desired temperature in the environmental chamber, the specimen is allowed to settle in its new environment for further ~20mins to ensure that it reached the target temperature. Following the achievement of the target temperature, quasi-static tensile test is carried out with an applied strain rate of $0.005 \pm 0.002\,\mathrm{min}^{-1}$ [25] until failure. The test setup used for this set of tests is schematically illustrated in Figure 6-2.

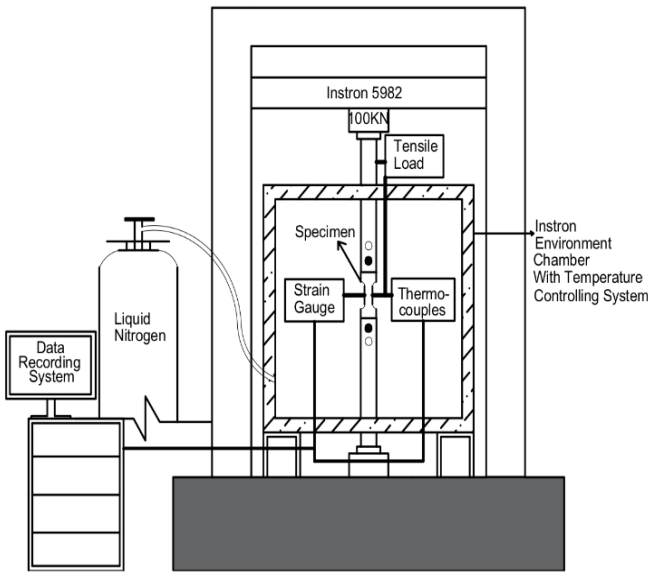

Figure 6-2. Test setup for sub-zero temperature tests

6.3. Results and Discussion

In order to study the mechanical response of UHSS tubes under extreme cooling conditions, the stress-strain curves, characteristic tensile strengths, and parameters indicating the ductility of the tested specimens are discussed. In addition to the ultimate tensile strength (f_u), the characteristic tensile strengths are defined as the tensile strengths at certain strain levels including 0.2%, 0.5%, 1.5% and 2.0% strains and are shown as $f_{0.2}$, $f_{0.5}$, $f_{1.5}$ and $f_{2.0}$. Illustration of the aforementioned strain and strength values are presented in Figure 6-3. As can be understood from this figure, unlike the $f_{1.5}$ and $f_{2.0}$ strengths for which the total strain (both elastic and plastic strains) are considered, the $f_{0.2}$ and $f_{0.5}$ strengths are calculated by excluding the elastic strain. It is also important to note that in most research works, the elastic strain in not excluded for derivation of $f_{0.5}$ strength [26, 27]. However, since the 0.5% strains of the stress-strain curves obtained from this research are usually within the yield stage, the elastic strain for this strength is excluded in this paper.

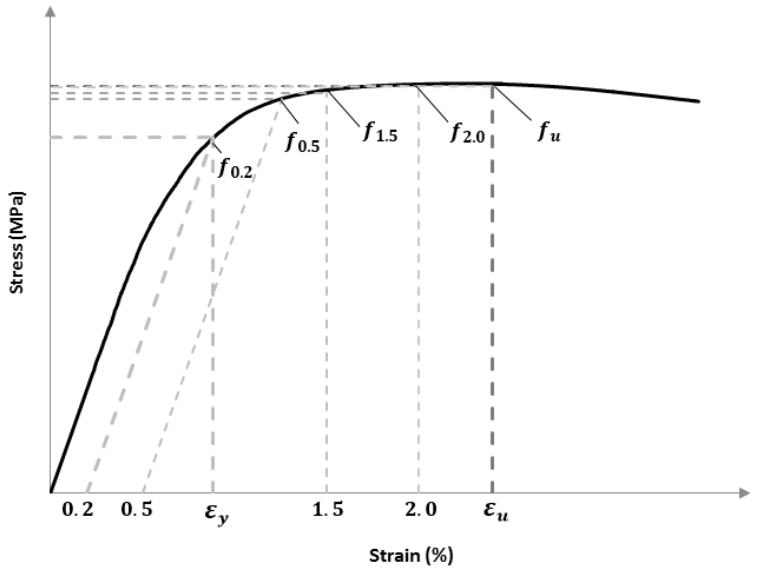

Figure 6-3. Description of characteristic tensile strengths and strains on a typical stress-strain curve

6.3.1. Stress-strain curves

The stress-strain curves of the UHSS specimens after water-quenching (WQ) cooling tests are presented in Figure 6-4. In order to understand the effect of the extreme cooling rate, i.e. water-quenching, the stress-strain curves obtained in Ref. [16] for the UHSS specimens cooled from different fire temperatures to room temperature with natural air-cooling (AC) method are also included in this figure. The UHSS-C***T***-AC and UHSS-C***T***-WQ labels represent the UHSS specimens **c**ooled from fire temperature ***T*** to room temperature with natural **a**ir-**c**ooling and **w**ater-**q**uenching methods, respectively. Also, the UHSS-**RT** curve represents the virgin UHSS specimen tested at **r**oom **t**emperature. The stress-strain curves are reported up to the onset of necking. The reason for not showing these curves after necking is that due to the changes in the specimen's cross section during necking, the engineering strain readings in this region are not accurate as they are not uniform. By comparing the stress-strain curves obtained for the UHSS specimens cooled from different fire temperatures with both cooling methods, it is seen that cooling rate does not affect the results for UHSS cooled from 600°C to room temperature. This is because 600°C is not in the temperature range where the identity of the phases present in UHSS are changed. Therefore, the water-quenching cooling tests for fire temperatures below 600°C are not presented as the cooling rate, even at its extreme condition, does not affect the results. It can be observed from UHSS-C750-AC and WQ stress-strain curves, and UHSS-C800-AC and WQ curves that for the UHSS cooled from 750°C and 800°C to room temperature, the water-quenching cooling method results in a much higher residual strength compared to the natural air-cooling method. From comparison of UHSS-C750-AC and WQ stress-strain curves, it can be also inferred that the UHSS material water-quenched from 750°C experiences much less uniform elongation compared to the air-cooled one, meaning that the higher cooling rate from this temperature makes UHSS comparatively less ductile. On the contrary, it can be seen from Figure 6-4 that unlike 750°C and 800°C temperatures, the strength of the UHSS specimen cooled from 700°C with water-quenching technique (UHSS-C700-WQ) is ~13% lower than that of the air-cooled specimen (UHSS-C700-AC). This shows that similar to 600°C fire temperature, 700°C is not in the temperature range where the identity of the phases in UHSS microstructure are not significantly changed and probably only a small amount of austenite is formed at this temperature. For better comparison of the results obtained

from the UHSS water-quenched and air-cooled from 700°C, microstructural evaluation has been conducted (see Section 6.4).

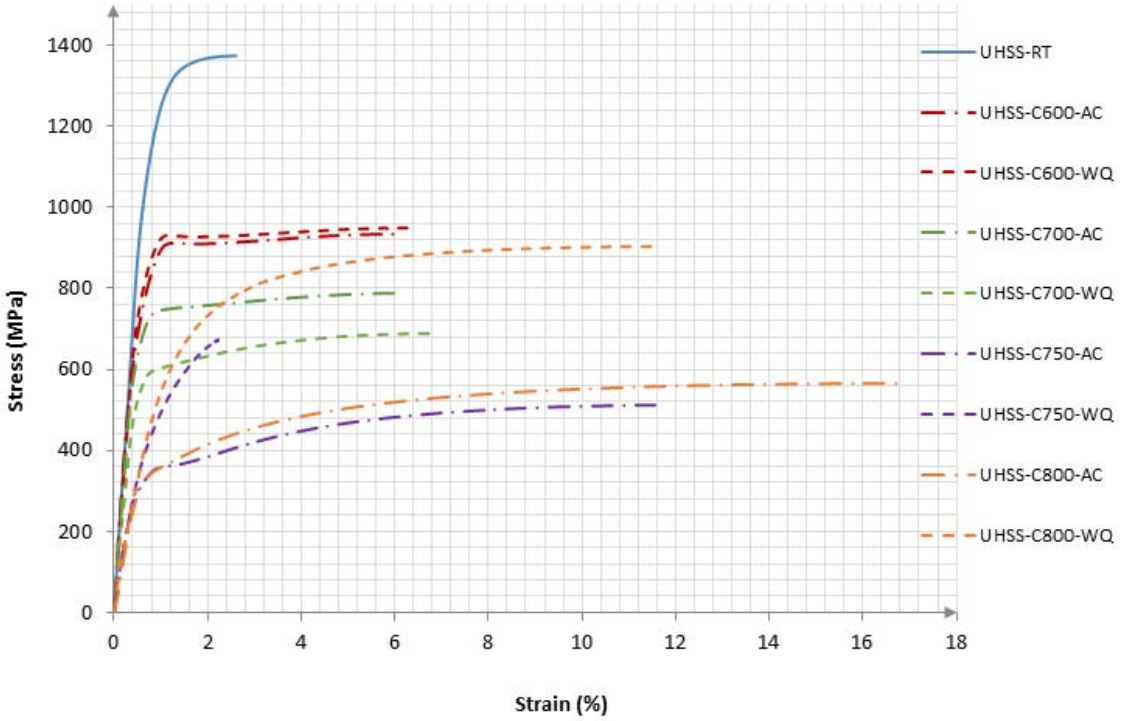

Figure 6-4. Stress-strain curves of UHSS specimens tested at room temperature after being cooled from various fire temperatures using different cooling methods: Air Cooling (AC) and Water Quenching (WQ)

In Figure 6-5, the stress-strain curves of the UHSS specimens cooled from room temperature to sub-zero temperatures are presented. The UHSS-C(-40) and UHSS-C(-80) curves represent the stress-strain curves of the UHSS specimens cooled from room temperature to -40°C and -80°C, respectively. The reason that only these two sub-zero temperatures are considered is that the minimum temperature the environmental chamber can be cooled to is -80°C and lower temperatures are not practical in civil engineering applications. In addition, the variation of strength is not very significant and thus only two temperature suffices to show the trend and analyse the behaviour of UHSS at low temperatures. Comparing the three stress-strain curves shown in Figure 6-5, it can be seen that considering the linear elastic stiffness of all three materials to be constant in their respective nature, their mechanical properties are found to be affected by decrements in temperature. As expected, by decreasing the temperature down to -80°C, the UHSS material becomes less ductile, meaning that it finds higher strength and a

considerably lower uniform elongation. It is worth noting that the importance of performing these tests is mainly to quantify the decrease in ductility of UHSS under sub-zero temperatures which is presented and discussed in section 6.3.3.

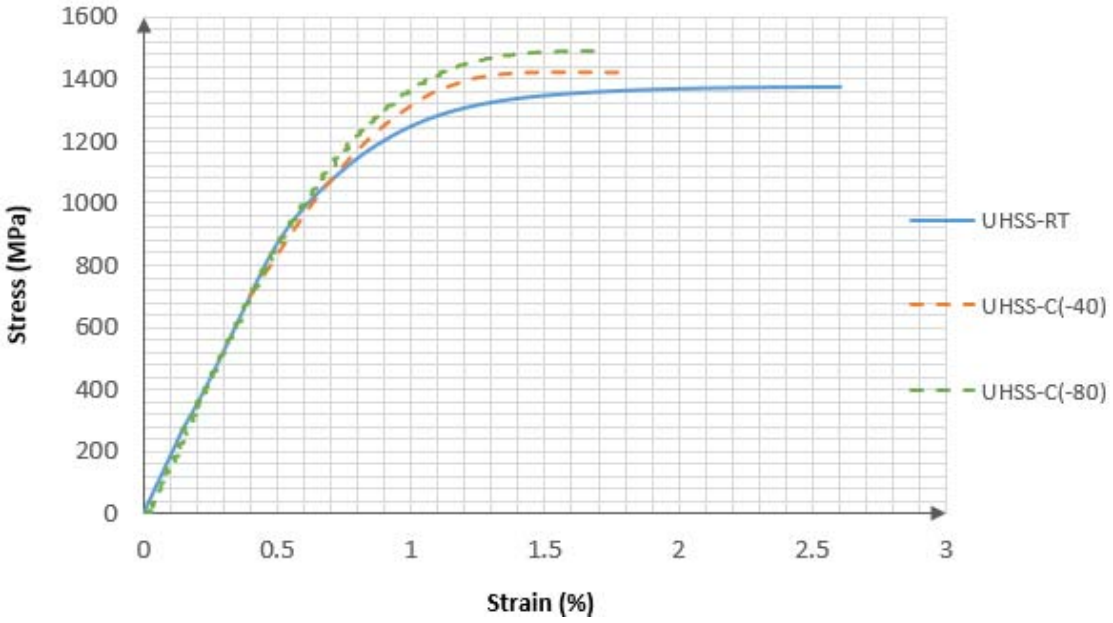

Figure 6-5. Stress-strain curves of UHSS specimens tested at sub-zero temperatures

6.3.2. Strength

To evaluate the changes in the residual strength of the water-quenched UHSS specimens compared to the original strength values, the characteristic strength values obtained from water-quenching cooling tests (noted by WQ index) are normalised with respect to those obtained for the virgin UHSS at room temperature (noted by RT index) and presented in Table 6-2. It can be inferred from the results of this table that for UHSS specimens water-quenched from temperatures below 750°C, the values of the characteristic strengths at different strain levels do not vary for a constant temperature. However, these values change significantly for 750°C and 800°C temperatures, which shows the difference between the strain hardening progress of the UHSS specimens water-quenched from these temperatures and the original ones tested at room temperature. Also, comparing the strength values of WQ cooling tests for 600°C and 700°C temperatures, a considerable reduction can be observed, which is the same behaviour that reported for the air-cooled UHSS specimens in Ref. [16]. The $f_{1.5,WQ} / f_{1.5,RT}$

and $f_{u,WQ}/f_{u,RT}$ values of the UHSS water-quenched from 750°C, however, do not exhibit a considerable difference from those for the 700°C. Because of the greatly extended elastic-plastic transition in the C750-WQ curve, the strength values at lower strain levels ($f_{0.2,WQ}/f_{0.2,RT}$ and $f_{0.5,WQ}/f_{0.5,RT}$) are less than those of all other temperatures. The reason of not reporting the strength at the 2.0% strain level for this test was the small uniform elongation value in the UHSS-C750-WQ curve that did not allow the UHSS to experience 2.0% strain prior to necking. The general trend of the residual strength variation with respect to the maximum fire temperature in water-quenching cooling tests must be categorised into temperatures equal or below 700°C, i.e. low fire temperatures, and above 700°C, i.e. high fire temperatures. In low fire temperatures, similar to the air-cooled samples, water-quenched samples are also experiencing a reduction in the residual strength values as the temperature increases. However, for the UHSS specimens cooled from high fire temperatures with water-quenching technique, a general trend cannot be accurately defined as new phases are formed and transformation of the phases during cooling from these temperatures is strongly dependent on the cooling rate. In Section 6.4, the relationship between these temperature ranges and the phases present in the microstructure is explained more deeply.

In Table 6-3, for better understanding of the extreme cooling rate effect, the ratio of the residual strength values of UHSS water-quenched from different fire temperatures (noted by WQ index) with respect to the air-cooled ones (noted by AC index) are presented. The results of the UHSS cooled from 600°C to room temperature clearly show no dependence on the cooling rate. For the 700°C temperature exposure, the water-quenched UHSS specimens exhibit an average of ~16% less strength than the air-cooled ones. To understand the reason behind this unexpected behaviour, comparison of the bulk microstructure of the air-cooled and water-quenched samples are performed in the next section to provide more insights into this phenomenon. Moving on to high fire temperatures, i.e. above 700°C, it can be seen that the ratio of the strength values of the water-quenched specimens to those of air-cooled UHSS specimens signifies the strong effect of the cooling rate on the residual strength of UHSS after fire. For the UHSS specimens water-quenched from 750°C and 800°C to room temperature, respectively, the strength values are in average ~35% and ~70% higher than the air cooled ones.

Table 6-2. Variation of strength of UHSS after cooling down from various fire temperatures by water-quenching (WQ) method with respect to that of virgin UHSS at room temperature (RT)

Temperature	600°C	700°C	750°C	800°C
$\frac{f_{0.2,WQ}}{f_{0.2,RT}}$	0.67	0.47	0.26	0.34
$\frac{f_{0.5,WQ}}{f_{0.5,RT}}$	0.69	0.46	0.35	0.44
$\frac{f_{1.5,WQ}}{f_{1.5,RT}}$	0.68	0.47	0.49	0.56
$\frac{f_{2.0,WQ}}{f_{2.0,RT}}$	0.67	0.47		0.58
$\frac{f_{u,WQ}}{f_{u,RT}}$	0.69	0.50	0.49	0.66

Table 6-3. Ratio of strength of UHSS after cooling down from various fire temperatures by water-quenching (WQ) method and natural air-cooling (AC)

Temperature	600°C	700°C	750°C	800°C
$\frac{f_{0.2,WQ}}{f_{0.2,AC}}$	1.03	0.82	1.00	1.32
$\frac{f_{0.5,WQ}}{f_{0.5,AC}}$	1.01	0.81	1.30	1.65
$\frac{f_{1.5,WQ}}{f_{1.5,AC}}$	1.01	0.84	1.78	1.97
$\frac{f_{2.0,WQ}}{f_{2.0,AC}}$	1.01	0.85		1.92
$\frac{f_{u,WQ}}{f_{u,AC}}$	1.01	0.87	1.31	1.60

To quantify the changes in strength of the UHSS cooled from the ambient state to harsh low temperatures, the strength values at different strain levels for UHSS specimens tested at sub-zero temperatures (noted by SZ index) are normalised with respect to the room

temperature values as presented in Table 6-4. It can be seen that in average, the strength increases up to 8% and 12% when cooled to -40°C and -80°C, respectively.

Table 6-4. Variation of strength of UHSS at sub-zero temperatures

Temperature	-40°C	-80°C
$\frac{f_{0.2,SZ}}{f_{0.2,RT}}$	1.053	1.105
$\frac{f_{0.5,SZ}}{f_{0.5,RT}}$	1.079	1.119
$\frac{f_{1.5,SZ}}{f_{1.5,RT}}$	1.057	1.107
$\frac{f_{2.0,SZ}}{f_{2.0,RT}}$		
$\frac{f_{u,SZ}}{f_{u,RT}}$	1.033	1.085

6.3.3. Ductility

The ductility of a material can be evaluated by different parameters depending on its application. In this paper, one reason to evaluate the ductility of UHSS under extreme cooling conditions is to determine if the material can develop sufficient plastic deformation under these conditions. The civil engineering codes of practice including AS4100 [28], AS/NZS 4600 [29] and Eurocode 3 [30] have set some requirements, among which, the ratios of $f_u/f_{0.2}$ and $\varepsilon_u/\varepsilon_y$ are discussed in this study. Note that in order to develop sufficient plastic deformation to perform plastic analysis on mild steel structures, AS4100 [28] and Eurocode 3 [30] standards require $f_u/f_{0.2} \geq 1.2$, while AS/NZS 4600 [29] suggest $f_u/f_{0.2} \geq 1.08$. Eurocode 3 [30] also sets a minimum limit of 20 for $\varepsilon_u/\varepsilon_y$.

The ratios of $f_u/f_{0.2}$ and $\varepsilon_u/\varepsilon_y$ for UHSS cooled from different fire temperatures with water-quenching technique (noted by WQ index) are illustrated in Table 6-5. From the values of $f_u/f_{0.2}$ presented in this table, it can be seen that for all the specimens water-quenched from different fire temperatures, this ratio is within the limits set out by the standards, as the minimum ratio is 1.21 (above both 1.08 and 1.2). However, looking at

the ratio of $\varepsilon_u/\varepsilon_y$ obtained from the water-quenching tests, it can be seen that the UHSS specimens do not meet the requirement suggested by Eurocode 3 [30], as neither of them are above 20.

Table 6-5. Variation of the ratios of $f_u/f_{0.2}$ and $\varepsilon_u/\varepsilon_y$ after cooling from different high fire temperatures

Temperature	**600°C**	**700°C**	**750°C**	**800°C**
$(f_u/f_{0.2})_{WQ}$	1.21	1.25	2.17	2.25
$(\varepsilon_u/\varepsilon_y)_{WQ}$	10.53	11.88	4.90	18.11

To better understand the effect of extreme cooling rate on the ductility of UHSS after cooling from fire, the values of the ratios discussed in Table 6-5 are normalised with respect to those for the air-cooled UHSS (noted by AC index) and presented in Table 6-6. It can be understood from the results that for low temperatures, i.e. 600°C and 700°C, the ratio of $f_u/f_{0.2}$ for the water-quenched UHSS and the air-cooled one are almost the same, which shows the minor effect of cooling rate on the post-fire ductility of UHSS. Also, the difference between the ratio of $\varepsilon_u/\varepsilon_y$ for water-quenched samples and air-cooled samples at low temperatures is not significant compared to that of UHSS cooled from high temperatures. So, neither of $f_u/f_{0.2}$ or $\varepsilon_u/\varepsilon_y$ exhibit major sensitivity to cooling rate when UHSS is cooled from low fire temperatures. However, for UHSS cooled from high fire temperatures, i.e. above 700°C, the $f_u/f_{0.2}$ ratio of the water-quenched UHSS is up to 31% higher than the air-cooled UHSS, whereas, the $\varepsilon_u/\varepsilon_y$ ratio of the water-quenched UHSS is up to 76% lower than the air-cooled one. The reason for the unexpected increase in the $f_u/f_{0.2}$ ratio is the extended elastic-plastic transition in the stress-strain curves of UHSS-C750-WQ and UHSS-C800-WQ, which leads to higher values of ultimate tensile stress (f_u) compared to the 0.2% proof stress ($f_{0.2}$). The significant decrease in $\varepsilon_u/\varepsilon_y$ is however quite expected as UHSS becomes very brittle when water-quenched and thus the necking occurs much earlier than the air-cooled UHSS.

Table 6-6. Variation of the ratios of $f_u/f_{0.2}$ and $\varepsilon_u/\varepsilon_y$ after cooling from different high fire temperatures

Temperature	600°C	700°C	750°C	800°C
$\frac{(f_u/f_{0.2})_{WQ}}{(f_u/f_{0.2})_{AC}}$	0.99	1.07	1.31	1.21
$\frac{(\varepsilon_u/\varepsilon_y)_{WQ}}{(\varepsilon_u/\varepsilon_y)_{AC}}$	1.06	1.14	0.24	0.58

An important reason for conducting the sub-zero temperature tests on UHSS, was to quantify the ductility parameters to check whether or not it can develop enough plastic strain. Table 6-7 presents the $f_u/f_{0.2}$ and $\varepsilon_u/\varepsilon_y$ ratios for the UHSS tested at room temperature (RT) and sub-zero temperatures of -40°C and -80°C. From the values presented in this table, it can be understood that while the requirements set out by the standards for $f_u/f_{0.2}$ are met, the values of $\varepsilon_u/\varepsilon_y$ for UHSS at sub-zero temperatures of down to -80°C are much lower than the minimum limit of 20 suggested by Eurocode 3 [30]. This reduction in $\varepsilon_u/\varepsilon_y$ value of the UHSS specimens subjected to sub-zero temperatures can be justified by the Considère criterion [31], where as a consequence of the ultimate strength increase, the yielding and necking points (defining ε_y and ε_u, respectively) are moved closer to each other on the stress-strain curve.

Table 6-7. $f_u/f_{0.2}$ and $\varepsilon_u/\varepsilon_y$ values at room temperature and after cooling down to sub-zero temperatures

Temperature	RT	-40°C	-80°C
$f_u/f_{0.2}$	1.174	1.199	1.200
$\varepsilon_u/\varepsilon_y$	3.106	2.209	2.034

Another good parameter showing the ductility of a material is the total strain energy absorbed per unit volume. Calculating this parameter can be determined by computing the area under the stress-strain curves as:

$$U^* = \int_0^{\varepsilon} \sigma \, d\varepsilon \tag{6-1}$$

The values of engineering stress (σ) and strain (ε) after necking are not accurate due to the non-uniform deformation of the specimens. Therefore, in this study the value of U^* is calculated up to the onset of necking and so, in Eq. (6-1), the upper limit of integral is the uniform elongation, i.e. $\varepsilon = \varepsilon_u$.

In Table 6-8, the normalised values of the strain energy absorbed per unit volume for the UHSS cooled from different fire temperatures by water quenching technique (U^*_{WQ}) with respect to that of the original UHSS tested at room temperature (U^*_{RT}) are illustrated. In addition, to discuss the effect of extreme cooling rate, the ratio of U^*_{WQ} with respect to the corresponding value for the air-cooled UHSS (U^*_{AC}) are also presented. It can be seen that except for the 750°C fire temperature, while there is a general increasing trend for the energy absorption of the UHSS water-quenched from different fire temperatures as the temperature increases, a significant difference cannot be observed between the results of the air-cooled (AC) and water-quenched (WQ) UHSS specimens. This means that, cooling of UHSS from most fire temperatures (except for 750°C) increases its energy absorption almost to the same extent for both cooling methods, which is due to the dependence of U^* value on both stress and strain values (see Eq. (6-1)). Although the values of strain for the water-quenched specimens are lower than the air-cooled ones, due to their higher stress values, there is not a significant difference between the U^* values of UHSS cooled from fire by the two cooling methods. The reason for the low value of energy absorption for the UHSS water-quenched from 750°C (65% lower than the virgin UHSS and 80% lower than the air-cooled one) is the low value of its uniform elongation (~2.2%).

Table 6-8. Variation of strain energy after cooling down from various fire temperatures to room temperature

Temperature	**600°C**	**700°C**	**750°C**	**800°C**
(U^*_{WQ}/U^*_{RT})	1.92	1.46	0.35	3.15
(U^*_{WQ}/U^*_{AC})	1.06	0.97	0.20	1.08

For a UHSS material subjected to low temperatures, an overall decrease in the ductility of the material is expected. However, apart from a qualitative analysis, it is important to specify the degree of ductility reduction at these low temperatures. Thus, the values of the energy absorption of the UHSS at sub-zero temperatures (U^*_{SZ}) are normalised with respect to the original room temperature value (U^*_{RT}). From Table 6-9, it can be seen that the energy absorption of the UHSS is reduced by up to ~39% when subjected to sub-zero temperatures. However, there is not a significant difference between the U^*_{SZ} values for UHSS subjected to -40°C and -80°C, meaning that once UHSS is subjected to sub-zero temperatures of as low as -40°C, it loses a large fraction of its ability to absorb strain energy and by further decrease of temperature, the strain energy absorption is no more decreased.

Table 6-9. Variation of strain energy after cooling down to sub-zero temperatures

Temperature	**-40°C**	**-80°C**
(U^*_{SZ}/U^*_{RT})	0.63	0.61

6.3.4. Investigation of steel grade effect

To investigate the effect of steel grade on the mechanical behaviour of steel under extreme cooling conditions, two lower strength grades of steel, Grade 800 high strength steel (HSS) and Grade 350 mild steel (MS), are also discussed and their behaviour is compared with that of Grade 1200 steel (UHSS). Figure 6-6 illustrates the plots of the thermodynamic stability of the phases present in the microstructure of these steel materials. These plots were calculated using the software package Thermo-Calc [32] and TCFe7 steel data base. From these plots, the percentage of each phase at different temperatures can be understood for MS, HSS and UHSS materials. Due to the importance of the retained Austenite phase, the percentage values of this phase at different temperatures are also illustrated next to these plots. It can be seen that for each of these steel alloys, there is a critical temperature (around 700°C) that the green curve representing the Austenite phase is appeared and the identity of the phases present in the microstructure of the material changes. This critical temperature specifies the boundary between the low and high fire temperatures for each steel alloy. Further details about these plots are presented in Refs [3, 16] and the phase changes in the

microstructure of UHSS cooled from different fire temperatures are explained in section 4 of this paper.

Figures 6-7 and 6-8 present the HSS and MS stress-strain curves obtained from the water-quenching cooling tests, in which the effect of extreme cooling rate is evaluated. For comparison purposes, the stress-strain curves obtained in Ref. [16] for HSS and MS materials cooled from fire temperatures with natural air-cooling method are also included in these figures. Similar to the labelling system used in the previous sections, HSS(or MS)-C***T***-AC and HSS(or MS)-C***T***-WQ labels represent the HSS(or MS) specimens tested at room temperature after **c**ooling from fire temperature ***T*** with **a**ir-**c**ooling and **w**ater-**q**uenching methods, respectively. Also, the HSS-RT and MS-RT stress-strain curves are related to the virgin HSS and MS materials tested at room temperature. It is important to note that since the mechanical properties of both HSS and MS materials are not significantly changed when cooled from fire temperatures below 700°C [16], the minimum fire temperature considered for these materials is 700°C.

The stress-strain curves of the air-cooled and water-quenched HSS specimens indicate that the post-fire mechanical behaviour of the HSS material cooled from fire temperatures below 750°C, is not significantly affected by the cooling rate. The only considerable difference that can be observed between the HSS-C750-AC and HSS-C750-WQ curves is the pronounced yield point in the stress-strain curve of the air-cooled HSS, which disappears in the water-quenched sample. Also, during transformation from elastic to plastic deformation, the water-quenched HSS specimen exhibits continuous yielding behaviour and thus a lower yield strength compared to the air-cooled HSS specimen which exhibits a yield plateau. When HSS is cooled from 800°C to room temperature, the strength of the water-quenched specimen (HSS-C800-WQ) is higher than the air-cooled one (HSS-C800-AC), meaning that the extreme cooling rate is able to affect the mechanical response of the HSS cooled from this fire temperature. This result was expected from the calculated plots of the thermodynamic stability of the phases present in HSS microstructure [3, 16] (Figure 6-6b), according to which, temperatures above 750°C are considered as high fire temperatures for this material. Regarding the uniform elongation of the tested HSS materials, while the uniform elongation of the HSS air-cooled and water-quenched from 750°C to room temperature are quite the same, the uniform elongation of the HSS water-quenched from 800°C to room temperature is

smaller than that of the air-cooled one. Also, although the strength in HSS-C700-AC and WQ curves are almost the same, they have a considerable difference in uniform elongation.

From the stress-strain curves shown in Figure 6-8, it can be seen that unlike HSS, MS specimens cooled from different fire temperatures with the natural air-cooling and water-quenching methods exhibit very different mechanical responses. Even for fire temperature exposure of 700°C, the water-quenched MS specimen shows quite higher strength compared to the air-cooled MS, such that its residual strength is almost equal to the virgin MS material (MS-RT). For fire temperature exposures of 750°C and 800°C, the difference between the mechanical response of the water-quenched and air-cooled samples is very significant. The ultimate tensile strength of the MS specimen water-quenched from 750°C and 800°C to room temperature (MS-C750-WQ and MS-C800-WQ), respectively, increases by ~50% and ~87% of that of the air-cooled samples (MS-C750-AC and MS-C800-AC) and ~24% and ~37% of that of the virgin MS tested at room temperature (MS-RT). Regarding the effect of cooling rate on the ductility of the MS cooled from fire, it can be seen that the uniform elongation of the MS material water quenched from fire temperatures of up to 800°C is reduced to as low as 40% of the air-cooled samples. As the maximum temperature the MS has experienced during fire increases, more strength increase and uniform elongation reduction is observed. These results also show that when cooling from high fire temperatures (above 700°C) with extreme cooling rates, the microstructure of MS can significantly change leading to a very different mechanical response compared to that of the MS naturally air-cooled from fire at its own rate.

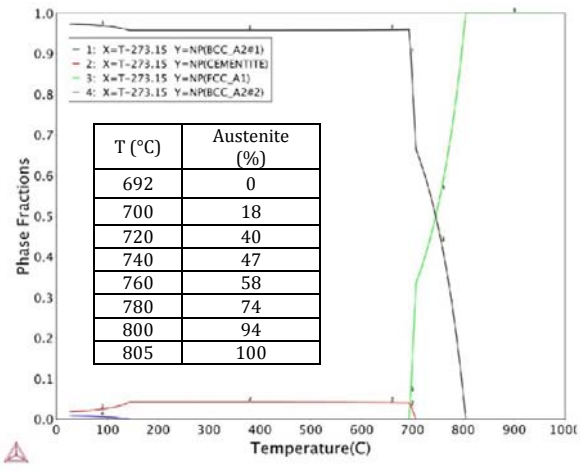

T (°C)	Austenite (%)
692	0
700	18
720	40
740	47
760	58
780	74
800	94
805	100

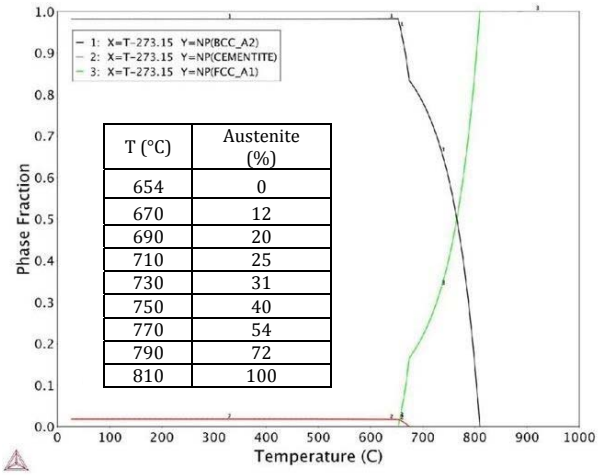

T (°C)	Austenite (%)
654	0
670	12
690	20
710	25
730	31
750	40
770	54
790	72
810	100

(a) **(b)**

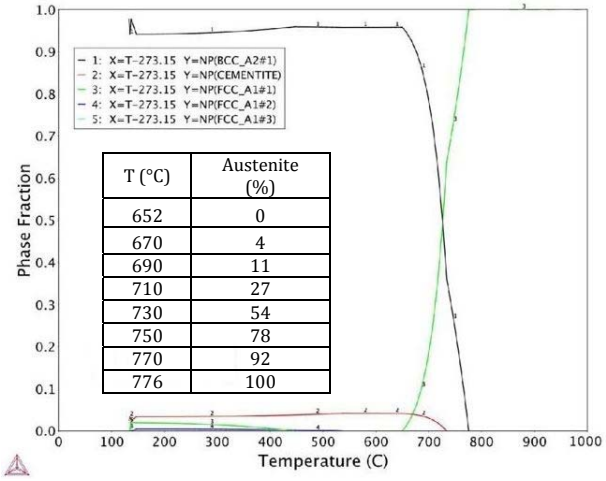

T (°C)	Austenite (%)
652	0
670	4
690	11
710	27
730	54
750	78
770	92
776	100

(c)

Figure 6-6. The plots of the thermal stability of ferrite (BCC), cementite and austenite (FCC) phases in a)MS, b)HSS and c)UHSS calculated in Ref. [3] as a function of temperature using the software package, Thermo-Calc [32]

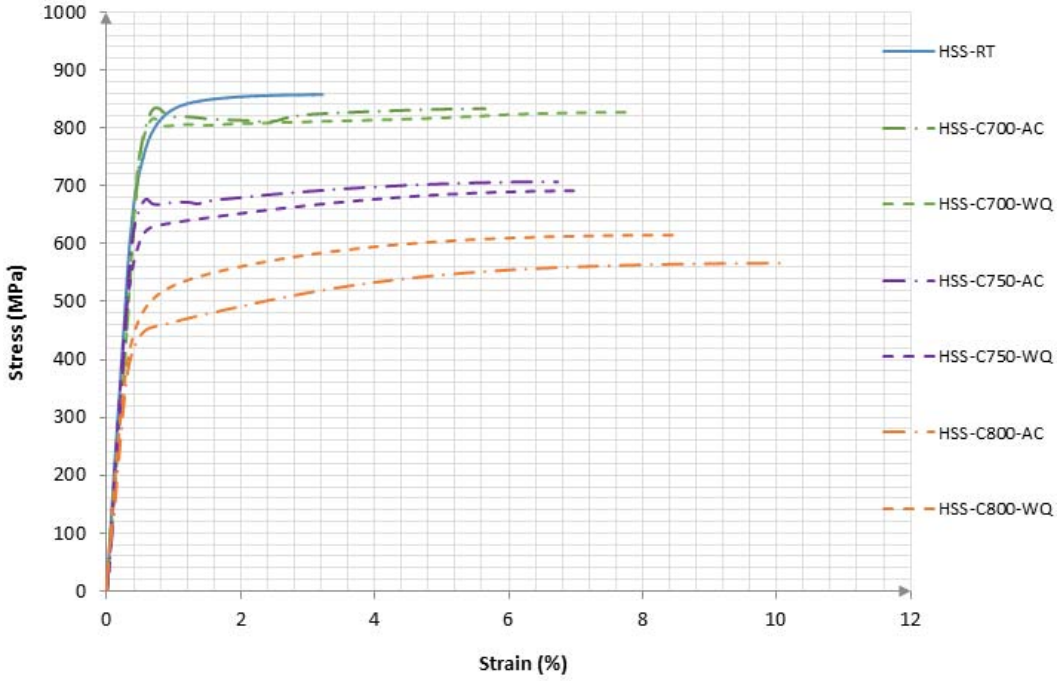

Figure 6-7. Stress-strain curves of HSS specimens tested at room temperature after being cooled from various fire temperatures using different cooling methods: Air Cooling (AC) and Water Quenching (WQ)

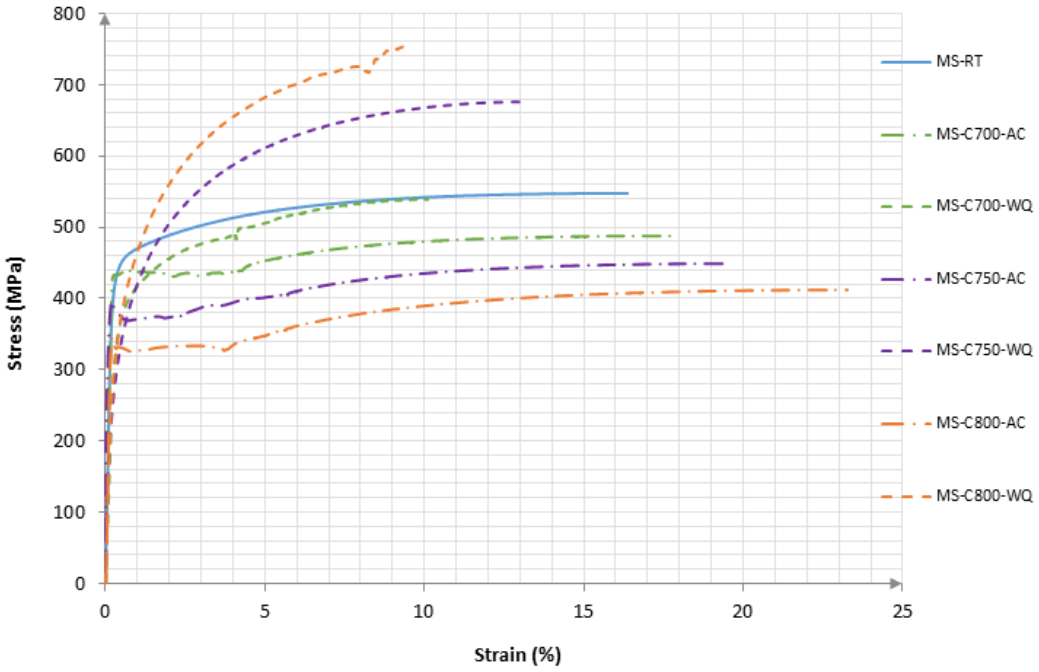

Figure 6-8. Stress-strain curves of MS specimens tested at room temperature after being cooled from various fire temperatures using different cooling methods: Air Cooling (AC) and Water Quenching (WQ)

The effect of steel grade on the mechanical response of steel cooled to extreme low temperatures was also investigated in this study. For comparison purposes, the stress-strain curves of HSS and MS at sub-zero temperatures are illustrated in Figures 6-9 and 6-10. In general, for all three materials, as the temperatures decrease, the yield strength and ultimate tensile strength increase, while the yield strain and uniform elongation decrease indicating that the materials become strong, yet less ductile as expected [33]. By comparing the curves in Figures 6-5, 6-9 and 6-10, it can be observed that out of all three materials, HSS had the most significant variation of the ultimate tensile strength with ~10% and ~15% increase when cooled from room temperature to -40°C and -80°C, respectively. The ultimate strength of UHSS and MS on the other hand had an increase of ~3% and ~5% when cooled from the ambient state to -40°C, and ~8.5% and ~7% when cooled to -80°C. Considering the ductility of the three grades of steel at low temperatures, they all experienced a considerable reduction in their uniform elongation with decrease in temperature. UHSS in particular had the lowest uniform elongation at different subzero temperatures but had yield strains higher than HSS. This phenomenon can be attributed to the higher yield strength of UHSS specimens resulted due to the roundness they portrayed in their stress-strain curves as they gradually transitioned from the elastic to the plastic state.

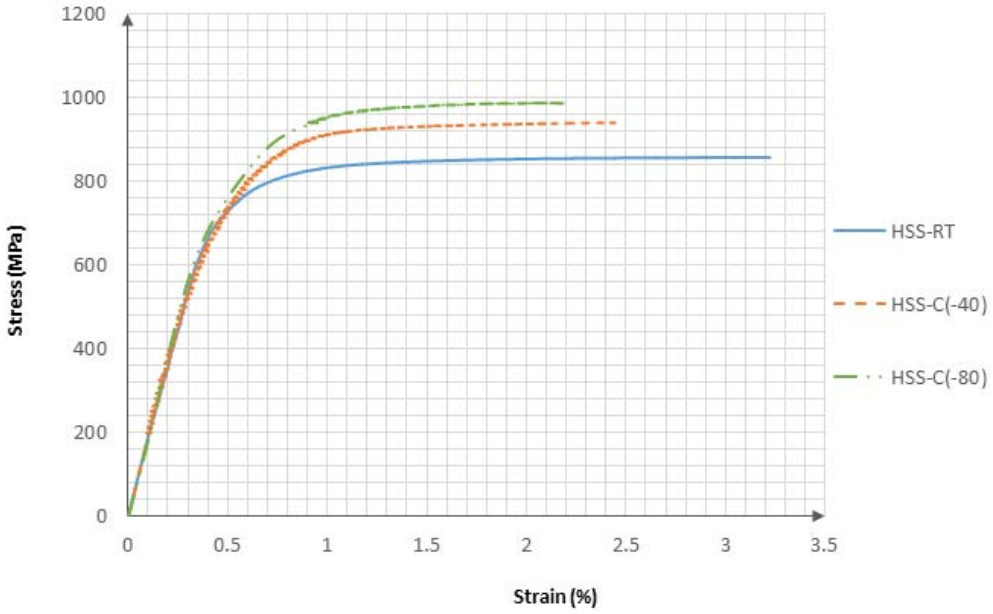

Figure 6-9. Stress-strain curves of HSS specimens tested at sub-zero temperatures

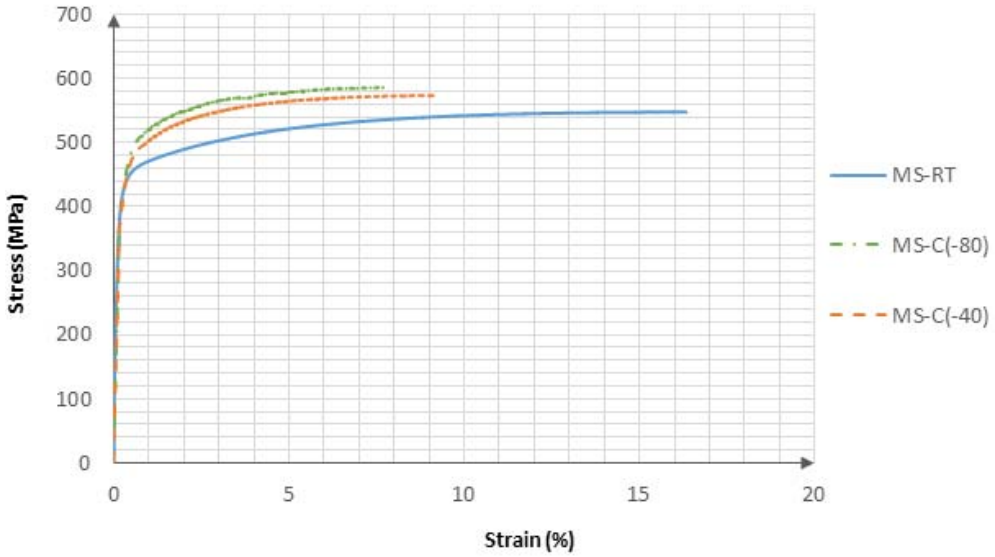

Figure 6-10. Stress-strain curves of MS specimens tested at sub-zero temperatures

6.4. Microstructure characterization

The UHSS material considered in this study derives its ultra-high strength from a tempered martensitic microstructure [34]. The SEM micrographs of the bulk microstructure of the virgin UHSS material obtained in Ref. [3], are shown in Figure 6-11. In these images, the lath shaped microstructure represents the martensitic microstructure, and the dark regions and the small white particles in the background are the ferrite and cementite phases, respectively. Martensite is very strong and brittle microstructure, which is tempered in order to provide enough ductility for engineering applications.

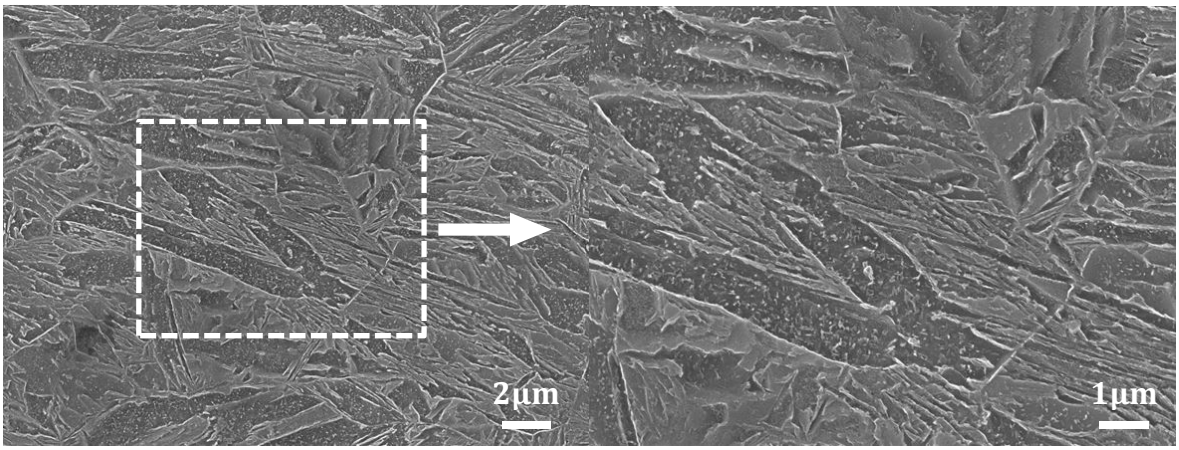

Figure 6-11. SEM micrographs of the bulk microstructure of the virgin UHSS specimen at ambient state [3]

Exposure of UHSS to low fire temperatures which are in 'tempering temperature range of martensite', continues the tempering process of martensite and subsequently removes carbon atoms from the solid solution. Since, the strength of the martensitic microstructure depends on carbon atom concentration in the solid solution, heating up the material to elevated temperatures leads to further softening of the material. When UHSS is heated up and cooled to room temperature, depending on whether the elevated temperature is in the low fire temperature (below 700°C) or high fire temperature (above 700°C) ranges, the microstructure of the cooled UHSS can be very different. According to the discussion made on the calculated thermodynamic stability phase diagrams (Figure 6-6) in Ref. [16], when UHSS is cooled from low fire temperatures, the residual strength of the material is mainly controlled by the maximum fire temperature and the time it was subjected to that temperature while the cooling rate does not affect the residual mechanical response. However, if UHSS is exposed to high fire temperatures, the identity of the phases present in the microstructure is changed and new phase called austenite is created. When UHSS cools from these fire temperatures to room temperature, depending on the steel chemical composition and the cooling rate, the austenite may be converted to ferrite and cementite [35-39]. However, it is predicted that the faster the cooling rate of fire is, the higher is the possibility that the original martensite microstructure is re-created. In this section, in order to have a better insight on the effect of extreme cooling rate on the microstructure of UHSS after cooling from fire, optical micrographs of UHSS cooled from fire temperatures of 700°C, 750°C and 800°C to room temperature with both natural air-cooling and water-quenching methods are illustrated in Figures 6-12 to 6-14. The images are taken from the bulk microstructure of the gauge length of the cooled specimens, close enough to the fracture surface such that the temperature gradient effect is minimised and far enough such that it is not affected by necking of the gauge length.

From the images depicted in Figure 6-12, it can be seen that the microstructures of the UHSS cooled from 700°C to room temperature with air-cooling (UHSS-C700-AC) and water-quenching methods (UHSS-C700-WQ) are very similar. Since 700°C is very close to the eutectoid reaction temperature of UHSS, when the tempered martensite is heated up to 700°C, there should be no or very little austenite formation. Therefore, the microstructures of both air-cooled and water quenched specimens are mostly tempered martensite and thus, they look very similar. The reason for the difference between the

UHSS-C700-AC and WQ stress-strain curves can be formation of a very small amount of austenite in the microstructure of UHSS at 700°C which did not transform to martensite and remained as austenite when water-quenched, while transformed to pearlite when air-cooled to room temperature. Since austenite is softer than pearlite, the strength of the UHSS water-quenched from 700°C is less than that of the one air-cooled to room temperature.

For the UHSS specimens cooled from 750°C to room temperature, based on the thermodynamic stability of the phase diagrams shown in Figure 6-6, formation of austenite phase at 750°C is expected. Starting from the microstructure of the UHSS water-quenched from 750°C to room temperature (UHSS-C750-WQ), which is the closest to the microstructure of UHSS at 750°C, it can be seen that the austenite islands that were present at 750°C, have transformed to fresh martensite. Therefore, islands of fresh martensite in a background of tempered martensite can be observed in the micrographs of Figure 6-13b. The micrographs obtained for the UHSS air-cooled from 750°C to room temperature (UHSS-C750-AC) look very different from the UHSS-C750-WQ ones. At 750°C, the microstructure should look like the one for UHSS-C750-WQ sample (just austenite and martensite); when it is water-quenched, it transforms to martensite and nothing else really changes. In addition to that, the shape of UHSS-C750-WQ stress-strain curve shows the existence of martensite in its microstructure. However, when UHSS is air-cooled from 750°C to room temperature (Figure 6-13a), austenite is not transformed to the martensite anymore and is transformed to either ferrite and cementite, or bainite, neither of which are as strong as the martensite and this is why the UHSS-C750-AC stress-strain curve is lower than the UHSS-C750-WQ one (Figure 6-4).

Looking at the micrographs shown in Figure 6-14b and d, it can be seen that the microstructure of the UHSS water-quenched from 800°C to room temperature (UHSS-C800-WQ) is almost similar to that of UHSS-C750-WQ, except that the islands of austenite were bigger and took up more of the volume at 800°C. This is because almost 100% austenite was formed at 800°C and when UHSS was water-quenched to room temperature, the austenite transformed to martensite. Therefore, UHSS-C800-WQ is mostly martensite and is very strong. This is also supported by the shape of the UHSS-C800-WQ stress-strain curve which illustrates an extended elasto-plastic transition. For the UHSS naturally air-cooled from 800°C to room temperature (UHSS-C800-AC),

austenite islands are transformed to bainite or ferrite. From the images shown in Figure 6-14a and c, it seems that the majority of the microstructure is ferrite and there is a little bit of small martensite islands in the microstructure, but not as much as in that of UHSS-C800-WQ.

In addition, from Figure 6-4, it can be seen that the UHSS-C800-AC and UHSS-C750-AC stress-strain curves are quite similar. Although at 800°C, more austenite is formed compared to 750°C, when the UHSS specimens are air-cooled from these temperatures, all austenite are transformed and so the microstructures of UHSS-C800-AC and UHSS-C750-AC are quite similar. However, UHSS-800-WQ and UHSS-750-WQ are different because different amounts of martensite presents in them. It is important to note that the water-quenching cooling tests carried out on UHSS specimens in this paper are not simulating the direct-quenching technique conducted on UHSS materials during their manufacturing process. Thus, it cannot be expected that the exact original room temperature microstructure is formed after water-quenching the UHSS specimens from 750°C and 800°C to room temperature.

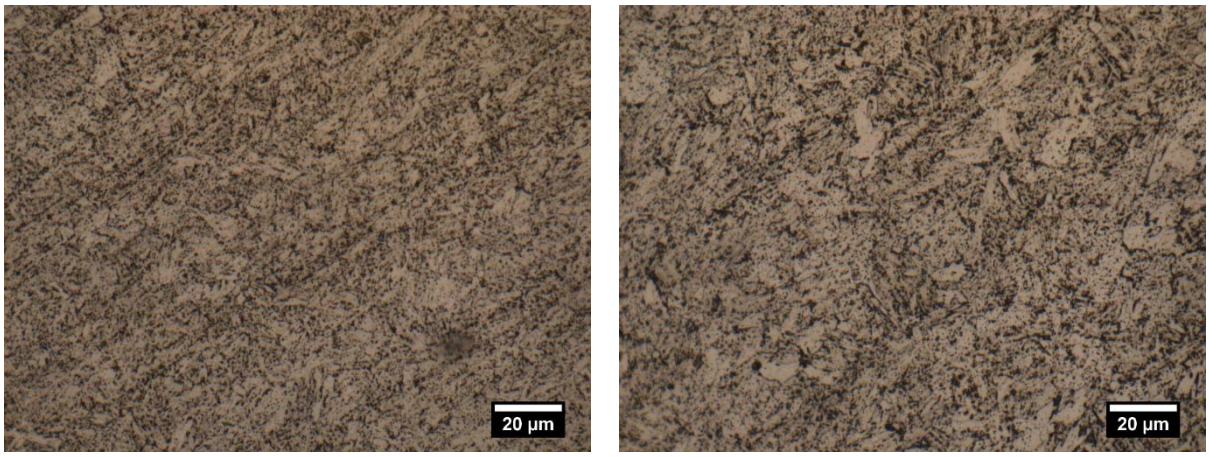

(a) **(b)**

Figure 6-12. Optical microscopic images of the bulk microstructure of the UHSS specimen cooled from 700°C to room temperature: a)with natural air-cooling method, and b)with water-quenching method

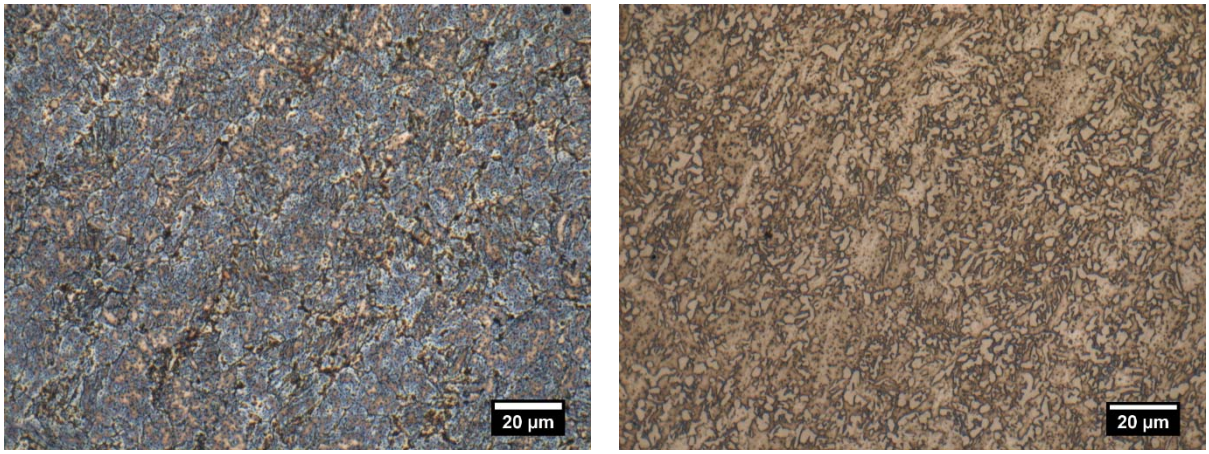

(a) **(b)**

Figure 6-13. Optical microscopic images of the bulk microstructure of the UHSS specimen cooled from 750°C to room temperature: a)with natural air-cooling method, and b)with water-quenching method

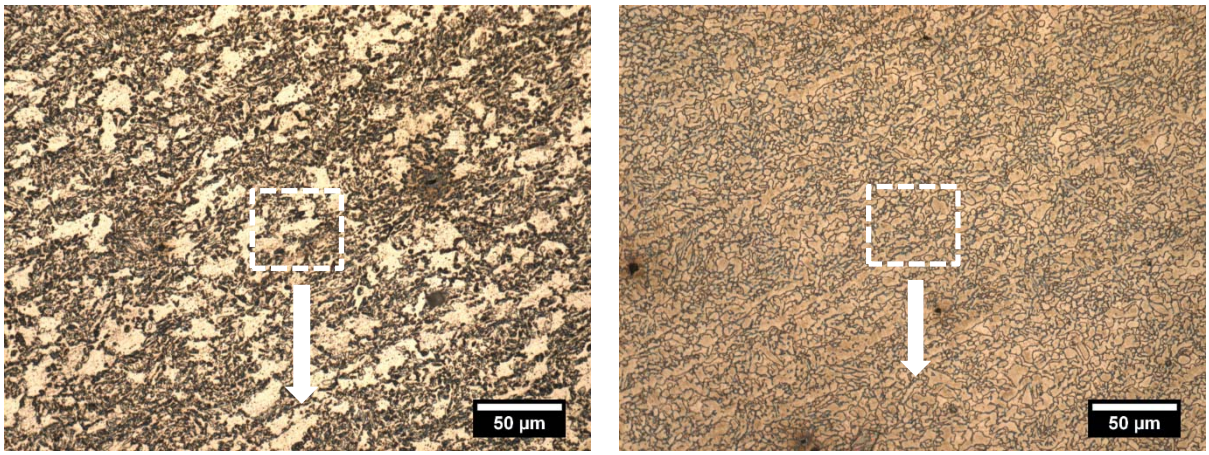

(a) **(b)**

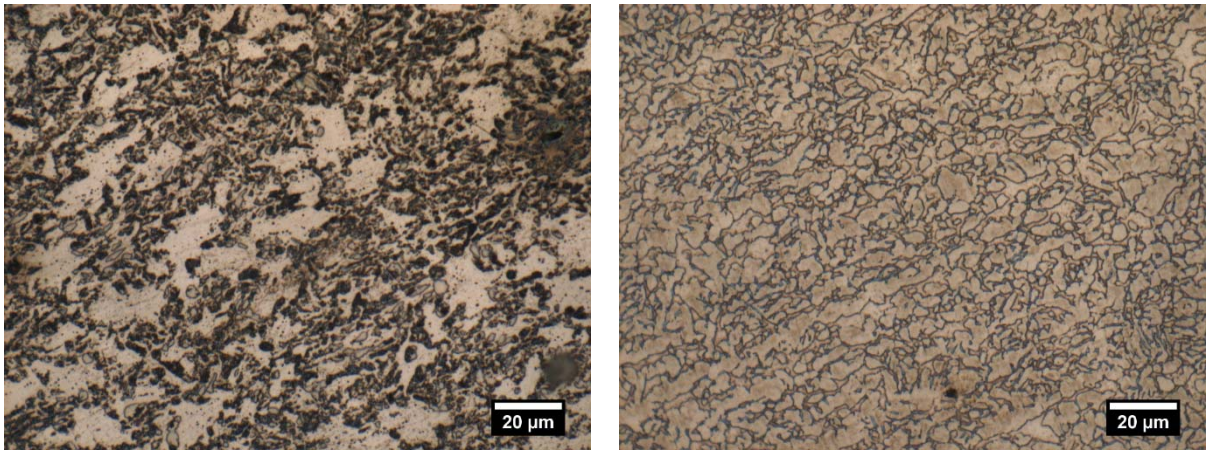

(c) **(d)**

Figure 6-14. Low and high magnification optical microscopic images of the bulk microstructure of the UHSS specimen cooled from 800°C to room temperature: a and c)with natural air-cooling method, and b and d)with water-quenching method

For the UHSS specimens cooled to sub-zero temperatures, since taking microscopic images at such low temperatures using the current microscopes was unlikely, for these specimens, no micrographs are provided in this paper. However, the changes observed in the mechanical behaviour of UHSS specimens cooled to sub-zero temperatures can be attributed to the decreased mobility of the dislocations in the microstructure of the martensitic UHSS material which led to a sudden decrease in its ductility and an increase in its strength at low temperatures [40].

6.5. Conclusion

The aim of this paper was to investigate the mechanical response of Grade 1200 UHSS under extreme cooling conditions defined as cooling from fire temperatures to room temperature with extremely high rate and cooling from room temperature to extremely low temperatures. Two sets of tests were designed to simulate these conditions: water-quenching cooling tests (simulating extremely high cooling rate) and sub-zero temperature tests (simulating extremely low temperatures). The stress-strain curves, strength and ductility of the UHSS specimens undergone these two sets of tests were evaluated. From the results of the water-quenching tests, it was concluded that while the cooling rate of fire does not have a major effect on the residual mechanical response of UHSS cooled from low fire temperatures (equal or below 700°C), it can seriously affect those of UHSS cooled from high fire temperatures (above 700°C). The ultimate tensile strength reduction obtained for the UHSS cooled from high fire temperature of 800°C with extremely high cooling rate (water-quenched) was 44% of the room temperature strength, but 60% higher than that of the UHSS cooled with a normal cooling rate (naturally air-cooled). However, the same water-quenched UHSS showed a lower uniform elongation compared to the air-cooled one, which indicates that UHSS becomes stronger, but also brittle when cooled from high fire temperatures with an extremely high cooling rate. This effect was also investigated for Grade 800 high strength steel (HSS) and Grade 350 mild steel (MS). Compared to the HSS material, MS exhibited a more sensitive behaviour with cooling rate increase, such that the residual ultimate tensile strength of the MS water-quenched from 800°C to room temperature, was 37% higher than that of the virgin MS. To provide better insights on the results obtained from the water-quenching tests, microstructures of the UHSS samples water-quenched from high fire

temperatures were compared to those of the air-cooled ones and the phase changes in their microstructure were discussed.

From the results obtained from the sub-zero temperature tests on UHSS, HSS and MS materials, it was observed that while HSS had the most significant variation of the ultimate tensile strength, i.e. ~15% increase when cooled from room temperature to -80°C, UHSS and MS experienced an increase of ~8.5% and ~7% when cooled to -80°C. Concerning the ductility of these materials at extremely low temperatures, UHSS in particular had the lowest uniform elongation at different subzero temperatures but due to the gradual elastic-plastic transition in its stress-strain curve, had yield strains higher than HSS.

Acknowledgement

The research work presented in this paper was supported by the Australian Government-Department of Education and also by Australian Research Council through a Discovery Project (DP150100442) awarded to the third and fourth authors. The authors thank SSAB Corporation for providing ultra-high strength and high strength steel tubes.

References

[1] M.A. Bradford, X.P. Liu, Flexural-torsional buckling of high-strength steel beams, Journal of Constructional Steel Research, 124 (2016) 122-131.
[2] F. Javidan, A. Heidarpour, X.L. Zhao, J. Minkkinen, Performance of innovative fabricated long hollow columns under axial compression, Journal of Constructional Steel Research, 106 (2015) 99-109.
[3] F. Azhari, A. Heidarpour, X.-L. Zhao, C.R. Hutchinson, Mechanical properties of ultra-high strength (Grade 1200) steel tubes under cooling phase of a fire: An experimental investigation, Construction and Building Materials, 93 (2015) 841-850.
[4] M. Nassirnia, A. Heidarpour, X.-L. Zhao, J. Minkkinen, Innovative hollow columns comprising corrugated plates and ultra high-strength steel tubes, Thin-Walled Structures, 101 (2016) 14-25.
[5] A. Heidarpour, S. Cevro, Q.-Y. Song, X.-L. Zhao, Behaviour of stub columns utilising mild-steel plates and VHS tubes under fire, Journal of Constructional Steel Research, 95 (2014) 220-229.
[6] S. Hosseini, A. Heidarpour, F. Collins, C.R. Hutchinson, Strain ageing effect on the temperature dependent mechanical properties of partially damaged structural mild-steel induced by high strain rate loading, Construction and Building Materials, 123 (2016) 454-463.
[7] Q.-Y. Song, A. Heidarpour, X.-L. Zhao, L.-H. Han, Post-earthquake fire behavior of welded steel I-beam to hollow column connections: An experimental investigation, Thin-Walled Structures, 98, Part A (2016) 143-153.
[8] F. Javidan, A. Heidarpour, X.-L. Zhao, H. Fallahi, Fundamental behaviour of high strength and ultra-high strength steel subjected to low cycle structural damage, Engineering Structures, 143 (2017) 427-440.
[9] S.N. Sadeghi, A. Heidarpour, X.-L. Zhao, R. Al-Mahaidi, An innovative I-beam to hybrid fabricated column connection: Experimental investigation, Engineering Structures, 148 (2017) 907-923.
[10] M. Farahi, A. Heidarpour, X.-L. Zhao, R. Al-Mahaidi, Compressive behaviour of concrete-filled double-skin sections consisting of corrugated plates, Engineering Structures, 111 (2016) 467-477.
[11] M. Mirmomeni, A. Heidarpour, X.-L. Zhao, C.R. Hutchinson, J.A. Packer, C. Wu, Fracture behaviour and microstructural evolution of structural mild steel under the multi-hazard loading of high-strain-rate load followed by elevated temperature, Construction and Building Materials, 122 (2016) 760-771.
[12] S. Sinaie, A. Heidarpour, X.L. Zhao, Stress–strain–temperature relation for cyclically-damaged structural mild steel, Engineering Structures, 77 (2014) 84-94.
[13] M. Amraei, T. Skriko, T. Björk, X.-L. Zhao, Plastic strain characteristics of butt-welded ultra-high strength steel (UHSS), Thin-Walled Structures, 109 (2016) 227-241.
[14] F. Azhari, A. Heidarpour, X.-L. Zhao, C.R. Hutchinson, Evaluating post-fire mechanical behavior of ultra-high strength (Grade1200) steel tubes, in: Structures in Fire, Proceedings of the Ninth International Conference, Princeton University, 2016.
[15] F. Azhari, A. Heidarpour, X.-L. Zhao, C.R. Hutchinson, Effect of creep strain on mechanical behaviour of ultra-high strength (Grade 1200) steel subject to cooling phase of a fire, Construction and Building Materials, 136 (2017) 18-30.

[16] F. Azhari, A. Heidarpour, X.-L. Zhao, C.R. Hutchinson, Post-fire mechanical response of ultra-high strength (Grade 1200) steel under high temperatures: Linking thermal stability and microstructure, Thin-Walled Structures, 119 (2017) 114-125.
[17] A. Heidarpour, N.S. Tofts, A.H. Korayem, X.-L. Zhao, C.R. Hutchinson, Mechanical properties of very high strength steel at elevated temperatures, Fire Safety Journal, 64 (2014) 27-35.
[18] C.G. Bailey, I.W. Burgess, R.J. Plank, Computer simulation of a full-scale structural fire test, Structural Engineer, 74 (1996) 93-100.
[19] J.A. El-Rimawi, I.W. Burgess, R.J. Plank, The treatment of strain reversal in structural members during the cooling phase of a fire, Journal of Constructional Steel Research, 37 (1996) 115-135.
[20] E.M. Aziz, V.K. Kodur, Effect of temperature and cooling regime on mechanical properties of high-strength low-alloy steel, Fire and Materials, 40 (2016) 926-939.
[21] W. Wang, T. Liu, J. Liu, Experimental study on post-fire mechanical properties of high strength Q460 steel, Journal of Constructional Steel Research, 114 (2015) 100-109.
[22] H.J. Frost, M.F. Ashby, Chapter 5-The B.C.C. transition metals: W, V, Cr, Nb, Mo, Ta and α-Fe in: Deformation-mechanism maps : the plasticity and creep of metals and ceramics, Pergamon Press, Oxford [Oxfordshire]; New York, 1982, pp. 30-42.
[23] J. Billingham, J.V. Sharp, Review of the Performance of High Strength Steels used Offshore (Research Report 105), in, Cranfield University, School of Industrial and Manufacturing Science, 2003.
[24] C.G. Soares, Y. Garbatov, Ships and Offshore Structures XIX, CRC Press, 2015.
[25] ASTM Standard E8/E8M, in: Standard Test Methods for Tension Testing of Methallic Materials, ASTM International, West Conshohocken, PA: USA, 2011.
[26] S.P. Chiew, M.S. Zhao, C.K. Lee, Mechanical properties of heat-treated high strength steel under fire/post-fire conditions, Journal of Constructional Steel Research, 98 (2014) 12-19.
[27] S. Gunalan, M. Mahendran, Experimental investigation of post-fire mechanical properties of cold-formed steels, Thin-Walled Structures, 84 (2014) 241-254.
[28] Australia Standards AS4100, Steel structures, Sydney, Australia, 1998.
[29] Australian/New Zealand Standard AS/NZS 4600, Cold-Formed Steel Structures, Standards Australia, Sydney, Australia and Standards New Zealand, Wellington, New Zealand, 2005.
[30] European Code 3,Eurocode 3: Design of Steel Structures, European Committee for Standardization, Brussels, Belgium, 2010.
[31] A. Considère, Annales des ponts et chaussées I sem, in, 1885, pp. 574.
[32] Thermo-Calc Software. [ONLINE] Available at: http://www.thermocalc.com/contact-us/thermo-calc-offices/, in, Foundation of Computational Thermodynamics, 1995.
[33] J.B. Yan, J.Y.R. Liew, M.H. Zhang, J.-Y. Wang, Mechanical properties of normal strength mild steel and high strength steel S690 in low temperature relevant to Arctic environment, Materials and Design, 61 (2014) 150-159.
[34] H.K.D.H. Bhadeshia, S.R. Honeycombe, Chapter 5 - Formation of Martensite, in: H.K.D.H.B.R. Honeycombe (Ed.) Steels (Third Edition)-Microstructure and Properties, Butterworth-Heinemann, Oxford, 2006, pp. 95-128.
[35] M. Gouné, F. Danoix, J. Ågren, Y. Bréchet, C.R. Hutchinson, M. Militzer, G. Purdy, S. van der Zwaag, H. Zurob, Overview of the current issues in austenite to ferrite transformation and the role of migrating interfaces therein for low alloyed steels, Materials Science and Engineering: R: Reports, 92 (2015) 1-38.

[36] D. Panahi, H. Van Landeghem, C.R. Hutchinson, G. Purdy, H.S. Zurob, New insights into the limit for non-partitioning ferrite growth, Acta Materialia, 86 (2015) 286-294.
[37] C. Qiu, H.S. Zurob, C.R. Hutchinson, The coupled solute drag effect during ferrite growth in Fe–C–Mn–Si alloys using controlled decarburization, Acta Materialia, 100 (2015) 333-343.
[38] C. Qiu, H.S. Zurob, D. Panahi, Y. Brechet, G.R. Purdy, C.R. Hutchinson, Quantifying the solute drag effect on ferrite growth in Fe-C-X alloys using controlled decarburization experiments, Metallurgical Transactions A, 44 (2013) 3472-3483.
[39] H.S. Zurob, D. Panahi, C.R. Hutchinson, Y. Brechet, G.R. Purdy, Self-Consistent Model for Planar Ferrite Growth in Fe-C-X Alloys, Metallurgical Transactions A, 44 (2013) 3456-3471.
[40] J. J.W. Morris, Dislocation Plasticity: an Overview, in: Encyclopedia of Materials Science and Technology, Elsevier Science, Amsterdam 2001.

Chapter 7

The effect of manufacturing process on the post-fire mechanical response of thin-walled ultra-high strength steel (Grade 1200) tubes

This chapter has been accepted for publication in the Journal of *Thin-Walled Structures*, Volume 132, November 2018, Pages 16-24.

DOI: 10.1016/j.tws.2018.08.011

Reprinted here with the Author Rights granted by Elsevier.

Table of Contents

Abstract

This study aims to investigate the effect of manufacturing process on the post-fire mechanical response of Grade 1200 ultra-high strength steel (UHSS) tubes. To this end, the post-fire mechanical properties of "direct-quenched" UHSS (UHSS-DQ) standard tensile coupons are compared to those made of "quenched and tempered" UHSS material (UHSS-QT) with similar original room temperature stress-strain responses. Thus, to compare the post-fire compression behaviour of UHSS-DQ tubular stub columns with those made of UHSS-QT material, a finite element (FE) model is developed in ABAQUS FE software with precise material properties extracted from the results of the post-fire tensile coupon tests. Quasi-static compression tests are then conducted on UHSS-QT tubular stub columns cooled from different fire temperatures to room temperature to validate the FE analysis. Using the results of the tensile coupon tests and the FE analysis on UHSS stub columns, it is shown that the manufacturing process substantially affects the mechanical properties of UHSS stub columns under cooling phase of a fire.

Key Words: ultra-high strength steel, stub columns, fire, cooling, manufacturing process, finite element analysis

7.1. Introduction

In recent years, due to the high strength to weight ratio of ultra-high strength structural steels (UHSS), researchers have attempted to investigate the potential of utilising this material in civil engineering construction [1-9]. As an example of the first practical applications of UHSS in the world, it can be referred to Nippon Steel & Sumitomo Metal Corporation, which applied these materials for the circular steel pipe columns, welded built-up H beams used as columns, and four-side-welded-box-type columns [8]. In addition, during the past decade, innovative fabricated columns composed of ultra-high strength steel (UHSS) tubes with nominal yield strength of 1200MPa have been proposed [4-6]. The superior performance of these innovative columns indicates the great potential of UHSS to be introduced as a structural material in production of sustainable structural members. However, there is lack of sufficient research addressing the behaviour of this type of steel under extreme structural loadings. Fire is one of the extreme hazards which can significantly damage the structure during its service life. After a structure is cooled from fire, the residual strength of the structural members should be accurately evaluated to decide whether or not it is possible to reuse them. To date, a number of researchers have addressed this issue by investigating the in-fire and post-fire mechanical behaviour of structural steels [10-24]. In recent years, the authors performed an extensive experimental study to investigate the post-fire tensile mechanical behaviour of Grade 1200 UHSS under fire [17-20]. The results showed a considerable reduction in residual strength of this material after being cooled from certain fire temperatures.

It has been reported in the literature that the mechanical behaviour of steel materials under fire conditions can be significantly affected by their manufacturing process technique [10, 25]. The ultra-high strength of UHSS materials is basically obtained by fast quenching techniques either in water or oil. If the cooling rate of the quenching process is sufficiently high, with a proper chemical composition of the steel, “martensite” phase might be formed which is very strong but also brittle [26]. Considering the great ductility these steels lose after the quenching process, different methods are used by manufacturing companies to compensate for this loss. The most applied method used for manufacturing the UHSS materials is the traditional quenching and tempering technique (QT). During this process, the material is quenched rapidly in several stages either in water or oil. Thus, through a final heat treatment, the steel is reheated to moderate

temperatures for a short time [27]. This process is called tempering, by which a certain level of the ductility of steel is recovered. In Ref. [27], Heidarpour et al. investigated the mechanical response of the quenched and tempered UHSS (i.e. UHSS-QT) at different elevated temperatures. They showed that the deterioration of the in-fire strength of UHSS-QT is greater than mild steel or high strength steel, which is due to the QT manufacturing process leading to a fundamentally different microstructure, with a different thermal stability. In recent years, a unique manufacturing process called the direct quenching technique (DQ) has been proposed by steel manufacturers [28]. Unlike the traditional QT technique where the material is quenched in several stages, in direct quenching method the material is quenched only in one stage. In Figure 7-1, the two techniques are compared by schematic diagrams. It is important to note that the UHSS material tested in Refs. [17-20] by the authors was also manufactured by using the DQ technique.

In this study, it is aimed to understand the effect of manufacturing process on the post-fire compressive behaviour of the UHSS tubular stub columns. To achieve this, standard tensile coupon tests are first conducted on direct-quenched, and quenched and tempered UHSS specimens (labelled as UHSS-DQ and UHSS-QT, respectively) after cooling from elevated temperatures of up to 800°C to room temperature. Comparing the results of these tests on UHSS-DQ and UHSS-QT tensile coupons, the effect of manufacturing process on the tensile stress-strain curves, and also the residual post-fire tensile strength and ductility of UHSS material is evaluated. Afterwards, using the precise material properties inputs obtained from the post-fire tensile tests, a finite element (FE) model is developed using the ABAQUS FE software [29] to compare the post-fire compressive behaviour of tubular stub columns made of UHSS-DQ and UHSS-QT materials . In order to validate the results of the FE model, quasi-static compression tests are conducted on UHSS-QT tubular stub columns cooled from different fire temperatures to the ambient state. After validation of the FE analysis, the effect of manufacturing process on the post-fire compressive behaviour of UHSS tubular stub columns is examined in which the load-displacement curves, and the strength and slenderness values of the two simulated stub columns are compared.

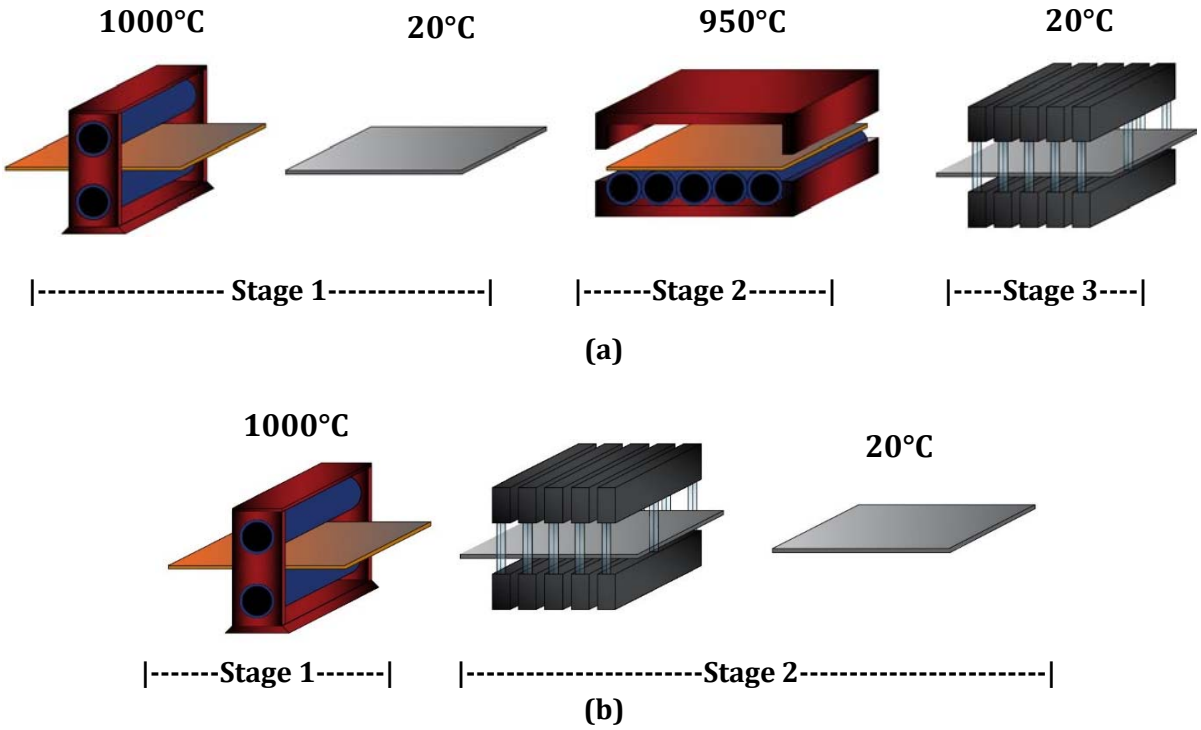

Figure 7-1. Schematic illustration of the a) traditional quenching and tempering manufacturing process of plates compared to the b) direct quenching one.

7.2. The effect of manufacturing process on the post-fire tensile behaviour of UHSS materials

7.2.1. Tensile coupon tests

The post-fire material properties of the UHSS-QT and UHSS-DQ materials studied in this paper, are measured by the results of tensile coupon tests. Using the waterjet cutting facility, the dog-bone specimens are extracted from two strips located at right angles (90°) to the tube weld line of the UHSS-QT (with $D = 38.1mm$ and $t = 1.8mm$) and UHSS-DQ tubes (with $D = 76.1mm$ and $t = 3.2mm$). The shape and dimensions of the coupons as well as their location in the UHSS tubes are indicated in Figure 7-2. In addition, the chemical compositions of the two UHSS materials are shown in Table 7-1. It can be seen that despite the different manufacturing techniques of these UHSS materials, except for a slight difference between their carbon (C) contents, their chemical compositions are quite similar.

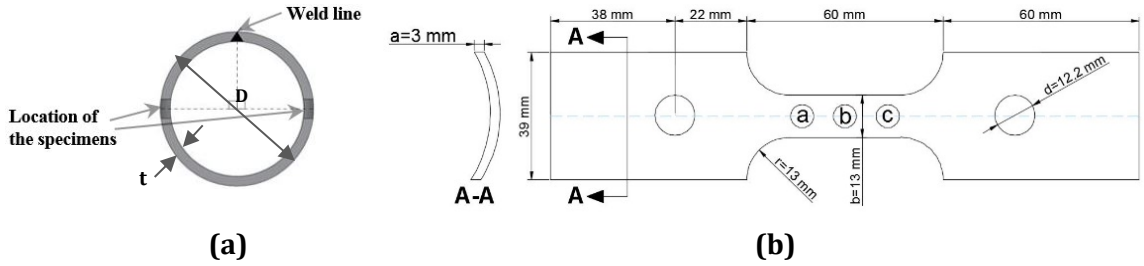

Figure 7-2. a) Tube section and b) dimensions of test specimens

Table 7-1. The chemical composition of test materials (wt%)

Material	C	Si	Mn	P	S	Cr	Ni	Mo	B
UHSS-QT	0.200	0.800	1.700	0.025	0.015	1.500	1.000	0.500	0.005
UHSS-DQ	0.230	0.800	1.700	0.025	0.015	1.500	1.000	0.500	0.005

The tensile coupons taken from UHSS tubes had an outward curvature representing the longitudinal residual stresses developed due to cold-forming process. In order to conduct the tensile coupon test, first, the specimens are mechanically flattened to be gripped inside the tensile loading machine. Then, they are heated up to elevated temperatures ranging from 470°C to 800°C inside a split furnace (model SF-16). Once the temperatures at the three thermocouples attached to points a, b and c on the specimen's gauge length (see Figure 7-2) are stabilised (after ~20 mins), they are air cooled to room temperature. Afterwards, using the Instron 5982 100kN testing machine, quasi-static tensile test is carried out at room temperature on the cooled specimens with an applied strain rate of $0.005 \pm 0.002\,\mathrm{min}^{-1}$. The strain of the specimen during the tensile test is recorded using the model 3448 High Temperature Contact Extensometer with approximate gauge length of 25 mm. The setup is similar to that used by the authors for the experiments conducted in Refs. [17-20]. It is worth noting that the reason for considering the minimum fire temperature of 470°C is that the results of the previous studies conducted on UHSS materials indicated that the post-fire mechanical properties of those subjected to temperatures below 470°C are not considerably changed [17-20].

7.2.2. Post-fire tensile mechanical properties of UHSS

From the tensile coupon tests conducted on the UHSS materials, nonlinear post-fire material properties are accurately obtained to be used as input material data for the FE analysis of UHSS tubular stub columns.

7.2.2.1. Stress-strain curves

The stress-strain curves of the tensile coupon tests are presented in Figure 7-3 for the UHSS-QT and UHSS-DQ specimens cooled from different fire temperatures to room temperature. The UHSS-QT-C*T* and UHSS-DQ-*CT* labels in the legend of these two figures, represent the UHSS-QT and UHSS-DQ tensile coupons cooled from temperature *T* to room temperature, respectively. Also, RT denotes the specimens tested at room temperature (RT) without experiencing fire. Due to the inaccurate strain readings after the necking of tensile coupons and the fact that the elongation of the material is not uniform after necking, the stress-strain curves are presented up to the onset of necking. From these curves, it can be observed that the material properties of both UHSS-QT and UHSS-DQ materials are dramatically changed by the increase of the maximum fire temperature they have experienced prior to cooling to room temperature.

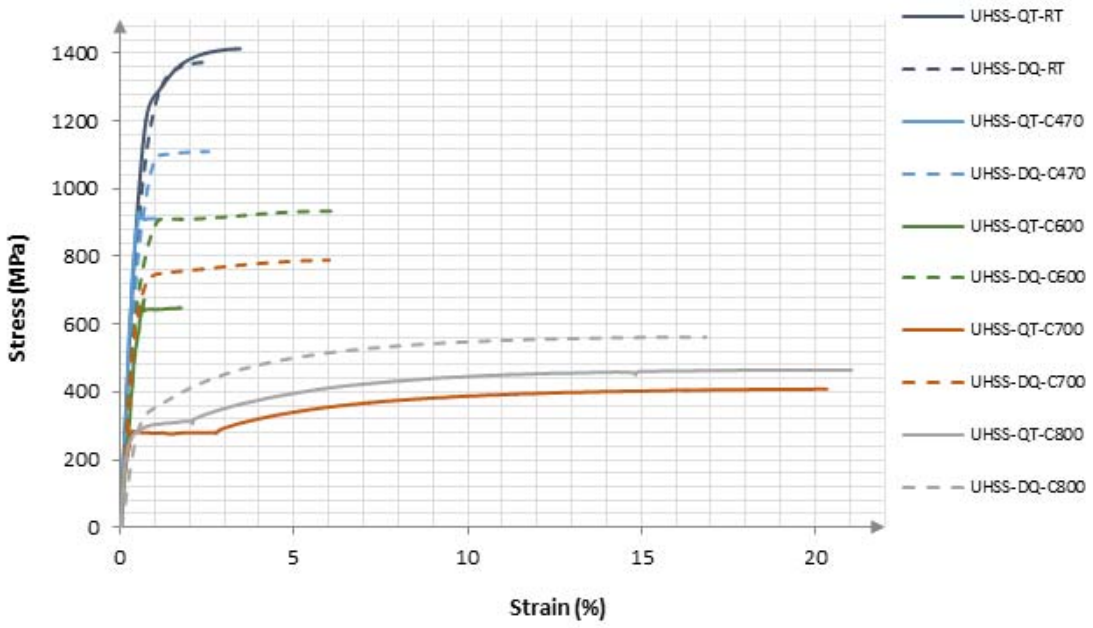

Figure 7-3. The engineering stress-strain curves of UHSS-QT and UHSS-DQ tensile coupons cooled from different fire temperatures to room temperature

7.2.2.2. Strength

In this section, the effect of manufacturing process on the post-fire tensile strength of UHSS material is evaluated. To achieve this, the tensile characteristic strengths at certain strain levels including 0.2%, 0.5%, 1.5% and 2.0% strains shown as $f_{0.2}$, $f_{0.5}$, $f_{1.5}$ and $f_{2.0}$, and also the ultimate tensile strength (f_u) are calculated for the UHSS-DQ and UHSS-QT tensile specimens. Illustration of these strain and strength values are presented in Figure 7-4.

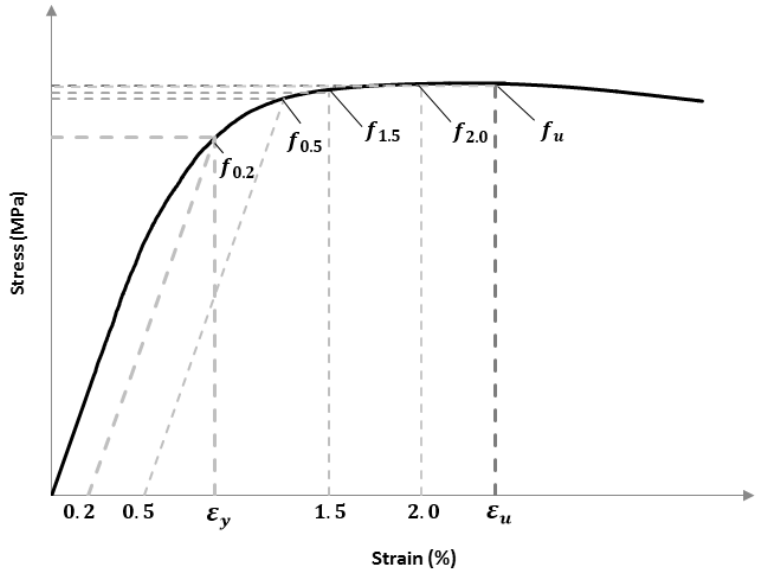

Figure 7-4. Description of characteristic tensile strengths and strains on a typical stress-strain curve

In Table 7-2, the values of the afore-mentioned tensile strengths for UHSS-DQ and UHSS-QT specimens cooled from different fire temperatures to room temperature (noted by *CT* index) are normalised with respect to those of the original room temperature specimens (noted by *RT* index). It is important to note that for some post-fire tensile tests carried out on UHSS-QT specimens, since the 1.5% and 2.0% strains are within the post-necking part of their stress-strain curves, the reduction factors of their corresponding strengths, i.e. $\frac{f_{1.5,CT}}{f_{1.5,RT}}$ and $\frac{f_{2.0,CT}}{f_{2.0,RT}}$, are not reported in Table 7-2.

Comparison of the general trend of the changes in the post-fire strength values of UHSS-DQ and UHSS-QT specimens indicates that the reduction in those of UHSS-QT is more significant than the UHSS-DQ specimens. This difference is specifically more considerable

for the values of the normalised ultimate tensile strength ($\frac{f_{u,CT}}{f_{u,RT}}$), such that the reduction of $f_{u,CT}$ for UHSS-QT cooled from 600°C to room temperature (54%), is close to that of UHSS-DQ cooled from 800°C to room temperature (59%). It can also be observed that the reduction in the strength of UHSS-QT specimens becomes stabilised after cooling from 700°C, such that the strength reduction values of the specimens cooled from 700°C and 800°C are very close to each other. Same phenomenon was observed in Ref. [20] for UHSS-DQ and fire temperatures of 750°C and 800°C, where the reason for this stabilization was linked to the formation of austenite phase in the microstructure of the UHSS-DQ after experiencing 750°C fire temperature. Therefore, following the same reasoning, it may be resulted that when UHSS-QT is exposed to fire temperature of 700°C, the steel phase is 100% austenite and its residual strength after cooling from temperatures above 700°C would be basically the same. In addition, the higher values of the ultimate tensile strength for the UHSS-QT and UHSS-DQ specimens cooled from 800°C indicates that the post-yield part of the UHSS-DQ-C800 and UHSS-QT-C800 stress-strain curves has a more rounded shape compared to that of other curves as shown in Figure 7-3. The reason behind this is the major microstructural changes in the two materials after exposing to this fire temperature, which allows them to experience significantly more strain hardening capacity compared to the original room temperature materials.

Table 7-2. Reduction factors of characteristic strengths for UHSS-DQ and UHSS-QT tensile coupons after cooling from various fire temperatures to room temperature (RT)

	Temperature (*T*) / **Material**	**470°C**	**600°C**	**700°C**	**800°C**
$\frac{f_{0.2,CT}}{f_{0.2,RT}}$	**UHSS-DQ**	0.850	0.650	0.575	0.258
	UHSS-QT	0.743	0.527	0.233	0.230
$\frac{f_{0.5,CT}}{f_{0.5,RT}}$	**UHSS-DQ**	0.840	0.687	0.565	0.269
	UHSS-QT	0.703	0.498	0.218	0.228
$\frac{f_{1.5,CT}}{f_{1.5,RT}}$	**UHSS-DQ**	0.818	0.676	0.558	0.285
	UHSS-QT		0.480	0.208	0.230
$\frac{f_{2.0,CT}}{f_{2.0,RT}}$	**UHSS-DQ**	0.808	0.667	0.553	0.301
	UHSS-QT			0.202	0.227
$\frac{f_{u,CT}}{f_{u,RT}}$	**UHSS-DQ**	0.809	0.681	0.574	0.411
	UHSS-QT	0.643	0.458	0.289	0.329

7.2.2.3. Ductility

In order to determine if the structure can undergo sufficient plastic deformation, it is important to evaluate the ductility of the construction materials. In this section, the effect of manufacturing process on the ductility of UHSS material is investigated. The ductility parameters considered for this end are $f_u/f_{0.2}$ and $\varepsilon_u/\varepsilon_y$, which according to AS4100 [30], AS/NZS 4600 [31] and Eurocode 3 [32] codes of practice, must meet certain requirements for the plastic analysis. Table 7-3 presents these ductility parameters for the UHSS-DQ and UHSS-QT materials cooled from different fire temperatures to room temperature. It can be observed that while the values of $f_u/f_{0.2}$ are close for the two UHSS materials cooled from fire temperatures below 600°C, their difference becomes considerable for higher temperatures. In addition, it can be observed that there is a considerable difference between the $\varepsilon_u/\varepsilon_y$ values of the UHSS-DQ and UHSS-QT materials cooled from different fire temperatures. In Ref. [20], based on the thermodynamic stability of the phases present in the microstructure of UHSS material, the authors of this paper defined two temperature regimes for the evaluation of the post-fire mechanical response of UHSS: the low fire temperatures (T≤ 600°C) and the high fire temperatures (T> 600°C). Considering this classification, it can be seen from Table 7-3 that for the low maximum fire temperatures, the values of $\varepsilon_u/\varepsilon_y$ for the UHSS-DQ specimens are up to 4 times larger than those for the UHSS-QT specimens. However, for the high maximum fire temperatures, compared to the UHSS-DQ specimens, UHSS-QT specimens experiences significantly higher $\varepsilon_u/\varepsilon_y$ after cooling from fire temperatures to room temperature. The reason is related to the variation of the uniform elongation (ε_u) and the yield strength (ε_y) for the UHSS materials cooled from the low and high fire temperature regimes. From Figure 7-3, it can be understood that the ε_u values for the UHSS-QT specimens cooled from low fire temperatures can be as small as 30% of those for the UHSS-DQ specimens; whereas the UHSS-QT specimens exposed to high fire temperatures, experience ε_u of up to 3.4 times higher than that of the UHSS-DQ specimens. On the other hand, from Figure 7-4, it is obvious that the values of ε_y have a direct linear relationship with the 0.2 proof strength ($f_{0.2}$) values. Thus, according to the values shown in Table 7-2 for the reduction of $f_{0.2}$ with the maximum fire temperature,

except for the UHSS specimens cooled from 700°C to room temperature, the difference between the ε_y values of the two materials is less than 20% for most temperatures. As a result, the variation of the values of $\varepsilon_u/\varepsilon_y$ for the UHSS materials cooled from both temperature regimes is mainly controlled by the changes in their ε_u values.

Table 7-3. Variation of the ratios of $f_u/f_{0.2}$ and $\varepsilon_u/\varepsilon_y$ for the UHSS-DQ and UHSS-QT tensile coupons cooled from various fire temperatures to room temperature (RT)

	Temperature (T) / Material	RT	470°C	600°C	700°C	800°C
$f_u/f_{0.2}$	**UHSS-DQ**	1.174	1.117	1.231	1.171	1.867
	UHSS-QT	1.154	0.999	1.005	1.434	1.648
$\varepsilon_u/\varepsilon_y$	**UHSS-DQ**	3.106	3.341	9.939	10.391	30.963
	UHSS-QT	4.426	1.811	2.409	52.349	54.703

7.3. The effect of manufacturing process on the post-fire compressive behaviour of UHSS stub columns

In order to investigate the effect of manufacturing process on the post-fire compressive behaviour of UHSS stub columns, the behaviour of two tubular sub columns made of UHSS-QT and UHSS-DQ materials after cooling from different fire temperatures to room temperature are discussed and compared. To this end, these stub column are numerically modelled using the commercial finite element (FE) software, ABAQUS [29]. In order to take into account the changes occurred in the material properties of these columns under cooling phase of a fire, the results of the experimental tensile tests presented in Section 7.2 of this paper are used as material inputs. The results of the FE analysis are then validated with the experimental tests conducted on the UHSS-QT tubular stub columns.

7.3.1. Stub column Modelling

In this section, the details of modelling the post-fire behaviour of UHSS-QT and UHSS-DQ tubular stub columns (SC) in ABAQUS FE package are explained. The developed FE model can be used for further case studies without the need to conduct experimental tests.

7.3.1.1. Initial Modelling

For modelling the UHSS-QT and UHSS-DQ stub-columns in ABAQUS, using the engineering stress-strain curves illustrated in Figure 7-3, the elastic modulus and the yield strength of the materials are directly extracted. However, in order to take into account the isotropic hardening behaviour of the materials, since the initially measured dimensions are no longer valid at this stage, the true stress (σ_t) and strain (ε_t) values calculated from the following equations are used:

$$\sigma_t = \sigma_e(1+\varepsilon_e), \quad \varepsilon_t = \ln(1+\varepsilon_e) \tag{7-1}$$

in which, ε_e and σ_e represent the engineering strain and stress values, respectively.

The external diameter (D) and the wall thickness (t) of the columns are chosen based on the real dimensions of the available UHSS-QT tubes, i.e. $D = 38.1mm$ and $t = 1.8mm$. The length of the stub columns are chosen using the guidelines set out by Johnston [33] which specifies a minimum stub column length of $L = 3D$ and the maximum length of $L = 20r_{\min}$, where $r_{\min}$ is the least radius of gyration ($r = \sqrt{I/A}$). Since based on the cross-section area dimensions used for the stub columns of this study, $3D < 20r_{\min}$, their length is considered to be $L = 3D$. For the FE modelling of these stub columns, due to their small thickness compared to their length and diameter, four-node reduced integration shell elements (S4R) with 6 degrees of freedom per node were used [29]. Mesh sensitivity analysis is performed and the mesh size of $2.4mm$ is used for the simulated stub columns. It is worth noting that the residual stresses resulted from the fabrication process are neglected in this simulation. However, since the stress-strain curves were obtained from the tensile coupons taken from the actual welded tubes, the residual stresses resulted from welding have been considered in the simulations.

In this study, special end fixtures are designed to avoid premature end failures (elephant buckling) of the stub columns during compression loading. The geometry and dimensions of the meshed stub columns and the end fixtures modelled in ABAQUS FE software are illustrated in Figure 7-5. As shown in Figure 7-5b, the plates used at the end fixtures are modelled as solid sections made of a rigid material with a much greater elastic modulus compared to that of UHSS material. Solid plates #1 and #2 of the end fixtures are

connected by the "Tie" constraint (Master surface: Solid plate #1, Slave surface: Solid plate #2). To model the interaction of Solid plate #2 and the outer surface of the UHSS stub-column, "General contact" with "Penalty friction formulation" (friction coefficient of 0.8) for the tangential contact behaviour, and "Hard contact" for the normal contact behaviour is used [29]. For the interaction of the UHSS stub column and Solid plate #1, "Surface-to-surface contact" with finite sliding, and tangential and normal contact properties similar to those used for the interaction of Solid plates #1 and #2, are used [29].

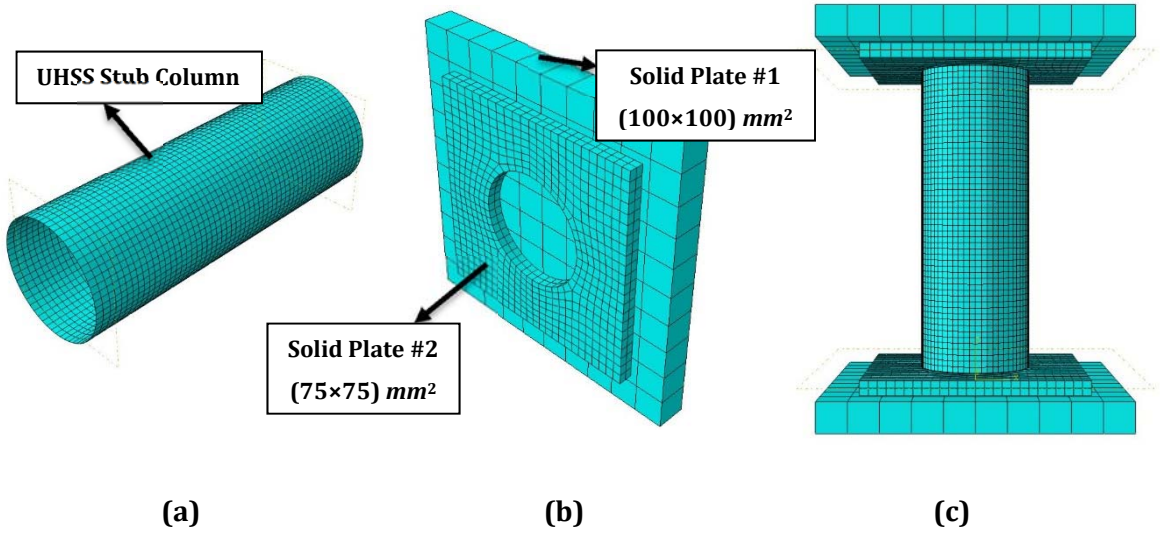

Figure 7-5. The finite element models of the a) tubular stub column, b) the anti-buckling end fixtures and c) the total assembly

7.3.1.2. FE analysis procedure

In order to take into account the unstable post-buckling behaviour of the modelled stub columns, displacement-controlled analysis must be performed. To achieve this goal two subsequent methods are used to simulate the compressive loading and the post-buckling analysis of the stub columns cooled from different fire temperatures to room temperature. In the first step, a "linear buckling analysis" is conducted on the stub column. While the reference point of the Solid plate #1 (Figure 7-5b) in the bottom fixture is completely fixed, the one for the top fixture has free axial displacement and a unit displacement is applied to it. From this step, the critical buckling displacements at different buckling modes are achieved. Examples of these mode shapes for UHSS-QT stub column cooled from 470°C to room temperature are illustrated in Figure 7-6. For the

sake of simplicity, it was assumed that the imperfect geometry of the columns could be represented by their first buckling mode shape. The "dynamic explicit analysis" is the next step of the nonlinear buckling analysis of the stub columns. In this step, initial imperfection data is given to the software as an important input data. In this study, this imperfection is considered as a factor of the displacement of the first mode of the linear buckling analysis. The factor is normally obtained based on the maximum imperfection of the experimental stub columns. However, in this study since the main goal of the FE analysis is comparison of the post-fire behaviour of two UHSS stub columns with different manufacturing processes, this factor is assumed to be 0.1 based on the measured imperfections available in the literature for UHSS tubes [4]. Noting that since the slenderness of the modelled UHSS circular hollow section is relatively low, it would be acceptable to use the imperfection value measured for a virgin section at room temperature.

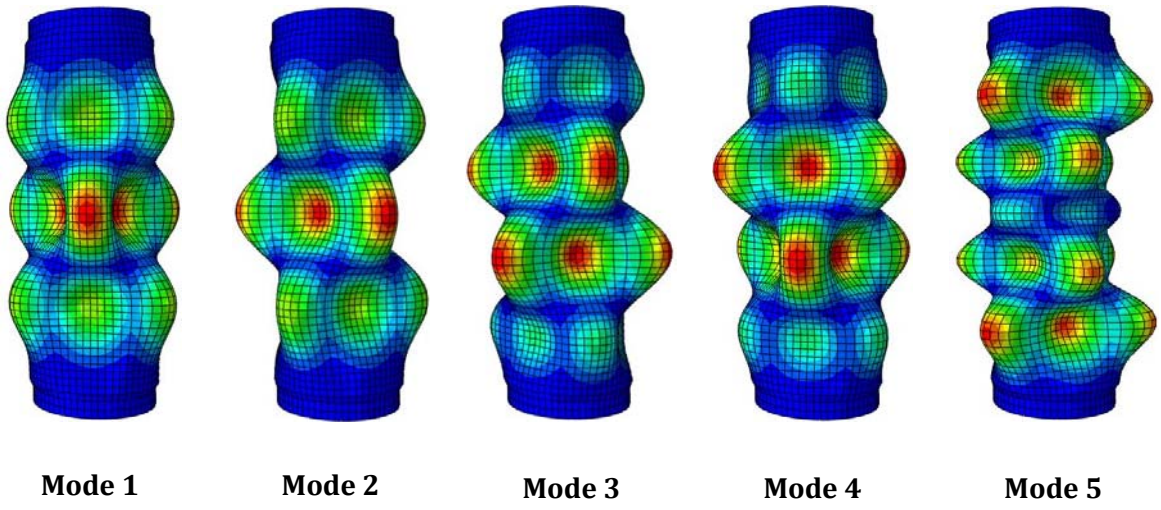

Figure 7-6. Illustration of the modes shapes resulted from the FE linear buckling analyses of the UHSS-QT stub column cooled from 470°C to room temperature

7.3.2. Verification of the FE analysis

7.3.2.1. Stub column experimental tests

In order to validate the FE analysis results experimental tests are conducted in which UHSS-QT tubular stub columns with the same nominal dimensions as those used in the numerical simulations (i.e. $D = 38.1mm$, $t = 1.8mm$ and $L = 3D$) are used. In order to simulate the post-fire conditions, the stub columns are located inside the split furnace

shown in Figure 7-7 . Similar to the procedure explained in Section 7.2.1 for the material coupon tests, they are heated up to different elevated temperatures and cooled to room temperature. The temperature of the stub columns along their height is recorded by three thermocouples attached to the top, middle and bottom of the columns. The status of the column inside the furnace and test setup of both heat-up and cooling phases are illustrated in Figure 7-7. It is worth noting that the furnace is split into three zones and heats up the specimen through a combination of convection and radiation, dependent on the test temperature. The variation of the stabilised maximum temperature recorded by the three thermocouples with the height of the columns are presented in Figure 7-8 for different tests. The *CT* curve represents the sample cooled from temperature *T* to room temperature. Also, to better illustrate the location of the temperature recordings, the column is schematically shown in this figure.

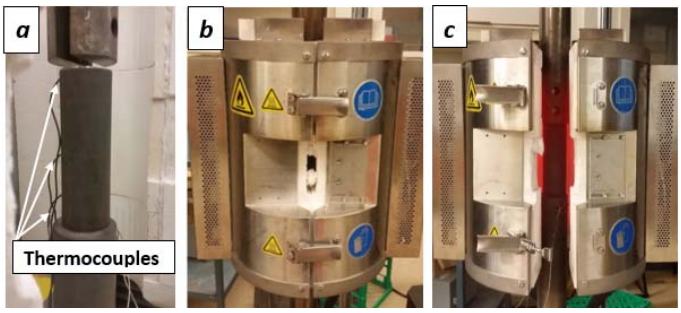

Figure 7-7. a) Status of the column inside the furnace and b) heat-up and c) cooling phases of the test

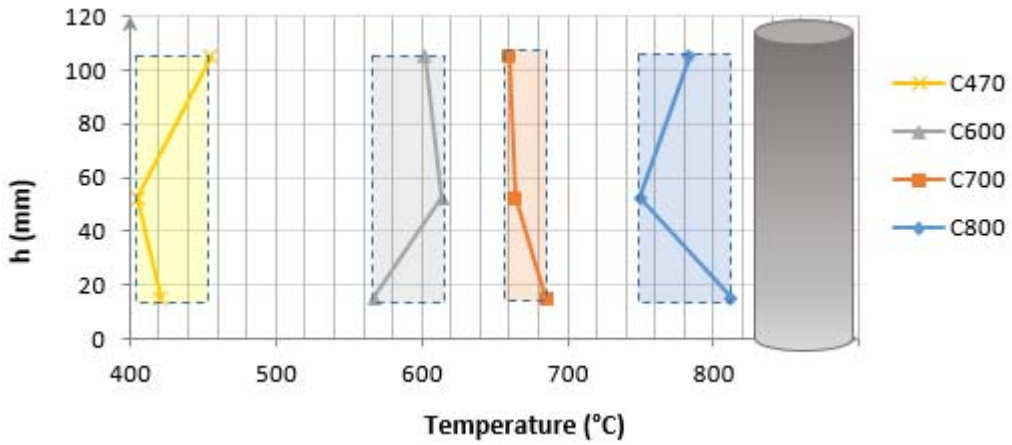

Figure 7-8. Temperature distribution of the heated columns along their height for different maximum fire temperatures.

To apply quasi-static compression load to the UHSS-QT stub columns cooled from different fire temperatures to the ambient state, Schimadzu testing machine with the capacity of 300kN is used. The displacement rate of $0.3 mm.\min^{-1}$ is applied to the top plate of the end fixture connected to the top of the stub columns. The geometry of the end fixtures are similar to those used in the numerical simulations (Figure 7-5b). The vertical deformation of the columns is recorded using an MTS non-contact laser extensometer. To derive exact strain values in both elastic and plastic region of the stress-strain curves and ensure strain uniformity along the height of the stub columns, reflective tapes are attached to two points with a ~4 mm distance in the middle of the column and also to the top and bottom of the end fixtures. The laser extensometer records the vertical displacement between the two middle reflective tapes, and the top and bottom ones to derive the elastic and plastic strains, respectively. The test setup for the compression loading of the columns is presented in Figure 7-9.

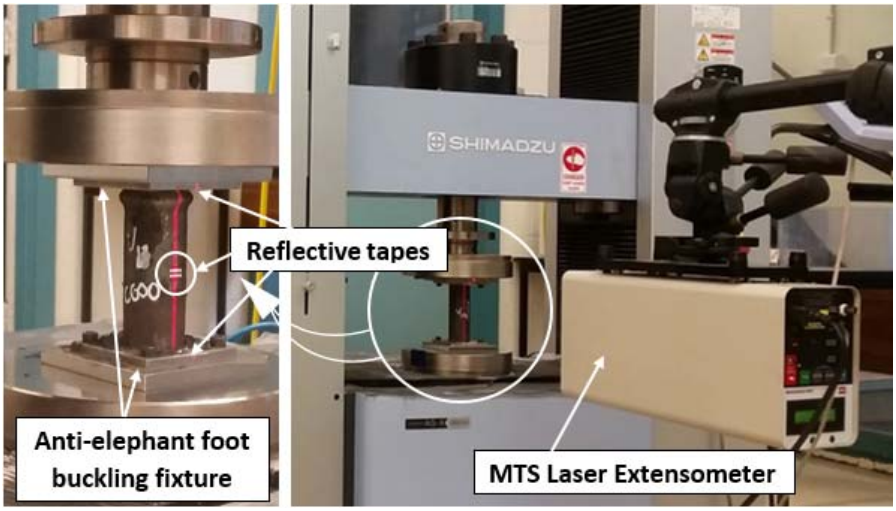

Figure 7-9. The test setup for compression loading of the UHSS stub-columns cooled from fire.

7.3.2.2. Stress-strain curves

In Figure 7-10, the post-fire stress-strain curves of the UHSS-QT stub columns (SC) obtained from both the experimental (Exp.) tests and the FE model (FEM) are presented. These curves are labelled as SC-UHSS-QT-C*T*-Exp. and SC-UHSS-QT-C*T*-FEM, respectively, where C*T* denotes cooling from fire temperature *T* to room temperature. Also, SC-UHSS-QT-RT-Exp. and SC-UHSS-QT-RT-FEM curves indicate the stress-strain curves of the UHSS-QT stub columns tested at room temperature (RT) without experiencing fire.

From Figure 7-10, it can be understood that the stress-strain curves obtained from the experimental tests and the FEM are in good agreement for the original room temperature stub columns and those cooled from different fire temperatures to room temperature, except for 600°C. The reason behind the difference between the experimental C600 test results and the FEM ones can be attributed to the temperature distribution along the heated column and the fact that this temperature (i.e. 600°C) is critical for the UHSS. From Figure 7-8, it can be understood that the temperature of the middle of the column exceeds 600°C. Besides, from the investigation conducted in [34], 600°C is defined as a critical temperature, above which the phases present in the material start changing in identity and thus the mechanical properties of UHSS above this temperature change considerably. Therefore, considering that the exact same heat-up and cooling conditions are present for the tensile coupons and the UHSS-QT stub columns cooled from different fire temperatures, one certain reason for this difference can be the temperature distribution along the column's height.

In addition, the experimental failure mechanism of the UHSS-QT stub column cooled from 470°C and subjected to compression loading at room temperature is compared to that of FE model, as illustrated in Figure 7-11. The general shape of all deformed columns cooled from different fire temperatures is quite similar due to their identical initial geometry and boundary conditions; therefore, only one maximum temperature (470°C) is considered for comparison of the deformed shape of the FE column with the experimental one. As can be observed from Figure 7-11, the deformed shapes obtained from numerical and experimental models are in a good agreement.

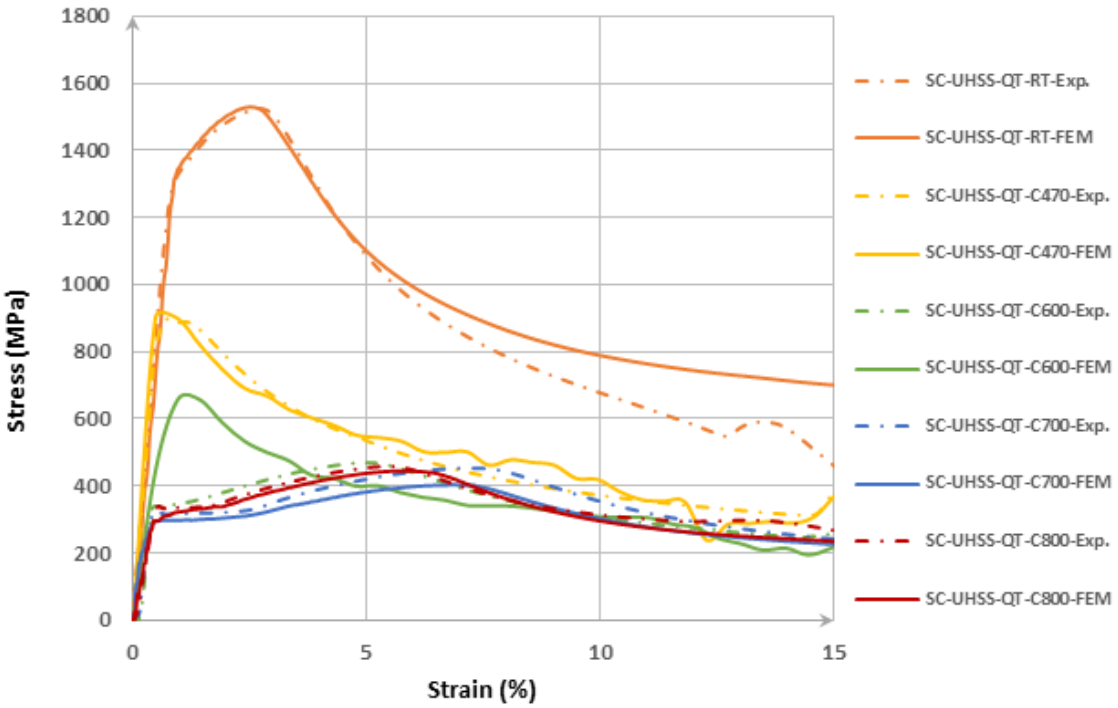

Figure 7-10. Comparison of the experimental and FE analysis results of the stress-strain curves of the UHSS-QT stub-columns cooled from different fire temperatures to room temperature.

Figure 7-11. Comparison of the failure mechanism of the experimental and FE Model for UHSS-QT stub column cooled from 470°C to room temperature

7.3.3. Post-fire compressive behaviour of UHSS stub-columns

7.3.3.1. Load-displacement curves

In this section, the post-fire load-displacement curves of the UHSS-DQ and UHSS-QT tubular stub columns are compared. Figure 7-12 depicts the compression force with respect to the axial displacement of these columns after cooling from different fire temperatures, which are obtained from the FE simulations explained and validated in Sections 7.3.1 and 7.3.2, respectively. The labelling system used in this figure is similar to that explained in Section 7.3.3. From these curves, it can be observed that by increasing the maximum fire temperature up to 800°C, the maximum loading capacity of both UHSS columns tested at room temperature are reduced up to 70%. As expected from the material coupon tests, the deterioration of the post-fire compressive load capacity of UHSS-DQ stub columns after experiencing fire temperatures of up to 700°C is considerably less significant than the UHSS-QT stub columns. The difference between the post-fire load-displacement curves of the UHSS-DQ and UHSS-QT stub columns however, becomes less considerable after they are cooled from 800°C to room temperature. This can be related to the formation of 100% austenite in the microstructure of both UHSS materials which was mentioned in Section 7.2.2.2. Comparing the general shape of the load-displacement curves of UHSS-QT and UHSS-DQ stub columns, it can also be inferred that the UHSS-DQ stub columns cooled from different fire temperatures undergo more plastic deformation.

Considering the fact that the original room temperature curves of the two simulated stub columns are quite similar, it can be understood that the manufacturing process of their construction materials plays an important role on their post-fire residual loading capacity.

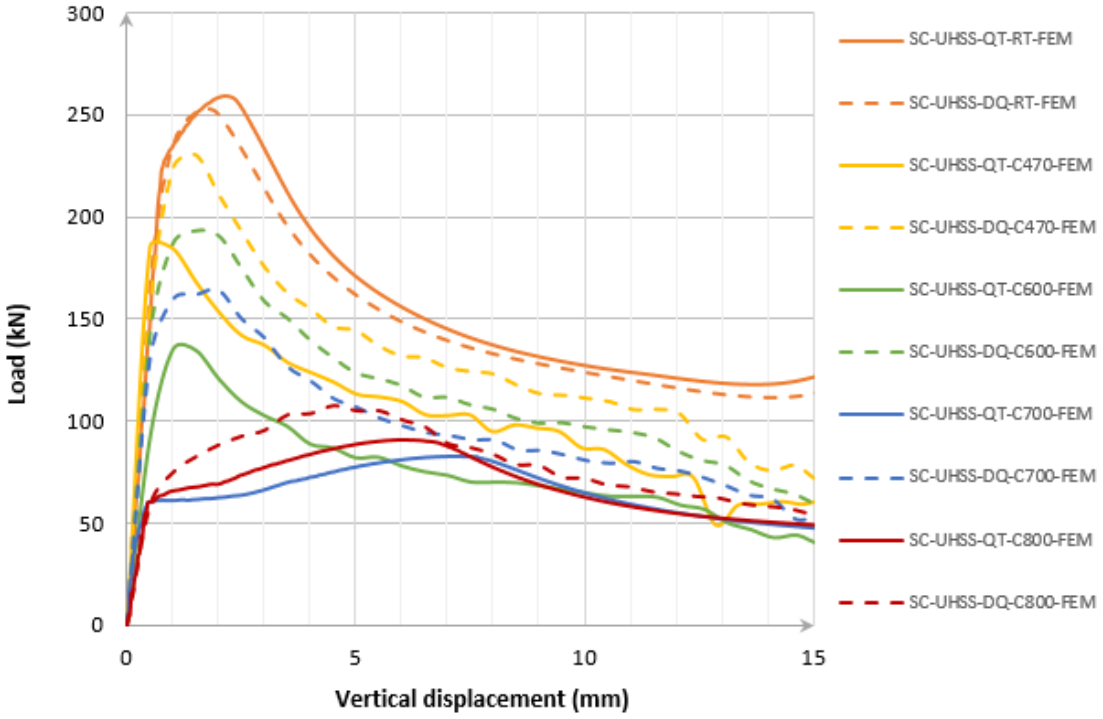

Figure 7-12. Comparison of the load-vertical displacement curves of UHSS-QT and UHSS-DQ stub-columns cooled from different fire temperatures to room temperature

7.3.3.2. Strength and slenderness

In this section, the post-fire strength and slenderness values of the UHSS-DQ and UHSS-QT stub columns (SC) are discussed and compared.

The values of 0.2% proof stress and ultimate strength for the two simulated stub columns cooled from different fire temperatures are normalised with respect to their corresponding room temperature values, i.e. $(\frac{f_{0.2,CT}}{f_{0.2,RT}})_{SC}$ and $(\frac{f_{u,CT}}{f_{u,RT}})_{SC}$, respectively, and presented in Table 7-4. The general decreasing trend of these strength reduction factors can be observed for both UHSS stub columns with increasing the maximum fire temperature. However, similar to the tensile strength values, the serious deterioration of the residual compressive strength for UHSS-QT stub columns starts after cooling from temperatures above 600°C, whereas this significant deduction occurs for UHSS-DQ stub columns after exposure to temperatures above 700°C. Nevertheless, both columns experience up to ~70-75% reduction in their ultimate compressive strength when cooled from 800°C to room temperature. Also, while the 0.2% proof strength reduction of the UHSS-QT stub column cooled from 700°C and 800°C is stabilised at ~77%, that for the

UHSS-DQ stub columns steadily increases up to ~84% when cooled from 800°C to room temperature.

In Table 7-4, the ultimate compressive strength of the UHSS-DQ and UHSS-QT stub columns ($f_{u,SC}$) cooled from different fire temperatures are also compared to the corresponding ultimate tensile strength (f_u) values obtained from the material tensile coupons by the following ratio:

$$r_{u,SC} = \frac{f_{u,SC}}{f_u} \tag{7-2}$$

From literature [35], it is known that the columns, for which the ultimate compressive strength values match their tensile coupon ones, i.e. the $r_{u,SC}$ values are close to 1, are failed under compression by cross section yielding. According to the $r_{u,SC}$ values presented in Table 7-4, it can be concluded that the original room temperature UHSS-DQ and UHSS-QT cross sections and those cooled from different fire temperatures to room temperature are mainly failed by yielding.

Another important parameter which is given in Table 7-5 is the slenderness parameter (λ) of the simulated UHSS-DQ and UHSS-QT stub columns cooled from different fire temperatures to room temperature. The values of λ for different stub columns are derived based on the definitions given by the available references for the yield slenderness limit of circular hollow-section (CHS). In the formulas presented in this Table, *D* and *t* are the outer diameter and wall thickness of the tube, respectively. *E* is the elastic modulus which is obtained using the strain values of the reflective tapes attached to the middle of the columns. It is worth mentioning that the elastic modulus of the columns exposed to different fire temperatures remains unchanged when cooled to room temperature [34]. Thus, the original room temperature elastic modulus is used for the stub columns cooled from different fire temperatures. Comparing the λ values presented in Table 7-5 with the yield slenderness limits set out by different standards, it can be interpreted that for the virgin UHSS-DQ and UHSS-QT stub columns, λ values are greater than the limits given by the standards. This means that if the values of slenderness limit set out by the standards are used, these sections should be categorised in "Class 4" and considered as slender sections. However, as stated above, the $r_{u,SC}$ values for the virgin UHSS-DQ and UHSS-QT

stub columns are close to 1 and therefore, the failure mode of UHSS-DQ and UHSS-QT stub columns is cross section yielding at room temperature. Therefore, the limits set out by the standards are too conservative if adopted for the design of a UHSS CHS at room temperature and to have an economical design, higher values of λ must be defined to differentiate the slender columns from compact ones. This is consistent with the yield slenderness limit suggested by Jiao et al. [36] for virgin UHSS-QT tube at room temperature, in which, considering the slenderness formula given by AS 4100 [37], a new limit of 258 (instead of 82) was proposed. On the other hand, the λ values of UHSS-DQ and UHSS-QT stub columns cooled from fire temperatures of up to 800°C, are well below the limits defined by the standards. Considering the close values of $r_{u,SC}$ to 1 for these columns, it can be concluded that these sections are also mainly failed by cross section yielding which is in accordance to the standards. While this paper only aims to identify the effect of manufacturing process on the slenderness limits and perform a comparison study between the slenderness of the tested columns and the limits set out by the standards, it is important to note that, in order to define the exact yield slenderness limits for the room temperature and post-fire behaviour of UHSS CHSs, excessive experiments on various sizes of UHSS columns are required.

Table 7-4. The strength reduction factors and the normalised slenderness values of the UHSS-DQ and UHSS-QT stub columns (SC) after cooling from various fire temperatures to room temperature (RT)

	Temperature / Material	**RT**	**470°C**	**600°C**	**700°C**	**800°C**
$(\frac{f_{0.2,CT}}{f_{0.2,RT}})_{SC}$	**UHSS-DQ**	1.000	0.816	0.645	0.559	0.163
	UHSS-QT	1.000	0.737	0.449	0.229	0.230
$(\frac{f_{u,CT}}{f_{u,RT}})_{SC}$	**UHSS-DQ**	1.000	0.755	0.633	0.537	0.353
	UHSS-QT	1.000	0.591	0.430	0.263	0.290
$r_{u,SC}$	**UHSS-DQ**	1.085	1.012	1.008	1.016	0.933
	UHSS-QT	1.082	0.993	1.015	0.984	0.955

Table 7-5. Slenderness parameters (λ) of UHSS-DQ and UHSS-DQ stub columns cooled from different fire temperatures based on the definitions given by different standards for cold-formed circular hollow sections (CHS)

References	Yield Slenderness limits	Temperature / Material	RT	470°C	600°C	700°C	800°C
AS 4100 [37]	$\lambda = (\frac{D}{t})(\frac{f_y}{250}) \leq 82$	UHSS-DQ	103.717	84.667	66.887	57.997	16.933
		UHSS-QT	103.717	76.454	46.567	23.707	23.876
EN-1993-1-1 [38]	$\lambda = (\frac{D}{t})(\frac{f_y}{235}) \leq 90$	UHSS-DQ	110.337	90.071	71.156	61.699	18.014
		UHSS-QT	110.337	81.334	49.539	25.220	25.400
AISI S100 [39]	$\lambda = (\frac{D}{t})(\frac{f_y}{E}) \leq 0.111$	UHSS-DQ	0.141	0.115	0.091	0.079	0.023
		UHSS-QT	0.123	0.091	0.055	0.028	0.028

7.3.3.3. Ductility

In order to compare the ductile post-fire compressive behaviour of the UHSS-DQ and UHSS-QT stub columns, the ductility factors introduced as $(f_u/f_{0.2})_{SC}$ and $(D_u/D_y)_{SC}$ are calculated. Noting that D_u and D_y, are the displacements corresponding to the ultimate compressive strength (or load) and the 0.2% proof strength (or load) of the stub columns, respectively. These displacements are extracted from the load-displacement curves illustrated in Figure 7-12. In Table 7-6, the afore-mentioned ductility factors are presented for the UHSS-DQ and UHSS-QT stub columns cooled from different fire temperatures to room temperature. It can be seen that while there is a general increasing trend for both ductility factors of the UHSS-DQ and UHSS-QT stub columns with increasing the maximum fire temperature, the changes in $(D_u/D_y)_{SC}$ is considerably more significant. This indicates that despite the strength reduction observed for the two UHSS stub columns after cooling from fire temperatures (Table 7-4), the ductility of the UHSS-DQ and UHSS-QT stub columns can be increased up to 6.1 and 4.7 times their original room temperature values, respectively. Also, comparing the two UHSS stub columns, it can be concluded that the UHSS-QT stub columns undergo more plastic deformation when cooling from high fire temperatures (above 600°C) to room temperature. This can be justified by the significant difference between the values of the

corresponding strain ratio (i.e. $\varepsilon_u/\varepsilon_y$) for the two UHSS materials cooled from high fire temperatures (Table 7-3). Similar to the reasoning given for the variation of $\varepsilon_u/\varepsilon_y$ ratio for the tensile coupons, the $(D_u/D_y)_{SC}$ values vary mainly due to the variation of D_u displacement. However, at low fire temperatures, a considerable difference cannot be observed between the ductility parameters of the UHSS-DQ and UHSS-QT stub columns cooled from fire temperatures to room temperature. The reason can be referred to the considerable difference in the microstructure of the materials of these columns after exposure to high fire temperatures, as a result of their different manufacturing process.

Table 7-6. Variation of the ratios of $f_u/f_{0.2}$ and $\varepsilon_u/\varepsilon_y$ for UHSS-DQ and UHSS-QT stub columns cooled from various fire temperatures to room temperature (RT)

	Temperature / Material	RT	470°C	600°C	700°C	800°C
$(f_u/f_{0.2})_{SC}$	**UHSS-DQ**	1.217	1.125	1.194	1.169	2.630
	UHSS-QT	1.248	1.000	1.196	1.436	1.574
$(D_u/D_y)_{SC}$	**UHSS-DQ**	2.347	1.873	2.278	3.271	14.370
	UHSS-QT	3.184	1.533	2.197	17.704	14.888

7.4. Conclusions

This paper investigated the effect of manufacturing process on the mechanical response of Grade 1200 ultra-high strength steel (UHSS) tubes under cooling phase of a fire. To achieve this, a comparison study was conducted on the post-fire tensile and compressive mechanical behaviour of “direct-quenched” and “quenched and tempered” UHSS tubes, i.e. UHSS-QT and UHSS-QT, respectively. Standard tensile coupon tests were first carried out on UHSS-DQ and UHSS-QT dog-bone specimens cooled from fire temperatures of up to 800°C to room temperature. The post-fire stress-strain curves and the residual strength and ductility of the two UHSS materials were then discussed and compared. It was shown that the reduction in the residual post-fire tensile strength of UHSS-QT specimens became maximum and stabilised at a lower temperature (700°C) compared to the UHSS-DQ specimens. The tensile coupon tests results also showed that the ductility of the two UHSS materials have a considerable difference when cooled from low and high

fire temperature regimes. Afterwards, using the precise post-fire material properties obtained from the tensile coupon tests, a finite element (FE) model was developed in ABAQUS FE software simulating the post-fire compression behaviour of UHSS-DQ and UHSS-QT tubular stub columns. The model was validated by the quasi-static compression tests conducted on UHSS-QT tubular stub columns after cooling from different fire temperatures to room temperature. The post-fire load-displacement curves, strength, slenderness and ductility of the UHSS-DQ and UHSS-QT stub columns were also compared. It was shown that while for the UHSS-QT stub columns cooled from fire temperatures, serious deterioration in their residual strength starts after exposure to temperatures above 600°C, this occurs for UHSS-DQ stub columns after exposure to temperatures above 700°C. The slenderness parameters of both stub columns which has a direct relationship with their 0.2% proof strength were compared to the limits set out by different standards. It was shown that except for the virgin room temperature columns, the slenderness values of the cooled ones are consistent with the yield slenderness limits defined by the standards. It was also indicated that while the ductility parameters of UHSS-DQ and UHSS-QT stub columns cooled from low fire temperatures do not exhibit a considerable difference, UHSS-QT stub columns experienced more plastic deformation when cooled from high fire temperatures.

Acknowledgement

The research work presented in this paper was supported by the Australian Government-Department of Education and also by Australian Research Council through a Discovery Project (DP150100442) awarded to the second and third authors.

References

[1] R. Bjorhovde, Development and use of high performance steel, Journal of Constructional Steel Research, 60 (2004) 393-400.
[2] G. Pocock, High strength steel use in Australia, Japan and the US, 2006.
[3] H. Ban, G. Shi, A review of research on high-strength steel structures, Proceedings of the Institution of Civil Engineers - Structures and Buildings, (2017) 1-17.
[4] F. Javidan, A. Heidarpour, X.-L. Zhao, J. Minkkinen, Application of high strength and ultra-high strength steel tubes in long hybrid compressive members: Experimental and numerical investigation, Thin-Walled Structures, 102 (2016) 273-285.
[5] M. Nassirnia, A. Heidarpour, X.-L. Zhao, J. Minkkinen, Innovative hollow columns comprising corrugated plates and ultra high-strength steel tubes, Thin-Walled Structures, 101 (2016) 14-25.
[6] M. Farahi, A. Heidarpour, X.-L. Zhao, R. Al-Mahaidi, 08.35: Compressive behavior of concrete filled double skin sections consisting of corrugated plates and ultra-high strength steel corner tubes, ce/papers, 1 (2017) 2120-2127.
[7] D.-H. Kim, J.-H. Kim, S. Chang, Material performance evaluation and super-tall building applicability of the 800 MPa high-strength steel plates for building structures, International Journal of Steel Structures, 14 (2014) 889-900.
[8] T. Kamo, M. Sasaki, Y. Watanabe, R. Ando, T. Suzuki, Ultra High Strength Steel for Sustainable Building Structures, in: Nippon Steel & Sumitomo Metal, Technical Report No. 110, September 2015.
[9] C.-H. Lee, Structural Performance of 800 MPa High-Strength Steel Members and Application to Highrise and Mega Building Structures, International Journal of High-Rise Buildings, 6 (2017) 249-259.
[10] S.P. Chiew, M.S. Zhao, C.K. Lee, Mechanical properties of heat-treated high strength steel under fire/post-fire conditions, Journal of Constructional Steel Research, 98 (2014) 12-19.
[11] S. Gunalan, M. Mahendran, Experimental investigation of post-fire mechanical properties of cold-formed steels, Thin-Walled Structures, 84 (2014) 241-254.
[12] J. Outinen, Mechanical properties of structural steel at elevated temperatures and after cooling down, in: 10th International Conference - Fire and Materials 2007.
[13] X. Qiang, F.S.K. Bijlaard, H. Kolstein, Post-fire mechanical properties of high strength structural steels S460 and S690, Engineering Structures, 35 (2012) 1-10.
[14] X. Qiang, F.S.K. Bijlaard, H. Kolstein, Post-fire performance of very high strength steel S960, Journal of Constructional Steel Research, 80 (2013) 235-242.
[15] W. Wang, T. Liu, J. Liu, Experimental study on post-fire mechanical properties of high strength Q460 steel, Journal of Constructional Steel Research, 114 (2015) 100-109.
[16] M. Amraei, T. Skriko, T. Björk, X.-L. Zhao, Plastic strain characteristics of butt-welded ultra-high strength steel (UHSS), Thin-Walled Structures, 109 (2016) 227-241.
[17] F. Azhari, A. Heidarpour, X.-L. Zhao, C.R. Hutchinson, Mechanical properties of ultra-high strength (Grade 1200) steel tubes under cooling phase of a fire: An experimental investigation, Construction and Building Materials, 93 (2015) 841-850.
[18] F. Azhari, A. Heidarpour, X.-L. Zhao, C.R. Hutchinson, Evaluating post-fire mechanical behavior of ultra-high strength (Grade1200) steel tubes, in: Structures in Fire, Proceedings of the Ninth International Conference, Princeton University, 2016.
[19] F. Azhari, A. Heidarpour, X.-L. Zhao, C.R. Hutchinson, Effect of creep strain on mechanical behaviour of ultra-high strength (Grade 1200) steel subject to cooling phase of a fire, Construction and Building Materials, 136 (2017) 18-30.

[20] F. Azhari, A. Heidarpour, X.-L. Zhao, C.R. Hutchinson, Post-fire mechanical response of ultra-high strength (Grade 1200) steel under high temperatures: Linking thermal stability and microstructure, Thin-Walled Structures, 119 (2017) 114-125.
[21] L. Kang, M. Suzuki, H. Ge, B. Wu, Experiment of ductile fracture performances of HSSS Q690 after a fire, Journal of Constructional Steel Research, 146 (2018) 109-121.
[22] X. Gao, X. Zhang, H. Liu, Z. Chen, H. Li, Residual mechanical properties of stainless steels S30408 and S31608 after fire exposure, Construction and Building Materials, 165 (2018) 82-92.
[23] W. Wang, B. Liu, V. Kodur, Effect of Temperature on Strength and Elastic Modulus of High-Strength Steel, Journal of Materials in Civil Engineering, 25 (2013) 174-182.
[24] J. Chen, B. Young, B. Uy, Behavior of High Strength Structural Steel at Elevated Temperatures, Journal of Structural Engineering, 132 (2006) 1948-1954.
[25] S. Kesawan, M. Mahendran, Post-fire mechanical properties of cold-formed steel hollow sections, Construction and Building Materials, 161 (2018) 26-36.
[26] H.K.D.H. Bhadeshia, S.R. Honeycombe, Chapter 5 - Formation of Martensite, in: H.K.D.H.B.R. Honeycombe (Ed.) Steels (Third Edition)-Microstructure and Properties, Butterworth-Heinemann, Oxford, 2006, pp. 95-128.
[27] A. Heidarpour, N.S. Tofts, A.H. Korayem, X.-L. Zhao, C.R. Hutchinson, Mechanical properties of very high strength steel at elevated temperatures, Fire Safety Journal, 64 (2014) 27-35.
[28] SSAB Manufacturing Company < https://www.ssab.com/ >, in, Stockholm, Sweden, 1878.
[29] ABAQUS Analysis User's Guide. A.S. Pachage, editor. Providence, RI, Simulia, 2012.
[30] Australia Standards AS4100, Steel structures, Sydney, Australia, 1998.
[31] Australian/New Zealand Standard AS/NZS 4600, Cold-Formed Steel Structures, Standards Australia, Sydney, Australia and Standards New Zealand, Wellington, New Zealand, 2005.
[32] European Code 3,Eurocode 3: Design of Steel Structures, European Committee for Standardization, Brussels, Belgium, 2010.
[33] R.D. Ziemian, Appendix B: Technical Memoranda of Structural Stability Research Council, in: Guide to Stability Design Criteria for Metal Structures, John Wiley & Sons, 2010, pp. 963-1029.
[34] F. Azhari, A. Heidarpour, X.L. Zhao, C.R. Hutchinson, Mechanical properties of ultra-high strength (Grade 1200) steel tubes under cooling phase of a fire: An experimental investigation, Construction and Building Materials, (2015).
[35] J.L. Ma, T.M. Chan, B. Young, Experimental Investigation on Stub-Column Behavior of Cold-Formed High-Strength Steel Tubular Sections, Journal of Structural Engineering (United States), 142 (2016).
[36] H. Jiao, X.L. Zhao, Imperfection, residual stress and yield slenderness limit of very high strength (VHS) circular steel tubes, Journal of Constructional Steel Research, 59 (2003) 233-249.
[37] AS (Australian Standard), in: "Steel structures." AS 4100, Sydney, Australia, 1998.
[38] CEN (European Committee for Standardization), in: "Eurocode 3: Design of steel structures—Part 1-1: General rules and rules for buildings." EN 1993-1-1, Brussels, Belgium, 2005.
[39] A. Standard, North American Specification for the Design of Cold-formed Steel Structural Members AISI S100, American Iron and Steel Institute, Washington DC, (2012).

Chapter 8

Conclusions and future work

Table of Contents

8.1. Summary of outcomes

Experimental tests conducted on Grade 1200 UHSS tubes subjected to fire temperatures and the following analytical and numerical investigations carried out in this thesis are the pre-requisite for using this material in structural members. Results and outcomes of each phase of this thesis are summarised below.

In chapters 2 and 3, an experimental study was performed to examine the in-fire and post-fire mechanical behaviour of the Grade 1200 UHSS tube subjected to fire temperatures ranging from 150°C to 800°C. The results obtained from the tensile tests conducted on the UHSS specimens at fire temperatures showed that the strength of UHSS deteriorates considerably when heated to temperatures above 300°C. The strength reduction becomes more significant as the fire temperature increases, such that the materials loses most of its strength at 800°C. According to the tensile tests conducted on the UHSS specimens at room temperature after cooling from fire temperatures, the reduction in the residual strength of UHSS starts when the material is cooled from fire temperatures equal and above 470°C. However, the most significant deterioration in the residual strength was observed after exposure to temperatures above 600°C. In addition, the results showed that when the UHSS is cooled from fire temperatures above ~750°C, the deterioration in the residual strength is stabilised, such that there is no more strength reduction after exposure to temperatures above 750°C. As for measurement of the ductility of the UHSS tube specimens cooled from elevated temperatures, different parameters (the uniform elongation, the energy absorption, etc.) were calculated. The general trend of the variation of these parameters with fire temperature indicated that the higher temperature the specimens have experienced, the more ductility is recovered. On the other hand, for the UHSS tube specimens tested at elevated temperatures, while there was no change in the uniform elongation with increasing the fire temperature, a general decreasing trend was observed for their energy absorption.

For understanding the effect of steel grade on the post-fire mechanical response of steel materials, the experimental tests results for the UHSS tube specimens were compared to those obtained for Grade 350 MS and Grade 800 HSS tube specimens. It was shown that unlike the UHSS, the deterioration in the residual strength of MS and HSS starts after

exposure to fire temperatures above 600°C and becomes significant when subjected to fire temperatures above 700°C.

To rationalise the changes occurred in the post-fire mechanical properties of the tested specimens, micrographs were obtained from their bulk microstructure both in their original sate and after being cooled from some critical fire temperatures to the ambient state. The microstructural reason for the resulted residual strength of the specimens subjected to cooling phase of fire was explained. The thermodynamic stability plots of the phases present in the microstructure of the UHSS, HSS and MS materials were calculated. Based on these curves, a recommendation was made to emphasise that the studies of the effect of elevated temperature exposures on the residual strengths of steels should be separated for two regimes of behaviour depending on the maximum temperature reached: the low temperature and high temperature regimes, the ranges of which depend on the alloy composition. For the steels examined in this study, the critical fire temperature dividing these two classes of temperatures is ~650-700°C. In the low temperature regime, while the post-fire behaviour of steel is insensitive to the cooling rates studied in this research, it strongly depends on the maximum fire temperature and less strongly on the time at elevated temperature. Insensitivity of the residual stress-strain behaviour of UHSS material to the cooling rate of fire was also experimentally shown by considering three different cooling rates. As opposed to the low temperature regime, it was shown that in the high temperature regime, the effect of cooling rate from fire is much stronger than the time and maximum fire temperature.

Using the modified version of the compound Ramberg-Osgood equations and the experimental results, an empirical material model was proposed for the post-fire behaviour of the UHSS material in terms of the maximum fire temperature and some of the original room temperature mechanical properties. The model showed a good accuracy in prediction of the post-fire stress-strain curves of the UHSS specimens cooled from different fire temperatures.

In chapter 4 of this thesis, the mechanical behaviour of Grade 1200 UHSS tube under a multi-phase loading scenario including fire and creep was experimentally examined. According to the stress-strain curves obtained from the experimental tests, for a constant value of sustained axial load ratio (β), with increasing the maximum fire temperature,

the deterioration in the residual strength became more significant as larger creep strains were experienced by the specimens. Furthermore, it was concluded that for a constant maximum fire temperature value, as the values of β were increased up to 0.85, the specimens experienced a considerable increase in the creep strain and consequently, a significant reduction in their residual strength (i.e. ~23% more reduction than the UHSS cooled from same fire temperature without experiencing creep). Therefore, the deterioration in the residual strength of the tested specimens during the considered multi-phase loading scenario, is directly related to the creep strain resulted from the existence of sustained axial load on the specimens during fire. As a result, the residual post-fire strength of a UHSS structural member is mainly controlled by the maximum fire temperature and the sustained loads applied to the member during fire. Chapter 4 also discussed the steel grade effect on the residual stress-strain behaviour of UHSS subject to fire and creep. To this end, Grade 800 HSS and Grade 350 MS tube specimens were undergone the same experimental tests with the maximum fire temperature of 700°C and axial load ratio of $\beta = 0.8$. From the comparison of the results obtained for the three grades of steel, it was concluded that the HSS was the most resistant material to creep, whereas the UHSS and MS materials experienced a substantial creep strain during fire. Comparing the resistance of the UHSS and MS materials to creep during a simulated fire exposure, it was shown that the UHSS was more sensitive to creep. Nevertheless, the residual strength of UHSS under such multi-phase loading scenario was still almost equal to that of the virgin MS at room temperature. This result can be an indication of the great potential of the UHSS material for being used as a construction material in structural members. For interpretation of the results, using the SEM method, micrographs were obtained from the UHSS specimens cooled from 700°C to room temperature, without experiencing creep strain and with creep strain caused by axial load ratio of $\beta = 0.8$ during heat-up and cooling phases. It was shown that the creep strain during fire further accelerates the tempering process and consequently, the cementite growth in the microstructure. Thus, the average size of cementite particles increases leading to a reduction in the residual strength of the martensitic UHSS.

After finishing the experimental investigations of the effect of severe temperature changes and the creep strain on the post-fire mechanical response of Grade 1200 UHSS tubes in chapters 2 to 4, using the experimental results and the Bernstain-Bézier

equations, a material model was proposed in Chapter 5. The model presented the relationship between the stress, strain, the maximum fire temperature and the sustained axial load ratio (β) for the UHSS material cooled from different fire temperatures to room temperature. The model was validated by showing its success in predicting the stress-strain curves for the UHSS cooled from fire temperatures which were not used in the calibration of the model. It is also capable of extrapolating the post-fire stress-strain curves of UHSS out of the temperature range of the available test data. The extrapolation technique works correctly provided that the same trend in the changes of the mechanical properties is continued and no unexpected material behaviour is observed. Another capability of the model was shown in predicting the instantaneous stress-induced strain (ε_σ) of UHSS subjected to a constant stress level, i.e. $\sigma = \text{Const.}$, in a transient fire. Thus, knowing ε_σ from the model and other strain components from the experimental tests, variation of the creep strain (ε_{cr}) of UHSS with the fire temperature for different constant stress values was obtained. It was shown that if the magnitude of the constant stress applied to the UHSS during fire is close to the ultimate tensile strength of UHSS at the elevated temperature, even if it has a small value, the material may experience a considerably large creep strain. Nevertheless, it is a general conclusion that the creep strain has a direct relationship with the magnitude of the constant stress and the fire temperature.

Following the conclusions made from the microstructural examinations conducted in chapters 2 and 3, chapter 6 mainly attempted to discuss the effect of extreme cooling rates on the post-fire mechanical response of UHSS cooled from fire temperatures, specifically the high temperature regime. The post-fire strength and ductility of the UHSS cooled from different fire temperatures to the ambient state with an extremely high cooling rate (water-quenched with ~3500°C/min average cooling rate) were compared to those of the UHSS naturally air-cooled to room temperature (~20°C/min average cooling rate). It was concluded from the results that while the cooling rate of fire has a significant effect on the residual mechanical response of UHSS cooled from high fire temperatures (above 700°C), it has a minor effect on those of UHSS cooled from low fire temperatures (equal or below 700°C). In addition, it was observed that the UHSS cooled from 800°C with an extremely high cooling rate (water-quenched) experienced 60% higher ultimate tensile strength compared to the air-cooled UHSS. On the other hand, the

same water-quenched UHSS undergone a lower uniform elongation compared to the air-cooled sample. Thus, it can be inferred that extremely high cooling rates from high fire temperatures makes the UHSS stronger, but also brittle. For better interpretation of the results, the microstructures of the tested UHSS specimens were discussed. Moreover, the steel grade effect was investigated by conducting a comparison study on Grade 800 HSS and Grade 350 MS. It was indicated that the effect of extreme cooling rate on the post-fire mechanical response of MS material is more significant compared to the HSS. In this chapter, in addition to the extreme cooling rate, as another extreme cooling condition, the extreme cooling temperatures were also simulated. The UHSS, HSS and MS materials were cooled from the ambient state to sub-zero temperatures of down to -80°C. According to the results, while the strength of the materials increased when cooled to sub-zero temperatures, the uniform elongation they experienced decreased and thus the material became stronger, but more brittle. When the three steel grades were cooled from room temperature to -80°C, the HSS material had the most significant increase in the ultimate tensile strength, i.e. ~15%, while UHSS and MS experienced an increase of ~8.5% and ~7%, respectively. In addition, the UHSS material exhibited the lowest uniform elongation at the simulated subzero temperatures. Nevertheless, because of the gradual elastic-plastic transition in its stress-strain curve, the yield strain of UHSS was higher than HSS.

In chapter 7 of this thesis, it was attempted to examine the manufacturing process effect on the post-fire mechanical response of Grade 1200 UHSS tubes. According to the experimental results obtained from the standard tensile coupon tests, compared to the UHSS material manufactured by the DQ technique (UHSS-DQ), that manufactured by the conventional QT method (UHSS-QT), showed more sensitivity to the temperature history when cooled from fire temperatures below 800°C to room temperature. For example, while there was a ~20% reduction in the ultimate tensile strength of the UHSS-DQ cooled from 470°C to room temperature, that for the UHSS-QT undergone the same test was ~35%. However, these strength reductions for the UHSS-DQ and UHSS-QT specimens cooled from 800°C to room temperature were close, i.e. 60% and 68%, respectively. The results also showed that while the reduction in the residual strength of UHSS-DQ is stabilised after 750°C temperature exposure, this stabilisation occurs for UHSS-QT at 700°C. For addressing the manufacturing process effect on the post-fire compression

behaviour of UHSS tubular stub-columns, a finite element model was developed using the results of the post-fire tensile tests carried out on UHSS-DQ and UHSS-QT tubes. The model was validated against the experimental compression tests conducted on UHSS-QT stub-columns cooled from different fire temperatures to room temperature. The detailed finite element modelling showed an acceptable agreement with the experimental post-fire behaviour of the tested stub-columns. Comparing the post-fire response of UHSS-QT and UHSS-DQ tubular stub-columns, it was shown that the UHSS-QT stub columns cooled from fire temperatures experienced the serious deterioration of the residual strength after exposure to temperatures above 600°C. However, this considerable strength reduction occurs for UHSS-DQ stub columns after exposure to temperatures above 700°C. The slenderness parameters of the simulated UHSS-DQ and UHSS-QT columns were also calculated. It was shown that unlike the cooled UHSS-DQ and UHSS-QT columns, the slenderness values of the virgin room temperature UHSS-DQ and UHSS-QT columns are consistent with the yield slenderness limits defined by the standards. However, the room temperature results of this study were consistent with the yield slenderness limit suggested by Jiao et al. [1] for virgin UHSS-QT tube at room temperature. Moreover, while the UHSS-QT stub columns experienced more plastic deformation when cooled from high fire temperatures, there is not a considerable difference between the ductility parameters of UHSS-DQ and UHSS-QT stub columns cooled from low fire temperatures.

8.2. Future work

The in-fire and post-fire mechancial response of different grades of steel tubes, with a focus on Grade 1200 UHSS, have been investigated during this PhD study. However, there are still other research problems which can be invetigated to further explore the behaviour of UHSS tubes under real fire conditions to enable their application in structural engineering fields. Some suggestions for future research work in this area are listed in the following sections.

8.2.1. The effect of strain rate on in-fire/post-fire mechanical response of UHSS

Although various experimental tests have been conducted on Grade 1200 UHSS specimens to simulate their behaviour under real fire conditions, the effect of strain rate has yet to be investigated. It is obvious that the creep strain caused in the material during fire can be considerably higher if strain rate is much higher than the moderate strain

levels defined by the standards (i.e. $0.005 \pm 0.002\,\text{min}^{-1}$ [2]). Therefore, the high strain rate can significantly affect the in-fire and post-fire strength reduction of UHSS and other steel grades. Thus, a potential future research can focus on the effect of high strain rates on the mechanical behaviour of UHSS (and other steel grades) at elevated temperatures and after cooling to room temperature. The high strain rate tests conducted on UHSS materials at elevated temperatures can be referred to as post-fire impact/blast multi-phase loading scenario.

8.2.2. Characterization of the post-necking true stress-strain response of UHSS tubes under in-fire/post-fire conditions

The in-fire and post-fire stress/strain results obtained during this PhD are only valid within the uniform strain regime. The necking phenomenon occurring during the tensile tests carried out on ductile materials such as steel, deviates the strain from the uniaxial state into a triaxial one [3]. Therefore, the readings of the strain values obtained from the uniaxial tensile tests are only accurate up to the onset of necking. While the true stress–strain curves are very important for the deformation analysis in theoretical plasticity and numerical simulations, there is a knowledge gap about the post-necking true stress-strain behaviour of steel materials under fire conditions. Thus, a potential future research can focus on this problem by introducing innovative correction methods for the non-uniform plastic deformation of the post-necking portion of the true stress-strain curves of UHSS (and other steel grades) under in-fire/post-fire conditions.

8.2.3. Large scale in-fire/post-fire tests on members composed of UHSS tubes

An innovative concept of prefabricated steel tube column has been developed by the Monash team which is composed of four Grade 1200 UHSS tubes welded to corners of four mild steel (MS) plates. While researchers from Monash University [4-7] have investigated the behaviour of these prefabricated columns at real scale under different loading scenarios, their response under fire and after cooling from fire temperatures have not been investigated. Knowing the precise nonlinear in-fire and post-fire mechanical behaviour of the materials used in these columns, numerical models can be developed to simulate their behaviour under real fire conditions. Experimental full-scale tests must be then conducted for validation of these models. The models can be used as powerful tools

for prediction of their behaviour under various loading scenarios including fire and creep, post-fire extreme loading, etc.

8.2.4. Analysis of multi-story UHSS buildings subjected to fire

In order to assess the behaviour of a multi-story UHSS building subjected to fire, numerical methods known as performance based methodologies can be used. The approach must use the experimental data on the performance of the material and structural systems, such as columns, subject to a realistic fire hazard. Due to the various uncertainties involved in characteristics of a fire hazard (such as heating rate, fire temperature, cooling rate, etc.), employing a probabilistic approach would be suitable to assess the in-fire/post-fire behaviour of these structures.

In the field of earthquake engineering, hazard analysis is conducted on multi-story buildings to describe the earthquake hazard in a probabilistic manner [8]. A hazard curve is produced by this analysis, which represents the variation of the ground motion parameters (as an intensity measure) with respect to the mean annual frequency (MAF) of exceedance [9]. Following the same concept, similar hazard analysis can be also created for the multi-story buildings subjected to fire. The hazard curve obtained from this analysis may show the relationship between the variation of maximum fire temperature (or any other characteristics of fire hazard) and the probability of collapse in a multi-story building at fire temperatures or after cooling to room temperature. This analysis can be then combined with structural analysis and the response of multi-story buildings under various characteristics of fire hazard (such as fire temperature) can be evaluated.

References

[1] H. Jiao, X.L. Zhao, Imperfection, residual stress and yield slenderness limit of very high strength (VHS) circular steel tubes, Journal of Constructional Steel Research, 59 (2003) 233-249.
[2] ASTM Standard E8/E8M, in: Standard Test Methods for Tension Testing of Methallic Materials, ASTM International, West Conshohocken, PA: USA, 2011.
[3] I.D.R. Fonseca, Correction of the post–necking true stress–strain data using instrumented nanoindentation, in, The University of North Carolina at Charlotte, 2014.
[4] M. Nassirnia, A. Heidarpour, X.-L. Zhao, J. Minkkinen, Innovative hollow columns comprising corrugated plates and ultra high-strength steel tubes, Thin-Walled Structures, 101 (2016) 14-25.
[5] F. Javidan, A. Heidarpour, X.-L. Zhao, J. Minkkinen, Application of high strength and ultra-high strength steel tubes in long hybrid compressive members: Experimental and numerical investigation, Thin-Walled Structures, 102 (2016) 273-285.
[6] M. Farahi, A. Heidarpour, X.-L. Zhao, R. Al-Mahaidi, 08.35: Compressive behavior of concrete filled double skin sections consisting of corrugated plates and ultra-high strength steel corner tubes, ce/papers, 1 (2017) 2120-2127.
[7] S.N. Sadeghi, A. Heidarpour, X.-L. Zhao, R. Al-Mahaidi, An innovative I-beam to hybrid fabricated column connection: Experimental investigation, Engineering Structures, 148 (2017) 907-923.
[8] S. Günay, K.M. Mosalam, PEER Performance-Based Earthquake Engineering Methodology, Revisited, Journal of Earthquake Engineering, 17 (2013) 829-858.
[9] Why Do Modern Probabilistic Seismic-Hazard Analyses Often Lead to Increased Hazard Estimates?, Bulletin of the Seismological Society of America, 96 (2006) 1967-1977.